Engineering of Combination Particles for Improved Therapeutic Efficacy

Amandeep Singh Dhillon

A thesis submitted for the degree of Doctor of Philosophy

University of Bath

Department of Pharmacy and Pharmacology

June 2010

……

Acknowledgements

There have been so many people involved in helping with the production of this thesis that it is hard to know where to begin. The ones that have done the most and inspired me the whole way are Professor Robert Price and Dr Jagdeep Shur. Without the constant encouragement shown by either Rob or Jag this work would probably have not been completed.

My deepest thanks goes to Rod, Steven, Kevin, Jo, Sarah and Don that have made sure that I have had the correct equipment in proper working order at hand. In addition, I would like to thank Ade for helping me fix my computer every time it broke and helping to keep me sane when faced with software issues.

To all of my friends that have helped me through the past four years, Harsh, Richard, Haggis, Hanne and most importantly Chonladda, as well as all of the undergraduate students who have taken part in the practical work, and all of my friends at home, a great big thank you for putting up with me and helping me get to the end.

Acknowledgment goes to Prosonix and the EPSRC for funding, without which, none of this work would have been possible.

And finally, but just as important as all of the others, I would like to thank my entire family, particularly my parents, Baldev and Kuldip, and my brother, Amardeep, for helping me get to this stage in my life. Without your love, support and encouragement, I would not have been in the place I am now.

Abstract

Combination based treatments have become increasingly popular in the treatment of several medical conditions in modern medicine due to the synergistic action possible from utilising several mechanistic pathways at once leading to an improved efficacy.

Patients suffering from Chronic Obstructive Pulmonary Disease (COPD) have been treated with the same drugs as asthmatic patients. Even though these compounds help with symptomatic control, none of the current formulations help with disease progression due to steroid resistance in these patients. Recent research has suggested that theophylline (THE) could be used to treat steroid resistance in COPD. However, this is only possible if the compounds reach the same site of action in the correct dose ratio.

However, for some compounds, improved efficacy may be achieved by improving the dissolution behaviour. A recent development in improving dissolution behaviour has been the crystal engineering of cocrystals, where a drug and a pharmaceutically excipient material are cocrystallised to form a new crystalline lattice. Current approaches are time consuming and the resultant crystals typically need further processing.

The development of the Solution Atomisation and by Xrystallisation by Sonication (SAX) process has previously been shown to be able to engineer individual particles containing two or more components in the correct stoichiometric ratios. The aim of this thesis is to assess the suitability of SAX to produce novel formulations for the treatment of COPD as well as the ability to produce cocrystals.

The SAX process was used to engineer particles containing a steroid, either budesonide (BUD) or fluticasone propionate (FP), as a combination or triple based therapy with the addition of theophylline (THE), salmeterol xinafoate (SX) and/or ipratropium bromide (IB). These particles were assessed via an array of techniques, and compared to micronized equivalent formulations in pressurised metered dose inhalers (pMDI's) and dry powder inhaler (DPI) formulations.

Cocrystals of carbamazepine (CBZ) and indomethacin (IND) with saccharin (SAC) were also produced via the SAX technique. In addition, cocrystals of CBZ with nicotinamide (NIC) were also produced via the same method. Physico-chemical properties were assessed compared to crystals formed by traditional methods of cocrystal manufacture.

Particles containing IB, SX and FP in the mass ratio 1:1.25:12.5 demonstrated a monomodal particle size distribution with XRPD analysis confirming the presence of the three compounds. However, DSC analysis did not show any distinct melting points therefore suggesting that the particles produced may have been amorphous. The presence of amorphous regions was confirmed by DVS analysis. *In-vitro* analysis of the triple formulation in both pMDI and DPI formulations suggest that a stable ratio of IB, SX and FP was maintained throughout the impactors used.

The combination particles contained either BUD or FP with THE. These particles were shown to be crystalline by XRPD analysis, which also confirmed the presence of both materials, and demonstrated a monomodal particle size distribution. *In-vitro* analysis suggested that the SAX produced particles with either FP or BUD with THE possibly fractured during fromulation preparation leading to a loss in the dose ratios throughout the stages of the impactor. However, the relative ratio of either FP or BUD to THE by mass, deposited on each stage showed greater consistency for the SAX formulations compared to the micronised equivalent. Dry powder inhaler (DPI) formulations showed no benefit in using the SAX particles compared to the micronised equivalent formulation for maintaining dose ratio consistency therefore confirming that the steroid and THE were co-processed rather then co-crystallised into one particle.

Crystalline particles containing SX, FP and THE in a 1:10:10 mass ratio were prepared via the SAX process. The resultant particles demonstrated a monomodal particle size distribution presenting a median equivalent volume diameter of 2.97 ± 0.01μm. XRPD analysis confirmed the presence of FP and THE. The presence of SX was confirmed by a melting endotherm in the DSC. *In-vitro* performance of both pMDI and DPI formulation for the triple API formulation suggested that the resultant particles did not maintain the dose ratios of three compounds.

Characterisation of the SAX produced cocrystals by DSC and XRPD confirmed the presence of the cocrystals with particle size distribution demonstrating a monomodal particle size distribution for all of the crystals produced.

The SAX process can be used to develop novel formulations for treatment of respiratory diseases, and can be suucessfuly applied for the rapid screening and large scale production of cocrystals in a single step operation.

Table of Contents

List of Abbreviations

%RD	Percentage of recovered dose
%w/v	Percentage weight-by-volume
%w/w	Percentage weight-by-weight
µg	Micrograms
µm	Micrometers
A	Surface area
Á	Angstroms
A*	Amplitude of wave
ACI	Andersen Cascade Impactor
API	Active Pharmaceutical Ingredient
AUC	Area under the curve
BCS	Biopharmaceutical Classification System
BUD	Budesonide
C	Concentration of drug at the surface
C&D	Capsules and device
C_{ae}	Cunningham slip correction factor
cAMP	Cyclic AMP (adenosine monophosphate)
CBZ	Carbamazepine
CFC	Chloroflurocarbon
CO_2	Carbon dioxide
COPD	Chronic Obstructive Pulmonary Disease
C_s	Concentration of drug in the solvent
CV	Coefficient of variation
d	Particle diameter

d_{10}	Cumulative diameter that accounts for 10% of all volume
d_{50}	Cumulative diameter that accounts for 50% of all volume
d_{90}	Cumulative diameter that accounts for 90% of all volume
dm/dt	Change in mass per unit time
DPI	Dry powder inhaler
DSC	Differential Scanning Calorimetry
DVS	Dynamic Vapour Sorption
ED	Emitted Dose
F	Filter
FDA	United States Food and Drug Administration
FP	Fluticasone propionate
FPD	Fine Particle Dose
FPF	Fine Particle Fraction
FPF_{ED}	Fine prarticle fraction as a function of emitted dose
FPF_{RD}	Fine particle fraction as a function of recovered dose
g	Acceleration due to gravity
GI	Gastro-intestinal
GOLD	Global Initiative on Obstructive Lung Disease
GR	Glucocorticod receptor
GSD	Geometric standard deviation
h	Boundry layer thickness
HDAC2	Histone deacetylase 2
HFA	Hydrofluoroalkane
HPLC	High Performance Liquid Chromatography
Hz	Hertz
I	Energy transmitted to liquid

IB	Ipratropium bromide
ICS	Inhaled corticosteroid
IL-8	Interlukin 8
IND	Indomethacin
k_1	Diffusion coefficient
kHz	Kilo hertz
kV	Kilo volts
LABA	Long acting β_2-agonist
LAMA	long acting muscarinic antagonist
LDI	Liquid dose inhaler
m	Meter
m/z	Mass-to-charge ratio
mA	Mili amps
min	Minutes
ml	Mili letters
mm	Mili meters
MOC	micro orifice collector
MP&T	Mouthpiece and throat
mRNA	Messenger RNA (ribonucleic acid)
N	Newtons
n	Number
NCE	New chemical entity
NF-κB	Nuclear factor κ B
NGI	Next Generation Impactor
nm	Nano meters

n_n	Number of circular nozzles in the stage
O/W	Oil-in-water
PDE	Phosphodiesterase enzymes
PKA	protein kinase A
pKa	Acid disassociation constant
pMDI	Pressurised metered dose inhaler
PS	Pre-seperator
Q	Volumatic air flow rate
R	Airway radius
R^2	coefficient of determination
RH	Relative humidity
rpm	Revolutions per minute
s	Seconds
S	Stage
SABA	Short acting β_2-agonist
SAC	Saccharin
SAMA	Short acting muscarinic antagonist
SAX	Solution Atomisation and Xrystallisation by Sonication
SD	Standard Deviation
SEM	Scanning electrom microscopy
ST_{50}	Stokes' number that gives a 50% chance of particle deposition
Stk	Stokes' number
SX	Salmeterol xinafoate
TGA	Thermo Gravametric Analysis
THE	Theophylline

U_t	Terminal velocity
UV	Ultra-violet
V	Air velocity
V_s	Velocity of sound in liquid
$W.g^{-1}$	Watts per gram
WHO	World Health Organisation
W_n	Nozzle Diameter
$\bar{x}$	Mean
XRPD	X-ray powder diffraction
ΔC	Change in concentration
η	Air viscosity
θ	Degrees
λ	Wavelength
ρ	Particle density
ρ_f	Density of liquid
ρ_p	Particle Density

Chapter 1 – Introduction.

1.1 Pharmaceutical combinations systems

Combination based treatments have become increasingly popular in the treatment of several medical conditions in modern medicine due to the synergistic action possible from utilising several mechanistic pathways at once.

Combination products combine two or more different single-entity products—a drug combined with another drug or a drug combined with a device. They may also be combined in multiple ways: physically, chemically, or otherwise; packaged together (co-packaged); or provided separately but specifically labelled for use together.

The largest challenge during development of combination products is the scale-up process, because additional quality control measures are required to determine the process scale-up parameter shift. During scale-up, combination products should require additional QC pressures along with a robust release-testing program. New technologies will require operations that are proven within acceptable ranges based on process scale-up and manufacturing limitation regarding device technology and delivery.

Combination products have proved to be highly effective in the treatment of respiratory diseases, either by the addition of a spacer device aiding the delivery of inhaled medication for children or by the combination of more then one chemical entity in either a dry powder inhaler of pressurised metered dose inhaler formulation.

1.2 Chronic Obstructive Pulmonary Disease (COPD)

The incidence of chronic obstructive pulmonary disease (COPD) is increasing globally, placing an increasing burden on health services in industrialised and developing countries (Mannino and Buist 2007; Pearce, it-Khaled et al. 2007). According to the latest World Health Organisation (WHO) estimates, COPD will become the third commonest cause of death by 2030 (Lopez and Mathers 2006). The Global Initiative on Obstructive Lung Disease (GOLD) defines COPD as “a disease state characterised by airflow limitation that is not fully reversible. The airflow limitation is usually progressive and associated with an abnormal inflammatory response of the lungs to noxious particles and gases” (Pauwels, Buist et al., 2001). This definition encompasses the idea that COPD is a chronic inflammatory disease, which is characterised by acceleration in the normal decline of lung function seen with age (Pauwels and Rabe, 2004). Amongst other inflammatory mediators, the key inflammatory cells that play a pivotal role in COPD include neutrophils, macrophages, T- and B-lymphocytes.

In developed countries, cigarette smoking is by far the commonest cause of COPD accounting for >95 % of cases, but there are several other risks factors, including air pollution, poor diet and occupational exposure (Barnes, Shapiro et al., 2003). Cigarette smoke extract can activate macrophages, which secrete many inflammatory proteins that orchestrate the inflammatory response in COPD (Barnes, Shapiro et al., 2003). Inflammatory mediators attract inflammatory cells such as neutrophils, which secrete proteases that contribute to alveolar destruction and mucus hyper-secretion (Barnes, Shapiro et al., 2003). Furthermore, macrophages generate reactive oxygen species and nitric oxide, which together with peroxynitrate may contribute to steroid therapy resistance in COPD (Barnes, 2004). COPD includes chronic obstructive bronchitis with fibrosis and obstruction of the small airways, and emphysema with enlargement of airspaces and destruction of lung parenchyma, loss of elasticity and closure of small airways (Barnes, Shapiro et al., 2003). Smoking induces many of these features. The slowly progressive airflow limitations in COPD eventually lead to disability and premature death.

Remodeling and narrowing of small airways and destruction of the lung parenchyma are the primary causes of airflow limitation in COPD, which are a direct result of chronic inflammation in the lung periphery.

Studies have shown that the inflammatory response in small airways increases as the disease progresses. The primary pattern of inflammation in COPD is characterised with increased numbers of macrophages in the airways. Macrophages play an important role in the inflammatory process in the COPD lung, through the release of pro-inflammatory mediators. For example, T lymphocytes with predominance of CD8+ (cytotoxic) T cells and, in more severe diseases, B lymphocytes with increased numbers of neutrophils in the airway lumen. Many of these inflammatory mediators serve to amplify the inflammatory response in COPD. Oxidative stress is an important amplifying mechanism and may increase the expression of inflammatory genes through impairing the activity of histone deacetylase 2 (HDAC2), which is required to switch off inflammatory genes.

The molecular basis of this amplification of inflammation has been related to the role of reduced HDAC activity in COPD. HDAC plays a critical role in the suppression of gene expression by reversing the hyperacetylation of core histones. HDAC activity is reduced in alveolar macrophages of cigarette smokers compared with nonsmokers, and this reduction is correlated with increased expression of inflammatory genes in these cells. There is also a reduction in total HDAC activity in peripheral lung, bronchial biopsies, and alveolar macrophages from COPD patients, and this reduction is correlated with disease severity. HDAC2 is required for the deacetylation-activated

nuclear glucocorticoid receptor and therefore the expression of inflammatory genes. The reduced activity of HDAC2 in COPD patients is associated with increased acetylation of glucocorticoid receptor, which may be a major mechanism accounting for corticosteroid resistance in COPD.

1.2.1 Treatment options for COPD

In order to manage COPD, therapies are required to control symptoms, reduce exacerbations and improve health status in patients. The first-line treatments for COPD are long-acting β_2-agonists (LABA), symptomatic bronchodilators (anti-muscarinic agents) and inhaled corticosteroids (ICS), which are employed to aid bronchodilation and reduce inflammation, respectively (Johnson and Rennard 2001; Barnes 2002; Barnes 2003; Barnes 2008).

1.2.1.1 β_2-agonists

β_2-agonists are the main bronchodilators used for the treatment of respiratory diseases. Ligand binding of the β_2-agonists to the β_2-agonists receptor results in the activation of the G_s protein. This then results in the enhanced production of cyclic adenosine monophosphate (cAMP), which leads to the activation of cAMP-dependant protein kinase A (PKA). As a result, myosine light chain is phosphorylated and inactivated. At the same time, Ca^{2+}-Mg^{2+}-ATPase is activated in the edoplasmic reticulum resulting in a decrease in intracellular Ca^{2+} level and therefore reducing Ca^{2+}-dependent actin-myosin interaction and the resultant relaxation in airway smooth muscles (Cazzola, Testi et al. 2002; Caramori and Adcock 2003; Keating and McCormack 2007).

In addition, β_2-receptors have been found on other cells including basophils, eosinophils, neturophils and lymphocytes (Lichtenstein and Margolis 1968). The activation of these receptors also results in the increase in intracellular cAMP which leads onto the inhibition of inflammatory mediator release (Lichtenstein and Margolis 1968; Barnes 1999). This suggests that β_2-agonists could reduce inflammation within the lung by reducing inflammatory mediator release. However, mast cells and lymphocytes rapidly become desensitised to the action of β_2-agonists (Johnson and Coleman 1995).

Short acting β_2-agonists (SABA's) are the first line treatment for respiratory diseases as they provide a rapid onset of action, generally 1 - 5 min, and provide symptomatic relief. Long acting β_2-agonists (LABA's), such as salmeterol xinafoate (SX), have also been developed. LABA's demonstrate a greater selectivity for β_2 receptors compared to SABA's (D'Alonzo, Nathan et al. 1994; Kamada, Spahn et al. 1994). As a result, LABA's provide better prophylactic control. However, due to the fact that LABA's do not

control inflammation, the addition of an inhaled corticosteroid (ICS) to a LABA should aid in the long-term control of asthma and chronic obstructive pulmonary disease symptoms.

In addition to the above mechanisms, β_2-agonists may induce glucocorticoid receptor translocation thus preparing the receptor to be more responsive to activation by ICS (Adcock, Maneechotesuwan et al. 2002; Barnes 2002). Recent studies have shown that the combination of LABA and ICS provide better control of asthmatic symptoms compared to using individual compounds (Barnes 2001; Mahler, Wire et al. 2002; Buhl 2003; Nelson, Chapman et al. 2003; Ankerst 2005).

1.2.1.2 Anti-muscarinic compounds

Bronchial smooth muscle tone is controlled by the parasympathetic nervous system. Postganglionic nerve fibres release acetylcholine which acts at muscarinic M_3-receptors resulting in an increase in bronchial tone (Gross 1988; Barnes 1993; Jacoby and Fryer 2001). In addition to this, stimulation of the muscarinic receptors in the airway gland increases secretion of mucus (Gross 1988; Hoffman and Taylor 2001).

Small doses of atropine can reduce saliva and bronchial secretions as well as reduce bronchoconstriction, hence resulting in its use in the early 1900's (Gross 1988), by competitive inhibition of the muscarinic receptors in the lung. However, atropine can also reduce mucociliary clearance. Newer anti-muscarinic compounds (such as ipratropium bromide, IB, and tiotropium) have a reduced inhibitory effect on mucociliary clearance compared to atropine (Gross 1988) while still being a competitive antagonist at M_3 receptors (Pakes, Brogden et al. 1980; Gross 1988; Jacoby and Fryer 2001).

Ipratropium is a short acting anti-muscarinic compound (short acting muscarinic antagonist, SAMA). This has a maximal response in 30-90 minutes with a total duration of action of 4-6 hours (Barnes 1999; Littner, Ilowite et al. 2000; van Noord, Bantje et al. 2000). This implies that it needs to be taken 3 to 4 times a day, thus making patient compliance an issue. Tiotropium is a long acting anti-muscarinic compound (long acting muscarinic antagonist, LAMA), which has a slower onset of action but offer a 24 hour duration of action resulting in a once-a-day dose and therefore improving patient compliance (Barnes 1999; Littner, Ilowite et al. 2000; van Noord, Bantje et al. 2000).

Anti-muscarinic compounds are more effective then β_2-agonists in COPD patients than in asthmatics (Littner, Ilowite et al. 2000; van Noord, Bantje et al. 2000; Jacoby and Fryer 2001; Barnes 2003). However, the combination of both and anti-muscarinic and β_2-agonists results in synergistic activity at a greater level than doubling the dose of either component on their own (Bryant 1985; Gross 1988; Bryant and Rogers 1992).

1.2.1.3 Inhaled Corticosteroids (ICS)

Glucocorticoids are mainly used in the treatment of inflammatory diseases. Asthmatics that are treated with inhaled corticosteroids (ICS) demonstrate a reduced responsiveness to trigger factors such as histamine in terms of sensitivity and degree of narrowing (Caramori and Adcock 2003). However, this may take several months to occur and is reversed on cessation of treatment. In contrast, the long term treatment with either oral or inhaled steroids in COPD patients provides no long term benefit, except for about 10% of the COPD population who are thought to have concomitant asthma (Barnes 2000; Caramori and Adcock 2003; Barnes 2008).

ICS work by activating the glucocorticoid receptor (GR) within cells via the disassociation from inhibitory proteins and subsequent changes in the receptor complex (Adcock, Maneechotesuwan et al. 2002; Caramori and Adcock 2003; Adcock and Chung 2008; Barnes 2008). This complex can then act on gene transcription in several ways. The first being the direct inhibition of NF-κB production and, therefore, inhibiting the inflammatory effects of cytokines (Barnes, Pedersen et al. 1998; Adcock, Maneechotesuwan et al. 2002; Caramori and Adcock 2003). ICS's can also work by the recruitment of histone deacetylase 2 (HDAC2), which act to result in the deacetalyation of the gene resulting in the suppression of gene transcription (Barnes 1998; Adcock, Maneechotesuwan et al. 2002; Barnes 2005).

The increased oxidative and nitrative stress caused by cigarette smoke may have reduced the activity and expression of HDAC2 in COPD patients (Barnes, Ito et al. 2004; Barnes and Stockley 2005; Ito, Ito et al. 2005; Barnes 2006; Ito, Yamamura et al. 2006; Barnes 2008; Barnes 2008). As a result, steroids have little or no effect at reducing inflammation in COPD patients.

Glucocorticoids have been found to have a beneficial action in the production and survival of β_2-agonist receptors (Mak, Nishikawa et al. 1995; Barnes 2001; Adcock, Maneechotesuwan et al. 2002; Barnes 2002) due to the fact that there are several glucocorticoid receptor elements in the promoter sequence for the human β_2-agonist receptor gene (Adcock, Maneechotesuwan et al. 2002). The activation of the gene results in increased β_2-agonist receptor mRNA being produced and thus leading to an increase in the total number of β_2-agonist receptors; therefore combating β_2-agonist receptor down regulation (Hadcock, Wang et al. 1989; Adcock, Maneechotesuwan et al. 2002).

1.2.1.4 Phosphodiesterase inhibitors

Theophylline (THE) is the cheapest of all drugs used for the treatment of asthma. Its use has declined due to β_2-agonists being safe to use with more tolerable side-effects. However, THE, which is available in an oral dosage form, is still used for the treatment of persistent asthma (The British Thoracic Society 2008). Its main mode of action is by the inhibition of phosphodiesterase enzymes (PDE) which catalyse the breakdown of cAMP (Cushley and Holgate 1985; Beavo and Reifsnyder 1990). This results in an increase in the intracellular levels of cAMP, resulting in reduced bronchoconstriction as for the β_2-agonists.

The inhibition of inflammatory mediator synthesis and release from inflammatory cells has been found to be caused by inhibiting PDE IV (Torphy and Undem 1991; Torphy, Undem et al. 1993; Page 1999), while inhibiting PDE III and IV results in bronchodilation (Torphy, Undem et al. 1993). THE is a non-selective PDE inhibitor and, therefore, will block PDE III and IV as well as others.

THE has also been found to be a competitive antagonist at the adenosine receptor (Fredholm and Persson 1982). Adenosine has been found to trigger bronchoconstriction and induce immunological mediator release from mast cells in asthmatic patients (Cushley, Tattersfield et al. 1984; Peachell, Columbo et al. 1988). Interestingly, the bronchoconstriction does not occur in isolated bronchial smooth muscle, but only in lungs of asthmatic patients (Cushley, Tattersfield et al. 1984). THE may also reduce the inflammatory response in asthmatic patients by inhibiting the adenosine receptor (Feoktistov, Biaggioni et al. 1998). This has been shown to be true by Culpitt et al. who demonstrated that THE can reduce inflammatory cells in COPD patients by 22% (Culpitt, de Matos et al. 2002).

Recent work has shown that the addition of THE to an ICS in asthmatic patients demonstrates the same effect as increasing the dose of ICS (Evans, Taylor et al. 1997; Markham and Faulds 1998). In some cases, the amount of THE needed is well below the dose required for bronchodilation (Evans, Taylor et al. 1997). However, this does not always appear to be the case (Lim, Jatakanon et al. 2000; Adachi, Aizawa et al. 2008).

In COPD patients, THE proves to be beneficial by helping to reduce exacerbations and improve lung function (Kirsten, Wegner et al. 1993; Cyr, Beauchesne et al. 2008). This response was for plasma levels lower than that required for bronchodilation (Kirsten, Wegner et al. 1993). This suggests that, at lower concentrations, THE may have another mechanism of action.

One explanation could be the activation of histone deacetylase (HDAC) (Ito, Lim et al. 2002; Cosio, Tsaprouni et al. 2004; Barnes 2008). As previously mentioned, HDAC recruitment by ICS's results in the deacetylation of inflammatory genes therefore reducing their transcription (Barnes 1998; Adcock, Maneechotesuwan et al. 2002; Barnes 2005). This suggests that THE may be beneficial in COPD patients for the reversal of steroid resistance (Barnes, Ito et al. 2004; Cosio, Tsaprouni et al. 2004; Barnes and Stockley 2005; Barnes 2008).

A significant amount of work has been done on the treatment of asthma, while current therapies for chronic obstructive pulmonary disease (COPD) have had to rely on these treatments developed for asthma.

1.2.1.5 Inhaled combination therapy for COPD

Inhalation dosage forms combining a LABA and ICS are available in both pressurised metered dose inhaler (pMDI) and dry powder inhaler (DPI) platforms (Keating and McCormack 2007). Of the inhalation products available, the combination of salmeterol xinafoate (SX, LABA) and fluticasone propionate (FP, ICS) (Seretide®/Advair®, GlaxoSmithKline, UK) has gained wide-spread acceptance with both physicians and patients, and is currently listed amongst the top ten best-selling pharmaceutical products with annual sales of approximately £5 billon forecasted for 2009 (Davis 2008). This combination based therapy shows greater efficacy compared with monotherapy treatments with the individual components (Calverley, Pauwels et al. 2003; Bergmann, Lindemann et al. 2004; Calverley, Anderson et al. 2007; Cazzola, Ando et al. 2007), with reduced mortality rates in COPD above and beyond that achieved by individual therapies (Sin and Man 2007).

The enhanced clinical benefit of combining both classes of compounds in a single formulation may be related to additive effects of administering both agents simultaneously to the lung, because they have complementary modes of action and target different aspects of the underlying disease pathophysiology (Barnes 2002; Nelson 2005). However, the increased clinical efficacy of inhaled therapies combining SX and FP have been reported to be more than just additive affects of co-administering both agents, but may be due to synergistic interactions of the two classes of compounds at the receptor, molecular and cellular level (Nelson, Chapman et al. 2003).

The synergistic effects of co-administered SX and FP have been previously investigated on human bronchial human cells in the inhibition of the pro-inflammatory chemokine interleukin-8 (IL-8) (Barnes, Qiu et al. 2006; Kent, Smyth et al. 2008; Mortaz, Rad et al. 2008). This chemokine plays a key role in the inflammatory

processes of severe asthma and COPD wherein it acts as a potent neutrophil chemo-attractant up-regulated in response to inflammatory stimuli such as cigarette smoke or bacterial products (Barnes 2004; Kent, Smyth et al. 2008). The recruitment (and subsequent activation) of large numbers of inflammatory cells to the lungs in response to increased IL-8 secretion leads to the tissue damage that typifies pathophysiologies observed in severe asthma and COPD (Dean, Dai et al. 1993). Previous studies have shown enhancement of the inhibition in IL-8 production when SX was combined with FP, which was related to improved clinical health status and reduced daily symptoms in patients (Calverley, Pauwels et al. 2003; Calverley, Boonsawat et al. 2003).

The synergistic action between SX and FP is thought only to occur when both drugs reach the same target cell in the required concentrations (Nelson, Chapman et al. 2003). The administration of both drugs from a single inhalation dosage form is, therefore, likely to enhance the probability of co-deposition in comparison to monotherapy treatment with the individual active agents. Furthermore, recent studies have shown that the opportunity for co-deposition of SX and FP particles in the airways is further enhanced in the Advair pMDI formulation as a result of particle co-association within the delivery device (Nelson, Chapman et al. 2003; Theophilus, Moore et al. 2006).

1.3 Respiratory Drug Delivery Systems

In essence, there are three main drug delivery systems employed to deliver therapeutics to the lungs: pressurised metered dose inhalers (pMDIs), dry powder inhalers (DPIs) and nebulisers (Hickey and Dunbar, 1997). All three systems are used to treat local conditions within the lung, for example, in asthma and COPD (Lalor and Hickey, 1996).

1.3.1 Nebulisers

Nebulisers are devices used to convert aqueous solutions or aqueous suspensions of drug into an aerosol (Clarke, 1995). Nebulisers apply either compressed gas or ultrasonic energy for the aerosolisation of the aqueous based solution, which is then inhaled by the patient (Dalby and Suman, 2003). Unlike other devices, they do not require the use of a complicated breathing manoeuvers and, by extending the time of operation, they can be used to deliver large doses (de Boer, Hagedoorn et al., 2003). However, due to the need for an external power supply, high running costs and the prolonged amount of time required to deliver an adequate dose (typically 10 to 15 minutes), nebulisers are typically limited to hospital and non-ambulatory patients (Garcia-Contreras and Hickey, 2003). Recent developments in nebuliser technology are beginning to overcome some of these problems, allowing accurate metering of

doses and increasing portability, which has led to the development of the liquid dose inhalers (LDIs) (Dalby and Suman 2003; Dalby, Spallek et al. 2004).

1.3.2 Pressurised Metered Dose Inhalers (pMDIs)

Since 1956, pressurised metered dose inhalers (pMDIs) have been the drug delivery system of choice for respiratory diseases because of a result of their cheap, robust and convenient characteristics (Hickey and Dunbar, 1997). Traditionally, these devices consist of a solution or suspension of fine drug particles in a chlorofluorocarbon (CFC) propellant sealed in a canister at high pressure (Biddiscombe, Melchor et al., 1987). The formulation may also contain formulation additives including surfactants and co-solvents (McDonald and Martin, 2000). The propellant is the main component of pMDI formulations and performs the role of solvent and dispersion medium for drug substance and other excipients (Young, Price et al., 2003a). Actuation of the inhaler results in the release of a metered volume of this solution or suspension, which is driven by the high vapour pressure within the canister, which in turn emerges at a high velocity through a narrow orifice (Smyth, Hickey et al., 2006). This process, combined with evaporation of the propellant, results in an aerosol of drug particles in the respirable size range that are able to enter and deposit in the respiratory tract (Berry, Kline et al., 2003). Despite pMDIs being the most frequently prescribed inhalation dosage form, the fact remains that most patients cannot use them correctly (Virchow, Crompton et al., 2008). This is because the high speed aerosol plume generated by a pMDI requires the patient to use accurate co-ordination of inspiration and inhaler activation to ensure correct inhalation and deposition of the drug in the lung (Virchow, Crompton et al., 2008). Even with the correct inhalation technique, pMDIs are inefficient, often delivering less than 1/3 of the emitted dose to the lungs (Virchow, Crompton et al., 2008). In addition to these problems, the introduction of the Montreal Protocol results in the phase out of chlorofluorocarbon (CFC) propellant gas in all aerosol-based products, including pMDIs. As a result, all pharmaceutical CFC-based pMDI products were re-formulated using hydrofluoroalkanes (HFAs) propellant and replaced (Richards, Hirst et al., 2001). The difficulties and expense, incurred in re-formulating pMDI products and long term issues regarding the future of HFA-based propellants, have prevented companies to launch new drugs as pMDI formulations (McDonald and Martin, 2000).

1.3.3 Dry Powder Inhalers (DPIs)

Dry powder inhalers (DPIs) permit a metered dose of drug to be delivered to the airways as a dry powder aerosol (Timsina, Martin et al., 1994). A patent from 1950, by Mack R. Fields, described the first metered dose DPI for the delivery of medicaments

to lungs (Fields, 1950). Later, DPIs were successfully introduced as a propellant-free alternative to the pMDI (McDonald and Martin, 2000). Currently, the spectrum of application of DPIs has become much broader, due to the high lung deposition that can be attained and their suitability for pulmonary delivery of therapeutic peptides and proteins both for local and systemic conditions (Byron and Patton, 1994).

DPIs are breath-actuated drug delivery systems, which enable a respirable cloud to be produced in response to the patient's inspiratory effort (Timsina, Martin et al., 1994). DPIs may therefore have many advantages over pMDIs (Hannemann, 1999; Newman and Busse, 2002; Virchow, Crompton et al., 2008). Firstly, DPIs do not need a propellant, which has been the driving force behind the introduction of a large number of novel DPI devices in recent years (Timsina, Martin et al., 1994). The second benefit is that DPIs eliminate the need for patient co-ordination of actuation and inhalation (Newman and Busse, 2002). Finally, in DPIs, the particles are travelling at a slower rate, therefore, an excessive drug loss due to impaction in the throat is avoided (Pauwels, Newman et al., 1997).

Successful deposition of drug particles into the lung requires the delivery of particles with a mass median aerodynamic diameter (MMAD) less than 5 μm (Heyder, Gebhart et al., 1986; Timsina, Martin et al., 1994; Prime, Atkins et al., 1997). A control of particle size of medicaments to be delivered by DPIs is typically achieved through high-energy micronisation techniques (Thibert and Tawashi, 1999), although numerous other technologies, for example, spray drying (Li, Seville et al., 2005) and supercritical fluid technologies (Shekunov, Feeley et al., 2003) have been evaluated. However, respirable sized particles exhibit high surface energies, which lead to particle aggregation, poor flow and entrainment properties, and thereby make re-dispersion of the drug a difficult process (Feeley, York et al., 1998).

The most common method employed to solve the problems associated with cohesive respirable powder materials is to formulate the drug with an excipient, traditionally lactose monohydrate (Bell, Hartley et al., 1971). The micronised drug is blended with carrier particles of a much larger size range (usually 20-100 μm), whereby the drug particles form an interactive mixture with the surfaces of the coarse lactose particles (Ganderton, 1992). The turbulent airflow generated within the device upon forced inspiration should be sufficient to fluidise the formulation from the device and to de-aggregate the drug particles from the carrier particles (Telko and Hickey, 2005; Shur, Harris et al., 2008). The drug particles are then entrained into the airstream, which enables the drug particle to enter the lungs (Shur, Harris et al., 2008). The carrier particles are subsequently deposited in the oropharynx of the patient. Although high levels of turbulence are required to be engineered into the device for efficient

deaggregation (Louey, Van Oort et al., 2006), there is a need to balance the resistance of the inhaler to airflow and in inhaling through the device at a flow rate which produces optimum drug delivery (Crowder and Hickey, 2006). One way to provide high levels of turbulence without imposing large increase in airflow resistance is the use and placement of grids of varying mesh sizes (Helgesson, Jennings et al., 2005; Telko and Hickey, 2005).

There are currently three types of DPIs available on the market. These include a single-dose, multidose and reservoir-based device (Prime, Atkins et al., 1997; Malcolmson and Embleton, 1998; Smith and Parry-Billings, 2003). Early DPI devices were all unit-dose systems and were dependent on loading and triggering procedures. The Spinhaler® and Rotahaler® are two early examples of DPI technologies. Both utilise pre-metered doses packed into hard gelatin capsules although different mechanisms of powder delivery and power technology are employed (Vidgren, Karkkainen et al., 1987).

Multidose pre-metered DPIs include the successful Diskhaler® and Diskus® devices from GlaxoSmithKline. The Diskhaler® employs individual doses contained within blisters (4 or 8 blisters) on a disk. On actuation, a needle pierces the upper and lower surfaces of a blister. As the patient inhales, the contents of the blister are dispersed into the airstream. The drug particles are dissociated from the carrier and a fraction delivered to the lung. On re-priming the device, the disk rotates to expose the next blister to the piercing needle (Prime, Atkins et al., 1997)(Hillery, Lloyd et al. 2001). The Accuhaler® DPI device, produced by GSK, retains the blister pack and unit-dose approach of the Diskhaler®, but has the advantage of holding additional doses. The pack consists of a coiled, double-foil strip of 60 blisters, each containing one dose of drug powder formulated with a lactose carrier (Malcolmson and Embleton, 1998).

Reservoir DPIs contain all the doses in a bulk reservoir, and each dose is dispensed from this reservoir by manipulation of the device prior to inhalation (Smith and Parry-Billings, 2003). The first device employing a multi-dose reservoir was the Turbuhaler (Newman, Moren et al., 1991). The dose is metered into conical cavities by rotating the base of the inhaler. The inhaled airstream dislodges the drug from the cavities and dispersion continues in the inhalation channels, which are helical to induce turbulent flow (Helgesson, Jennings et al., 2005). A desiccant is employed to ensure that the powder reservoir remains dry during the shelf life of the inhaler. Other examples of reservoir DPI device are the Easyhaler® (Ranbaxy, UK Ltd), Clickhaler® (Vectura plc, Chippenham, UK) and Pulvinal® (Chiesi Farmaceutici SpA, Parma, Italy).

Every DPI device exhibit an internal resistance which determines the peak inspiratory flow rate that a patient can achieve when using the device (Harris 2007). As flow rate will inevitably be linked with inhaler performance, it is essential that such factors are considered in any *In-vitro* comparative testing of DPIs (Harris 2007). Successful development of DPI systems requires development on two integrated fronts: device engineering and powder formulation (Timsina, Martin et al. 1994).

1.3.4 Problems with current combination formulations.

In a DPI the patient's inhalation breath is used to disassociate the fine drug particles from the surface of the carrier particle, therefore allowing the drug particles to be delivered into the deep lung (Telko and Hickey 2005). The amount of drug liberated from the surface of the carrier particle will be largely dependent on the interfacial forces between the fine drug components and the carrier and the deaggregation energy generated within a device during forced inspiration (Jones, Harris et al. 2008).

Pressurised metered dose inhalers (pMDI's) demonstrate a similar problem where the two micronised components are accurately weighed into a canister and suspended in a suitable propellant. In this situation, the drug molecules are suspended within the propellant and may exhibit inter-particulate forces resulting in agglomeration of the drug molecules and therefore a reduced fine particle dose. Alternatively, the particles may interact with the surface of the pMDI canister and reduce the amount of drug available for delivery into the lungs. The amount of interaction will be dependent on the canister material as well as the surface properties of the drug molecule (Traini 2005).

As a result, the prospect of co-depositing of both actives to the same site of action in the correct dose ratio is rather limited and cannot be adequately controlled (Taki and Marriott; Taki, Zeng et al. 2006). Hence, these dosage forms may be subjected to greater variability in fine particle delivery of each active.

In addition, the two drugs will exhibit different densities and particle size distributions. This will result in different deposition mechanisms, will be discussed shortly, and therefore result in the loss of synergistic action between the drugs.

One method for overcoming this problem may be to develop novel devices that allow for each drug component to be formulated separately but delivered together. This could result in larger devices, making them harder to carry and use.

Alternatively, the two drug components could be dissolved within a pMDI propellant in the correct ratio (Lewis, Meakin et al. 2006). This would allow for each droplet to contain the correct ratio of both components. However, stability may be an issue

depending on the chemical stability of the drug component within the propellant solution.

Another method for the provision of a combination formulation, that may work in both DPI and pMDI formulations is the development of novel particles that contain both components.

1.4 Drug deposition in the lungs.

The human lung has evolved in such a way as to prevent entry of and facilitate the removal of unwanted and harmful material from reaching the respiratory sections. This has been accomplished by a collection of mechanisms (Lippmann, Yeates et al. 1980). The first of which is the presence of ciliated epithelial cells on the conducting airways which have a mucus layer suspended on top (Gurney 1991; Boucher 1994). If a large particle is deposited on the conducting airways, which consist of the trachea, bronchi and bronchioles, the insoluble particle becomes stuck in the mucus layer. The rhythmic beating of the cilia results in the movement of the mucus layer back up the airway towards the throat where it can be swallowed. Unfortunately, this allows for the drug to be absorbed into the body via the intestines and have a systemic effect.

Once past the trachea, the airway splits or bifurcates into the bronchi. From here, the airways branch out over 32 bifurcations until reaching the alveoli (Gurney 1991). At each bifurcation, the airways become narrower and the air velocity reduces. This, in combination with the bifurcation angle, results in the active filtering of particles and microbes by the lungs. As a result, the lugs provide a unique challenge in delivering medication to a specific site within the lungs.

The three main mechanisms for drug deposition within the lungs are inertial impaction, sedimentation and Brownian motion. In addition to these, interception and electrostatic precipitation may also lead to drug deposition.

1.4.1 Inertial impaction.

Inertial impaction is the major mechanism of drug deposition in the conducting airways (Asgharian and Anjilvel 1994). At each bifurcation, the direction of airflow changes. However, a large, or dense particle may not be able to lose its inertia resulting in impaction on the airway wall (Martonen, Katz et al. 1992). The probability of impaction of a particle travelling in an airway is related to its Stokes' number (Stk) using equation 1.1:

$$Stk = \frac{\rho_p d^2 V}{18\eta R} \qquad \text{Equation 1.1}$$

where ρ_p is the particle density, d is the particle diameter, V is the air velocity, η is the air viscosity and R is the airway radius. A higher Stokes' number means a greater probability of deposition (Morrison 1974; Martonen and Katz 1993; Crowder, Rosati et al. 2002).

1.4.2 Sedimentation

Sedimentation occurs as a result of gravity acting on a particle within the respiratory tract (Clark and Egan 1994). The terminal velocity of a particle in a laminar air-flow (U_t) is described by Stokes' law (Stokes 1908):

$$U_t = \frac{\rho d^2 g}{18\eta} \qquad \text{Equation 1.2}$$

where ρ is the particle density, d is the particle diameter, g is the acceleration due to gravity and η is the air viscosity. However, the viscosity of air is constant ($1.9 \times 10^{-7} Nm^{-2}s$) and acceleration due to gravity is also constant ($9.8\ ms^{-2}$). Therefore, the terminal velocity can be simplified to:

$$U_t = 2.9 \times 10^6 \rho d^2 \qquad \text{Equation 1.3}$$

As can be seen, the terminal velocity is dependent on only the particle density and diameter. However, the particle must have sufficient time to settle in the airway (Taulbee and Yu 1975). As a result, this is the major mechanism of deposition in the bronchioles.

1.4.3 Brownian Motion

Brownian motion is caused by the constant bombardment of air particles against particles. This results in the particles demonstrating a 'random walk'. As the particle size decreases, the velocity of the particle will increase (Aulton 2002; Florence and Attwood 2006).

1.4.4 Interception

Interception occurs when a particle moving within the airstream makes contact with the respiratory surface(Taulbee and Yu 1975). Elongated particles are most likely to deposit in this manner. However, as the typical size of drug particles used in respiratory drug delivery is much smaller than that of the airways, this mechanism of deposition is relatively unimportant in most cases (Martonen and Katz 1993).

1.4.5 Electrostatic precipitation

During aerosolisation, drug particles may become electrostatically charged (Yeomans, Rogers et al. 1949). In theory, charged particles may influence the deposition mechanism either through the induction of an image charge on the respiratory surface and subsequent electrostatic attraction or via the repulsion between like charged aerosol particles directing them towards the airway walls (Balashazy and Hofmann 1993).

1.5 Improving clinical efficacy for oral medication.

Solubility of active pharmaceutical ingredients (APIs) is major concern during development of a drug product, since poor aqueous solubility of the API may lead to sub-optimal efficacy in patients owing to their slow dissolution in biological fluids. This is particularly true when APIs are delivered via the oral route of administration.

1.5.1 Drug dissolution.

The solubility of a substance is the amount of substance that has passed into solution when equilibrium is attained between the solution and excess. On administration of an oral dosage form, the drug is released from a matrix and dissolves in the surrounding gastrointestinal (GI) fluid to form a solution, as shown in figure 1.1.

The dissolution of a drug crystal begins with the drug and aqueous media interacting to transform a solid phase into a solute molecule, resulting in a supersaturated layer of solute above the surface of the crystal. Following this, solutes diffuse into the bulk of the liquid. If the drug is soluble in the liquid, this whole process will happen rapidly. However, if the drug is poorly water soluble, the liberation of a solid to a solute will increase the time needed to fully dissolve the compound. A drug substance is considered highly soluble when the highest dose strength is soluble in 250 ml or less of aqueous medium over the pH range of 1 – 7.5 (Mannhold, Kubinyi et al. 2003). Hence, the process of drug dissolution is limited by the intrinsic solubility of the API in the GI fluid, which is primarily water.

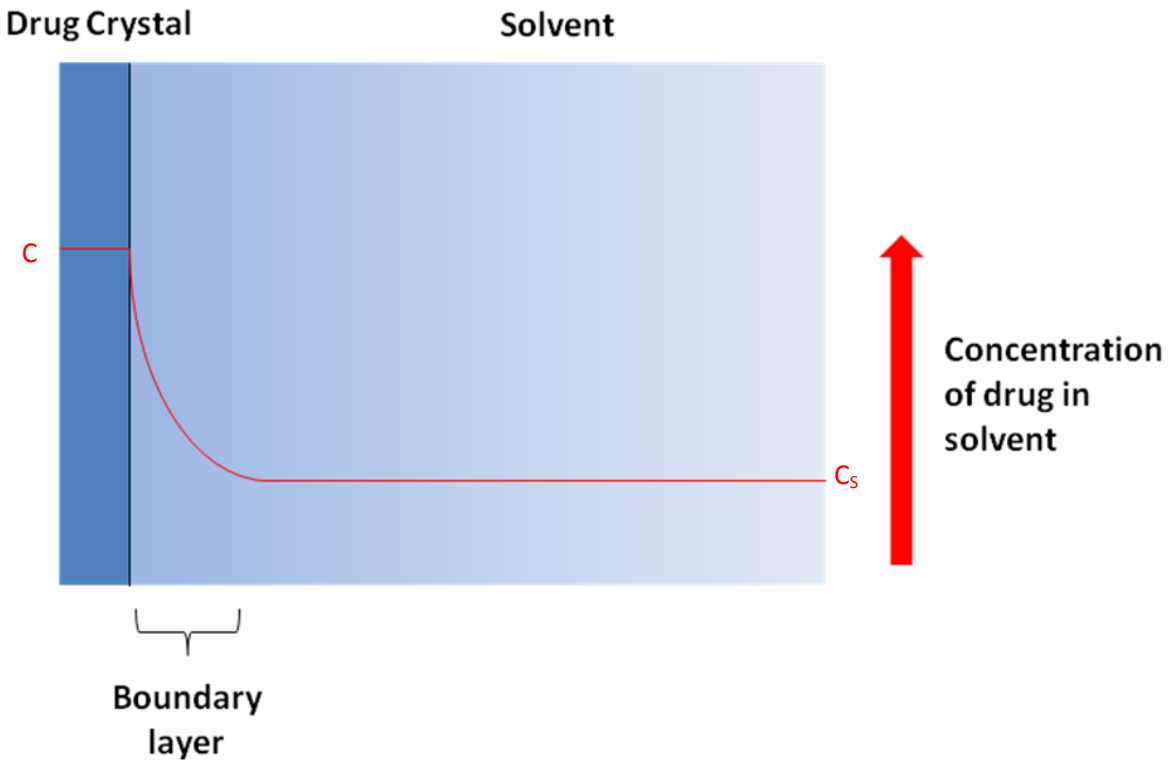

Figure 1.1: *Schematic showing how drug concentration varies with distance from a drug crystal surface in a solvent where C is the concentration of drug at the surface of the particle and C_S is the concentration of drug in the solvent (edited from Aulton 2002).*

Once the drug is in solution, it passes across the membranes of cells lining the GI tract and absorbed into the systemic circulation before being distributed around the body until it reaches the target site, as shown in Figure 1.2 (2002; Aulton 2002). Hence, the oral absorption and bioavailability of an API is largely dependent on the extent of drug solubility in the biological fluids and permeability.

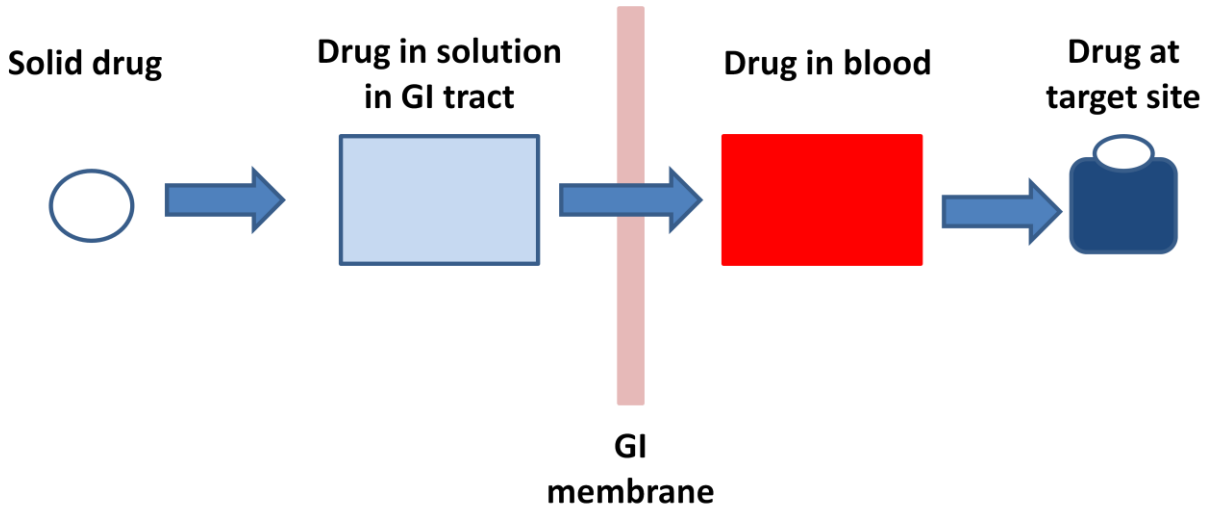

Figure 1.2: *Schematic of how oral medication reaches the target receptor (edited from Aulton 2002)*

If the compound has a high bioavailability (proportion of dose reaching the blood stream compared to an equivalent dose given by intra-venous injection) then the rate-limiting step would be the rate of dissolution of the drug into the GI fluid.

In an effort to speed up the drug regulatory process, the FDA adopted a guidance to the industry in the form of the Biopharmaceutical Classification System (BCS, established by Dr. Amidon) with which to identify bioequivalence tests. The BCS recommends a class of immediate-release solid oral dosage forms for which bioequivalence may be assessed based on *In-vitro* dissolution tests. Hence, this may be used to justify a biowaiver based on the fact that observed differences in the bioavailability of two immediate release preparations containing the same drug result primarily from *in vivo* dissolution differences in the GI tract (Mannhold, Kubinyi et al. 2003). The BCS system classifies drugs as follows:

- Class I – high permeability, high solubility.
- Class II – high permeability, low solubility.
- Class III – low permeability, high solubility.
- Class IV – low permeability, low solubility.

The BCS biowaiver for *in vivo* bioequivalence studies requires excipients to be in a dosage form used previously in FDA approved immediate-release solid dosage forms, having a wide therapeutic window and showing rapid and similar dissolution, high solubility and high permeability.

The issue of low API aqueous solubility presents an ever-growing challenge to the pharmaceutical industry, one that must be met to maintain and enhance research and development pipelines. This is particularly important in an industry that is intensely competitive. Accordingly, pharmaceutical companies are increasingly adopting strategies using emerging formulation technologies to deal with solubility and bioavailability issues at the earliest possible opportunity.

A recent BCS classification of the 130 orally administered drugs on the World Health Organisation (WHO) model list of essential medicines found that, of the 61 that could be classified approximately one-quarter were poorly soluble, with 17 % in class II and 10 % in class IV (Lindenberg, Kopp et al. 2004).

In recent years, drug molecules with limited aqueous solubility are becoming increasingly prevalent due to pharmaceutical companies searching extensively for new therapeutic molecules during drug discovery programs. Currently, over 40 % of new chemical entities (NCEs) present intrinsic solubilities (solubility of neutral or unionized form) of less than 1 $\mu g.ml^{-1}$. Furthermore, it has been reported that approximately one-third of compounds synthesised in medicinal chemistry laboratories have an aqueous solubility less than 10 $\mu g.ml^{-1}$, another third have solubility ranging from 10 to 100 $\mu g.ml^{-1}$ whilst the solubility of the remaining third is greater than 100 $\mu g.ml^{-1}$. As a result, the pharmaceutical industries have a large number of compounds that have not been developed due to the fact that they are poorly water soluble and difficult to formulate.

1.5.2 Improving solubility/dissolution rate

The dissolution rate from a single spherical particle is defined by the Noyes-Whitney equation which states that “the rate of mass transfer of solute through the diffusion layer (boundary layer) is proportional to the area available for migration, the concentration difference across the boundary layer and is inversely proportional to the thickness of the boundary layer” or simplified in equation 1.4 (Aulton 2002; Florence and Attwood 2006):

$$\frac{dm}{dt} = \frac{k_1 A \Delta C}{h} \qquad \text{Equation 1.4}$$

Where k_1 is the constant known as the diffusion coefficient (D), A is the surface area available for migration ΔC is the difference in drug concentration across the boundary layer (C_S-C from figure 1.1) and h is the boundary layer thickness. For drugs that are readily absorbed from the GI tract, such as those in groups I and II of the BCS system, the drug is removed from solution before reaching saturation. In this situation, ΔC can be approximated as C_S as shown in equation 1.5:

$$\frac{dm}{dt} = \frac{DAC_S}{h}$$ Equation 1.5

From equation 1.5, one method that can be of use in improving drug solubility/dissolution rates could be by reducing the particle size into the micro- or even nano-meter range as this allows for a larger surface area (for the same amount of material) and, therefore, allow for a higher dissolution rate. This will not, however, increase the maximal concentration of the material in the liquid but will allow for a greater amount of the drug to be absorbed into the body as shown by Liversidge and Cundy, who compared the pharmacokinetics of crystalline and nanocrystalline Danazol in beagle dogs. They showed that the Area Under the Curve (AUC), and so the total amount of danazol absorbed into the dogs, increased from 1.0±0.4μgh/ml for the crystalline danazol to 16.5±3.2μgh/ml for the nanoparticle dispersion (Liversidge and Cundy 1995).

The main problem associated with particle size reduction is the amount of time needed to produce the correct particle size range. Liversidge and Cundy's nanoparticle formulation involved using a ball mill for 5 days in order to obtain an average particle size of 84.9nm. Along with this, the other major problem is that the large surface area also provides a large amount of contact area for the particles to agglomerate. In order to combat this, Liverside and Cundy stabilized the particles with polyvinylpyrrolidine (PVP, 1.5%w/w). The final problem with particle size reduction is that a lot of energy is needed in order to break down the particles. This in turn will damage the crystalline lattice resulting in some amorphous regions on the surface. These amorphous regions on the particles could result in an increased degradation of the product.

An alternative method for increasing dissolution is by making a salt of the compound. The salt selected for a compound depends on the drugs physico-chemical compounds, namely the acid disassociation (pKa) of the drug. If the drug is basic, an anionic salt is used, while a cationic salt can be used with an acidic drug.

Li et al demonstrated the effectiveness of different salts using Haloperidol as well as its Hydrochloride and Mesylate salts. The Haloperidol did not dissolve sufficiently in water for Li et al to measure via UV. The salts, however, allowed for sufficient Haloperidol to be dissolved for it to measurable. For example, the Haloperidol Hydrochloride salt dissolved sufficiently to produce a solution containing 0.02mg/ml of Haloperidol at saturation. The Haloperidol Mesylate salt results in a different saturation concentration (0.002mg/ml)(Li 2005).

The problem with using a salt is that the drug needs to be a strong acid or a strong base. Most compounds, however, are only mild acids and mild bases and so are not suitable for making into salts.

Another method for improving dissolution rates is by making an emulsion. In an emulsion there are at least two phases, an oil phase and an aqueous phase. For a hydrophobic compound, the internal phase will normally be the oil phase while the bulk of the solution will be aqueous, or water, phase. This is known as an oil-in-water (O/W) emulsion. Emulsifying compounds are also needed to stabilise the emulsion otherwise the two phases would separate. Stabilisers used have both a hydrophilic and a hydrophobic group so that they can interact with both the aqueous and oil phases of the emulsion.

As a drug with low aqueous solubility would be classed as being hydrophobic, it would be mostly dissolved in the oil phase of the emulsion. However, some of the drug will also be present in the aqueous phase, depending on its partition coefficient, it would be this portion of the drug that can be absorbed into the body if the emulsion is taken orally.

As emulsions contain oil and water phases, they are normally given as liquids. This can cause a problem as liquids can aid the degradation of drug molecules and so may have a short shelf life. Also, the oil phase is normally made from nut oil and so cannot be given to patients who are sensitive to nuts.

One way around these issues is to use cyclodextrin. Cyclodextrins consist of a ring of sugar molecules linked together. The number of sugar molecules range from 6 (α-cyclodextrin) to 8 (γ-cyclodextrin). The structure of the cyclodextrins are shown below in figure 1.3 (Biwer, Antranikian et al. 2002).

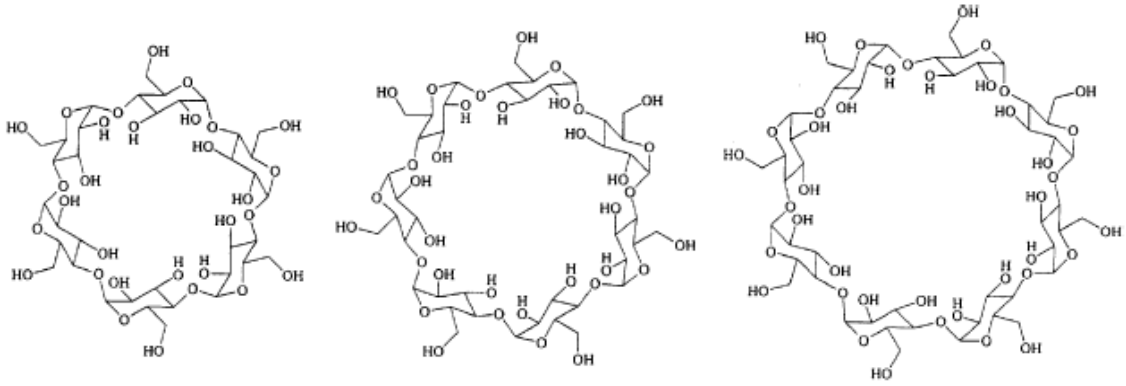

Figure 1.3: *Graphical representation of α-, β-, and γ- cyclodextrin respectively. (Biwer, Antranikian et al. 2002)*

Cyclodextrins have a hydrophobic region inside the ring with a hydrophilic exterior. This means that a hydrophobic drug could reside in the middle of the ring just like in the oil phase of the emulsion. Also, as the cyclodextrin is crystalline, the resulting drug-cyclodextrin complex is completely solid so can be formulated into a tablet. (Biwer, Antranikian et al. 2002)

Liversidge and Cundy (1995) also tested a danazol-cyclodextrin complex in their study and found that this formulation was as good as reducing the particle size into the nano-range but needed the addition of a very large amount of cyclodextrin in their formulation (50%w/w). At such high levels, cyclodextrins may be toxic via various processes. The first mechanism is by the solubilisation of cholesterol, resulting in lysis or the cell, and phospholipids from the cell membrane (Tetsumi and Kaneto 1997). In addition, the kidneys can be affected as they are the major organ responsible for their removal (Tetsumi and Kaneto 1997).

1.5.3 Novel method for improving drug solubility.

Hydrogen bonds can be viewed as a form of polar interaction where an electropositive hydrogen atom is between two electronegative atoms and bonded to one of them. Normally, the hydrogen is attached to a nitrogen or oxygen atom. In this situation, the atom attached to the hydrogen atom draws electrons away from the hydrogen forming a proton donor. The electrons from the second electronegative atom are then shared between the proton and the second electronegative group.

Recently, Almarrson et al have patented the production of pharmaceutical cocrystals containing a drug (carbamazepine) and a crystal former (such as saccharin or nicotinamide) joined together by hydrogen bonding of complimentary groups forming a new crystalline lattice. Cocrystals are where both components i.e. the active pharmaceutical ingredient (API) and cocrystal former are solid at room temperature. If the former is a liquid, the resultant crystal form is defined as a solvate (Almarsson and Zaworotko 2004; Almarsson, Hickey et al. 2007).

Hickey et al compared the solubility of the 1:1 molar ratio carbamazepine:saccharin cocrystal (200mg formulation with respect to anhydrous carbamazepine) with Tegretol 200mg immediate release tablets in fasted beagle dogs. They found that the elimination of the carbamazepine was unaffected by producing the cocrystal however the time to reach maximal plasma concentration was reduced from approximately 1.75 hours to about 1.0 hour on average. The area under the curve (AUC), and therefore the total amount of carbamazepine absorbed by the dogs, increased for the cocrystal suggesting that the cocrystallisation of saccharin into the crystalline lattice of the API improved the absorption of the carbamazepine (Hickey, Peterson et al. 2007)

Remenar et al have also shown using an anti-fungal agent, itraconazole, that cocrystals can be used to improve solubility. They showed that crystalline itraconazole has a much lower solubility then the amorphous form that is on the market (Sopranox) as shown in figure 1.4. The study, however, showed the dramatic effect that different cocrystal formers had on the rate of dissolution of the API, as shown in figure 1.4 (Remenar, Morissette et al. 2003).

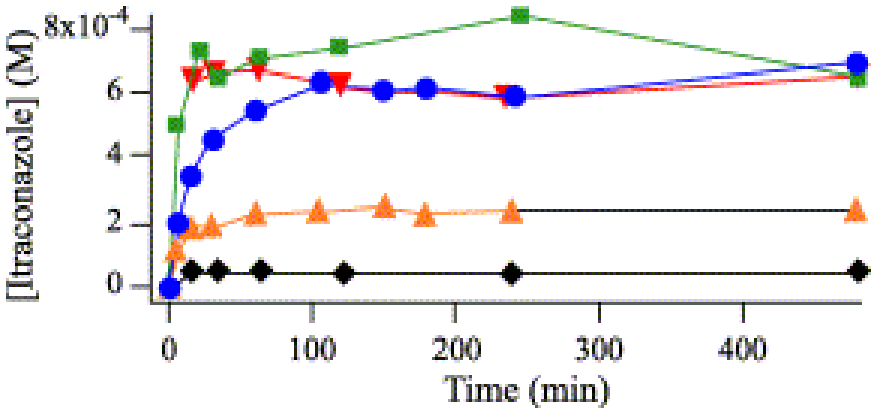

Figure 1.4: *Graph adapted from Remenar et al showing the effect of different cocrystals (orange, blue and red lines) on the solubility of crystalline Itracoanzole (black line) compared to the amorphous marketed product (green line).(Remenar, Morissette et al. 2003)*

1.5.3.1 Production of cocrystals.

The conventionally used method for producing cocrystals is via an evaporation based crystallisation method. The active pharmaceutical ingredient (API) and the crystal former are dissolved in a volatile solvent in the correct ratio. The volatile solvent is then allowed to evaporate forming a supersaturated solution for nucleation and crystal growth (Pedireddi, Jones et al. 1996; Fleischman, Kuduva et al. 2003; Almarsson and Zaworotko 2004; Vishweshwar, McMahon et al. 2006).

Another method for producing cocrystals is by co-milling the two components in a ball mill. A drop of a suitable solvent can also be used, and has been shown to increase the inter-conversion rate of cocrystal formation. This process is called solvent drop grinding. Both of these methods work by inducing amorphous regions on the API and the crystal former. These amorphous regions then interact to form the cocrystal (Jayasankar 2006; Vishweshwar, McMahon et al. 2006)

1.5.3.2 Limitations with current cocrystal methods.

The current methods for producing cocrystals do not produce ideal particles. For example, the solvent evaporation method does not produce a narrow particle size distribution without the need for further processing, which may influence the integrity of the cocrystals. Furthermore, due to the slow nature of evaporation, either the API and/or the cocrystal former may reach saturation before the other resulting in nucleation and growth of the pure API or cocrystal former as well as the cocrystal.

The ball milling process or solvent drop grinding process can only be used to make a small quantity of material. This material may also contain amorphous regions, which will interact with other materials or even increase the rate of degradation of the material. Furthermore, the industrial scale-up of such a process is limited.

1.6 Solution Atomisation and Xrystallisation by Sonication (SAX)

The Solution Atomisation and Xrystallisation by Sonication (SAX) process consists of three distinct phases: (a) production of an aerosol of a solution containing the drug via a suitable aerosol generator; (b) collecting the supersaturated droplets in a suitable non-solvent; (c) the use of ultrasonic energy to induce crystallisation of the particles (Kaerger and Price 2004; Pitchayajittipong, Shur et al. 2009). Figure 1.5 shows a schematic diagram of the lab-scale SAX equipment.

The atomiser produces spherical droplets that contain the drug in a volatile solvent of a specific particle size distribution. As the solvent evaporates, the droplets become highly super-saturated droplets which are collected in a crystallisation vessel that contains a suitable anti-solvent, which is preferably miscible with the solvent used to make the initial solution (Kaerger and Price 2004; Pitchayajittipong, Shur et al. 2009). The surface tension of the collecting solution in the crystallisation vessel should be low or possibly minimised to prevent structural changes to the droplet shape on impingement. The generation of micrometer-sized droplets of drug solution leads to rapid vaporisation of the solvent and the production of highly supersaturated droplets of the solute molecules. However, rapid crystallisation within these droplets does not readily occur because of the dramatic increase in the viscosity, which limits the mass transport properties of the solute molecules to form a critical nucleus for nucleation and subsequent crystal growth (Kaerger and Price 2004). To induce homogeneous nucleation requires a sufficient degree of molecular motion within the droplets. This process is aided by the application of sonic energy, which increases the molecular motion within the droplets and induces nucleation and growth of crystals.

The relative viscosity of these droplets will be drug specific and highly dependent on the rate of vaporisation of the drug solvent. The vaporisation process is dependent on a number of parameters including vapor pressure of the solvent, dimensions of the initial atomised droplet, solute-to-solvent composition, temperature, and flow rate. In the SAX process, the degree of vaporisation of the solvent is controlled by the separation distance between the atomiser and the non-solvent solution. As a batch process, the crystallised particles are filtered from the resulting suspension and dried over silica-gel at room temperature (Kaerger and Price 2004; Pitchayajittipong, Shur et al. 2009).

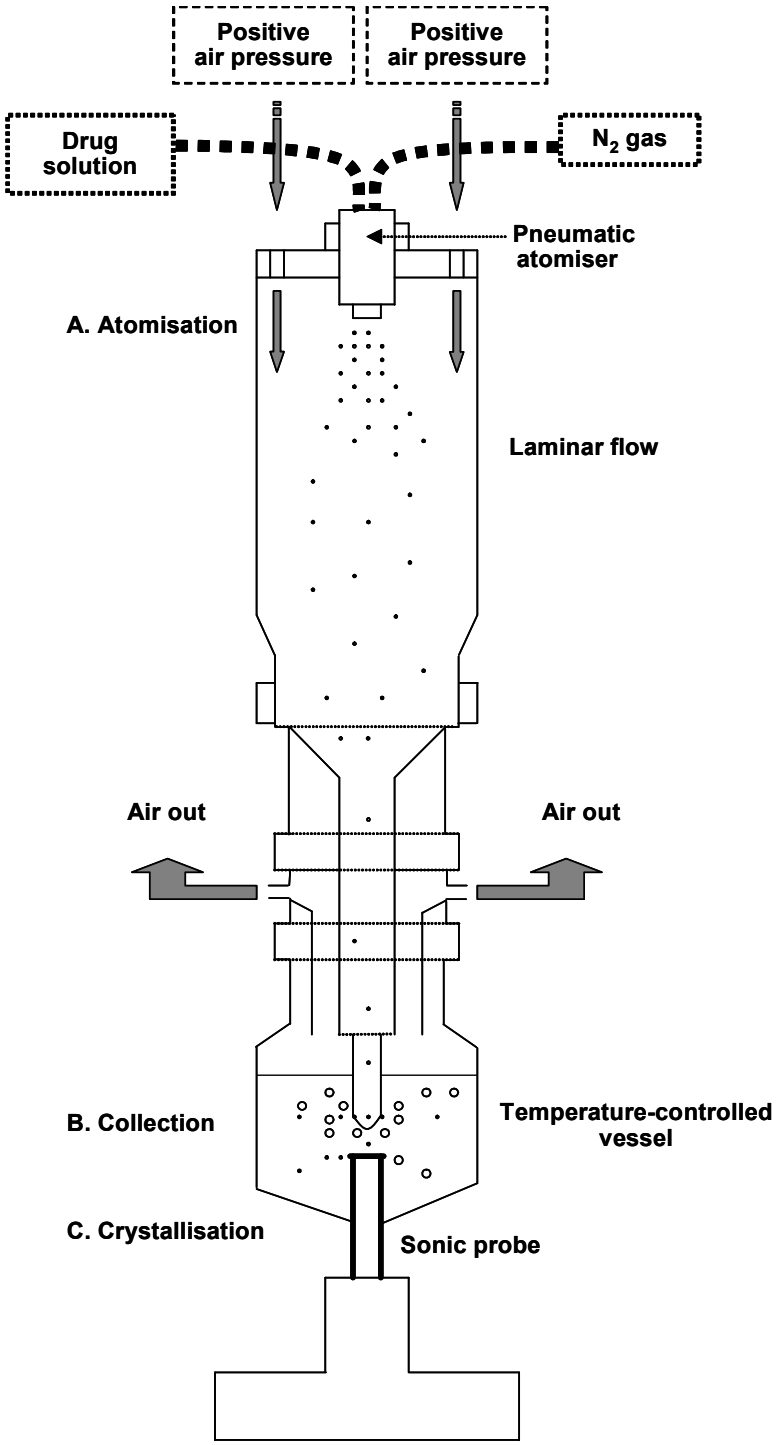

Figure 1.5: *Schematic diagram of the lab-scale version of the SAX experimental set-up*

By combining these processes and controlling relevant parameters, high-purity micron-sized sphere-like crystalline particles can be readily produced in a single droplet-to-particle operation. The major advantage of this low-cost technique relates to the use of any suitable aerosol generator, and the whole process can be carried out under atmospheric pressure and ambient conditions. Furthermore, it has the potential for batch and continuous processing at an industrial scale.

1.7 Aims of this study

This thesis will look at how SAX can be used to (1) develop novel particles that may be used in the treatment of COPD; and (2) produce cocrystals that could be used in oral formulations to improve the API's solubility and dissolution rate, therefore increasing its bioavailability.

The outline of this thesis in relation to the key aims is shown in figure 1.5:

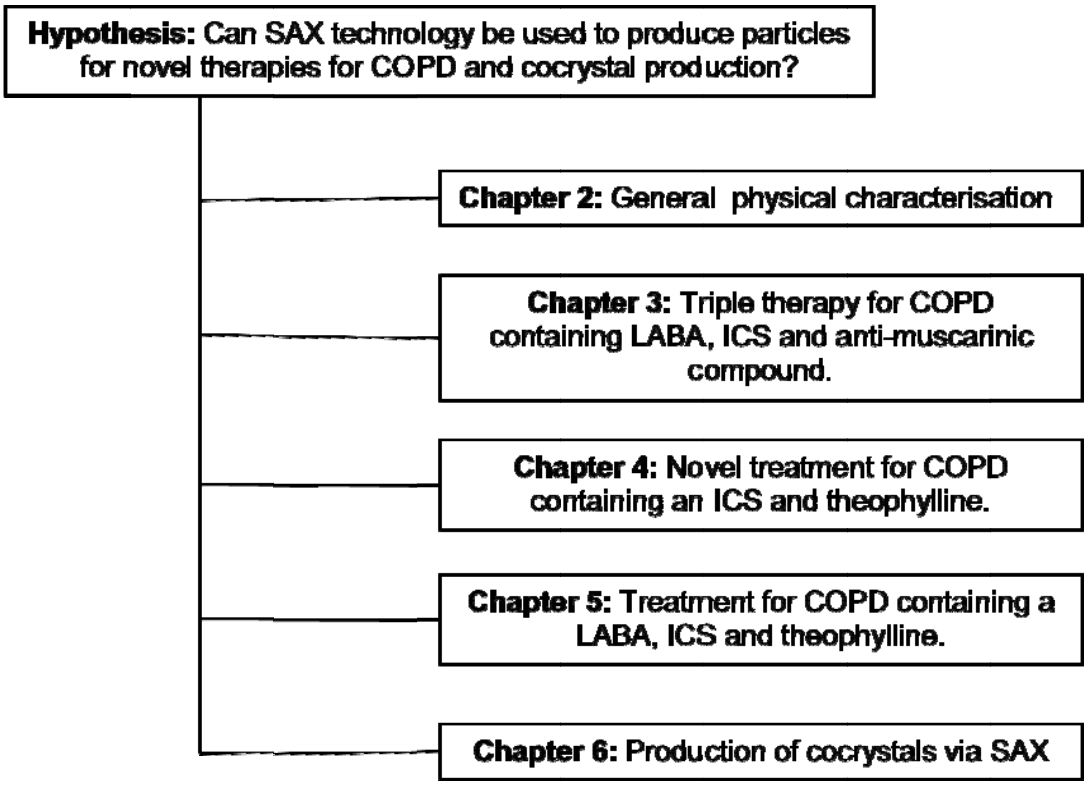

Figure 1.5: *Flow diagram of the structure of the thesis in relation to the key aim of the project.*

In Chapter 2, the drugs will be generally characterised in the term of physical properties of particles. Chapter 3 is related to the development of novel combination particles for the treatment of COPD. In Chapter 4, the SAX process has been applied to generate a triple formulation containing a LABA, ICS and theophylline for COPD. Chapter 5 looks at the formation of a triple formulation containing a LABA, ICS and an anti-muscarinic agent. Furthermore, all materials produced have been characterised by their physico-chemical properties and formulated in both pMDI and DPI formulations to investigate *in-vitro* performance. Finally, chapter 6 looks at the application of SAX in the controlled formation of cocrystals.

Chapter 2 - Materials and Methods

The importance of the physicochemical properties of drug and excipient components of dosage forms was highlighted in Chapter 1. Physicochemical properties such as particle size, shape and crystallinity can have a dramatic effect on the efficacy of dosage forms and drug product performance. This chapter describes the comprehensive physicochemical characterisation of the materials used throughout the study.

2.1 Materials

The materials used in this study are summarised in Table 2.1, All solvents, with the exception of perfluorodecalin (Flutec PC6, F2 Chemicals Limited, Lea Town, UK), were supplied by Fisher Scientific (Loughborough, UK) and were of at least analytical grade. Water was prepared by reverse osmosis (MiliQ, Molsheim, France).

Table 2.1: Sources of materials.

Materials	***Suppliers***
Micronised Fluticasone Propionate	Merck Generics, Potters Bar, UK
Micronised Salmeterol Xinafoate	Merck Generics, Potters Bar, UK
Micronised Budesonide	Scior, Milan, Italy
Anhydrous Theophylline	Forum Chemicals Ltd, Surrey, UK
Ipratropium Bromide	Amplachem Inc, Indiana, USA
Carbamazepine	Sigma-Aldrich, Gillingham, UK
Indomethacine	Sigma-Aldrich, Gillingham, UK
Nicotinamide	Acros Organics, Geel, Belgium
Saccharin	Acros Organics, Geel, Belgium
Lactose monohydrate – SV003	DMV-Fonterra, Vehgel, Netherlands

For the remainder of the thesis, fluticasone propionate, salmeterol xinafoate, budesonide, theophylline, ipratropium bromide, carbamazepine, indomethacine, nicotinamide and saccharin will be abbreviated to FP, SX, BUD, THE, IB, CBZ, IND, NIC and SAC, respectively.

2.1.1 Physico-chemical Properties

For the Solution Atomisation and Xrystalisation by Sonication process to be successful for combined particles, all of the components need to be dissolved in a suitable, highly volatile solution (Kaerger and Price 2004; Pitchayajittipong, Shur et al. 2009). This is easier to achieve if the compounds are all soluble in the same solvent.

Different solvents have different hydrophilic/hydrophobic behaviour. As a result, a more hydrophobic drug will be more likely to dissolve in a hydrophobic solvent (such as dichloromethane) compared to a more hydrophilic solvent (such as methanol). For this reason, for two or more compounds to dissolve in a single solvent, the partition coefficient (log P values) should be similar.

The log P values for the compounds used are listed in table 2.2 below.

Table 2.2: Log P values for all compounds (Tetko, Gasteiger et al. 2005; VCCLAB 2005)

Material	***Log P***
Fluticasone Propionate	3.7
Salmeterol Xinafoate	3.95 (Salmeterol only)
Budesonide	1.9
Anhydrous Theophylline	-0.2
Ipratropium Bromide	0.89
Carbamazepine	2.45
Indomethacine	4.27
Nicotinamide	-0.37
Saccharin	0.91

2.2 Material processing

The objective of pharmaceutical manufacturing is in the generation of dosage forms that enable reliable delivery of medicines to the human body. To achieve this, active pharmaceutical ingredients (APIs) must be processed to aid their inclusion in pharmaceutical dosage forms. This section describes the processing of two APIs utilised in this study and key process technologies utilised to produce API particles for this study.

2.2.1 Re-crystallisation of Theophylline (THE)

Two grams of anhydrous theophylline was dissolved in 50ml water and heated to 60°C by use of a hot-plate stirrer with the aid of a magnetic fly to form a saturated solution. The solution was allowed to naturally return to room temperature to induce a

supersaturated solution for nucleation and crystal growth. The resultant theophylline monohydrate crystals were isolated by filtration and subsequently heated for 24h at 110°C to produce anhydrous theophylline (Suihko, Ketolainen et al. 1997). The resultant powder was stored at <10% relative humidity until needed.

2.2.2 Re-crystallisation of Ipratropium Bromide (IB)

One gram of IB was dissolved in 25ml ethanol. The resulting solution was stirred by a magnetic stirrer while being gently heated by a hot-plate heater to 30°C for 24 hours to promote ethanol evaporation for IB crystal growth. The resultant crystals were scraped from the crystallisation vessel and stored at 0% relative humidity for 24 hours prior to use.

2.2.3 Air jet micronisation of re-crystallised THE and IB.

2.2.3.1 Introduction

Particle size of an API is a major variable in the delivery of the active to the lungs (Heyder, Gebhart et al. 1986; Park and Lee 2000; Telko and Hickey 2005). Drug particles with an aerodynamic diameter greater then 10μm will not reach the lungs (Taulbee and Yu 1975). Particles which have an aerodynamic diameter between 2.5 and 6μm will deposit in the conducting airways, while particles less then 2.5μm will deposit in the alveoli (Tsuda, Butler et al. 1994).

In order to achieve the required particle size distribution, many pharmaceutical companies employ a ‘top-down’ method where large drug particles are milled to produce micronised material (micronisation) with a geometric particle size between 1 and 5μm (Telko and Hickey 2005). The most common approach to achieve particle size reduction is air jet micronisation.

An air jet microniser employs high pressure air to accelerate large particles to collide with one another at high speed within a micronisation chamber (Williams, Brown et al. 1999; Rasenack and Muller 2004). These impaction events results in the fracturing of the larger crystals into smaller particles (Akbarieh and Tawashi 1987).

The pressure within the micronisation chamber (ring) is a critical parameter as this provides the acceleration of the particles prior to collision. The air jets are placed tangentially to the ring, resulting in the air and particles making a circular motion around the ring (Austin and Trass 1997). The larger particles are maintained in this circular motion by centrifugal action while smaller particles lose their inertia and can be carried by the air flow away into the collection bag in the centre of the ring (Austin and Trass 1997).

During micronisaton, fresh material can be provided into the chamber via a feed hoper. The material can be drawn into the ring chamber via a Venturi effect due to the pressure drop caused by the air rushing past the feed inlet. However, due to the high pressures within the micronisation, pressurised air is used to transport material into the micronisation chamber. This is called the Venturi pressure.

The ring and Venturi pressures can be individually adjusted order to provide the most effective conditions for micronising the particles.

2.2.3.2 Method

Air jet microniation of the re-crystallised THE and IB was performed using an MC One® Jet Mill (Jetpharma, Balerna, Switzerland). The Venturi and ring pressures used are given in table 2.3 below

Table 2.3: Venturi and ring pressures used for micronisation.

Drug	Venturi (Bar)	Ring (Bar)	Number of Cycles
THE	6	4	5
IB	3	4	3

After each cycle, the resultant material was sized, using a HELOS laser diffraction sensor (Sympatec GmbH, Clausthal-Zellerfeld, Germany), as described below. If the d_{90} of the particle size distribution was not less than 6.0µm, then the material was passed through the mill for another cycle. The total number of micronisation cycles for each drug is listed in Table 2.2.

Once sufficient particle size reduction had occurred, the powder was stored at 0% RH and ambient temperature for 24 hours before use.

2.3 Scanning Electron Microscopy

2.3.1 Introduction

Scanning electron microscopy (SEM) produces high magnifcation images of surfaces by using electrons instead of light waves (Brittain, Bogdanowich et al. 1991). An electron gun emits a beam of high energy electrons, which travels downward through a series of magnetic lenses designed to focus the electrons to a very fine spot. A set of scanning coils enable the focused beam to raster scan the specimen being imaged. As the electron beam hits each spot of a conductive sample, secondary electrons are emitted from its surface. A detector counts these back-scattered electrons and sends

the signals to an amplifier. The final image is built up from the number of electrons emitted from each spot on the sample. Given the large amount of electrical energy, analysis is carried out in a vacuum and samples must be conductive. Non-conductive samples are coated with a thin layer of gold, a conducting material.

SEM are used pharmaceutically to qualitatively characterise topographical and morphological variations of materials.

2.3.2 Method

Powder samples were fixed to sticky carbon tabs mounted on aluminium stubs and excess powder removed with a puff of air. The resulting particles were then coated with gold using a splutter coater (model S150B, Edwards High Vacuum, Sussex, UK) and examined using a scanning electron microscope (model JSM6310, Japanese Electron Optics Ltd., Tokyo, Japan) at 15kV.

2.3.3 Results and discussion

Figure 2.1 shows the scanning electron micrograph images for micronised FP (a & b), micronised SX (c & d) and micronised BUD (e & f) at 1000x and 5000x magnification. The micronised FP and micronised SX particles appear to be plate-like in shape. In addition, the SEM's show that micronisation of FP may have produced a mono-dispersed particle size distribution with the same being true for SX. The micronised BUD particles appear to be mostly plate like in nature with some rounded particles. The images appear to suggest that there may be a degree of variability in particle size. In addition, the SEM's appear to show that micronised material forms aggregates.

Figure 2.2 shows the scanning electron micrograph images for the jet milled THE (a & b) and IB (c & d) at 1000x and 5000x magnification. Micronised THE particles appear to be rhombic in shape. The SEM images appears to suggest that there could be a broad particle size distribution. Micronised IB appears to form plate-like particles which also appear to possess a broad particle size distribution.

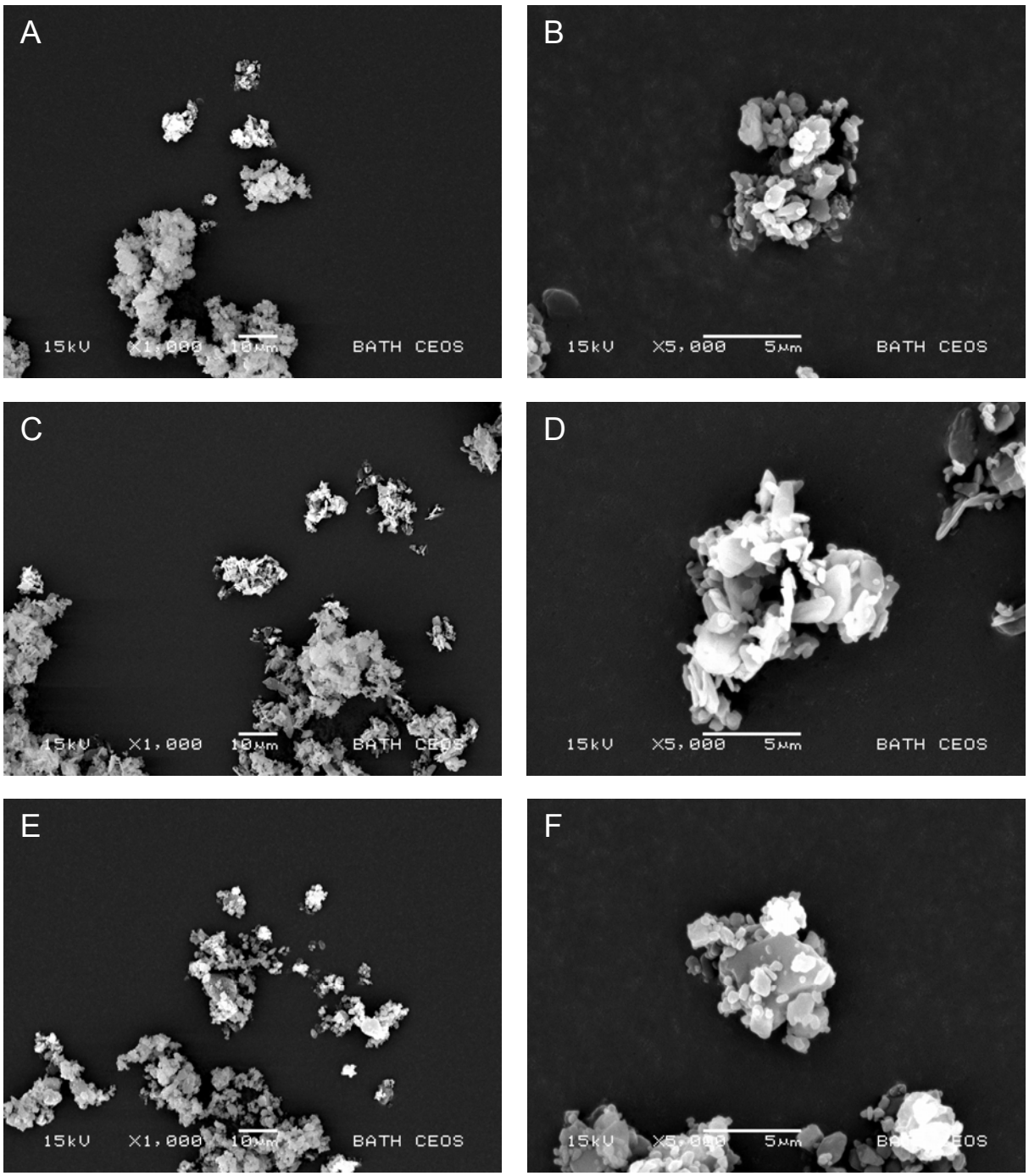

Figure 2.1: Representative SEM's of as supplied micronised FP (A and B), SX (C and D) and BUD (E and F) at 1000x and 5000x magnification.

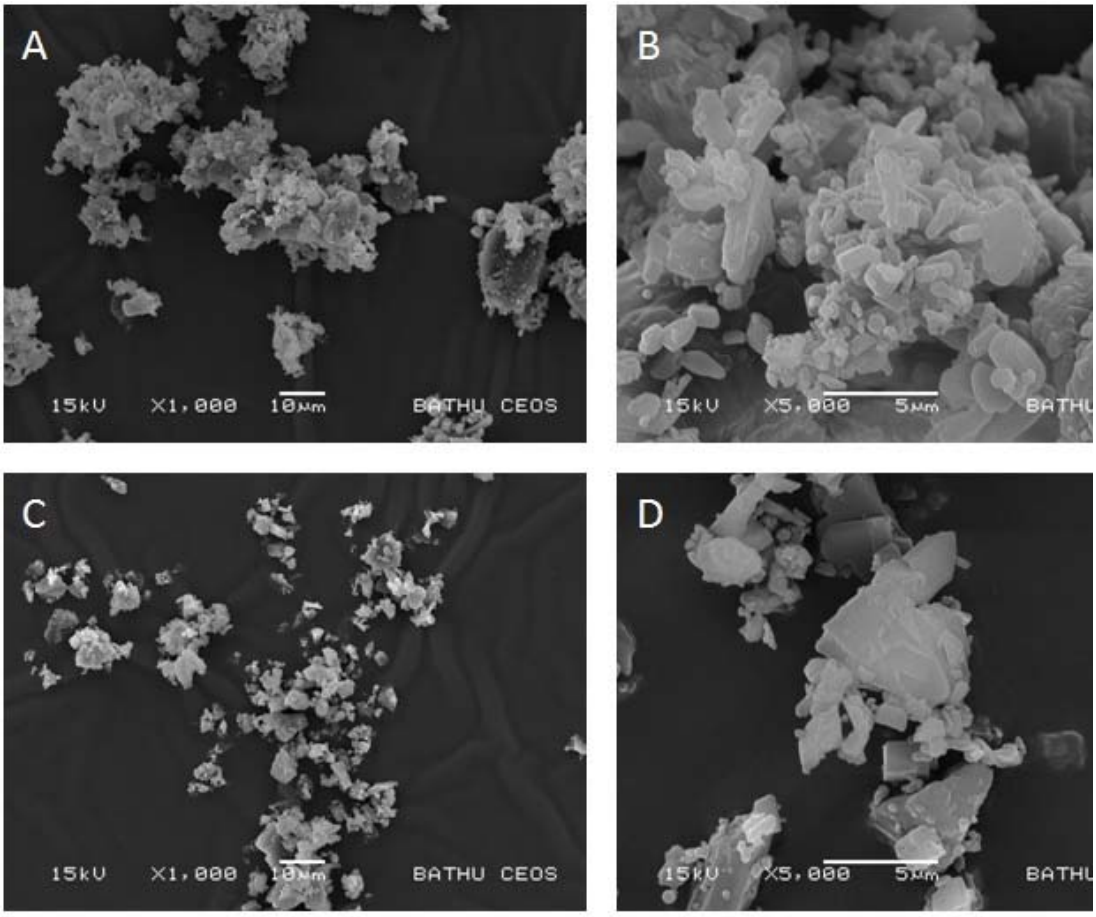

Figure 2.2: Representative SEM's of air jet micronised THE (A & B) and IB (C & D)

2.4 Particle Size Analysis

2.4.1 Introduction

Many different techniques for the measurement of particle size of powders are available, for example, sieving, sedimentation rates, microscopy, and impaction (Brittain, Bogdanowich et al. 1991). However, the technique chosen for this study is laser diffraction (low angle laser light scattering), which has the advantage of rapidly measuring particle size of an ensemble of particles (de Boer, Gjaltema et al. 2002; Guchardi, Frei et al. 2008).

Particle size analysis by laser diffraction is based on the principle that light is scattered by particles in its path (Shekunov, Chattopadhyay et al. 2007), with smaller particles causing light to be scattered at larger angles (Bosquillon, Lombry et al. 2001). In such a particle sizer, a beam of coherent, monochromatic laser light, is directed at a cell containing the particles to be sized and then, the pattern and intensity of the scattered light is detected via a photodetector. When a sample with a polydisperse particle size distribution is analysed, the resultant scattering pattern is achieved by integration of the scattering patterns of the particles. This pattern can then be used to derive a volume-

weighted distribution of volume equivalent diameters by applying one of several mathematical models which describes the scattering of light by particles and the comparison of experimental and theoretical diffractograms (Shekunov, Chattopadhyay et al. 2007). The mathematical models for calculating the particle size from the diffraction pattern are extremely complex. As a result, laser diffraction particle size distributions show the distribution based on spherical particles rather than the actual size of each particle (Allen 1990; Washington 1992).

These phenomena can be described by the Fraunhoffer diffraction or Mie theory. Mie theory requires knowledge of the refractive index of the particles and makes the assumption that they are smooth spheres (Mie 1908). The Mie theory states that the induction of light scattering is triggered by the difference between the refractive indices of the particle and the surrounding medium (Mie 1908). It can be difficult to apply Mie theory for the derivation of the particle size distribution of pharmaceutical materials, due to their variable shape, roughness and unknown refractive index. In these situations and when particle size is significantly greater than the wavelength of the light, it can be considered more appropriate to apply the Fraunhofer approximation to derive the particle size distribution (Shekunov, Chattopadhyay et al. 2007). This technique only describes the diffraction of light at the contour of the particle and makes the assumptions that only forward light scattering occurs and the particle size is much larger than the wavelength of the light (Shekunov, Chattopadhyay et al. 2007). Therefore, the Fraunhofer approximation was applied to derive particle size distribution.

2.4.2 Method

2.4.2.1 Dry dispersion

Particle sizing was carried out in the dry state by using a dry disperser. This process was employed for particles that were to be delivered via inhalation as these would be diluted in air when in use. Powders were dispersed using compressed air at 3 bar through a RODOS dry disperser fed by an ASPIROS micro-dosing unit before sizing using a HELOS laser diffraction sensor (all from Sympatec GmbH, Clausthal-Zellerfeld, Germany). The particle size analysis was performed using WINDOX 4.0 software (Sympatec GmbH, Clausthal-Zellerfeld, Germany). Size distribution and values presented are the average of three determinations.

2.4.2.2 Wet dispersion.

Particle sizing was carried out in wet cell with a small quantity of the particles being re-dispersed in a 0.1% w/v of lecithin (BDH Ltd., Poole, UK) in cyclohexane or perfluorodecalin by sonicating for 5 minutes. The resultant suspension was then diluted

down to 50 ml in the cuvette and particle size measured using a HELOS laser diffraction sensor (Sympatec GmbH, Clausthal-Zellerfeld, Germany). The particle size analysis was performed using WINDOX 4.0 software (Sympatec GmbH, Clausthal-Zellerfeld, Germany). Size distribution and values presented are the average of three determinations.

2.4.3 Results and Discussion.

2.4.3.1 Inhaled micronised drug

In addition to providing a graphical representation of the particle size distribution, particle size measurements were summarised using the d_{10}, d_{50} and d_{90} values for the samples, as shown in Table 2.4. The d_{50} values for all of the micronised compounds were 1.81 µm, 2.13 µm, 1.60 µm, 4.15 µm, and 2.81 µm for FP, SX, BUD, THE and IB, respectively. As all of the d_{90} values, except for micronized THE, are less then 6.0µm the micronised compounds are suitable for inhaled delivery

In order to achieve effective drug delivery to the lungs, particle size distribution of the API is critical and needs to be fully characterised. All micronised compounds were assessed using the dry dispersion method mentioned above as this would dilute the drug particles in air, therefore mimicking the effect of delivery from an inhaler. Figure 2.3 shows the cumulative distribution for all of the micronised compounds. For THE and IB, the particle size distributions for the final milling cycles are shown.

The particle size distribution of micronised THE is the largest for all of the compound (d_{10}=1.26, d_{50}=4.15, d_{90}=9.33µm). However, the particle size distribution did not change for three consecutive cycles through the mill and, therefore, this was taken as the smallest particle size distribution obtainable for anhydrous theophylline. The next largest particle size distribution obtained was for IB (d_{10}=0.83, d_{50}=2.81, d_{90}=6.71µm). This could suggest that the smaller scale MC One® Jet Mill may not be able to produce sufficient energy to adequately micronize material with respect to that of the as-received material which was micronized with an industrial micronizer.

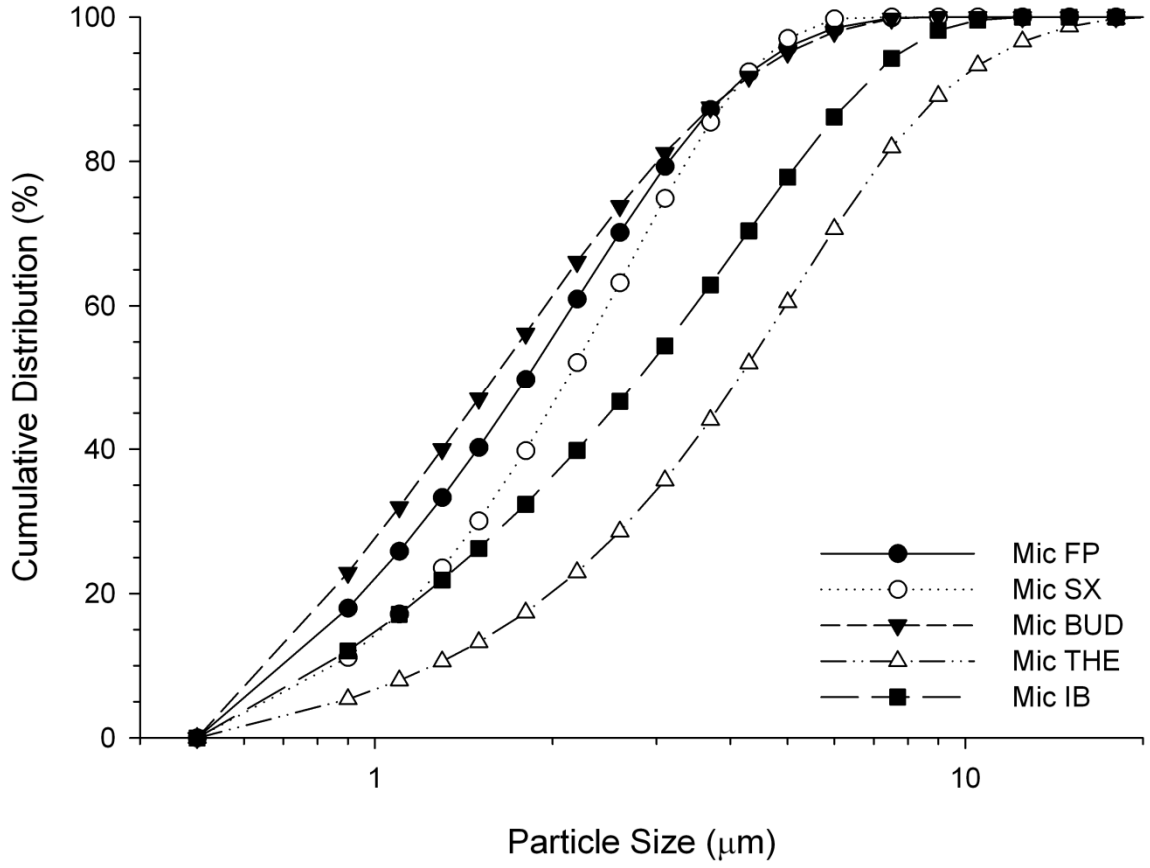

Figure 2.3 Particle size distribution of the micronised compounds.

Table 2.4 Summary particle size statistics of the micronised compounds.

	$d_{10\%}$ (μm) ± SD	$d_{50\%}$ (μm) ± SD	$d_{90\%}$ (μm) ± SD
Micronised FP	0.72 ± 0.01	1.81 ± 0.01	4.03 ± 0.05
Micronised SX	0.86 ± 0.01	2.13 ± 0.01	4.10 ± 0.01
Micronised BUD	0.63 ± 0.01	1.60 ± 0.01	4.05 ± 0.04
Micronised THE	1.26 ± 0.02	4.15 ± 0.03	9.33 ± 0.12
Micronised IB	0.83 ± 0.03	2.81 ± 0.10	6.71 ± 0.09

2.5 Differential Scanning Calorimetry

2.5.1 Introduction

Differential scanning calorimetry (DSC) is used to investigate the crystalline nature of pharmaceutical materials (Brittain, Bogdanowich et al. 1991; Buckton 1997). A DSC measures energy differences associated with chemical and physical changes in the sample including crystallisation, melting, and decomposition in relation to a ramping change in temperature (Duncanhewitt and Grant 1986). This is achieved by measuring the heat flow required to maintain the sample and reference at the same temperature during heating and cooling (Buckton 1997). There are two types of DSCs in common use. In a power compensated DSC, the temperatures of the sample and reference are controlled independently using separate furnaces (Wendlandt 1986). Temperature differences of the sample and reference are made identical by varying the power input to the two furnaces; this energy difference is calculated as a function of sample temperature. In a heat flux DSC, which was used in this study, a single furnace is utilised so the sample and reference are heated by a single source. An enthalpy change in the sample causes a difference in the temperature of the sample relative to the reference (Wendlandt 1986).

2.5.2 Method

Study material thermal properties were investigated using a differential scanning calorimeter (DSC 2920, TA Instruments, Surrey, UK) calibrated with an indium standard. For most materials, approximately 1-5 mg of the sample was accurately weighed into an aluminium pan and crimped with a lid to form a hermetic seal. The sample and reference (identical, but empty, hermetically sealed pan) were heated at the rate of $10^{\circ}C.min^{-1}$ from $30^{\circ}C$ to $350^{\circ}C$. The calorimeter head was continually flushed with dry nitrogen gas at $0.3\ L.min^{-1}$ during all measurements.

2.5.3 Results and discussion

2.5.3.1 Micronised drugs

Figure 2.4A shows the DSC thermogram of micronised FP. As shown, there is a single melt endotherm with an onset temperature of 284.50°C and a peak melting temperature of 292.92°C. The melt is immediately followed by an exothermic event suggesting subsequent degradation of FP.

The SX thermogram (figure 2.4B) is complex in comparison to FP. As shown, there are two endothermic reactions, the first having an onset of melt of 123.89°C (peak melting temperature 125.95°C) and the second having an onset of 137.33°C (peak melting temperature 140.64°C). Between these melts, there appears to be an exothermic

response with a peak temperature of 131.29°C. This type of response is indicative of the melting of a polymorphic form, then recrystalising into a second, more stable form which then goes on to melt at a higher temperature. In the case of SX, it is thought that SX form I has an onset of melt of ~126°C which then recrystallises to SX form II at ~132°C before melting at ~141°C. For SX the form II seeds are thought to be induced during micronisation of SX form I, which enable the recrystallisation event seen in the DSC (Beach, Latham et al. 1999; Tong, Shekunov et al. 2003).

The DSC thermogram of BUD is similar to that seen for FP in that there is a single melt followed by degradation, as seen in figure 2.4C. The onset of melt for BUD is 258.13°C with a peak melting point of 261.86°C.

Figure 2.5 shows the DSC thermograms for the micronised THE and IB (a and b respectively) samples both of which were identical to the as-received DSC thermograms of the raw materials (data not shown). THE demonstrates a single melt with an onset melting point of 271.75°C and a peak melting point of 273.21°C which is slightly lower than the 275°C noted in the literature (Ebisuzaki, Boyle et al. 1997). This slight shift in melting point may be due to a small impurity within the crystalline lattice.

The DSC thermogram for micronised IB is very complex in comparison to all the other DSC thermograms (figure 2.5B). As can be seen, there appears to be four distinct endothermic events. The first of which has an onset of melt of 115.71°C (peak melting point of 121.44°C). The second melt has a calculated onset of melt of 222.26°C but appears to start melting at ~183°C and has a peak melting point of 230.65°C. This melt also appears to have a shoulder, which suggests that there may be another event occurring at the same time. The second melt immediately precedes the third melt which has an onset of melt of 250.90°C (peak melting point of 251.44°C). The final melting endotherms may be due to degradation of the IB.

Similar results have been seen by Corrigan *et.al,* who suggested that the endotherms between 80 and 120°C could be attributed to water loss from within the lattice. This water loss was confirmed by TGA (Corrigan, Corrigan et al. 2006). While the endothermic event at ~230°C is related to the melt of anhydrous IB (Corrigan, Corrigan et al. 2006).

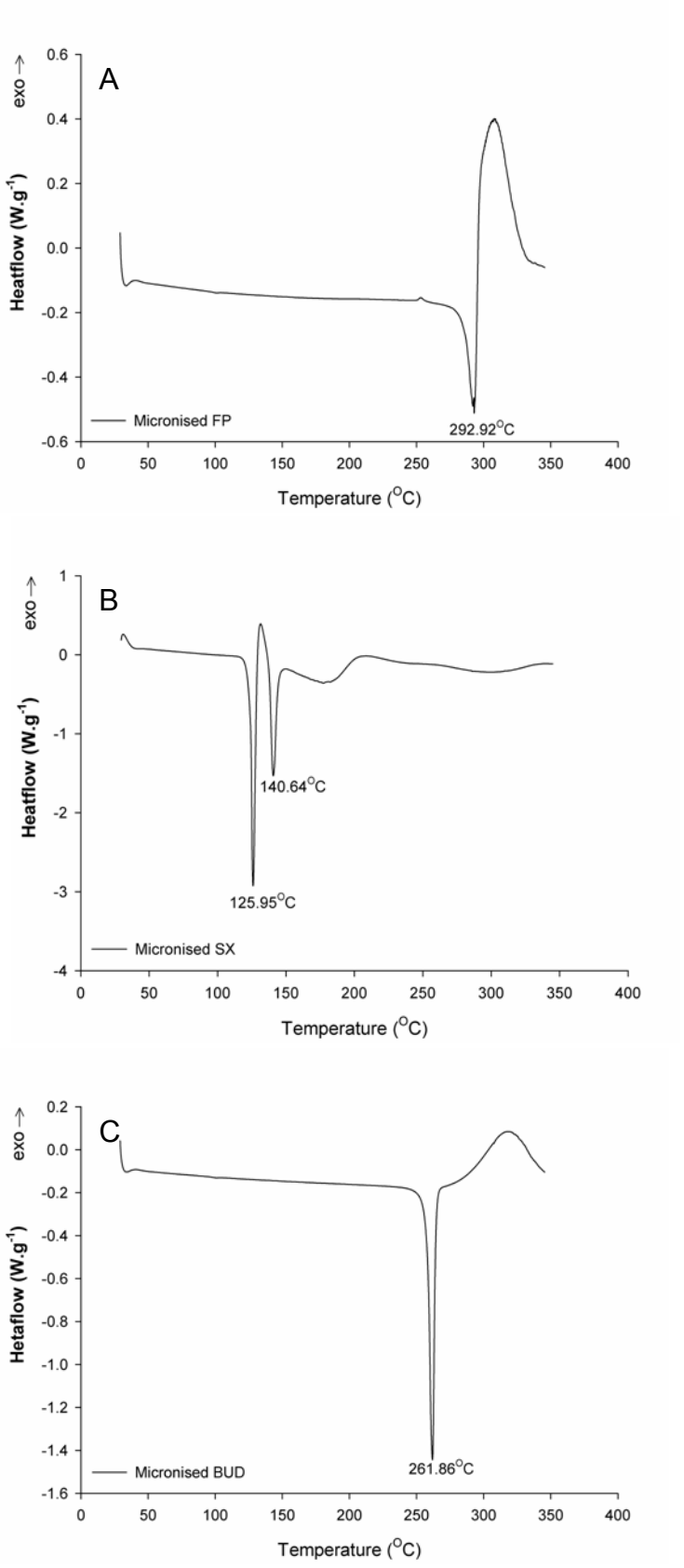

Figure 2.4: DSC thermograms of the micronised drugs. A=FP B=SX C=BUD

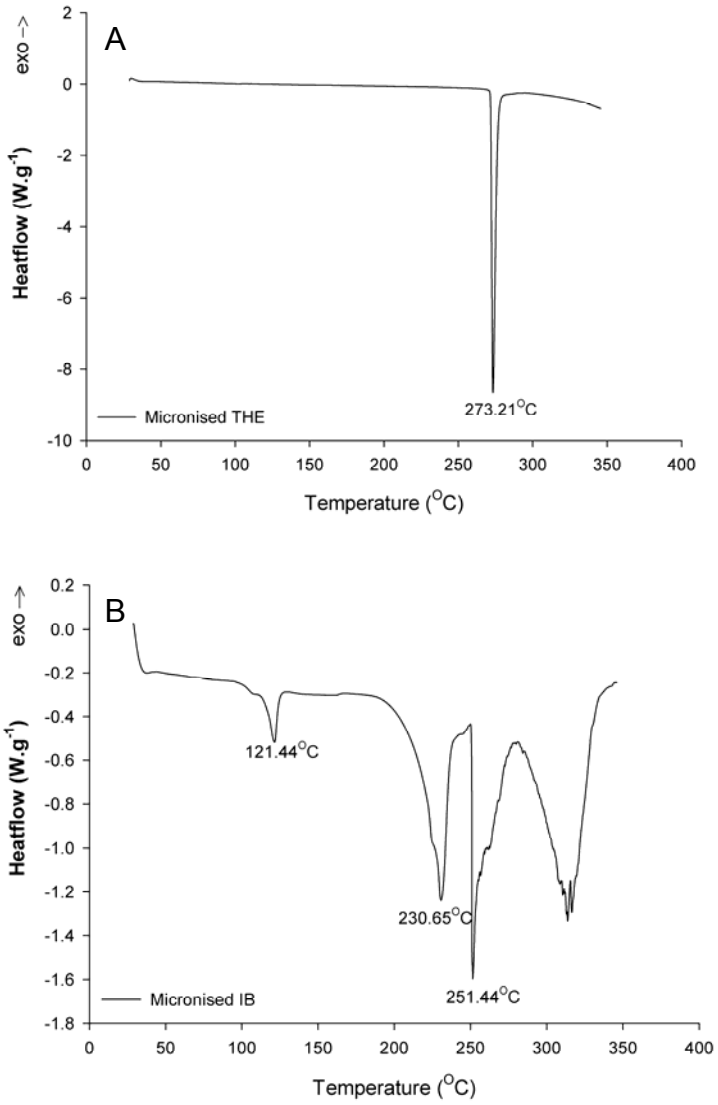

Figure 2.5: DSC thermogram of micronised THE (A) and micronised IB (B).

2.5.3.2 Cocrystal raw materials.

The DSC thermogram for CBZ depicts two distinct melting endothermic reactions. These peaks are related to different forms of CBZ melting at different temperatures due to their relative stability. The first melt has an onset of melt of 173.23°C and a peak melting temperature of 175.95°C. This relates to the melting of CBZ form III which then recrystallises to form CBZ form I. Unexpectedly, the recrystallisation of form III to form I is not seen in the DSC. CBZ form I has an onset of melt of 191.38°C and a peak melting temperature of 193.54°C. These results echo those found by others (Behme and Brooke 1991; Rustichelli, Gamberini et al. 2000; McGregor, Saunders et al. 2004). Form II may be crystallised from ethanol, as described by Rustichelli *et.al,* however, this recrystallises into form I after melting at 183°C.

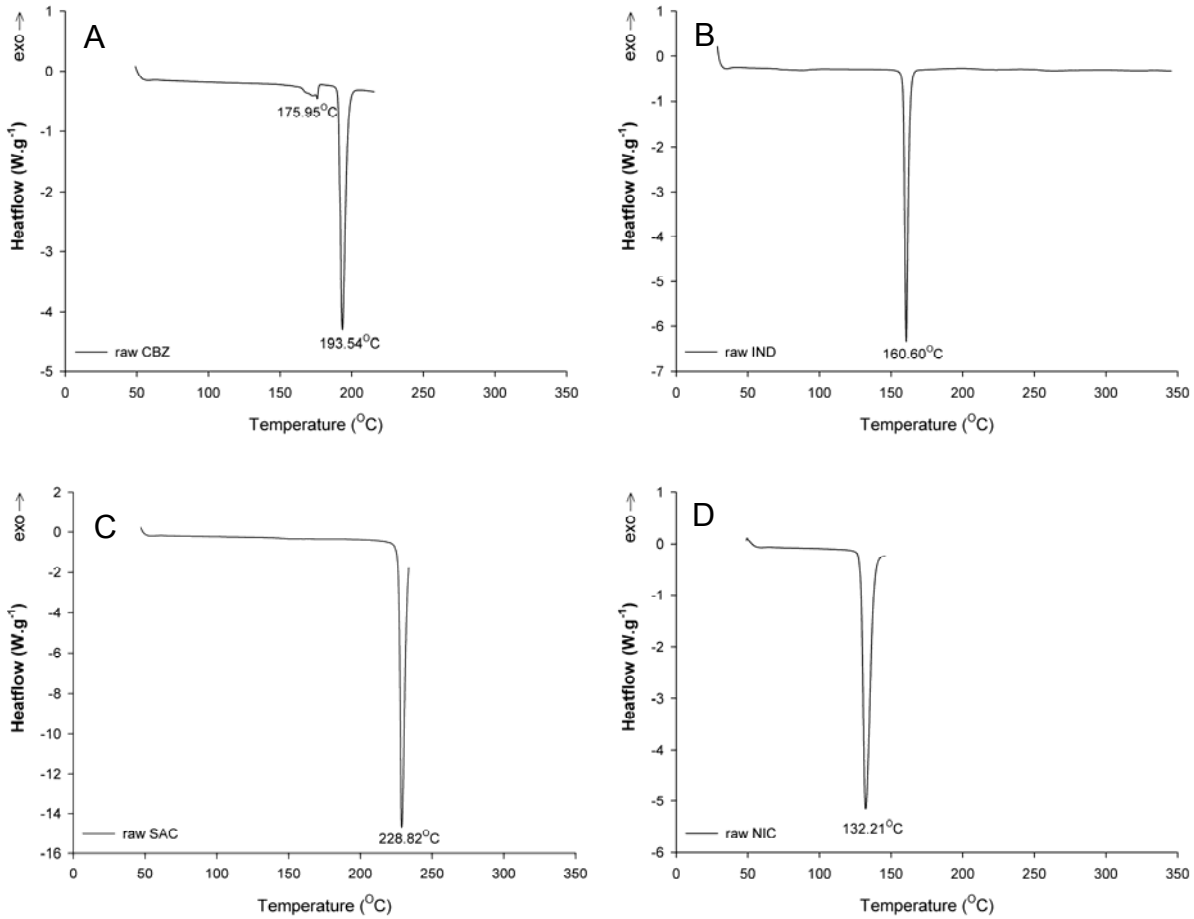

Figure 2.6: DSC thermograms of the raw materials used to produce cocrsyatals

A=CBZ, B=IND, C=SAC, D=NIC

The DSC thermograms for IND, SAC and NIC (figures 2.6 B, C and D respectively) demonstrated one polymorph each with IND having an onset of melt at 158.64°C, SAC melting at 226.99°C and NIC melting at 129.01°C. The melting point for IND relates to the γ-form (Minoru, Bruno et al. 1994; Basavoju, Boström et al. 2008). In addition, the melting points for SAC and NIC correlate with data produced by others (2006; Basavoju, Boström et al. 2008). As can be seen, each compound has a distinctive melting point completely separate from any of the other compounds.

2.6 X-ray powder diffraction (XRPD)

2.6.1 Introduction

X-ray powder diffraction (XRPD) is used to confirm the identity and crystallinity of the study materials (Buckton 1997). Every crystalline form of a compound has a unique X-ray powder pattern. XRPD was, therefore, utilised to identify the respective polymorphic forms of the compounds (Suryabarayanan and Brittain 1995). More

importantly, this is necessary as amorphous materials are thermodynamically unstable and have a propensity to recrystallise during storage (Buckton 1997).

A parallel and monochromatic X-ray beam incident on a crystalline solid is scattered in all directions. At certain angles, the scattered radiation is in phase with itself and so is reinforced (Suryabarayanan and Brittain 1995). This phenomenon occurs whenever Bragg's law is satisfied:

$$n\lambda = 2d_p \sin\theta \qquad \text{Equation 2.1}$$

where n is an integer (the order of reflection), λ is the wavelength of the X-rays, d_p is the distance between the planes of the crystal and θ is the angle between the incident X-rays and the crystal surface(Suryabarayanan and Brittain 1995).

Every crystalline solid leads to the diffraction of X-rays at a unique combination of angles, enabling identification of the material and its polymorph. In addition, amorphous materials do not create scattering at well defined angles, allowing them to be distinguished from crystalline samples. XRPD is able to detect amorphous content at the lower limit of approximately 10% w/w (Buckton 1997).

2.6.2 Method

XRPD spectra were obtained using a Phillips analytical X-ray powder diffractometer (Cambridge, UK) with a CuK $_\alpha$ source ($\lambda = 1.5418\,\mathring{A}$) operated at 40 kV and 25 mA or Bruker D8 Advance Powder Diffraction system (Coventry, UK). A single sweep between diffraction angles (2θ) 5˚ and 50˚ with a step size of 0.02˚ and step time of 13 seconds was employed for each measurement.

2.6.3 Results and Discussion

2.6.3.1 Micronised drugs

Figure 2.7 depicts the XRPD spectra for FP (A), SX (B) and BUD (C). All diffractograms show distinct peaks in each spectrum, thus, suggesting that all three compounds are predominantly crystalline in nature. In addition, the spectrums confirmed each drugs identity (Beach, Latham et al. 1999; Louey, Van Oort et al. 2004; Steckel, Pichert et al. 2004).

Figure 2.8 depicts the XRPD spectra of THE (A) and IB (B) before and after recrystallisation and micronisation. As can be seen, the recrystallisation and subsequent micronisation has not changed the peaks for either THE or IB. In addition to this, both pre- and post micronisation demonstrates distinct peaks suggesting that

the compounds are predominantly crystalline. The spectrums also confirm the identity of each compound (Ando, Ishii et al. 1995; Smith, Hammond et al. 2001; H. Abdine, Heba et al. 2003; Taylor, Hickey et al. 2006).

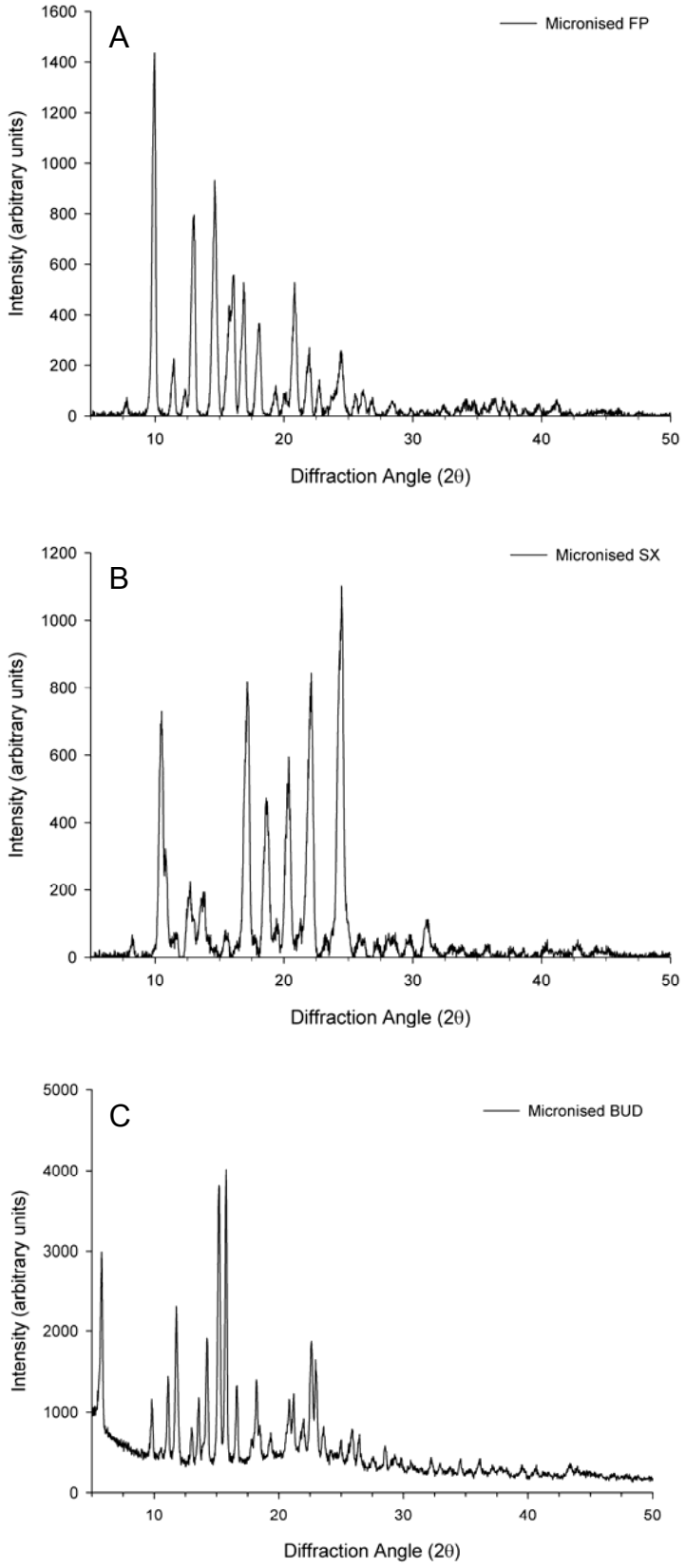

Figure 2.7: XRPD diffractogram of micronised FP (A), SX (B) and BUD (C).

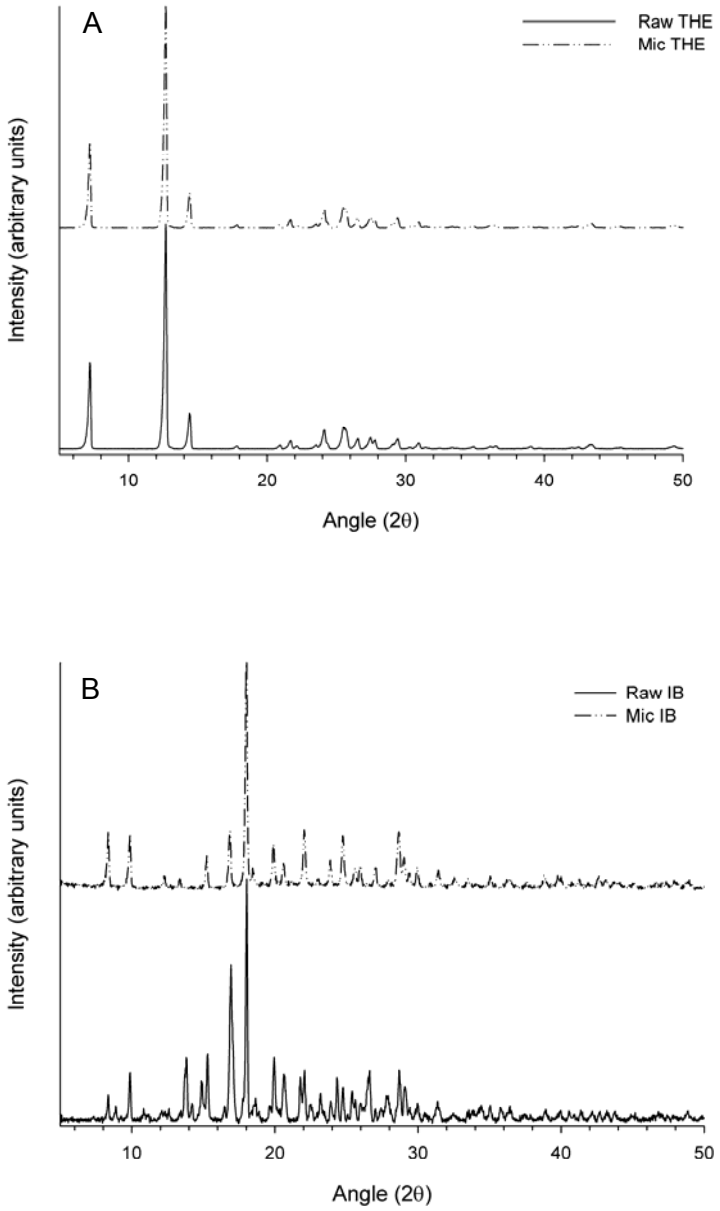

Figure 2.8: XRPD diffractogram of THE vs mic THE (a) and IB vs mic IB(b)

2.6.3.2 Cocrystal raw material

The XRPD spectra for CBZ, IND, SAC and NIC are shown in figure 2.9. As can be seen, each compound has a specific characteristic diffractogram with sharp peaks proving that the compounds were crystalline before being used to produce cocrystalls. In addition, the spectrums also confirm the identity of each compound (Fleischman, Kuduva et al. 2003; Basavoju, Boström et al. 2008).

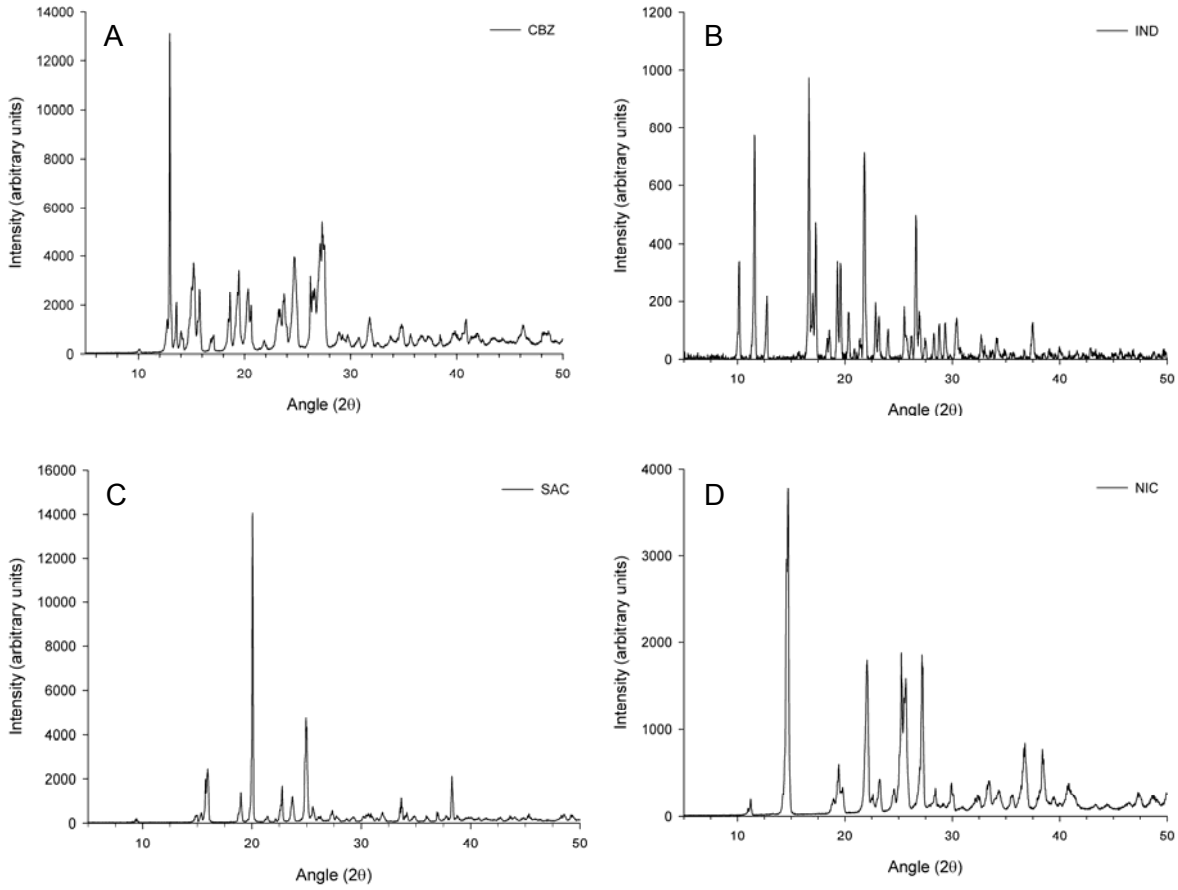

Figure 2.9: XRPD diffractogram of CBZ (a), IND (b), SAC (c) and NIC (d)

2.7 Dynamic Vapour Sorption

2.7.1 Introduction

Dynamic vapour sorption (DVS) is generally used to investigate the effect of humidity on the water sorption and desorption of materials (Buckton 1997). The hydrophilic/hydrophobic nature of materials may affect interparticulate forces, therefore, DVS is widely applied to investigate the stability and crystallinity of a material at elevation conditions of relative humidity (% RH) (Young, Edge et al. 2005).

A DVS instrument employs a Cahn microbalance housed within a temperature-controlled incubator. The twin pans of the microbalance (one for the sample, one as a reference) are contained within glass cells perfused with nitrogen, the relative humidity of which is controlled by a mass flow controller that mixes dry and water saturated gas (Buckton and Darcey 1999).

The instrument can be used to measure changes in sample mass upon exposure to varying humidity. Amorphous materials are thermodynamically unstable, which enables

their detection by DVS as they absorb water molecules from the atmosphere during the experiment (Pfeiffer-Brodka, Langguth et al. 2003). This relates to the plasticisation of the amorphous phase, progressively lowering its glass transition temperature until it falls below the experimental temperature. At this point, molecules in the amorphous phase have sufficient mobility to align and so recrystallise, resulting in the expulsion of the absorbed vapour, which can be seen as a rapid loss of mass on the DVS trace (Buckton 1997). The presence of amorphous materials can be deduced from DVS traces showing >1% mass increase or rapid mass loss with increasing humidity (Buckton 1997).

2.7.2 Method

DVS experiments were performed with a DVS-1 instrument (Surface Measurement Systems Ltd., London, UK). Approximately 50mg of sample was weighed into the sample pan and its mass continually recorded during exposure to two humidity cycles of 0-90% RH in 10% RH steps at 25°C. Equilibrium mass, as defined by a specific change in mass to time ratio of 0.0002dm/dt was achieved for ten minutes before progression to the next step of the cycle.

2.7.3 Results and discussion

2.7.3.1 Micronised drugs

The DVS moisture isotherms for FP, SX and BUD (figure 2.10) showed >0.1% w/w mass increase or mass loss during the first cycle with BUD taking up more moisture then either FP or SX (0.09%, 0.05% and 0.07% w/w respectively) at 90% RH.

Micronised FP showed an increase in mass of 0.007% w/w after the first desorption cycle with a further 0.003%w/w increase in mass after the second cycle. The total amount of water taken up by the material in either cycle is small enough to be due to error within the equipment. Therefore, confirming the crystalline state of FP.

Micronised SX showed no difference in weight after the first cycle. However, a difference between the rate of uptake in the first cycle compared to that in the second cycle between 20 and 80 %RH can be seen. This difference in uptake rates is not consistent with a recrystallisation event, which is characterised by a larger uptake of water during the fist cycle then in the second. The desorption cycles showed no difference. This may suggest that any amorphous material was on the surface so that all of the water vapour could have been removed during the desorption cycle.

BUD showed an increase in mass of 0.007% w/w after the first cycle. There appears to be an inflection in the cycle1 sorption curve at 70% RH, however, this change is too small to be anything significant.

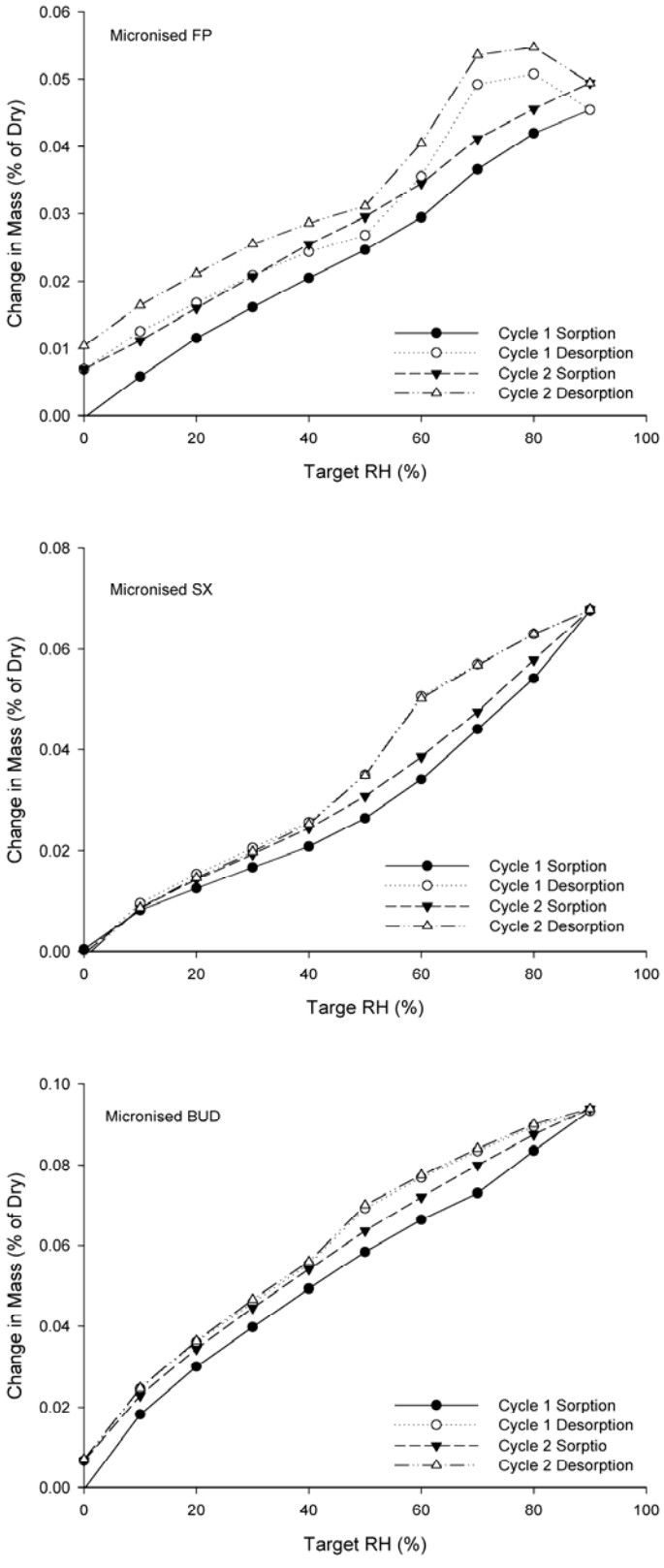

Figure 2.10: DVS moisture sorption isotherms at 25°C for FP, SX and BUD.

Figure 2.11 shows the DVS moisture isotherm for THE as supplied (a) and after micronisation (b). After the first cycle, as supplied THE demonstrates a mass increase of ~0.002% w/w with the second sorption cycle showing a smooth increase in the amount of water adsorbed by the sample between 10 and 80% RH and a sharper rise at 90% RH. The maximum mass increase is ~0.02% w/w with respect to dry as supplied THE.

In contrast to this, the micronised THE (figure 2.11B) shows a larger maximal mass increase of ~0.08% w/w with respect to the dry weight. This may be due to the geometric particle size distribution being smaller, resulting in a greater surface area, and therefore allowing for more water to be adsorbed onto the surface (Brittain 1995; Lodewyckx and Vansant 1997). Micronised THE shows a steady increase in mass as the humidity is increased from 0 to 70% RH. After this, there is a sharp rise in mass until a maximum at 90% RH. After the desorption cycle, the mass does not go back to 0% w/w at 0% RH, but shows in increase in mass from the starting material of ~0.035% w/w. This suggests the formation of an irreversible hydrate during the first sorption cycle. Surprisingly, the mass increase for either the as supplied THE or the micronised THE at 90% RH is not sufficient to be related to the formation of a hydrate as a 9% w/w increase is needed to indicate the conversion of THE into theophylline monohydrate (Vora, Buckton et al. 2004). Vora *et.al.* also found that the monohydrate formation was reversed when the relative humidity was reduced to 5% RH with no further mass loss when this was reduced to 0% RH.

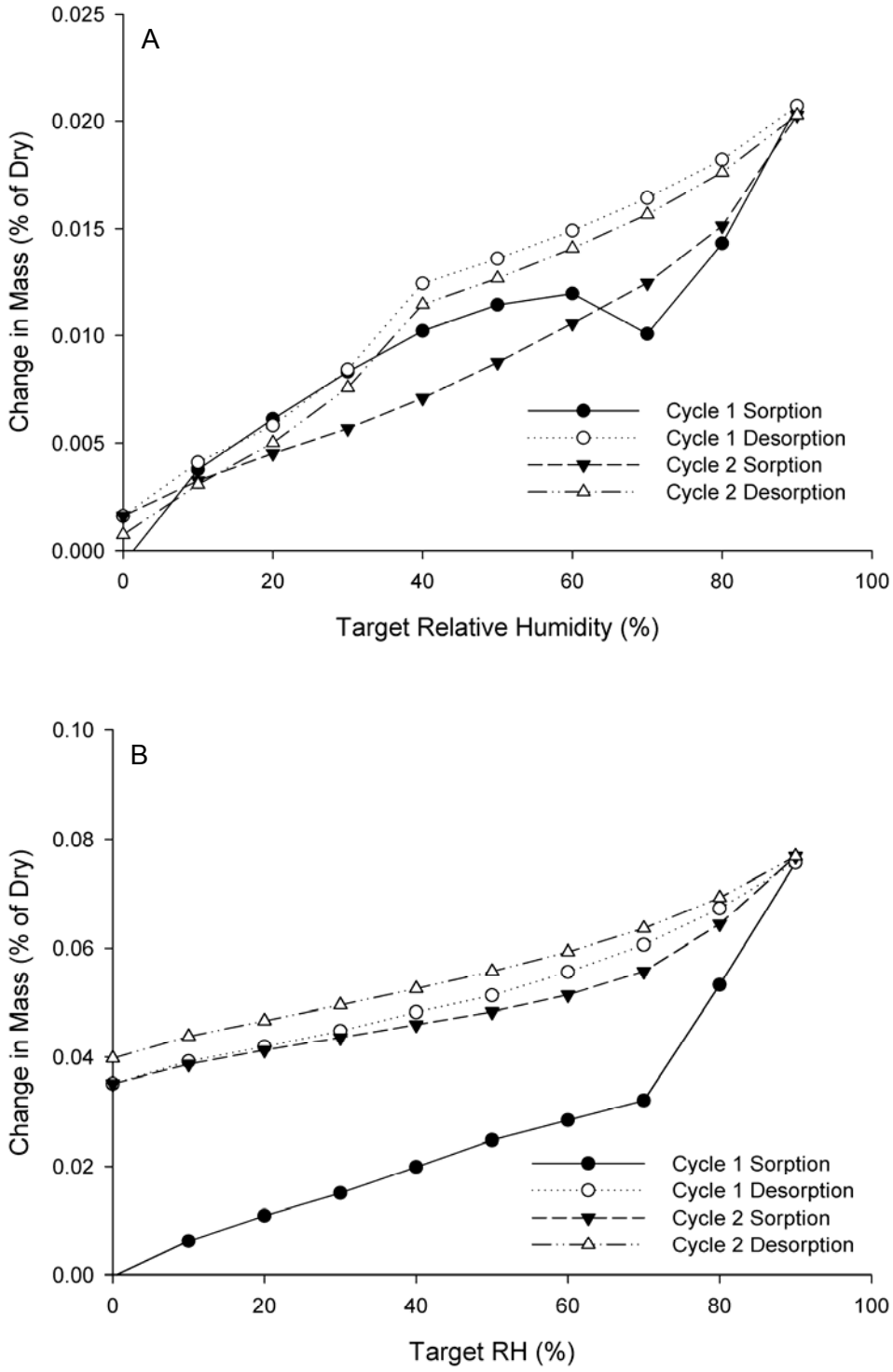

Figure 2.11:DVS moisture sorption isotherms at 25°C for THE as supplied (a) and after micronisation (b).

Figure 2.12 shows the DVS isothermal plot for IB as supplied (a) and after micronisation (b) at 25°C. As can be seen, the as supplied IB demonstrates a gradual increase in mass up until 60% RH. After this point, the mass increase is much more pronounced until it reaches a maximal mass change of ~2.9% w/w. During desorption, the mass drop was insignificant at 10% RH (~2.8% w/w), however, when the % RH

was reduced to 0%, the mass dropped to ~2.5% w/w. This mass drop between that at 90% RH and 0% RH was similar to the total water sorption for IB monohydrate demonstrated by others (Elajnaf, Carter et al. 2007). In addition, the failure of the DVS to completly remove all of the water vapour was has been seen by others (Taylor, Hickey et al. 2006), and confirms the formation of a monohydrate.

However, for complete conversion of anhydrous IB to form a monohydrate, a total of ~4% mass increase would have been observed (Abdine, Belal Heba et al. 2003; Corrigan, Corrigan et al. 2006). Therefore, this may suggest that some of the IB may already have formed a monohydrate. This also correlates with the DSC results which demonstrated an endothermic event occurring at ~120°C which relates to the removal of water from the lattice (Corrigan, Corrigan et al. 2006).

Micronised IB demonstrated a similar response to moisture as the as supplied IB (figure 2.12B). However, the response was heightened due to the increased surface area of the micronised material (Brittain 1995; Lodewyckx and Vansant 1997).

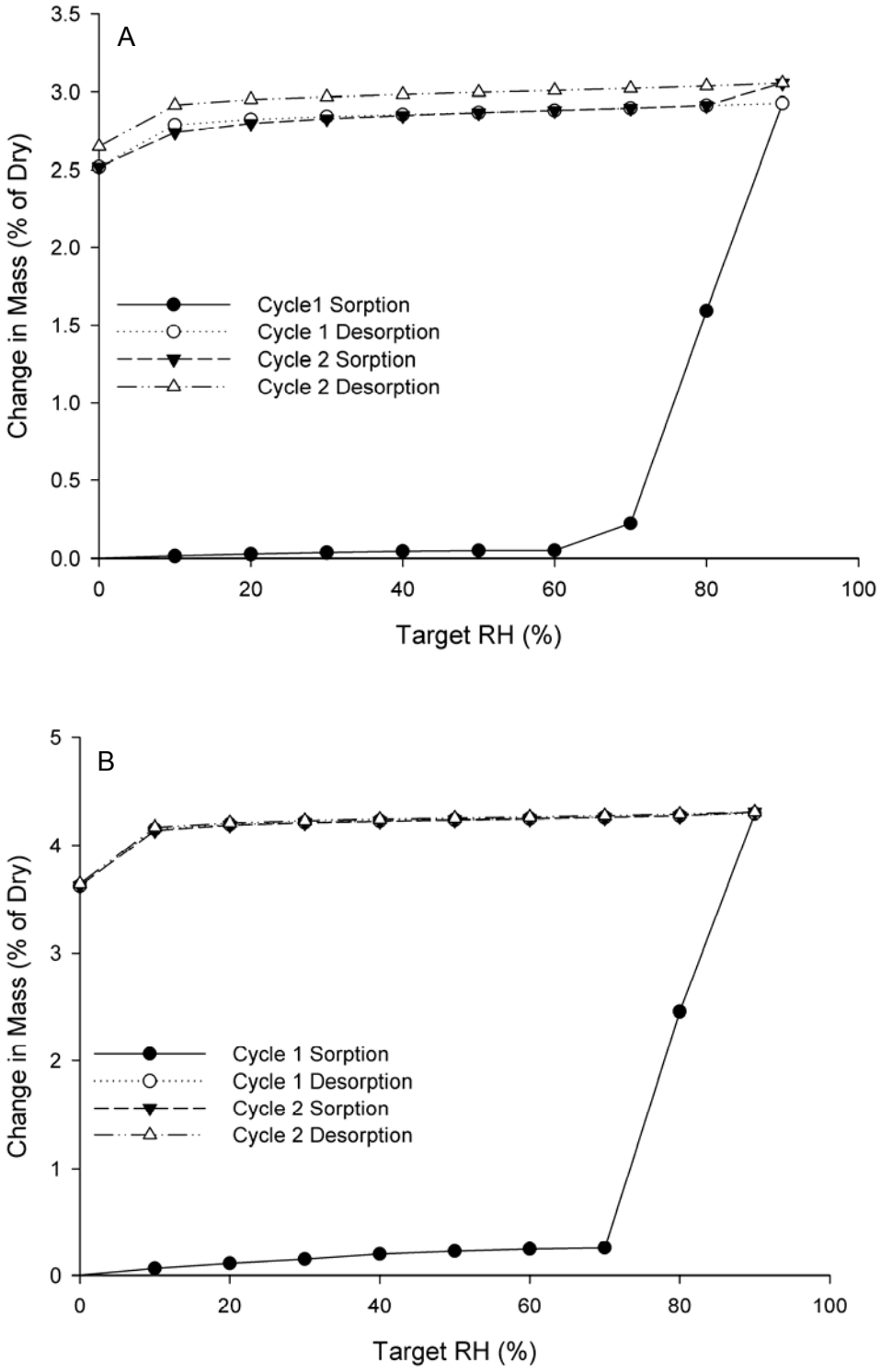

Figure 2.12: DVS moisture sorption isotherms at 25°C for IB as supplied (a) and after micronisation (b).

2.7.3.2 Cocrystal raw material

Figure 2.13 shows the DVS isothermal plot for CBZ, IND, NIC and SAC at 25°C. As can be seen, CBZ, NIC and SAC form hydrates (Jayasankar, Good et al. 2007) which

are irreversible on drying. In addition to this, both NIC and SAC demonstrate a recrystallisation even at 60 and 70% RH respectively.

CBZ showed a maximal mass increase of ~0.01% w/w at 90% RH with no loss during the desorption cycle. The second sorption cycle showed an increase in mass up to ~0.011% w/w with very little loss during the desorption cycle.

The IND DVS isotherm demonstrates that pure IND can produce a reversible hydrate. The mass change increases gradually as the relative humidity is increased from 0 to 20% RH. A large mass increase is seen at 30% RH suggesting that between 20 and 30% RH, IND is converted to a hydrate. The mass then gradually increases to a maximum at 90% RH. During the desorption cycle, the mass change appears to be constant between 90 and 10% RH. As the humidity is decreased further, the mass change drops to 0% w/w and, therefore, back to the starting material.

NIC showed a gradual increase in mass up to 40% RH, which stayed the same at 50% RH but was followed by a mass drop at 60% RH, suggesting that there had been a re-crystallisation. After this, the mass drastically increased between 70 and 90% RH up to 0.155% w/w. During desorption, the mass loss between 90 and 80% RH was identical to the mass gain in the same region. The rate of decline then reduced between 80 and 60% RH with a final drop in mass at 50% RH to ~0.016% w/w with only minimal loss after this to 0% RH (~0.014% w/w). During the second cycle, the mass increase was minimal at 60% RH, after which point, the mass increased in line with the desorption cycle up to 90% RH. This suggests that bellow 60% RH, one hydration form exists while humidity's above 60% will result in a second hydration.

SAC demonstrates a similar result as NIC with 20% RH having little effect on the mass with only ~0.001% w/w mass increase from dry. Between 20 and 40% RH, the mass increases to ~0.006% w/w and stays at this level until 60% RH. At 70% RH, the SAC recrystallises as signified by a mass drop to 0.0006% w/w. This is followed by a slight increase at 80% RH then a large rise at 90% RH to ~0.04% w/w.

During desorption, SAC demonstrates a gradual decrease in mass between 90 and 50% RH down to ~0.003% w/w change from dry. Unpredictably, the mass of the sample increases as the humidity is decreased further to ~0.005% w/w at 0% RH. The second sorption cycle follows the desorption line up to 50% RH then stabilises until the humidity reaches 80% RH before increasing again to ~0.04% w/w at 90% RH. The second desorption cycle then follows the first, thus suggesting that high levels of humidity (90% RH) are needed to form a solvate which can be slowly reversed.

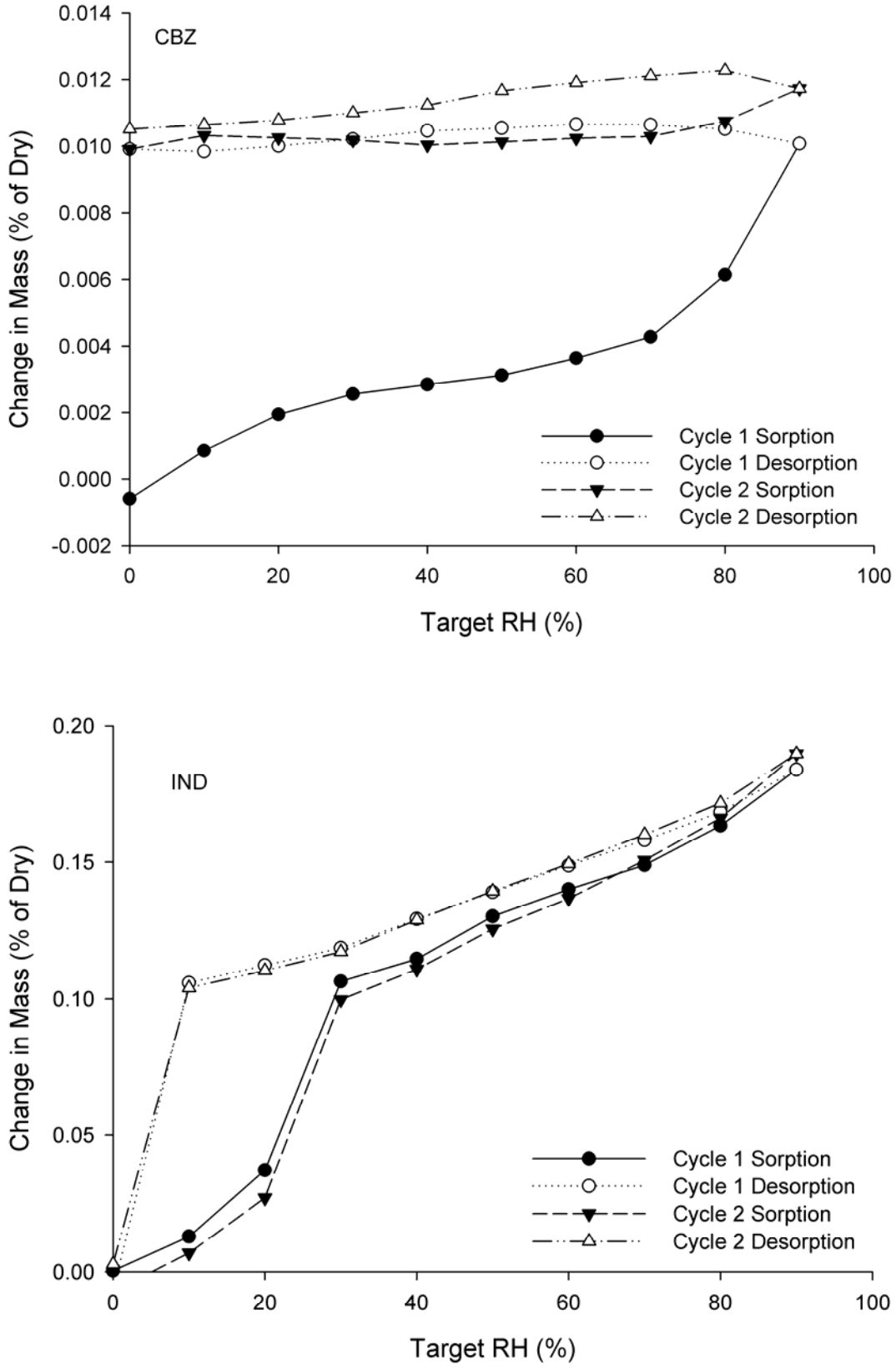

Figure 2.13: (Continued on next page) DVS moisture sorption isotherms at 25°C for CBZ and IND.

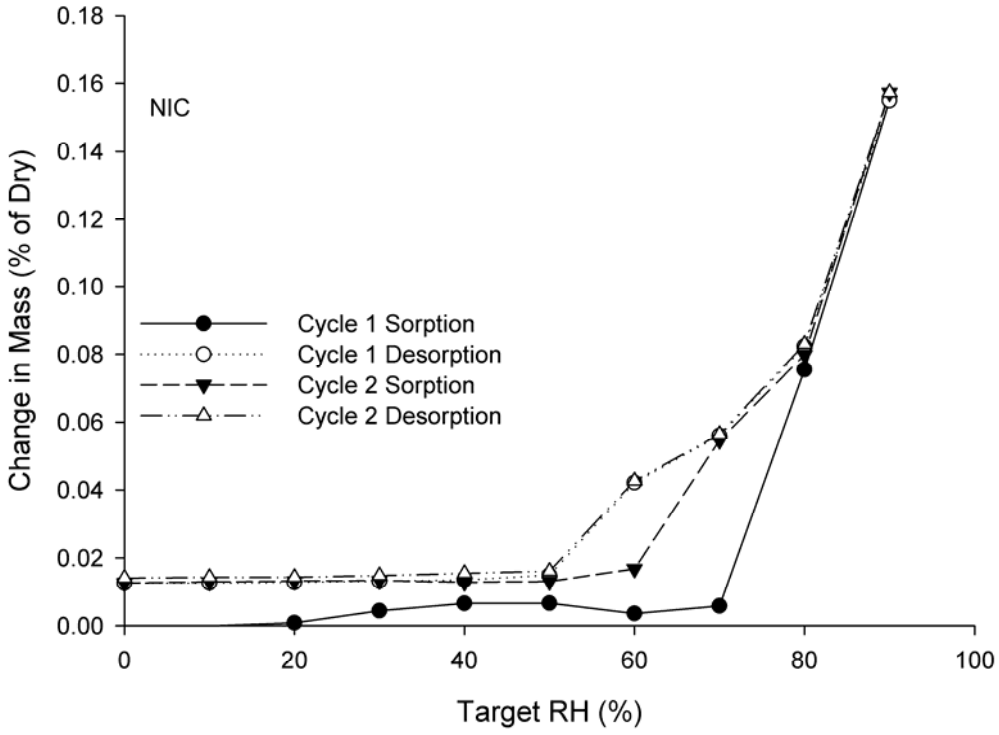

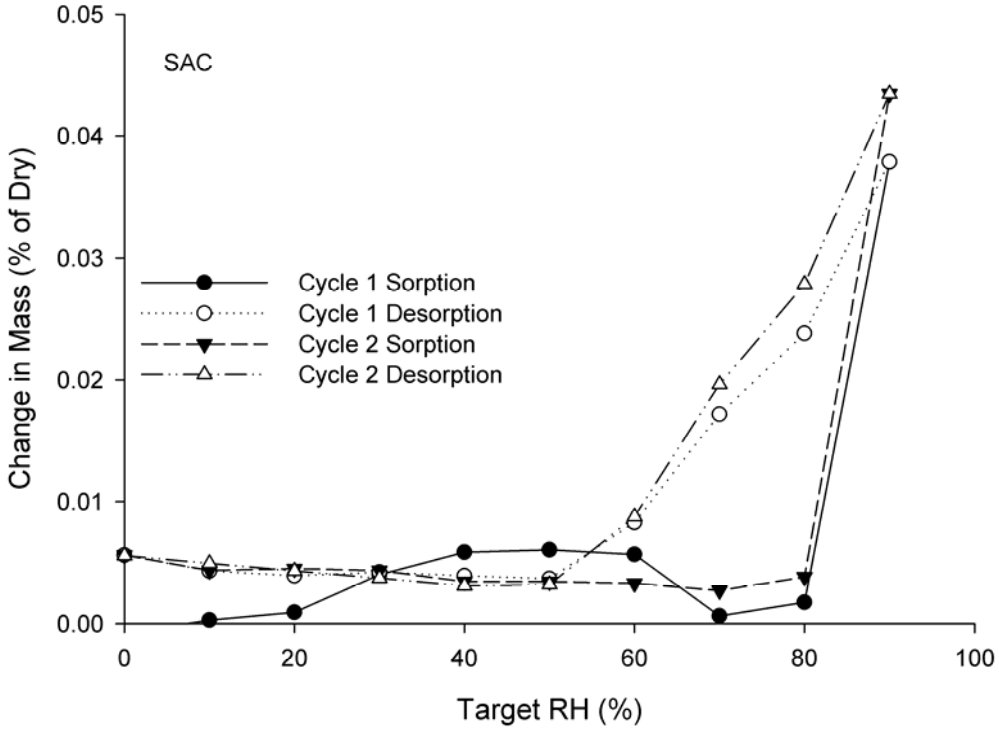

Figure 2.13: (Continued from previous page) DVS moisture sorption isotherms at 25°C for NIC and SAC

Chapter 3 - Novel Triple Based Formulations for the Treatment of COPD

3.1 Introduction

Chronic obstructive pulmonary disease (COPD) is a complex disease condition of the airways, characterized by airflow limitation and airway inflammation (Pauwels and Rabe 2004; Mannino and Buist 2007). With limited treatment options to slow the relentless progression of these diseases, chronic respiratory diseases constitute a serious public health problem in all countries throughout the world (Pauwels and Rabe 2004; Mannino and Buist 2007). The only proven way of slowing the deterioration in lung function is by smoking cessation (Barnes 2003; 2004; Cazzola, Hanania et al. 2008). In addition, many of the drug treatments cannot completely reverse either the bronchoconstriction or inflammation (Jacoby and Fryer 2001; Barnes 2003; Caramori and Adcock 2003).

However, COPD patients appear to have an increased vagal cholinergic tone. This is controlled by muscarinic receptors with bronchoconstriction resulting from activation of M_3 muscarinic receptors on the airway smooth muscle (Jacoby and Fryer 2001; Pauwels, Buist et al. 2001). Anti-muscarinic compounds, such as ipratropium bromide (IB), block the muscarinic receptor and reduce the effect of acetylcholine. This appears to be the only pathway whereby bronchoconstriction in COPD patients can be reversed (Barnes 2000; Jacoby and Fryer 2001; Cazzola, Hanania et al. 2008).

The addition of an anti-muscarinic compound to salmeterol xinafoate (SX) and fluticasone propionate (FP), a long acting β_2-agonist (LABA) and an inhaled corticosteroid (ICS) respectively, may result in a greater therapeutic effect in COPD patients (Rodrigo and Rodrigo 2003; Aaron, Vandemheen et al. 2007; Singh, Brooks et al. 2008). This is related to the additive action of targeting multiple pathways to promote bronchodilation.

IB has a short duration of action (about 4-6 hours)(Pauwels, Buist et al. 2001) and, may result in the patient needing to take 3 or 4 doses a day (British Medical Association and Royal Pharmaceutical Society of Great Britain 2009). The long acting anti-muscarinic, tiotropium, can be given once daily (British Medical Association and Royal Pharmaceutical Society of Great Britain 2009).

The addition of another compound to the treatment regimen for COPD patients may result in a complicated treatment regimen (Stempel, Stoloff et al. 2005) and may result in poor compliance due to the added complexity (Keating and McCormack 2007). This

reason, along with the added benefits of providing multiple compounds in one inhaler, has driven the development of combination inhalers for the treatment of COPD (Barnes 2002).

Previous work has shown that combination particles, containing SX and FP, can be produced via SAX. These particles allow for a consistent dose ratio of SX and FP to be delivered throughout an impactor compared to individually micronised components formulated in the same way (Pitchayajittipong, Shur et al. 2009). The addition of IB to SX and FP may allow for greater contol of a patients disease by helping to reduce vagal tone, while improving patent compliance by reducing the total number of inhalers the patient needs to use.

3.2 Materials

Micronised FP and SX were obtained from sources stated in Chapter 2, as was IB and lactose monohydrate. All organic solvents were of at least analytical grade and were supplied by Fisher Chemicals (Loughborough, UK). Water was prepared by MilliQ from reverse osmosis (Millipore, Molsheim, France).

3.3 Methods

3.3.1 The Production of SAX-produced IB:SX:FP Particles

Combination SAX IB:SX:FP particles were prepared by atomisation of a 1.9% w/v solution containing IB:SX:FP in the ratio 1:1.25:12.5 in an acetone: methanol 20:1 co-solvent mixture. This ratio corresponds to the dose equivalent ratio for each of the three drugs when used by patients. Atomisation was conducted using a SU11 co-axial two-fluid atomiser with an internal mix (Spraying Systems Co., Illinois, USA). The atomiser was used at a sprayed rate of 4 $ml.min^{-1}$ with air pressure at 2.5 bar in the lab scale of the SAX process over 60 cm of separation distance including positive pressure 30 $L.min^{-1}$. The resultant droplets were collected in a non-solvent of perfluorodecalin (F2 Systems) at 5˚C, and continually exposed to sonic energy using a sonic horn (P100, Sonic Systems, Somerset, UK) operating at a fixed wavelength of 20 kHz and capable of inducing a maximum power output of 750 W. The ultrasonic horn (horn diameter ~13 mm) was immersed 5 mm in the processing liquid to aid nucleation and crystal growth. The resulting combined SAX particles were isolated using supercritical CO_2 extraction of perfluorodecalin, as described in Chapter 2.

Supercritical fluid extraction has been shown to have no, or very little effect on the final product morphology or crystal habit (Pitchayajittipong, Shur et al. 2009), and, therefore, will not be assessed as a variable in this thesis.

3.3.2. Formulation Production

3.3.2.1: Pressurised metered dose inhalers (pMDI's)

Drug-only pressurised metered dose inhaler (pMDI) formulations containing 1.18% w/w of combination SAX particles of IB, SX and FP was produced by weighing an appropriate amount of material into an aluminium canister (Bespak, King's Lynn, UK) before being sealed with a 50 µl metering valve (Bespak, King's Lynn, UK) and the appropriate amount of HFA-134a (Ineos Fluor, Runcorn, UK) propellant being added. The canisters were sonicated for 20 minutes and allowed to stand for 24 hours before testing. An equivalent formulation containing micronised IB, micronised SX and micronised FP was also prepared.

3.3.2.2: Dry powder inhaler (DPI) formulation

A carrier based DPI formulation, containing 0.16% w/w combined SAX IB:SX:FP, was prepared by geometric blending with Respitose SV003 grade of lactose monohydrate. The combined SAX particles and SV003 lactose were mixed in a 15 ml glass tube for 60 seconds in a Whirlimixer (Fisons Scientific Equipment, Loughborough, UK). The resultant blend was further processed using a Turbula mixer (Willy A Bachofen AG, Basel, Switzerland) at 46 rpm for 45 minutes.

In order to compare the *in-vitro* inhalation performance of SAX particles, a micronised combination formulation containing 0.0100% w/w of micronised IB, 0.0125% w/w of micronised SX and 0.1250% w/w micronised FP, was prepared by geometric blending sieved lactose monohydrate (Respitose SV003). The drug and SV003 lactose were mixed in a 15 ml glass tube for 60 seconds in a Whirlimixer (Fisons Scientific Equipment, Loughborough, UK). The resultant blend was then mixed using a Turbula mixer (Willy A Bachofen AG, Basel, Switzerland) at 46 rpm for 45 minutes. All formulations were stored at 44 % RH and 25 °C for 24 h before formulation testing.

3.3.3 Content uniformity determination

Upon blending of the DPI formulation, the content uniformity of formulations was assessed. Each blend was spread over a clean surface and ten samples of 25 $\pm$ 1 mg taken from random positions. Each sample was dissolved with 15 minutes sonication in 100 ml final volume of 0.6% w/v aqueous ammonium acetate (Sigma-Aldrich, Gillingham, UK): methanol (25:75 v/v) and drug concentration assessed by high performance liquid chromatography (HPLC). The proportion of drug in each sample was calculated and the content uniformity expressed as the coefficient of variation (*CV*):

$$CV = \frac{SD \times 100}{\bar{x}} \qquad \text{Equation 3.1}$$

where $\bar{x}$ is the mean drug proportion and SD is the standard deviation.

3.3.4 Capsule filling

The DPI formulations were manually loaded into size 3 hydroxypropyl methylcellulose (HPMC) capsules (Qualicaps, Madrid, Spain). Fill weight was 25 ± 1 mg, giving a nominal dose of 40 ± 1.6 µg total drug per capsule for each formulations used. Filled capsules were stored in a sealed container containing a saturated solution of potassium carbonate, giving a relative humidity of 44% (Rockland 1960), for at least 24 hours prior to analysis.

3.3.5 *In-vitro* performance analysis

Inertial impaction has been the pharmacopoeial and industry standard technique for the determination of drug aerosol particle size distribution (Marple, Roberts et al. 2003). It allows the aerodynamic size distribution of the entire inhaled dose to be characterised in a way that is specific to the drug (Marple, Roberts et al. 2003). An impactor is a device into which the aerosolised formulation is drawn, under an airstream at a defined flow rate. It passes through a series of stages, which consists of a plate containing a number of nozzles or jets with a defined diameter located above a flat collection surface. As the aerosol passes from stage-to-stage, the jet sizes become progressively smaller. As the airstream passes through each stage, it changes direction. Any airborne particles will be subject to two forces: their momentum, which acts to keep them travelling in their current direction; and the hydrodynamic forces exerted by the air travelling in the new direction (Marple, Roberts et al. 2003). Particles with a larger momentum, which is a function of their mass and thus diameter, will be less likely to relax into a change in direction of the air flow, and may impact on the collection surface, removing them from the airstream (see Figure 3.1) (Henningson and Ahlberg 1994).

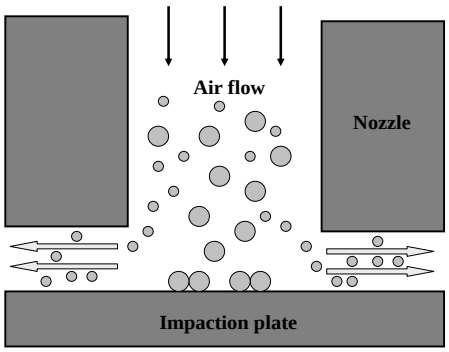

Figure 3.1: The impactor consisting of a nozzle and an impaction plate

For a given nozzle diameter, particles above a certain size (the cut-off diameter) will impact on the collection surface. In practice, the efficiency with which particles of varying sizes impact in a given stage follows a sigmoidal function. Therefore, the cut-off diameter for a given stage is characterised by the aerodynamic diameter at which 50% of particles impact (C_{50}) (Marple, Roberts et al. 2003). The cut-off diameter of a stage can be described using Stokes' law (Marple, Roberts et al. 2003):

$$C_{50} = \sqrt{\frac{9\pi\eta n_n W_n}{4\rho_p C_{ae} Q}} \times \sqrt{St_{50}} \qquad \text{Equation 3.2}$$

where η is the viscosity of air, n_n is the number of circular nozzles in the stage, W_n is the nozzle diameter, ρ_p is the particle density, C_{ae} is the Cunningham slip correction factor, Q is the volumetric air flow rate and $\sqrt{St_{50}}$ is the square root of the Stokes' number that gives a 50% chance of particle deposition, which is ~0.49 for a well-designed impactor.

By passing the aerosolised formulation through an impactor and then recovering and quantifying the amount of drug deposited on each stage, the aerodynamic particle size distribution can be determined. In order to mimic the anatomy of the respiratory tract, impactors also feature an induction port that is placed between the inhaler and the stages. This contains a 90˚ bend and acts as a very simple model of the mouth and throat, enabling deposition in this area to be approximated.

3.3.5.1 Andersen Cascade Impactor (ACI)

In-vitro pMDI performance was assessed using an Andersen Cascade Impactor (ACI, Copley Scientific, Nottingham, UK, figure 3.2), which consists of a metal throat piece, 8 stainless steel stages and a final filter stage to collect any fine material. When operated at 28.3 ±1.5 $L.min^{-1}$, the cut-off diameters for each stage exhibit as detailed in table 3.1. The fine particle dose (FPD) can be defined as the mass of drug deposited on stage 3 and bellow (<4.7µm).

Table 3.1: Cut-off diameters for each stage of the ACI when used at 28.3 $L.min^{-1}$ (British Pharmacopoeia Commission 2003)

Stage	Cut-off Diameter (µm)
0	9.0
1	5.8
2	4.7
3	3.3
4	2.1
5	1.1
6	0.7
7	0.4

Figure 3.2: Andersen cascade impactor (taken from www.copleyscienticfic.co.uk)

Prior to assembly, each impaction plate was immersed in a 1% v/v solution of silicon oil (Acros Organics, Geel, Belgium) in hexane and allowed to air dry. The ACI was then assembled and connected to a vacuum pump (Gaast, Benton Harbour, MI, USA) *via* a solenoid valve. The flow rate at the inlet to the throat was set to 28.3 $L.min^{-1}$ using a digital flow meter - model DFM 2000 (Copley Scientific Ltd., Nottingham, UK).

For each analysis, the first five shots of each pMDI were fired to waste following shaking the can for 10s between each actuation. The pMDIs were inserted into a specially constructed mouthpiece and actuated in a fixed position. With the pump on, the solenoid valve was opened for 12s. A 3s delay was employed, after the pump was engaged, to allow equilibrium of the pump before the actuator was pressed for 4s to allow sufficient time for firing. After this, the pump was allowed to continue for a further 5s before the solenoid valve was closed, as illustrated in figure 3.3. Three consecutive doses, with vigorous shaking of the canister between each dose, for each formulation were released into the impactor.

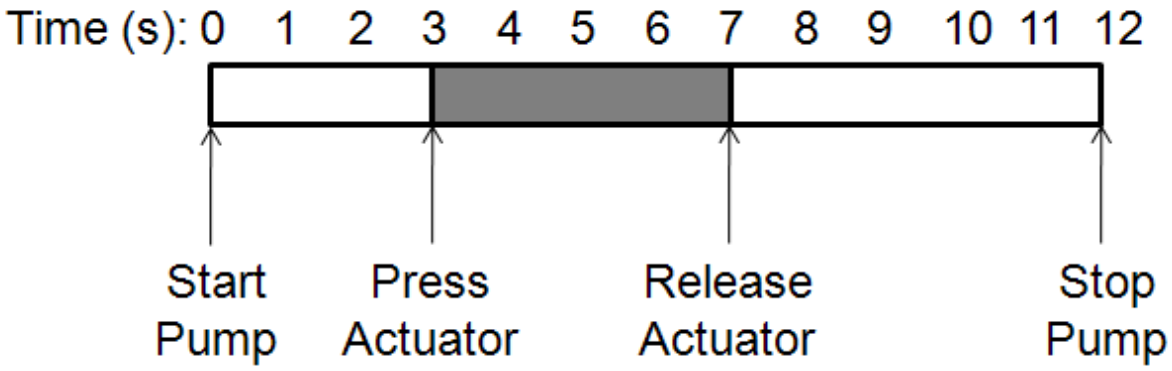

Figure 3.3: Graphical representation of pump time showing when actuator is depressed.

The pMDI actuator, mouthpiece adaptor, throat assembly, collection plates from stage zero to seven and filter stage were thoroughly rinsed into suitable volumetric flasks with dilution solvent (0.6% w/v aqueous ammonium acetate: methanol, 25:75 v/v) and made up to the mark. The actuator, mouthpiece adaptor, throat assembly and ACI collection plates were then washed in water and rinsed with distilled water followed by methanol, and dried at 40°C in an oven for 30 min. The ACI components were left to cool for 30 min, reassembled and re-used. For each formulation, ACI investigations were carried out in triplicate. All samples were analysed by high performance liquid chromatography (HPLC), from which the mass of drug deposited on each stage could be determined.

The emitted dose (ED) was defined as the mass of drug recovered from all parts of the ACI and mouthpiece adaptor. The fine particle dose (FPD) was the mass of drug

recovered from stage 3 and below of the ACI and the fine particle fraction (FPF_{ED}) was the FPD expressed as a percentage of the ED.

3.3.5.2 Next Generation Impactor (NGI)

In-vitro DPI performance was assessed using a Next Generation Impactor (NGI, Copley Scientific Ltd, Nottingham, UK, figure 3.4), which consists of a metal throat piece, pre-separator, 8 stages, of which the final stage is a micro orifice collector (MOC), which performs the role of a filter. When operated at 85 $L.min^{-1}$, the cut-off diameters for each stage exhibit as detailed in table 3.2. The FPD can be defined as the mass of drug deposited on stage 3 and bellow (<3.72μm).

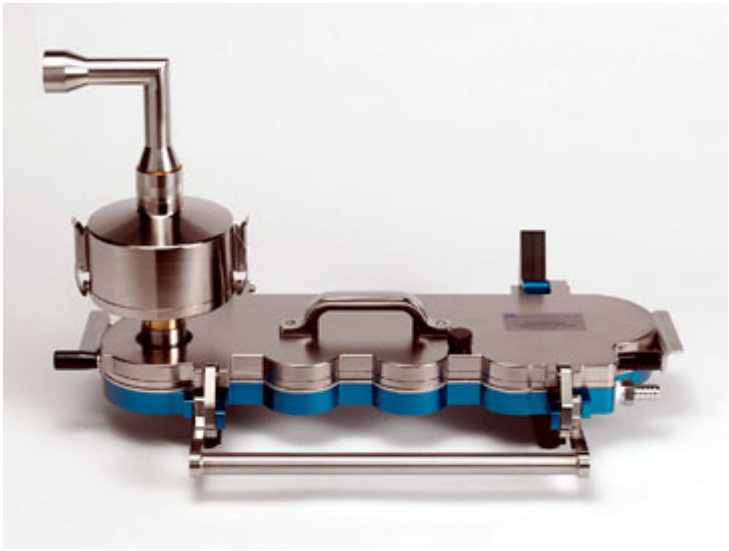

Figure 3.4: Next Generation Impactor with pre-separator and throat piece assembly (taken from www.copleyscienticfic.co.uk)

Table 3.2: Cut-off diameters for each stage of the NGI when used at 85 $L.min^{-1}$ (Marple, Olson et al. 2003)

Stage	Cut-off Diameter (μm)
Pre-separator	11.05
1	6.68
2	3.72
3	2.37
4	1.41
5	0.78
6	0.45
7	0.27
MOC	0.09

The NGI was used to investigate the performance of the DPI formulations. The NGI collection cups were immersed in a 1% v/v solution of silicon oil (Acros Organics, Geel, Belgium) in hexane and allowed to air dry. The NGI was then assembled with pre-separator (containing 15 ml of wash solvent) and connected to a vacuum pump (Gaast, Benton Harbour, MI, USA) *via* a solenoid valve. The flow rate at the inlet to the throat was set to 85 $L.min^{-1}$ using a digital flow meter (DFM 2000, Copley Scientific Ltd., Nottingham, UK). An Aerolizer DPI device was attached to the throat of the NGI using a specially created mouthpiece. A capsule was inserted in the Aerolizer and pierced by eight sharp pins to generate four small holes at each end of the capsule. The contents of the capsule were then aerosolised into the NGI by drawing air through the apparatus at 85 $L.min^{-1}$ for 2.8 seconds (controlled by the solenoid valve). Once the contents of five capsules were aerosolised, and the device, capsule and each stage were thoroughly rinsed into suitable volumetric flasks with dilution solvent (25%, 0.6% w/v aqueous ammonium acetate, 75% methanol) and made up to the mark. The concentration of drug in each solution was investigated by HPLC, from which the mass of drug deposited on each stage of the NGI could be determined at stages 1 to 7 and the MOC. The NGI was subsequently washed in water and methanol, dried in an oven, and allowed to cool to room temperature before re-use.

Each formulation was tested in triplicate. The emitted dose (ED) was defined as the mass of drug recovered from all parts of the NGI and the mouthpiece. The fine particle dose (FPD) was the mass of drug recovered from stage 3 and below of the NGI and the fine particle fraction (FPF_{ED}) was the FPD expressed as a percentage of the ED.

3.3.6 High Performance Liquid Chromatography

Drug concentrations were determined by HPLC. The HPLC system consisted of a Shimadzu LC -2010AHT coupled with an LCMS-2010EV quadruple mass analyser coupled with electrospray and atmospheric pressure chemical ionization (Dionex, Camberley, UK). Data were collected and analysed using Chromeleon software (Dionex, Camberley, UK). Unknown sample concentration was determined from duplicate injections by comparison of peak area with reference peaks from external standard solutions of known concentration.

All compounds were analysed using the HPLC. This employed a 4.6 mm x 150 mm C18(2) 5µm Hypersil column (Phenomenex, Macclesfield, Cheshire, UK). The flow rate was 0.5 $ml.min^{-1}$; with the injection volume of 50 µl. the mobile phase used was 75:25 (v/v) 0.6% w/v aqueous ammonium acetate:methanol. IB and SX drug concentrations were assessed using mass spectroscopy with IB having a m/z of 332.2 and SX having an m/z of 416.2, while FP was detected with a detection wavelength of 228nm. Drug

retention times were 3.51, 7.21 and 11.24 minutes for IB, SX, and FP respectively, so a run time of 15 minutes was employed.

The relationship between drug concentration (0.025, 0.05, 0.25, 0.5 and 2.5 $\mu g.ml^{-1}$ for IB and SX and 0.25, 0.5, 2.5, 5.0 and 25 $\mu g.ml^{-1}$ for FP) and peak area for each drug was found to be linear, with linear regression analysis yielding a coefficient of determination (R^2) of 0.9995 for IB and SX and 0.9987 for FP (Figure 3.5). Calibration curves were produced prior to each experimental assay.

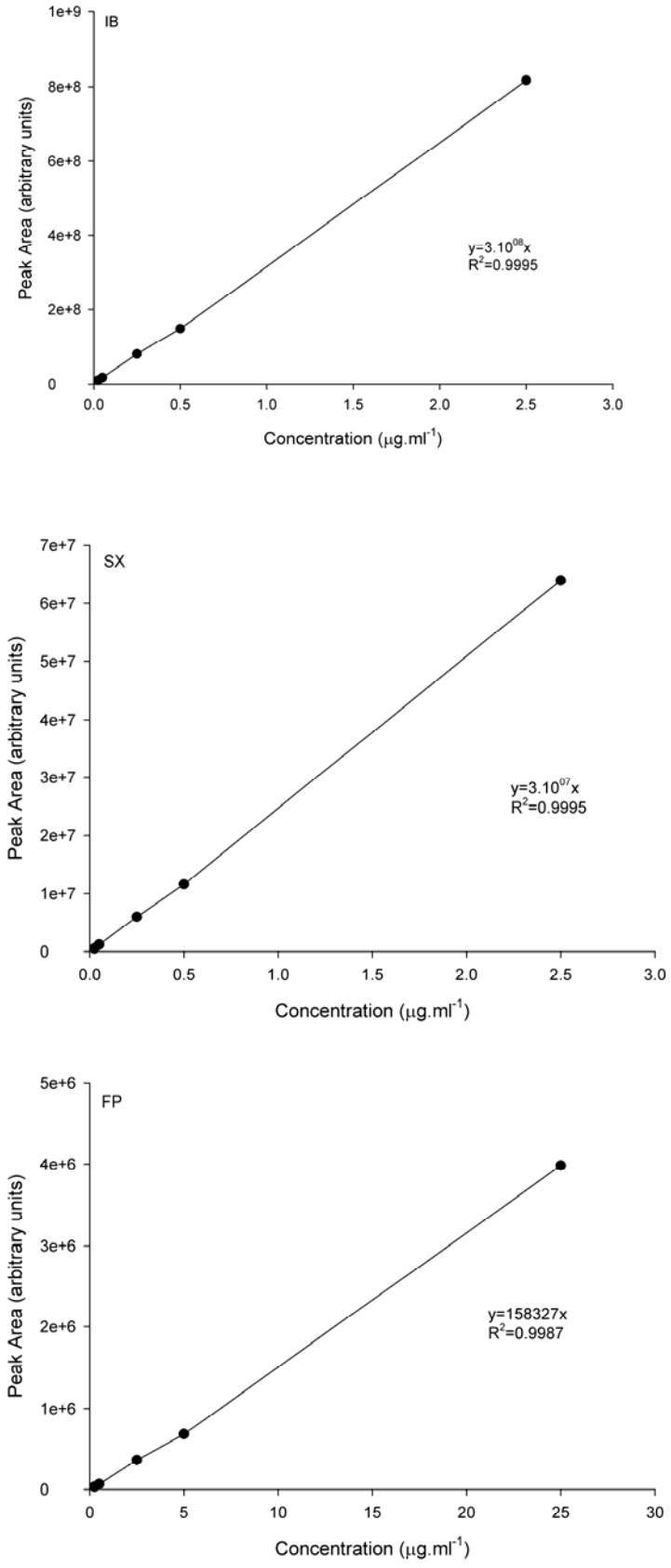

Figure 3.5: Representative HPLC calibration curves for IB, SX and FP.

3.4 Results and discussion

3.4.1 Physical characterisation

Figure 3.6 shows the scanning electron images depicting the morphology of micronised IB particles (a) and SAX IB particles produced from a methanol solution (b). The micronised particles appear to form irregular shaped particles of varying sizes while the SAX particles appear to be much smaller and needle shaped with a smaller particle size distribution. For the micronised particles, the largest particle appears to be approximately 5μm in diameter while the SAX particles are about 4μm in length.

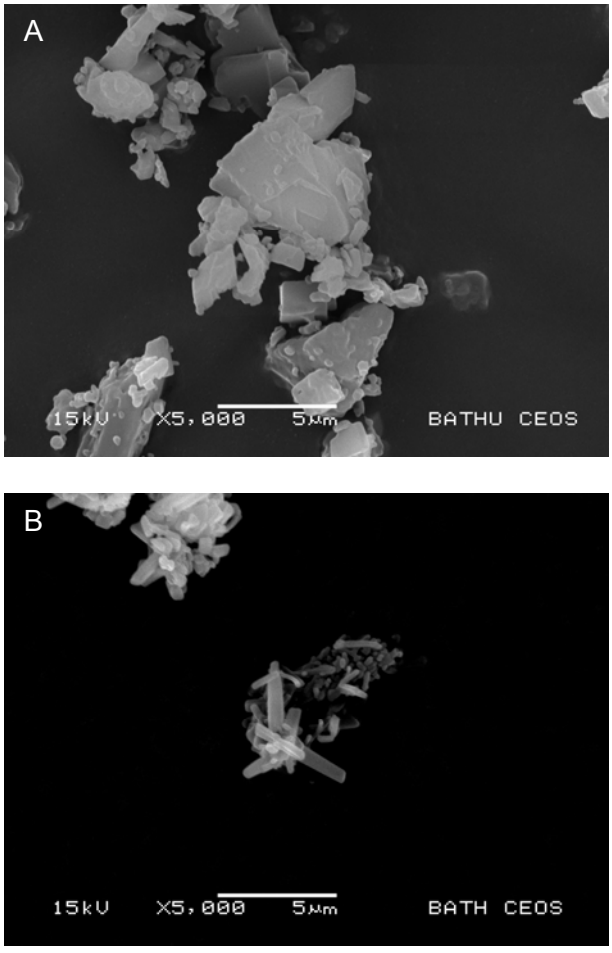

Figure 3.6: SEM micrograph of micronised IB (A) and SAX IB (B).

Figure 3.7 shows the SEM micrograph images of the SAX produced IB:SX:FP (1:1.25:12.5 ratio by mass) particles. The particles appear to be spherical in nature. This suggested that the vapour pressure of the acetone:methanol mixture was sufficient to allow for sufficient evaporation of the droplet before reaching the anti-solvent. As a result, the highly viscous droplet maintained the spherical nature during crystallisation.

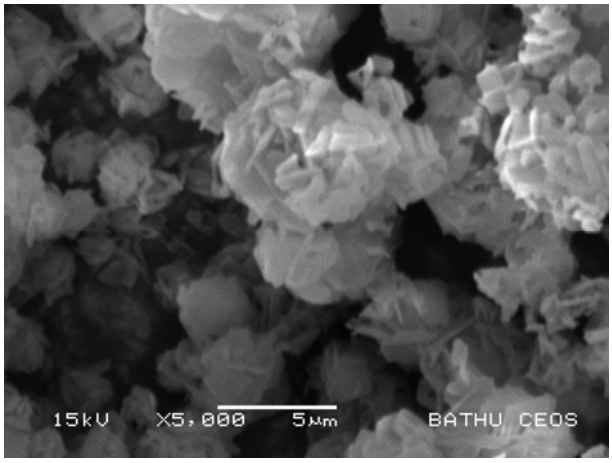

Figure 3.7: SEM micrograph images of SAX produced IB:SX:FP (1:1.25:12.5 ratio by mass) particles .

Figure 3.8 shows the DVS isotherm of the SAX engineered IB:SX:FP particles. As shown, there was a gradual increase in mass between 0%RH and 60%RH. After this point, the mass increase plateaus between 70 and 80%RH. These data suggest that a re-crystallisation event may have occurred (Buckton and Darcy 1995; Elamin, Sebhatu et al. 1995; Buckton 1997; Buckton and Darcey 1999).

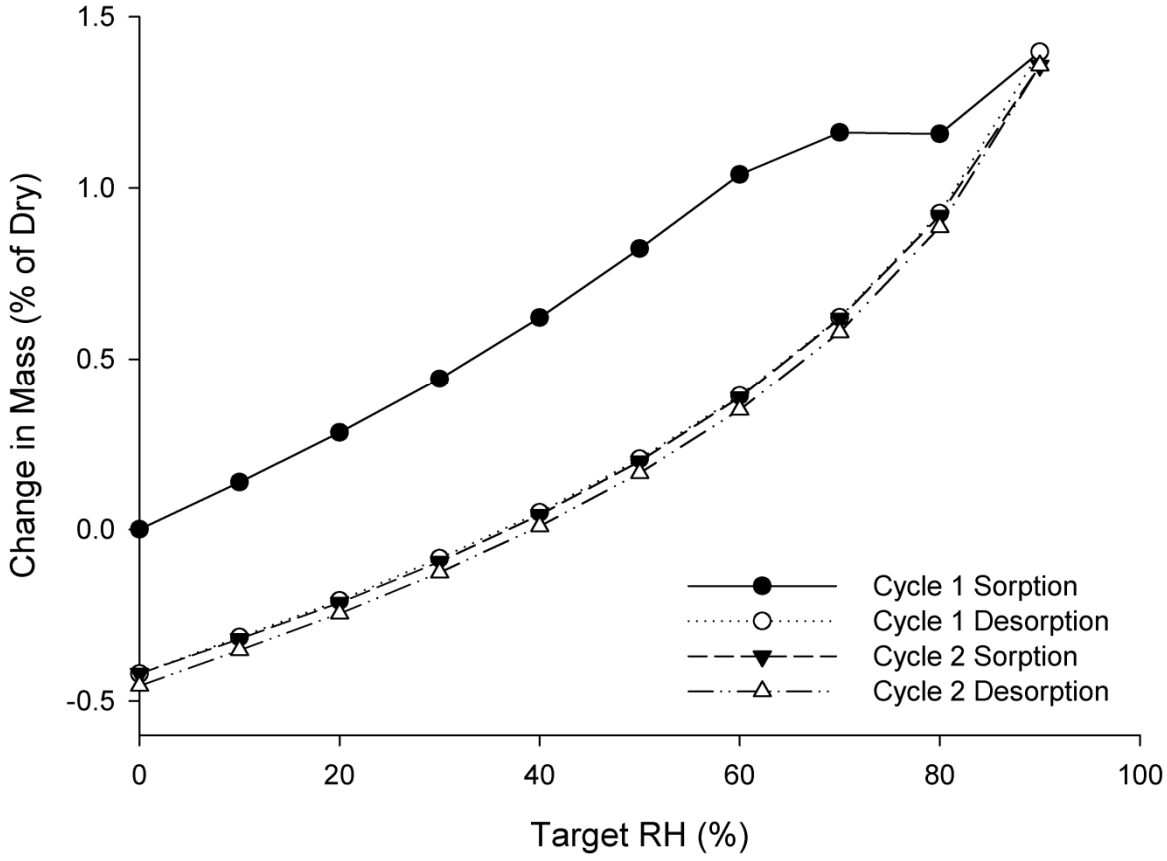

Figure 3.8: DVS isotherm plot for SAX engineered IB:SX:FP (1:1.25:12.5 ratio by mass) at 25°C.

The re-crystallisation can be seen in Figure 3.9, which shows the real-time mass and humidity change of the sample during the DVS experiment. There appears to have been a re-crystallisation event above 60% RH. These results are inconsistent with the DVS traces from the raw materials, as seen in chapter 2.

After these re-crystallisation events, the desorption and second sorption-desorption followed the same curve, but at a lower weight due to the vapour/moisture lost during the first sorption cycle.

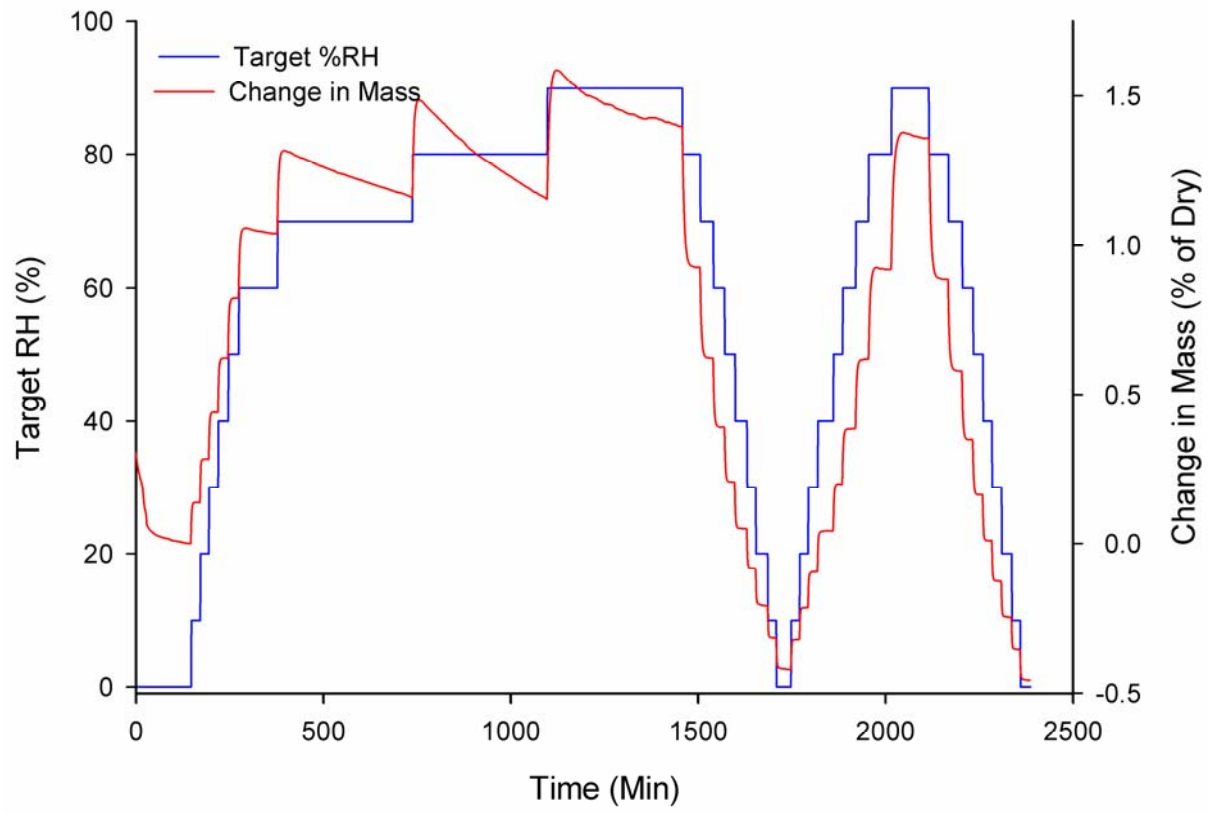

Figure 3.9: Real time DVS data for IB:SX:FP particles produced by SAX at 25°C.

Despite the level of amorphous content, XRPD analysis demonstrated sharp peaks in the diffractogram suggesting that the particles had less than 10% amorphous content (Salekigerhardt, Ahlneck et al. 1994; Buckton and Darcey 1999) (Figure 3.10). The majority of the peaks in the XRPD diffractogram relate to the presence of FP in the sample. These data suggest that the IB and SX may not have been incorporated into the sample that was analysed.

Closer inspection of the results may suggest that the peak at 13.61° 2θ could be indicative of both IB and SX. In addition to this, the peak at 15.12° 2θ may also be for IB and the peak at 17.00° 2θ may represent all three compounds.

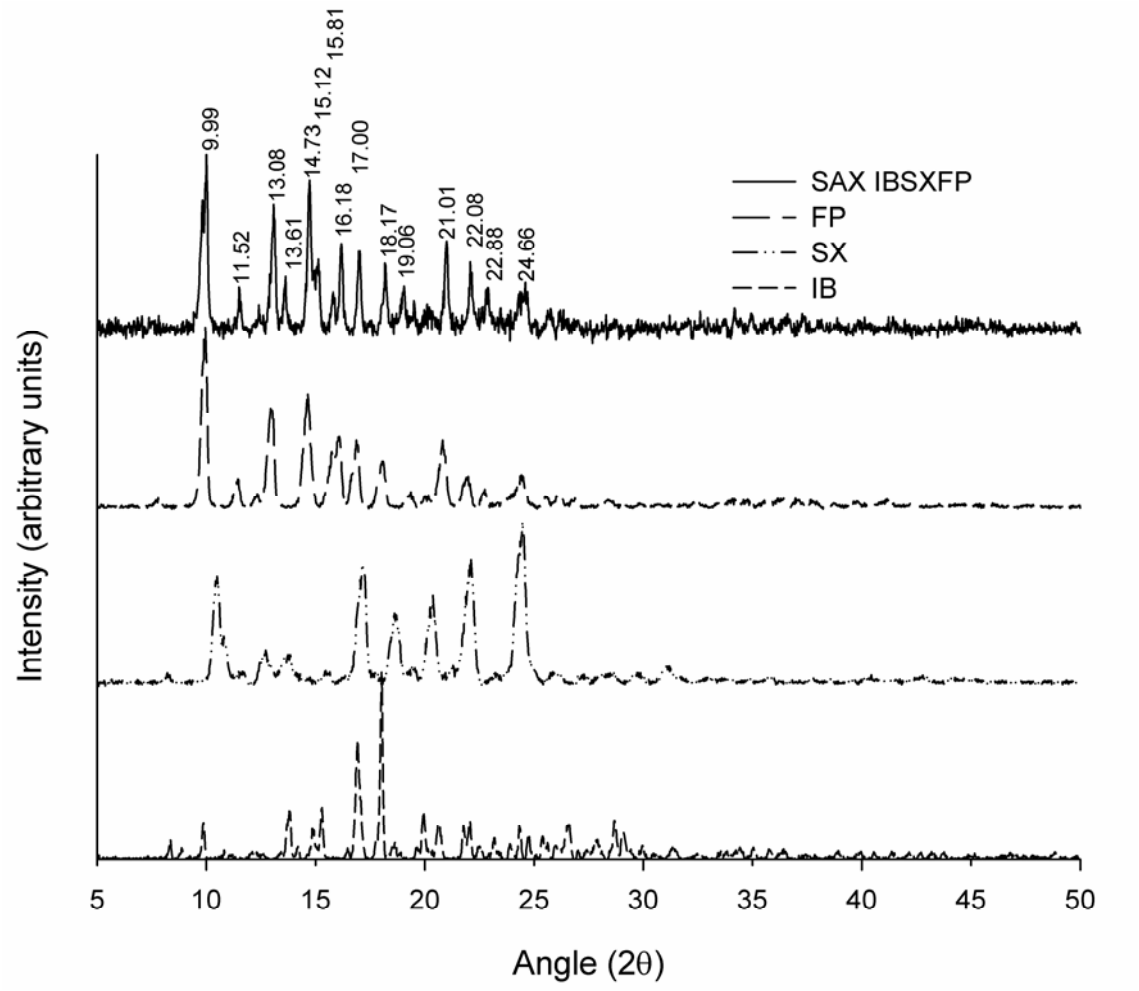

Figure 3.10:XRPD Difractogran for SAX engineered IB:SX:FP (1:1.25:12.5 by mass) particles compared to raw materials.

The lack of peaks representing SX was also seen by Pitchayajittipong *et.al* in the SX:FP 1:10 particles produced by SAX (Pitchayajittipong, Shur et al. 2009). These data suggest that the amount of FP within the sample has the greatest impact on the XRPD with the other compounds of insufficient concentration to be able to produce peaks of sufficient intensity to show up in the diffractogram.

Pitchayajittipong *et.al* were able to demonstrate the presence of SX within the sample via the use of DSC analysis (Pitchayajittipong, Shur et al. 2009). However, the DSC trace for the SAX engineered IB:SX:FP particles did not demonstrate any endothermic responses, indicative of a melt, over the entire heating range, as depicted in Figure 3.11. In addition to this, a total of five exothermic responses could be seen: the first at 88.24°C; second at 199.72°C; third at 261.79°C which flows into 4th at 279.25°C which is immediately followed by the fifth at 290.34°C. These could indicate the re-

crystallisation of a material. However, if this was the case, then an endothermic melt would have been expected at a higher temperature after the re-crystallisation.

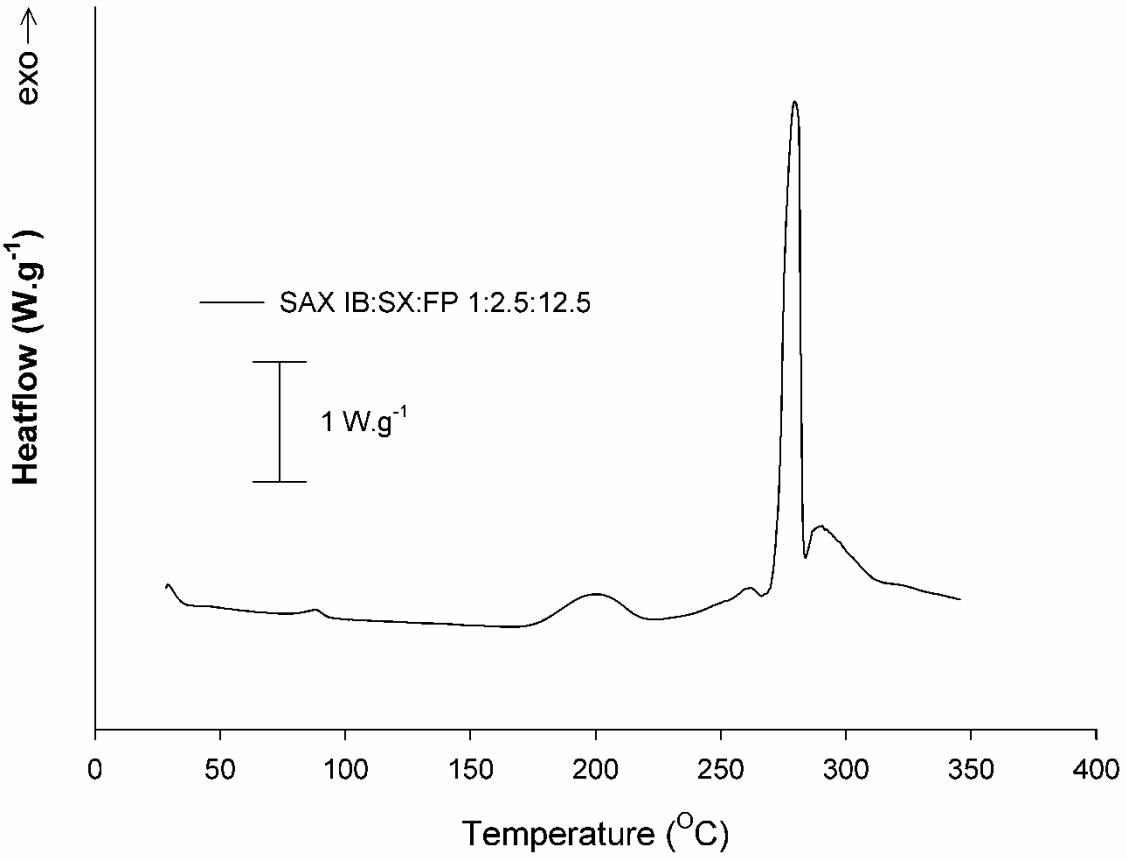

Figure 3.11: DSC thermogram for SAX engineered IB:SX:FP (1:1.25:12.5 by mass) particles.

In addition, DSC analysis of the post-DVS material produced a similar DSC trace with the exception of the peak at 88.24°C. These data suggested that the exothermic response at 88.24°C may have been the re-crystallisation of the sample with the remainder of the DSC thermogram representing a true response of the sample to temperature.

A possible explanation for this could be due to the perfluorodecalin reducing the amount of energy transmitted to the liquid (I) from the ultrasonic probe due to its high density (1.917g.cm^{-3} at 25°C 1 atmosphere pressure), as seen in equation 3.3:

$$I = \frac{A^{*2}}{2\rho_f V_s} \qquad \text{Equation 3.3}$$

Where A^* is the amplitude of the wave, ρ_f is the density of the liquid and V_s is the velocity of sound in the liquid. This would result in a reduced amount of energy being available for nucleation and, therefore, the particles may not have had sufficient nucleation sites within the particle to allow for crystal growth resulting in amorphous formation (Botsaris and Mullins 1976; Mullin 1992; Shekunov and York 2000).

Figure 3.12 shows the particle size data for the SAX engineered IB:SX:FP particles compared to the micronised equivalent. The data is also summarised in table 3.3. The d_{10} data suggested that the particles are larger than the micronised particles and this continues with the d_{50}. However, the d_{90} shows that the SAX particles are smaller than the micronised IB. These data suggest that the SAX engineered particles may not be able to penetrate to the lower stages of the impactor as the micronised particles but the system appears to have provided better particle size control with the particles demonstrating a narrower distribution compared to the micronized compounds.

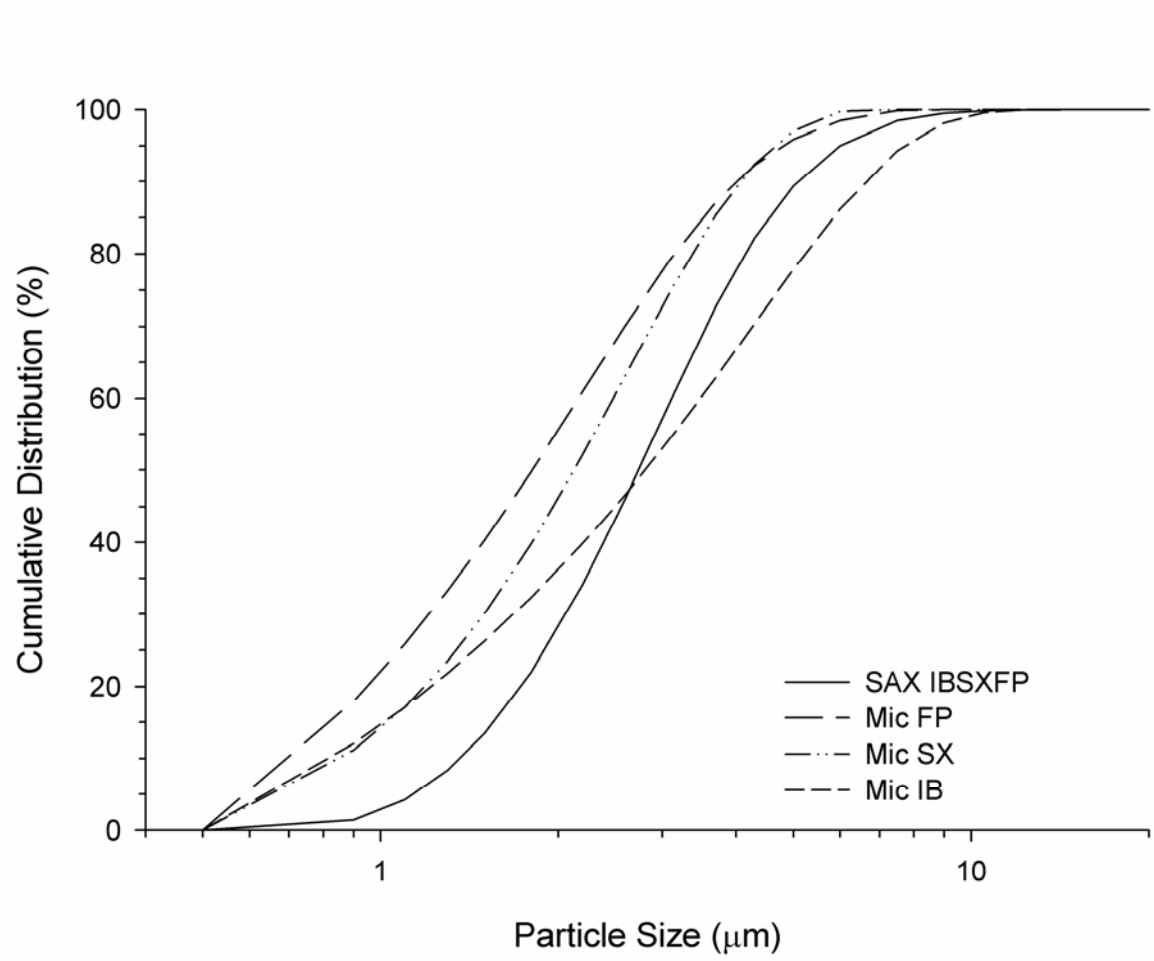

Figure 3.12: Particle size distribution of SAX produced IB:SX:FP 1:1.25:12.5 particles compared to micronised IB, micronised SX and micronised FP.

Table 3.3: Particle size distribution of micronised IB, micronised SX, micronised FP and SAX engineered IB:SX:FP 1:1.25:12.5 particles

	Particle Size (µm ± SD)		
	d_{10}	d_{50}	d_{90}
IB	0.83 ± 0.03	2.81 ± 0.10	6.71 ± 0.09
SX	0.86 ± 0.01	2.13 ± 0.01	4.10 ± 0.01
FP	0.72 ± 0.01	1.81 ± 0.01	4.03 ± 0.05
IBSXFP	1.34 ± 0.09	2.74 ± 0.12	5.12 ± 0.21

3.4.2 *In-vitro* performance of pMDI formulations containing IB, SX, FP

Figure 3.13 shows the fine particle fraction of the emitted dose (FPF_{ED}) for the SAX formulation pMDI compared to the micronised equivalent. These data, along with the mass deposited on each stage, emitted dose (ED), fine particle dose (FPD), the mass median aerodynamic diameter (MMAD) and the geometric standard deviation of the MMAD (GSD), are also represented in table 3.4.

Aerosolisation of the pMDI formulation containing micronised forms of the APIs resulted in significantly greater ($P<0.05$) amount of FP delivered to the lower stages of the ACI compared to the other compounds. This could be due to the micronised FP demonstrating a slightly smaller particle size distribution then the other compounds. There was no significant difference between the FPF_{ED} for micronised IB and micronised SX.

Compared to the micronised formulation, the SAX particles demonstrated a lower FPF_{ED} with the micronised IB and micronised FP demonstrating a significant ($P<0.05$) higher FPF_{ED} compared to the SAX formulation. These differences maybe related to the particle size distribution of the SAX particles, which were larger than the micronised particles, therefore resulting in greater deposition at the upper-stages of the impactor.

In addition, the FPF_{ED} for IB in the SAX formulation was lower than that for SX and FP within the SAX formulation. These data suggest that the IB was separated from the FP and SX either during formulation or during firing of the pMDI canister. There were no significant differences between the emitted dose across the formulations for IB or FP. However, the dose of SX emitted from the SAX formulation appears to be twice the calculated dose per shot. In order to normalise this result, all the graphs below show

the mass on each stage relative to the total amount of drug recovered (% of recovered dose, %RD)

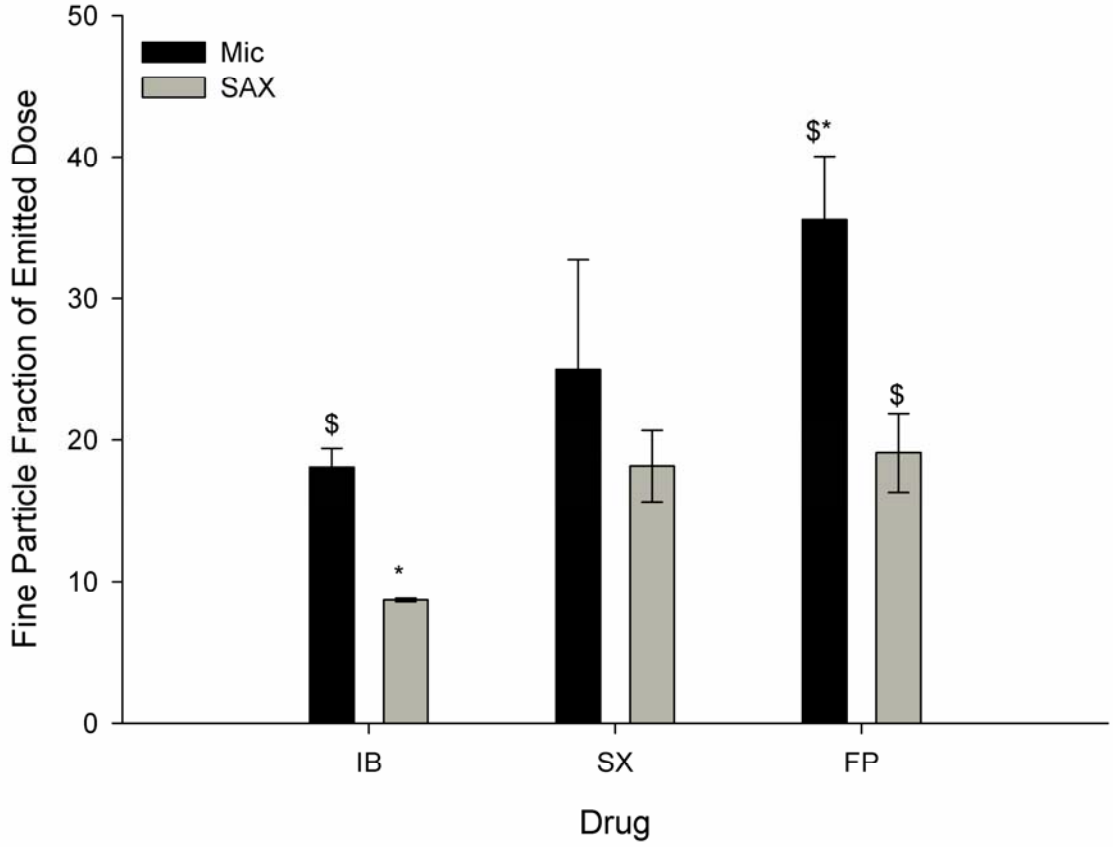

*Figure 3.13: Graphical representation of FPF_{ED} for all the compounds in both the SAX and micronised formulations. *=significant difference compared to compounds in same formulation $=significant difference across formulations (P<0.05)*

Table 3.4: ACI deposition per shoot of drug delivered from micronised IB:SX:FP 1:1.25:12.5 and SAX engineered IB:SX:FP 1:1.25:12.5 particles pMDI formulations;

IB=ipratropium bromide, SX=salmeterol xinafoate, FP=fluticasone propionate; MP&T= mouthpiece and throat; S=stage; F=filter.

Formulation	Drug	Mean Drug Deposition on Impactor Stages (µg±SD)											Mean ED (µg±SD)	Mean FPD (µg±SD)	Mean FPF_{ED} (%±SD)	MMAD µm (GSD)
		Device	MP &T	S0	S1	S2	S3	S4	S5	S6	S7	F				
Micronised	IB	8.64 ± 0.34	19.02 ± 0.53	2.56 ± 1.19	4.85 ± 0.33	3.61 ± 0.29	4.42 ± 0.24	1.71 ± 0.14	0.42 ± 0.11	0.03 ± 0.00	0.02 ± 0.01	0.01 ± 0.01	36.6 ± 1.5	6.6 ± 0.2	18.1 ± 1.3	5.55 (1.82)
	SX	9.53 ± 1.22	20.22 ± 2.23	2.91 ± 0.73	3.52 ± 0.64	3.84 ±0.63	4.82 ± 3.60	4.22 ± 0.60	1.38 ± 0.12	0.11 ± 0.02	0.00 ± 0.01	0.00 ± 0.00	41.0 ± 6.0	10.5 ± 4.3	25.0 ± 7.7	4.67 (1.74)
	FP	24.20 ± 2.22	148.47 ±34.83	22.26 ± 3.08	25.97 ± 3.81	29.05 ± 7.59	54.61 ± 3.99	44.64 ± 2.95	17.43 ± 4.42	3.88 ± 0.28	1.72 ± 0.14	0.68 ± 1.18	348.7 ± 40.0	123.0 ± 4.0	35.6 ± 4.5	3.95 (2.14)
SAX	IB	8.84 ± 0.63	17.84 ± 0.66	9.55 ± 0.78	2.74 ± 0.21	1.32 ± 0.04	1.51 ± 0.06	0.86 ± 0.07	0.44 ± 0.11	0.07 ± 0.02	0.04 ± 0.03	0.07 ± 0.04	34.4 ± 1.8	3.0 ± 0.1	8.7 ± 0.1	14.45 (3.42)
	SX	25.37 ± 1.01	48.85 ± 1.72	17.05 ± 1.26	12.48 ± 1.39	8.52 ± 1.21	8.68 ± 2.59	4.88 ± 0.96	3.90 ± 0.81	1.40 ± 0.29	0.40 ± 0.09	0.20 ± 0.00	106.4 ± 9.9	19.5 ± 4.6	18.1 ± 2.5	6.48 (2.65)
	FP	73.70 ± 8.15	148.36 ±15.35	53.98 ± 2.49	47.91 ± 2.39	33.19 ± 4.24	32.88 ± 8.51	17.96 ± 3.58	11.94 ± 2.99	3.80 ± 2.05	0.49 ± 0.84	0.69 ± 1.19	351.2 ± 37.3	67.8 ± 16.6	19.1 ± 2.8	6.44 (2.52)

Figure 3.13 shows the amount of drug deposited on each stage as a function of recovered dose, while Figure 3.14 shows the deposition profile only stages 0 to filter. The micronised formulation demonstrated a consistent dose ratio between SX and FP between the mouthpiece and stage 3 inclusive with IB only being deposited in a significantly ($P<0.05$) greater amount on stage 1. After stage 4, the dose ratio was variable.

The SAX formulation delivered a consistent ratio between SX and FP on almost all of the stages (except stages 2 and 7) form the mouthpiece onwards. The amount of IB, however, was generally lower on all of the stages, except for stage 0. This may indicate that the IB may have fractured from the rest of the particles during the formulation stage.

These data are also represented in figure 3.15 showing a normalised ratio of the %RD for all the drugs on stages 0 to filter. As can be seen, the relative ratio of IB, SX and FP appears to be consistent between stages 1 and 5 with the amount of IB varying for the other stages.

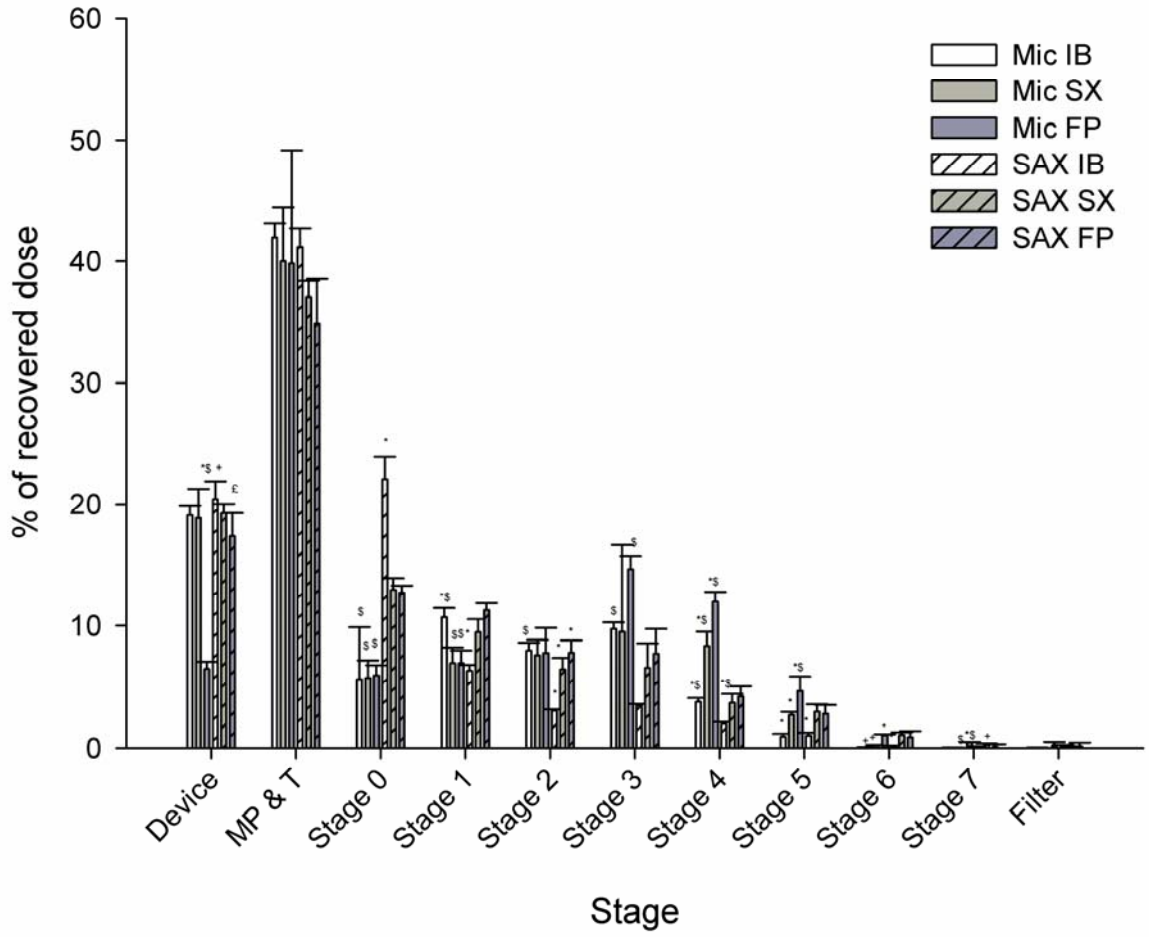

Figure 3.14: Graphical representation of the percentage of recovered dose (RD) collected on each stage of the ACI.=significant difference from other compounds in the same formulation, $=significant difference between same drug in different formulations, £=significant difference from $\%RD_{IB}$ in the same formulation, #=significant difference from $\%RD_{SX}$ in the same formulation and +=significant difference in $\%RD_{FP}$ in the same formulation (all $P<0.05$)*

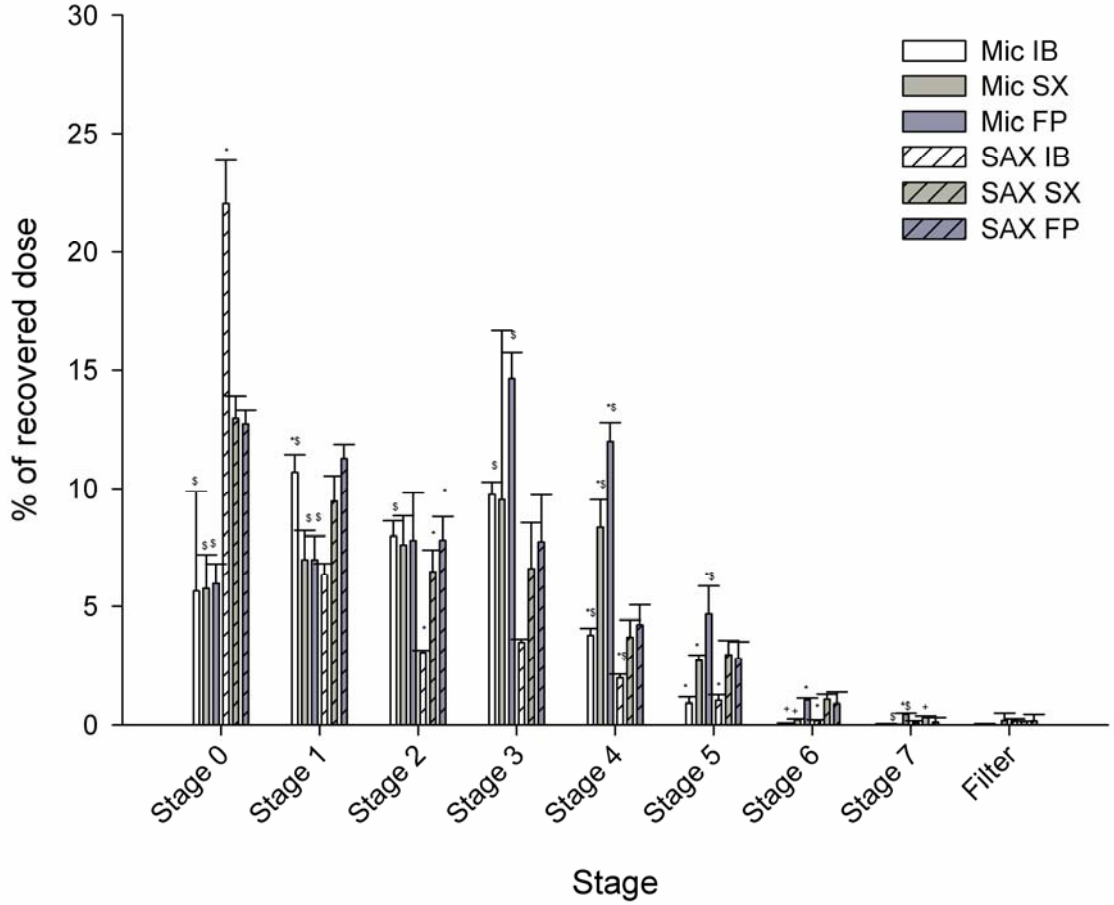

Figure 3.15: Graphical representation of the percentage of recovered dose (RD) collected on stages 0 to filter of the ACI.=significant difference from other compounds in the same formulation, $=significant difference between same drug in different formulations, £=significant difference from $\%RD_{IB}$ in the same formulation, #=significant difference from $\%RD_{SX}$ in the same formulation and +=significant difference in $\%RD_{FP}$ in the same formulation (all $P<0.05$)*

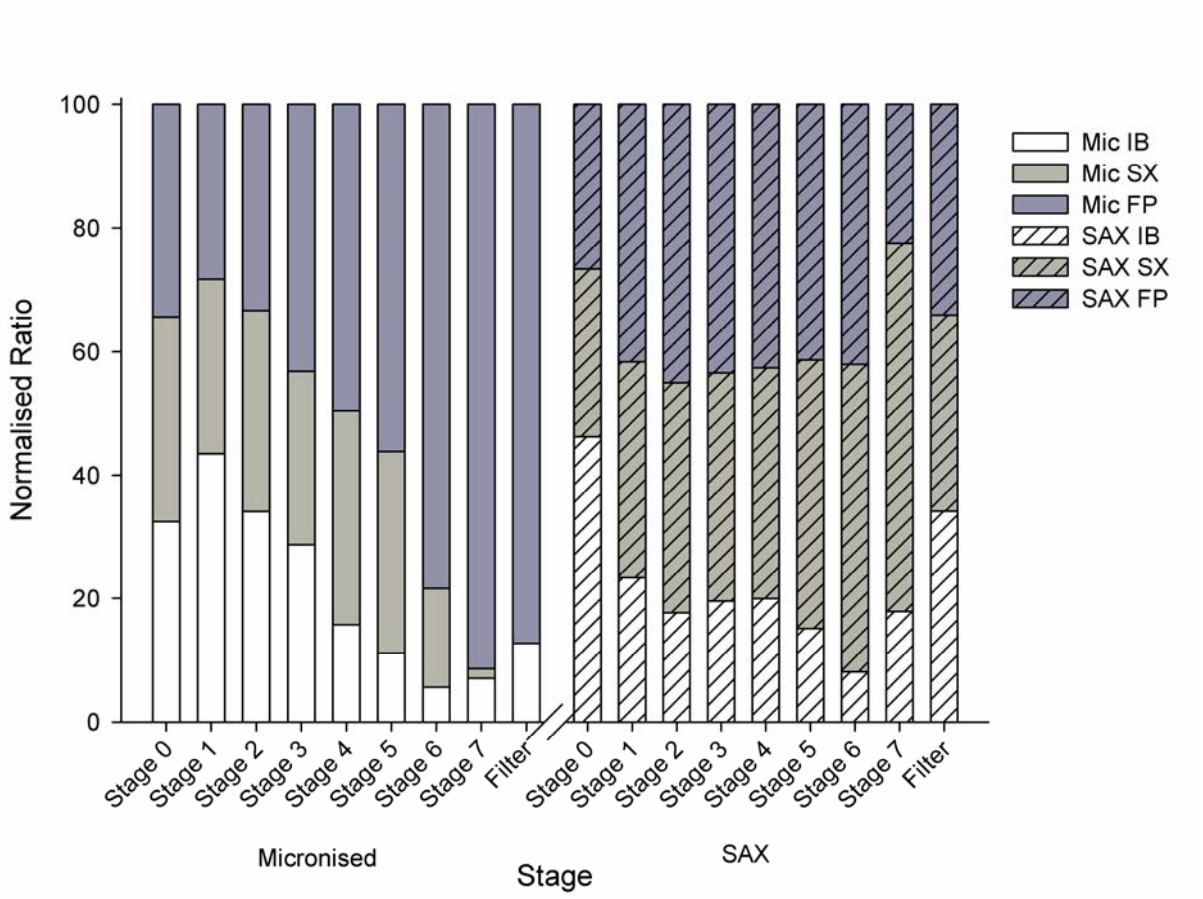

Figure 3.16:Graphical representation of the ratio between the %RD for each drug between stage 0 and filter of the ACI for both formulations.

3.4.3. *In-vitro* performance of DPI formulations containing IB, SX, FP

Table 3.5 shows the mass deposited on each stage of the NGI, as well as the content uniformity, emitted dose (ED), fine particle dose (FPD), the mass median aerodynamic diameter (MMAD) and the geometric standard deviation of the MMAD (GSD) for both formulations. Neither formulation produced demonstrated a formulation where all of the compounds had a CV <6%. However, it should be noted, that the CV for the SAX formulation were similar, while those for the micronised formulation varied dramatically.

Figure 3.16 shows the FPF_{ED} of IB, SX and FP from the micronised and SAX formulations. As can be seen, the micronised formulation demonstrated a significant difference between all three compounds within the formulation with SX demonstrating the greatest FPF_{ED} and IB the lowest. All of the drugs in the micronised formulation had significantly different ($P<0.05$) FPF_{ED} values. In addition, the FPF_{ED} did not differ across the formulations except for SX which showed a significantly ($P<0.05$) greater FPF_{ED} in the micronised formulation compared to the SAX. There was no significant difference in the FPF_{ED} between the drugs in the SAX formulation.

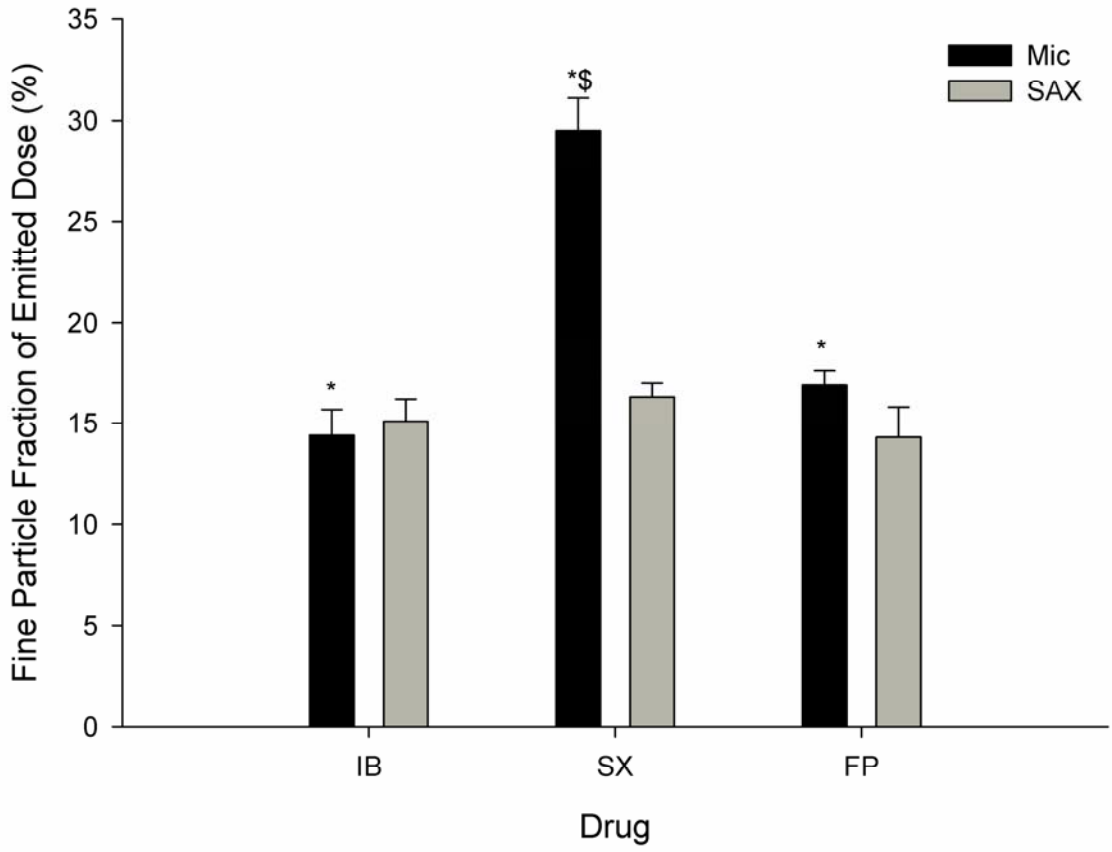

*Figure 3.17: Fine particle fraction of the emitted dose from the micronised and SAX formulations. *=significantly different (P<0.05) from others in formulation $= significantly different (P<0.05) from other formulation*

Table 3.5: NGI deposition per shoot of drug delivered from micronised IB:SX:FP 1:1.25:12.5 and SAX engineered IB:SX:FP 1:1.25:12.5 particles DPI formulations;

IB= ipratropium bromide, SX=salmeterol xinafoate, FP=fluticasone propionate; C&D= Capsules and Device; MP&T= mouthpiece and throat; PS=Pre-separator; S=stage; MOC= micro orifice collector.

Formulation	Drug	Mean Drug Deposition on Impactor Stages												Mean ED (µg±SD)	Mean FPD (µg±SD)	Mean FPF_{ED} (%±SD)	MMAD µm (GSD)
		CV (%)	C&D	MP &T	PS	S1	S2	S3	S4	S5	S6	S7	MOC				
Micronised	IB	10.06	9.99 ± 3.20	8.60 ± 1.31	15.75 ± 1.65	2.99 ±0.17	3.62 ±0.08	2.51 ±0.04	1.86 ±0.05	0.63 ±0.06	0.14 ±0.02	0.03 ±0.01	0.00 ±0.00	21.68 ± 1.75	3.10 ± 0.25	14.4 ± 1.28	4.19 (2.19)
	SX	36.45	11.25 ±1.63	3.44 ± 1.11	18.08 ±1.81	0.91 ±0.03	2.34 ±0.11	3.22 ±0.23	4.13 ±0.13	2.18 ±0.28	0.62 ±0.06	0.18 ±0.03	0.00 ±0.00	21.05 ± 2.10	6.20 ± 0.39	29.5 ± 1.60	2.33 (1.94)
	FP	0.85	93.86 ± 8.56	48.16 ± 4.06	304.93 ±15.13	12.65 ±1.92	28.63 ±1.28	33.52 ±2.51	31.57 ±1.52	12.02 ±1.06	2.38 ±0.40	0.51 ±0.19	0.00 ±0.00	284.62 ± 12.52	48.00 ± 2.82	16.9 ± 0.71	2.86 (1.71)
SAX	IB	13.09	7.54 ±3.11	5.58 ±0.83	9.65 ±0.28	2.65 ±0.05	3.34 ±0.10	1.97 ±0.08	1.15 ±0.08	0.49 ±0.05	0.14 ±0.01	0.03 ±0.02	0.01 ±0.00	15.00 ± 0.66	2.27 ± 0.13	15.1 ± 1.06	4.60 (2.34)
	SX	13.12	5.15 ±1.44	3.59 ±0.38	5.92 ±0.64	1.82 ±0.17	2.26 ±0.20	1.38 ±0.19	0.81 ±0.10	0.34 ±0.06	0.10 ±0.02	0.02 ±0.02	0.00 ±0.00	9.75 ± 0.97	1.59 ± 0.22	16.3 ± 0.67	4.07 (1.93)
	FP	10.51	35.04 ±18.85	46.15 ±14.72	107.40 ±6.83	30.84 ±0.46	27.25 ±0.63	15.66 ±0.58	10.57 ±0.43	6.00 ±0.33	2.43 ±0.19	0.43 ±0.39	0.00 ±0.00	148.03 ± 11.74	21.05 ± 1.00	14.3 ± 1.46	4.93 (2.79)

Figure 3.17 shows the %RD of each drug on all stages of the NGI with stages 1 to MOC being highlighted in Figure 3.18. There were very few differences between the formulations. Regardless of which stage is looked at, there appears to be at least one compound which demonstrates a significant difference to the %RD of the other compounds. The exceptions are the mouth piece and throat and stage 4 for the SAX formulation where all three compounds appear to have the same %RD.

The relative ratio of the %RD for each drug in both formulations can also be seen in Figure 3.19. The variation between the %RD for the drugs in the SAX formulation on each stage, was small in comparison to the micronised preparation.

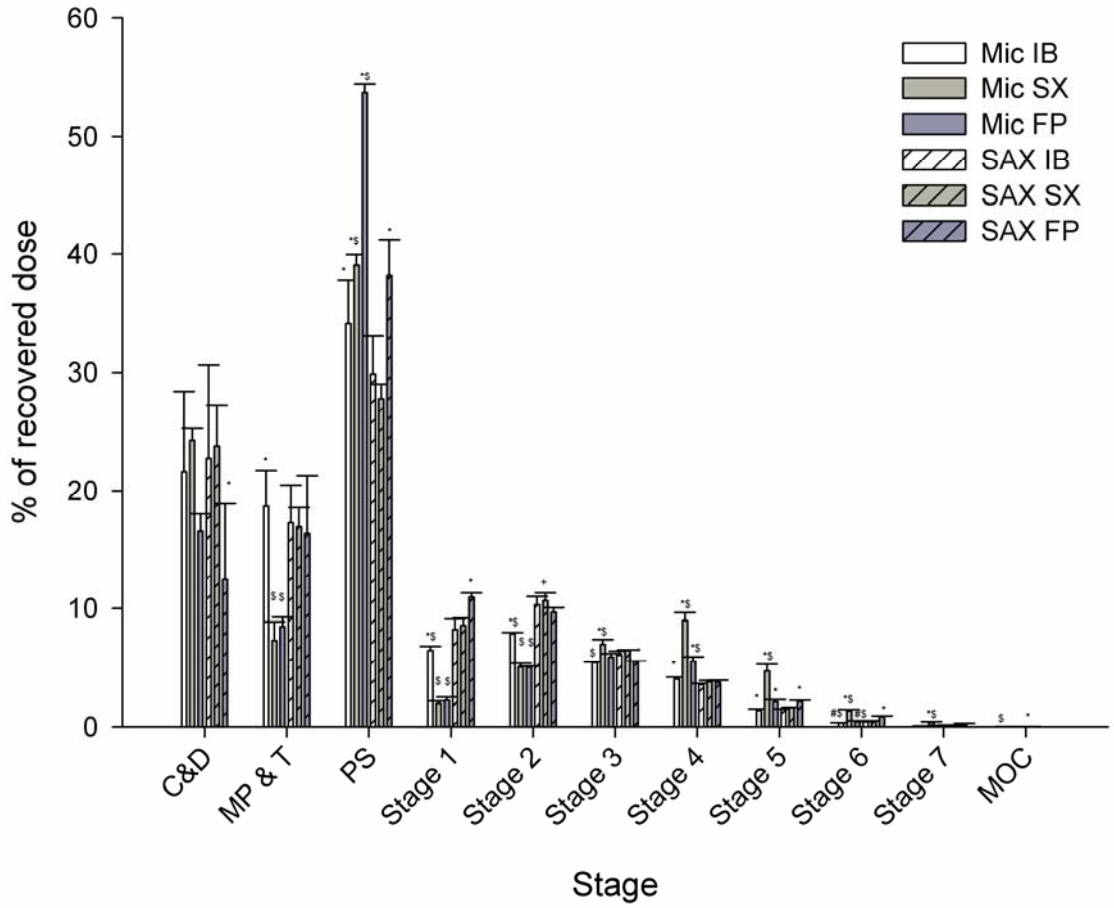

Figure 3.18: Graphical representation of the percentage of recovered dose (%RD) collected on each stage of the NGI.=significant difference from other compounds in the same formulation, $=significant difference between same drug in different formulations, £=significant difference from $\%RD_{IB}$ in the same formulation, #=significant difference from $\%RD_{SX}$ in the same formulation and +=significant difference in $\%RD_{FP}$ in the same formulation (all $P<0.05$)*

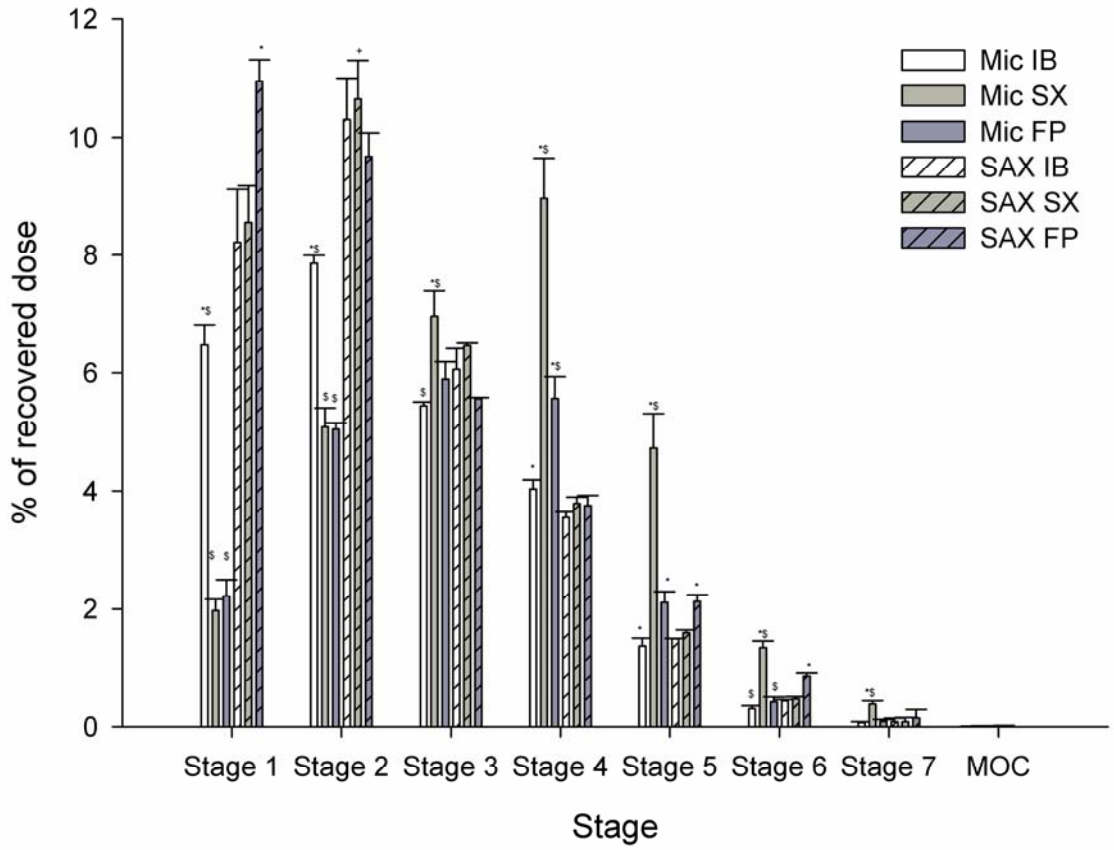

Figure 3.19: Graphical representation of the percentage of recovered dose (%RD) collected on each stage of the NGI.=significant difference from other compounds in the same formulation, $=significant difference between same drug in different formulations, £=significant difference from $\%RD_{IB}$ in the same formulation, #=significant difference from $\%RD_{SX}$ in the same formulation and +=significant difference in $\%RD_{SX}$ in the same formulation (all $P<0.05$)*

These data suggest that the amorphous content along with the shearing action of formulating the SAX particles, may have caused slight separation of the drugs during the formulation process but made very little difference to the final delivered ratio (Begat, Morton et al. 2004; Price 2005; Jones, Harris et al. 2008).

These data also indicacted that the processing of multiple drug component formulations via SAX allows for a more consistent dosing compared to conventional methods. As a result, the patient may benefit from the addition of an anti-muscarinic compound to a LABA and ICS without further complicating their regime (Rodrigo and Rodrigo 2003; Aaron, Vandemheen et al. 2007; Singh, Brooks et al. 2008).

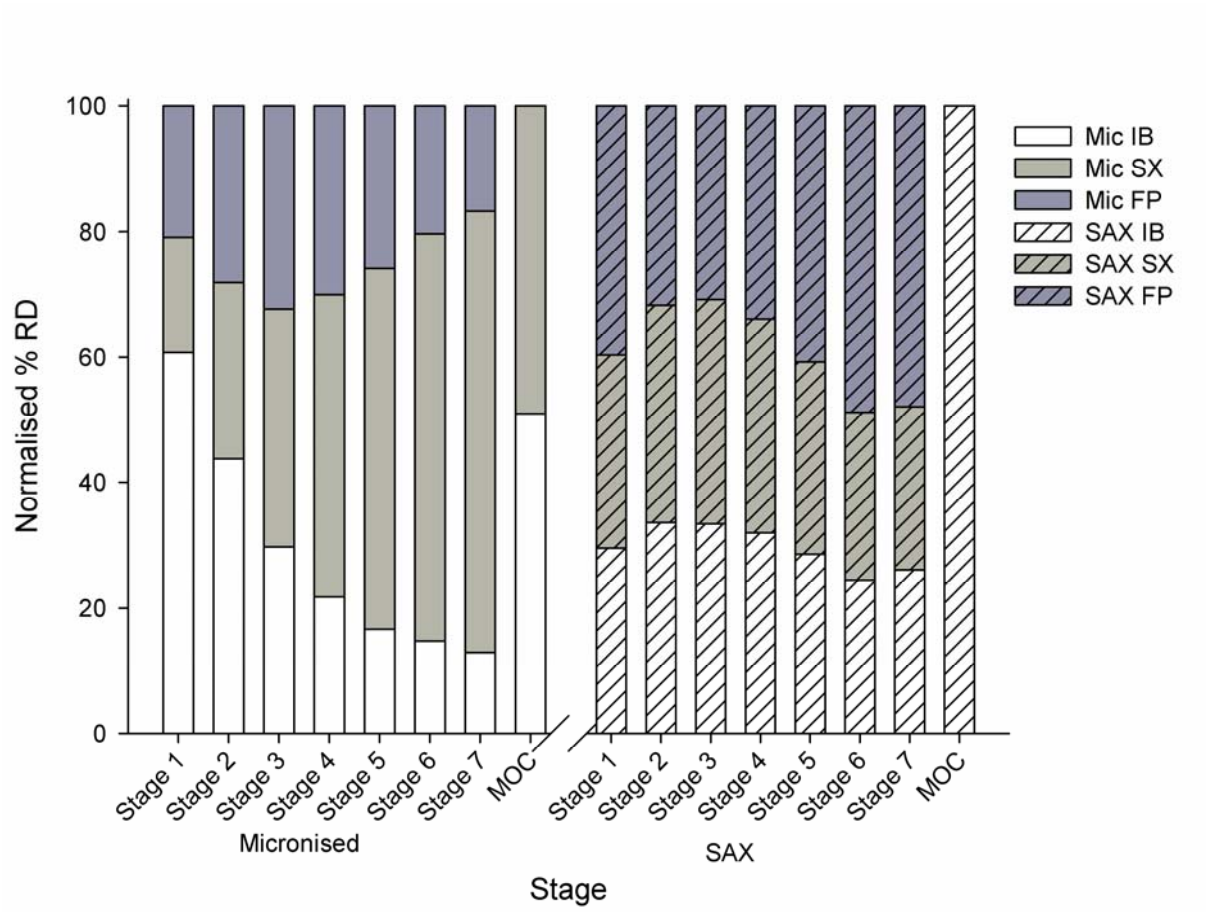

Figure 3.20:Graphical representation of the ratio between the %RD for each drug between stage 0 and filter of the NGI for both formulations.

3.5 Conclusion

The SAX process can be used to make particles that contain three different drug ingredients at varying concentration. However, the solvent selected must be volatile enough to ensure the droplets are highly viscous on reaching the anti-solvent. In addition, the anti-solvent may need to be of as low a density as possible in order to allow for maximal energy to be transferred to the particles to aid crystallisation.

Despite slight variations, the SAX process can be used to produce particles that contain a long acting β_2-agonist, an inhaled corticosteroid and an anti-muscarinic compound that, once formulated, allow for all three compounds to be co-deposited for synergistic action.

Chapter 4 - Combination of ICS and Theophylline for the Treatment of COPD

4.1 Introduction

4.1.1 Pathophysiology of COPD

Chronic obstructive pulmonary disease (COPD) is a complex disease condition of the lungs. According to the latest World Health Organisation (WHO) estimates, approximately 210 million have COPD (Halbert, Natoli et al. 2006) with WHO estimates suggesting that the disease will become the third commonest cause of death by 2030 (Lopez and Mathers 2006). With limited treatment options to slow the relentless progression of the disease, COPD constitutes a serious public health problem in all countries throughout the world (Bousquet, Dahk et al. 2007).

In developed countries, cigarette smoking is by far the commonest cause of COPD, but there are several other risk factors, including air pollution, poor diet and occupational exposure (Barnes, Shapiro et al. 2003). Cigarette smoke can activate macrophages, causing a drastic increase in the numbers found in the airways of COPD patients (Barnes 2004). Activated macrophages secrete many inflammatory proteins, such as IL-8 and NF-κB, which orchestrate the inflammatory response in COPD (Barnes, Shapiro et al. 2003; Barnes 2004; Barnes 2008).

The NF-κB is responsible for the up-regulation of many of the inflammatory proteins found in COPD patients, while IL-8 acts as a chemo-attractant that results in the infiltration of neutrophils into the lungs (Keatings, Jatakanon et al. 1997; Caramori and Adcock 2003; Barnes 2004; Barnes 2008). Finally, the macrophages also secrete elastase that can contribute towards the destruction of the alveoli (Barnes 2000; Caramori and Adcock 2003; Barnes 2004; Barnes 2008). The neutrophils that are attracted to the site of inflammation by IL-8 have been found to produce serine proteases which can also lead to the destruction of the alveoli walls (Barnes 2004). The same serine proteases have also been found to induce mucus secretion, resulting in the formation of a thick mucus plug (Barnes 2004). Neutrophils also release IL-8 and so may heighten the infiltration of more neutrophils to the site of inflammation (Barnes 2004).

4.1.2 Treatment Options to Control Inflammation.

Glucocorticoids are mainly used in the treatment of inflammatory diseases. Long term treatment with either oral or inhaled steroids in COPD patients provides no long term benefit, except for about 10% of the COPD population who are thought to have concomitant asthma (Barnes 2000; Caramori and Adcock 2003; Barnes 2008).

ICS work by activating the glucocorticoid receptor (GR) within cells via the disassociation from inhibitory proteins and subsequent changes in the receptor complex (Adcock, Maneechotesuwan et al. 2002; Caramori and Adcock 2003; Adcock and Chung 2008; Barnes 2008). This complex can then act on gene transcription in several ways. The first being the direct inhibition of NF-κB production and, therefore, inhibiting the inflammatory effects of cytokines (Barnes, Pedersen et al. 1998; Adcock, Maneechotesuwan et al. 2002; Caramori and Adcock 2003). ICS's can also work by the recruitment of histone deacetylase 2 (HDAC2) which act to result in the deacetalyation of the gene resulting in the suppression of gene transcription (Barnes 1998; Adcock, Maneechotesuwan et al. 2002; Barnes 2005).

The increased oxidative and nitrative stress caused by cigarette smoke may have reduced the activity and expression of HDAC2 in COPD patients (Barnes, Ito et al. 2004; Barnes and Stockley 2005; Ito, Ito et al. 2005; Barnes 2006; Ito, Yamamura et al. 2006; Barnes 2008; Barnes 2008). As a result, steroids have little or no effect at reducing inflammation in COPD patients.

Theophylline (THE) is a xanthine compound that has been used in the past as a bronchodilator. However, its use has gradually reduced over time due to its narrow therapeutic window and vast side-effect profile. Despite this, it is still used in the treatment of severe asthma.

Recent work has found that THE can be used by asthmatic patients, in combination with an ICS, to have the same effect as increasing the ICS dose at levels lower than that needed for bronchodilation (Barnes and Pauwels 1994; Ukena, Harnest et al. 1997; Barnes and Woolcock 1998; Markham and Faulds 1998; Lim, Jatakanon et al. 2000; Lim, Tomita et al. 2001). This is thought to be due to the activation of HDAC2 (Barnes and Pauwels 1994; Ito, Lim et al. 2002; Cosio, Tsaprouni et al. 2004; Barnes 2006). From this, it could be hypothesised that the combination delivery of a xanthine molecule, such as THE, and an ICS may restore some anti-inflammatory effect in patients with COPD

4.1.3 SAX Process

Solution Atomisation and Xrystallisation by Sonication (SAX™) has been designed as a 'bottom-up' process for producing crystalline particles with a defined particle size distribution (Kaerger and Price 2004; Pitchayajittipong, Shur et al. 2009). The SAX process consists of three processes: 1) atomisation of a solute in an appropriate solvent; 2) evaporation of the solvent resulting in a highly viscous, supersaturated droplet and; 3) collection of the droplets in an appropriate non-solvent using sonication to induce crystallisation (Kaerger and Price 2004; Pitchayajittipong, Shur et al. 2009).

The solution to be atomised would consist of a solute dissolved close to its saturation point in a highly volatile solvent. When atomised, this would result in a short drying time before the supersaturated droplet is formed and therefore a short time of flight before reaching the non-solvent will be sufficient. If the solvent has a lower vapour pressure or the solution is under-saturated, the droplets may not be supersaturated by the time they reach the non-solvent. In this situation, the solute will have sufficient time to agglomerate with another droplet before being crystallised and therefore particle size control could be lost.

Atomisation can be conducted by any suitable atomiser. The lab scale SAX system uses pneumatic atomisation as these allow for the production of particles in the 1-5μm range and are therefore suitable for inhalation (Pitchayajittipong, Shur et al. 2009). Dry N_2 gas is purged through the system to produce a laminar flow and aid the evaporation of the solvent from the droplets. The gas purge also helps direct the super-saturated particles through a 'bubbler' tube into the non-solvent with the added benefit that positive pressure helps to produce particles with a smaller particle size distribution (Pitchayajittipong, Shur et al. 2009).

The non-solvent should be appropriate for the solute in question and ideally be miscible with the solvent. In addition, the non-solvent should have a low surface tension in order to have minimal effect on the structural shape of the droplet on collection. The temperature of the non-solvent is controlled in order to control the crystal growth kinetics with lower temperatures allowing for the spherical nature of the particles to be maintained (Pitchayajittipong, Shur et al. 2009).

Highly viscous droplets do not allow for rapid crystallisation due to their low molecular mobility (Hancock and Zografi 1997; Kaerger and Price 2004; Pitchayajittipong, Shur et al. 2009). Ultrasonic energy is employed to increase molecular mobility and reduce the metastable zone width in order to form a stable cluster of molecules for crystal growth (Lorimer and Mason 1987; Hancock and Zografi 1997; Kaerger and Price 2004; Ruecroft, Hipkiss et al. 2005; Ruecroft 2007; Pitchayajittipong, Shur et al. 2009).

4.1.4 Aim

Current inhaled corticosteroids (such as fluticasone and budesonide) may be ineffective in dealing with inflammation in the lungs of a COPD patient due to HDAC inactivity (Barnes 1999; Barnes, Ito et al. 2004; Barnes 2006; Cazzola and Matera 2008). However, research has suggested that the addition of a xanthine molecule (such as theophylline) may help to reverse this (Cosio, Tsaprouni et al. 2004; Barnes and Stockley 2005; Barnes 2006; Barnes 2008; Cazzola, Hanania et al. 2008).

For this to be effective, both theophylline and the inhaled corticosteroid will need to reach the target cell in sufficient concentrations. Previous work has shown that fluticasone propionate and salmeterol xinafoate can be engineered into one particle allowing for the co-deposition of both molecules in the correct ratio (Pitchayajittipong, Shur et al. 2009). This work will look at combining an ICS with theophylline in order to deliver both molecules together and to potentially reverse steroid resistance in COPD patients.

4.2 Materials

Micronised FP and BUD were obtained from sources stated in Chapter 2, as was THE and lactose. All organic solvents were of at least analytical grade and were supplied by Fisher Chemicals (Loughborough, UK). Water was prepared by MilliQ from reverse osmosis (Molsheim, France).

4.3 Methods

4.3.1 Engineering combination particles containing FP:THE and BUD:THE using the SAX-process

Combined SAX FP:THE or BUD:THE particles were prepared by atomisation of a 2% w/v solution containing either FP:THE or BUD:THE in the ratio 1:1 in dichloromethane: methanol 50:50 solvent. Atomisation was conducted using a SU11 co-axial two-fluid atomiser with an internal mix (Spraying Systems Co., Illinois, USA). The atomiser was used at a sprayed rate of 4 $ml.min^{-1}$ with air pressure at 2.5 bar in the lab scale of the SAX process over 60 cm of separation distance including positive pressure 30 $L.min^{-1}$ in the system with an ultrasonic probe. The particles were collected in perfluorodecalin at 5˚C, and the resulting combined SAX particles were isolated using supercritical CO_2 extraction of perfluorodecalin, as described earlier.

4.3.2. Formulation Production

4.3.2.1: Pressurised metered dose inhalers (pMDI's)

Drug-only pressurised metered dose inhaler (pMDI) formulations containing 0.30 % w/w of combination SAX particles of FP and THE was produced by weighing an appropriate amount of material into an aluminium canister (Bespak, King's Lynn, UK) before being sealed with a 50 µl metering valve (Bespak, King's Lynn, UK) and ~10g of HFA-134a (Ineos Fluor, Runcorn, UK) propellant being added. Drug only pMDI formulatons conataining 0.2% w/w of combination SAX particles of BUD and THE was produced in the sameway as the FP:THE formulation. The canisters were then sonicated for 20 minutes and allowed to stand for 24 hours before testing. An equivalent formulation containing either micronized FP or micronised BUD and micronised THE was also prepared.

4.3.2.2: Dry powder inhaler (DPI) formulation

A carrier based DPI formulation, containing 1.6% w/w combined SAX FP:THE or BUD:THE particles, was prepared by geometric blending with Respitose SV003 grade of lactose monohydrate. The combined SAX particles and SV003 lactose monohydrate were mixed in a 15 ml glass tube for 60 seconds in a Whirlimixer (Fisons Scientific Equipment, Loughborough, UK). The resultant blend was further processed using a Turbula shaker-mixer (Willy A Bachofen AG, Basel, Switzerland) at 46 rpm for 45 minutes.

In order to compare the *in-vitro* inhalation performance of SAX particles, a micronised combination formulation containing 0.8% w/w of either micronised FP or micronised BUD and 0.8% w/w micronised THE, (ratio 1:1), was prepared by geometric blending SV003 lactose monohydrate. The drug and SV003 lactose were mixed in a 15 ml glass tube for 60 seconds in a Whirlimixer (Fisons Scientific Equipment, Loughborough, UK). The resultant blend was then mixed using a Turbula shaker-mixer (Willy A Bachofen AG, Basel, Switzerland) at 46 rpm for 45 minutes. Both formulations containing either combined SAX particles or micronised equivalent blends were stored at 44 % RH and 25 °C for 24 h before formulation testing.

4.3.3 Content Uniformity Determination

Upon blending of the DPI formulation, the content uniformity of formulations in both studies (I and II) was assessed. Each blend was spread over a clean surface and ten samples of 25 $\pm$ 1 mg taken from random positions. Each sample was dissolved with 15 minutes sonication in 100 ml final volume of 25% 0.6% w/v aqueous ammonium acetate (Sigma-Aldrich, Gillingham, UK) 75% methanol and drug concentration

assessed by high performance liquid chromatography (HPLC). The proportion of drug in each sample was calculated and the content uniformity expressed as the coefficient of variation (see Chapter 3, Equation 3.1).

4.3.4 Capsule Filling

The DPI formulations were manually loaded into size 3 hydroxypropyl methylcellulose (HPMC) capsules (Qualicaps, Madrid, Spain). Fill weight was 25 $\pm$ 1 mg, giving a nominal dose of 100 $\pm$ 4 µg per drug per capsule for each formulations used. Following filling, capsules were stored in a sealed container containing a saturated solution of potassium carbonate, giving a relative humidity of 44% (Rockland 1960), for at least 24 hours prior to analysis.

4.3.5 *In-Vitro* Performance Analaysis

4.3.5.1 Andersen Cascade Impactor (ACI)

In-vitro pMDI performance was assessed using an Andersen cascade impactor (ACI, Copley Scientific, Nottingham, UK). Prior to assembly, each impaction plate was immersed in a 1% v/v solution of silicon oil (Acros Organics, Geel, Belgium) in hexane and allowed to air dry. The ACI (Copley Scientific, Nottingham, UK) was then assembled and connected to a vacuum pump (Gaast, Benton Harbour, MI, USA) *via* a solenoid valve. The flow rate at the inlet to the throat was set to 28.3 $L.min^{-1}$ using a digital flow meter with model DFM 2000 (Copley Scientific Ltd., Nottingham, UK).

For each analysis, the first five shoots of each pMDI were shaken vigorously for 10s and fired to waste. The manufactured pMDIs were inserted into a specially constructed mouthpiece and actuated in a fixed position. A 3s delay was employed, after the pump was engaged, to allow equilibrium of the pump before the actuator was pressed for 4s to allow sufficient time for firing. After this, the pump was allowed to continue for a further 5s before stopping the pump, as in chapter 3. Three consecutive doses, with vigorous shaking of the canister between each dose, for each formulation were released into the impactor.

The pMDI actuator, mouthpiece adaptor, throat assembly, collection plates from stage zero to seven and filter stage were thoroughly rinsed into suitable volumetric flasks with dilution solvent (75:25 (V/V) 0.6% w/v aqueous ammonium acetate:methanol) and made up to the mark. The actuator, mouthpiece adaptor, throat assembly and ACI collection plates were then washed in water and rinsed with distilled water followed by methanol, and dried at 40°C in an oven for 30 min. The ACI components were left to cool for 30 min, reassembled and re-used. For each formulation, ACI investigations

were carried out in triplicate. All samples were analysed by high performance liquid chromatography (HPLC), from which the mass of drug deposited on each stage could be determined.

The emitted dose (ED) was defined as the mass of drug recovered from all parts of the ACI and mouthpiece adaptor. The fine particle dose (FPD) was the mass of drug recovered from stage 3 and below of the ACI and the fine particle fraction (FPF_{ED}) was the FPD expressed as a percentage of the ED.

4.3.5.2 Next Generation Impactor (NGI)

In-vitro DPI performance was assessed using a Next Generation Impactor (NGI, Copley Scientific Ltd, Nottingham, UK). The NGI collection cups were immersed in a 1% v/v solution of silicone oil (Acros Organics, Geel, Belgium) in hexane and allowed to air dry. The NGI was then assembled with pre-separator (containing 15 ml of wash solvent) and connected to a vacuum pump (Gaast, Benton Harbour, MI, USA) *via* a solenoid valve. The flow rate at the inlet to the throat was set to 85 $L.min^{-1}$ using a digital flow meter with model DFM 2000 (Copley Scientific Ltd., Nottingham, UK). An aerolizer was attached to the throat of the NGI using a specially created mouthpiece. A capsule was inserted in the aerolizer and pierced by eight sharp pins within this aerolizer to generate four small holes at each end of the capsule. The contents of the capsule were then aerosolised into the NGI by drawing air through the apparatus at 85 $L.min^{-1}$ for 2.8 seconds (controlled by the solenoid valve). Once the contents of three capsules were aerosolised in this way, the device was disconnected, and capsules and each stage were thoroughly rinsed into suitable volumetric flasks with dilution solvent (75:25 (V/V) 0.6% w/v aqueous ammonium acetate:methanol) and made up to the mark. The concentration of drug in each solution was investigated by HPLC, from which the mass of drug deposited on each stage of the NGI could be determined at stages 1 to 7 and the MOC. Between experiments, the NGI was washed in water and methanol, dried in an oven, and allowed to cool to room temperature before re-use.

Each formulation was tested in triplicate. The emitted dose (ED) was defined as the mass of drug recovered from all parts of the NGI and the mouthpiece. The fine particle dose (FPD) was the mass of drug recovered from stage 3 and below of the NGI and the fine particle fraction (FPF_{ED}) was the FPD expressed as a percentage of the ED.

4.3.6 High Performance Liquid Chromatography

Drug concentrations were determined by HPLC. The HPLC system consisted of a PU-980 intelligent HPLC pump, an AS950 intelligent autosampler and a UV-975 inteligent UV/VIS detector (all from Jasco, Japan). Data were collected and analysed using Azur

v4.0 software (Datalys, Saint Martin D'Heres, France). Unknown sample concentration was determined from duplicate injections by comparison of peak area with reference peaks from external standard solutions of known concentration.

All studies were analysed using the same HPLC method. This employed a 4.6 mm x 150 mm C18(2) 5 µm Hypersil column (Phenominex, Macclesfield, Cheshire, UK) and a mobile phase consisting of 25% 0.6% w/v aqueous ammonium acetate 75% methanol. The flow rate was 1.5 $ml.min^{-1}$; with the injection volume of 100 µl. Drug retention times were 1.28, 3.42 and 3.87 minutes for THE, BUD and FP respectively, so a run time of 5 minutes was employed. UV detection wavelength was 228 nm.

The relationship between drug concentration (0.1, 1, 5, 10 and 50 $\mu g.ml^{-1}$) and peak area for each drug was found to be linear, with linear regression analysis yielding a coefficient of determination (R^2) of 1.0 for FP and BUD and 0.997 for THE (Figure 4.1). Calibration curves were produced prior to each experimental assay.

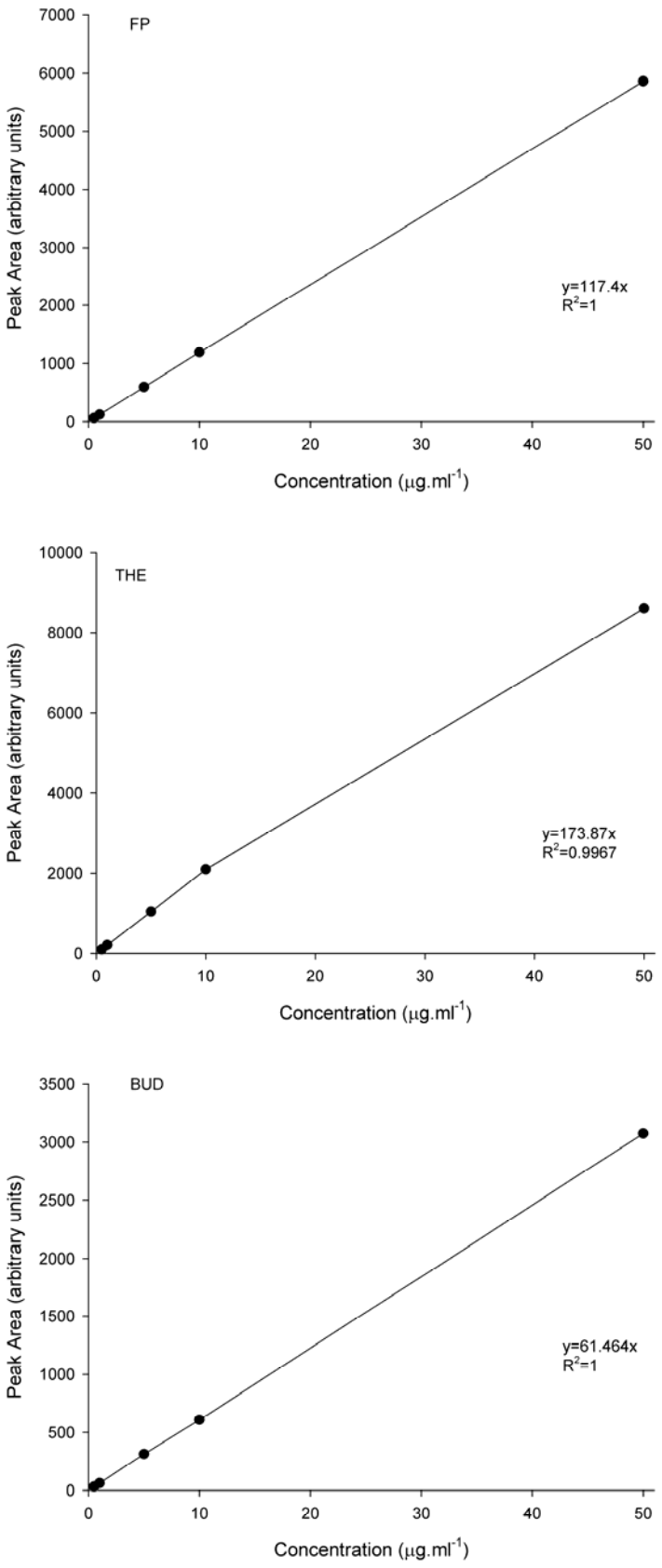

Figure 4.1: Representative HPLC calibration curves for FP, THE and BUD.

4.4 Results and Discussion

4.4.1 Physical characterisation

As for any crystallisation process, the solvent/anti-solvent combination can have a profound effect on the on the crystal morphology (Mullin 1992; Threlfall 2000). In addition, the SAX system allows for the temperature of the anti-solvent to be controlled. This can also have an effect on the particle morphology (Pitchayajittipong, Shur et al. 2009). As a result, the particles produced by the SAX process can look markedly different from micronised particles. Therefore, it is important to know how SAX can affect the morphology of a single drug on its own. Figure 4.2 shows the SEM micrograph images for micronised FP, BUD and THE compared to the SAX equivalent particles.

Micronised FP particles appear to be very small and of irregular shapes. Compared to this, the SAX FP particles appear to be more spherical and made up of a collection of flat plates twinned together. This is consistent with the spherical droplets being of a highly viscous nature when reaching the anti-solvent and the sonication having induced nucleation in many different points within the droplet.

Micronised BUD appears to be the same as micronised FP, however, the SAX processed BUD appears to be a collection of rectangular shaped crystals all joined together in the centre forming a roughly spherical nature.

Micronised THE appears to be larger than micronised FP and BUD and appears to form larger agglomerates compared to FP and BUD. SAX processed THE appears to be more plate-like that do not appear to form spherical agglomerates. This could suggest that the THE concentration in the solvent was not at saturation. Alternatively, the ethanol may have reduced the vapour pressure of dichloromethane sufficiently to prevent the formation of a highly viscous droplet before reaching the anti-solvent. Finally, the surface tension of the hexane may have been high enough to cause the droplet to flatten on impact (Pitchayajittipong, Shur et al. 2009).

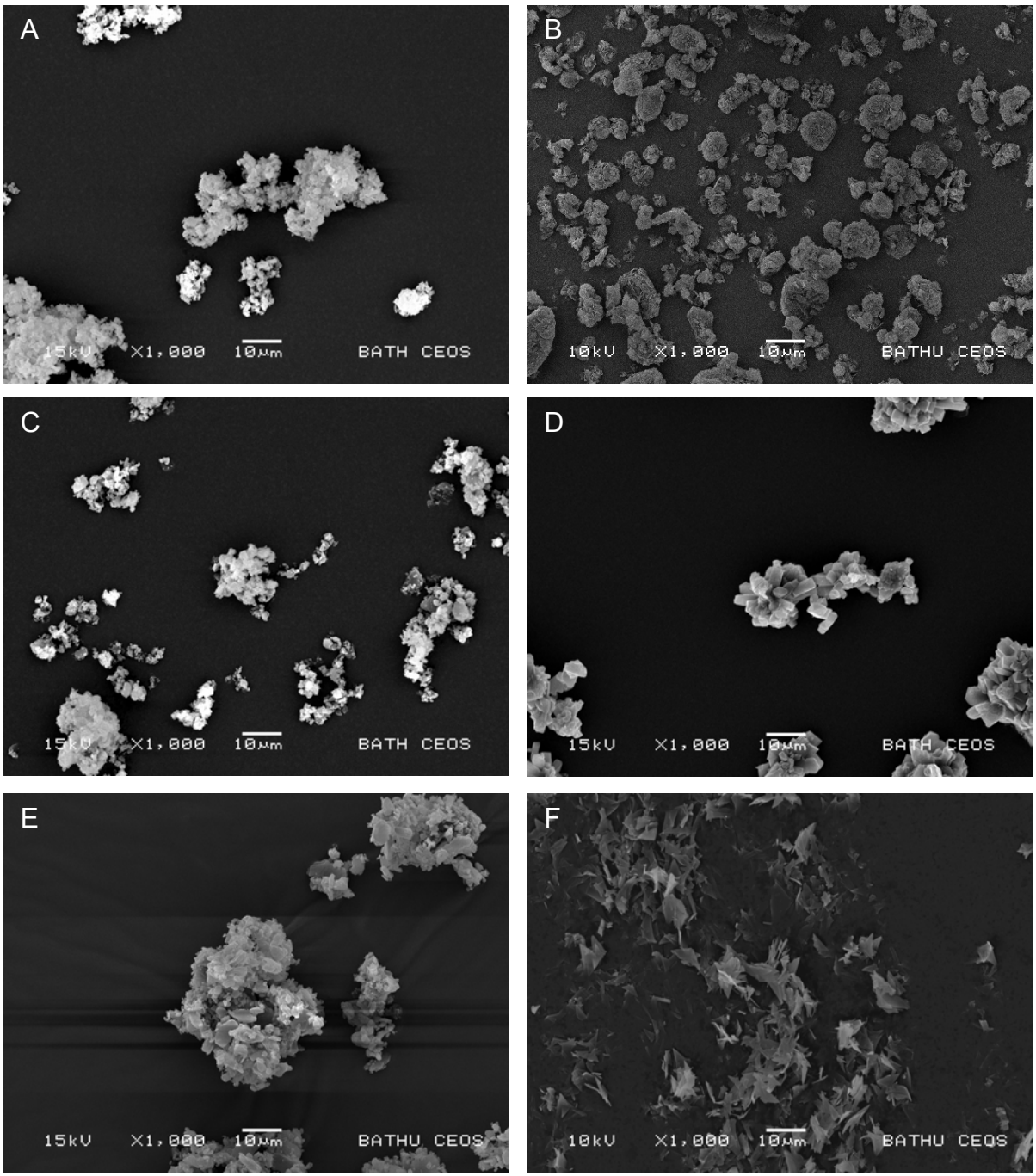

Figure 4.2: SEM micrograph images of micronised FP (a) SAX FP (b) micronised BUD (c) SAX BUD (d) Micronised THE (e) and SAX THE (f).

SAX produced particles containing THE with either FP or BUD are represented in figure 4.3. As shown, these appear to be vastly different from SAX FP, SAX BUD or SAX THE.

The SEM images of SAX produced FP:THE 1:1 show that the particles appear to form flat, needle shaped particles. Only one particle morphology can be seen. Even though the particles appear to be long needles, they may still be suitable for lung delivery (Pinkerton, Brody et al. 1983). In addition, all of the particles appear to be the same size.

In contrast, the SAX produced BUD:THE 1:1 particles appear to be a variety of different sizes, with some appearing to be larger than 10μm in length and others as small as 0.5μm. The particles all appear to be plate like in nature with the smaller particles forming agglomerates. These agglomerates may be difficult to separate, resulting in the production of larger particles, which may decrease the fine particle dose of the formulation.

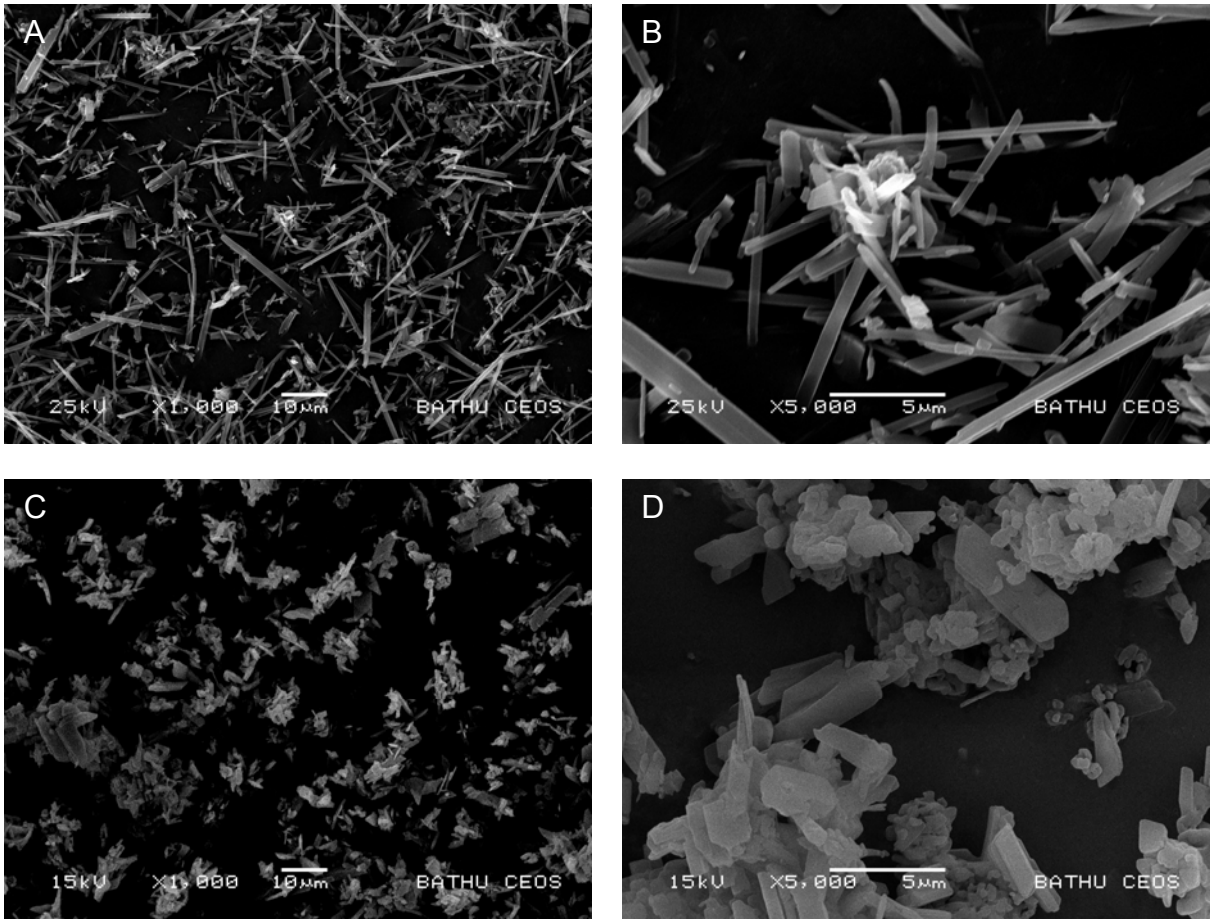

Figure 4.3: SEM micrograph images of SAX produced FP:THE 1:1 particles at 1000x (a) 5000x (b) magnification and SAX produced BUD:THE 1:1 particles at 1000x (c) and 5000x (d) magnification.

A graphical representation of the particle size distribution of the SAX produced FP:THE 1:1 particles compared to micronised FP and THE are shown in Figure 4.4 with the data being summarised in table 4.1. The particle size disribution of the SAX produced FP:THE 1:1 suggested a volume-weighted mediam diameter of 2.44 um. However, SEM analysis suggested that the FP:THE 1:1 particles are long needles with a length greater than 10μm. The descrepency between SEM and laser diffraction data may related to the fact the laser diffraction analysis of data fits the particle to an equivalent spherical diameter, and therefore the results are smaller than expected (Crower, Hickey et al. 2003; Shekunov, Chattopadhyay et al. 2007). The difference in the particle size ditribution between micronised FP and micronised THE suggest that the

1:1 mass ratio of FP:THE may not be maintained in the micronised formulation and therefore may separate out during aerosolisation resulting in THE not being available with the FP to reduce inflammation within the lungs.

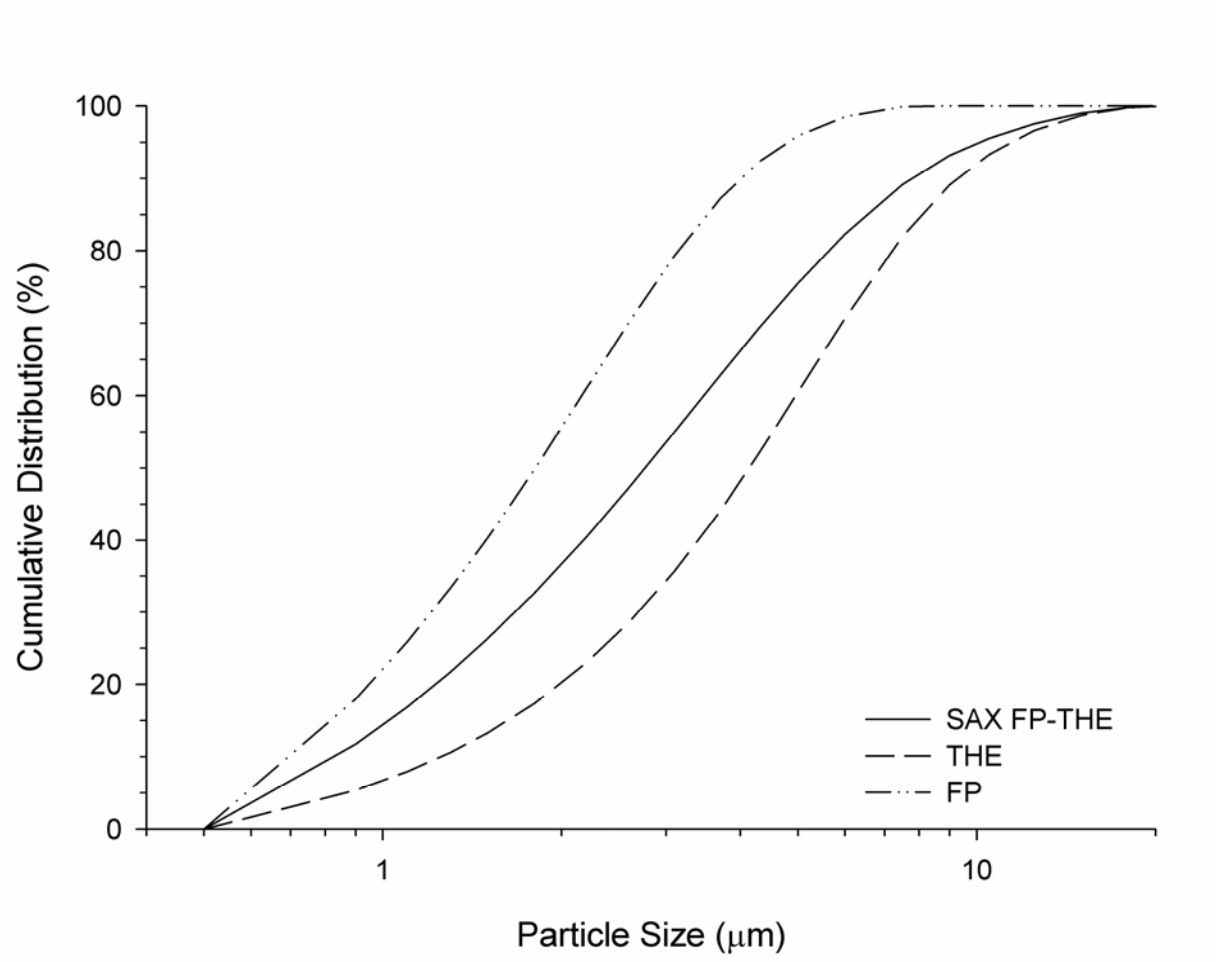

Figure 4.4: Particle size distribution of SAX produced FP:THE 1:1 particles compared to micronised FP and micronised THE.

Table 4.1: Particle size distribution of micronised THE, micronised FP and SAX engineered FP:THE 1:1 particles.

	Particle Size (μm) ±SD		
	d_{10}	d_{50}	d_{90}
THE	1.26 ± 0.02	4.15 ± 0.03	9.33 ±0.12
FP	0.72 ± 0.01	1.81 ± 0.01	4.03 ± 0.05
FP-THE	0.86 ± 0.08	2.77 ± 0.36	7.82 ± 0.45

Figure 4.5 shows a graphical representation of the particle size distribution of the SAX produced BUD:THE 1:1 particles compared to micronised BUD and THE with the data being summarised in table 4.2. As shown, the particle size distribution of the SAX produced BUD:THE 1:1 falls between that of micronised BUD and micronised THE.

The particle size distribution of BUD:THE has a smaller spread then that of FP:THE (~4µm between d_{10} and d_{90} for BUD:THE compared to ~7µm between d_{10} and d_{90} for FP:THE).

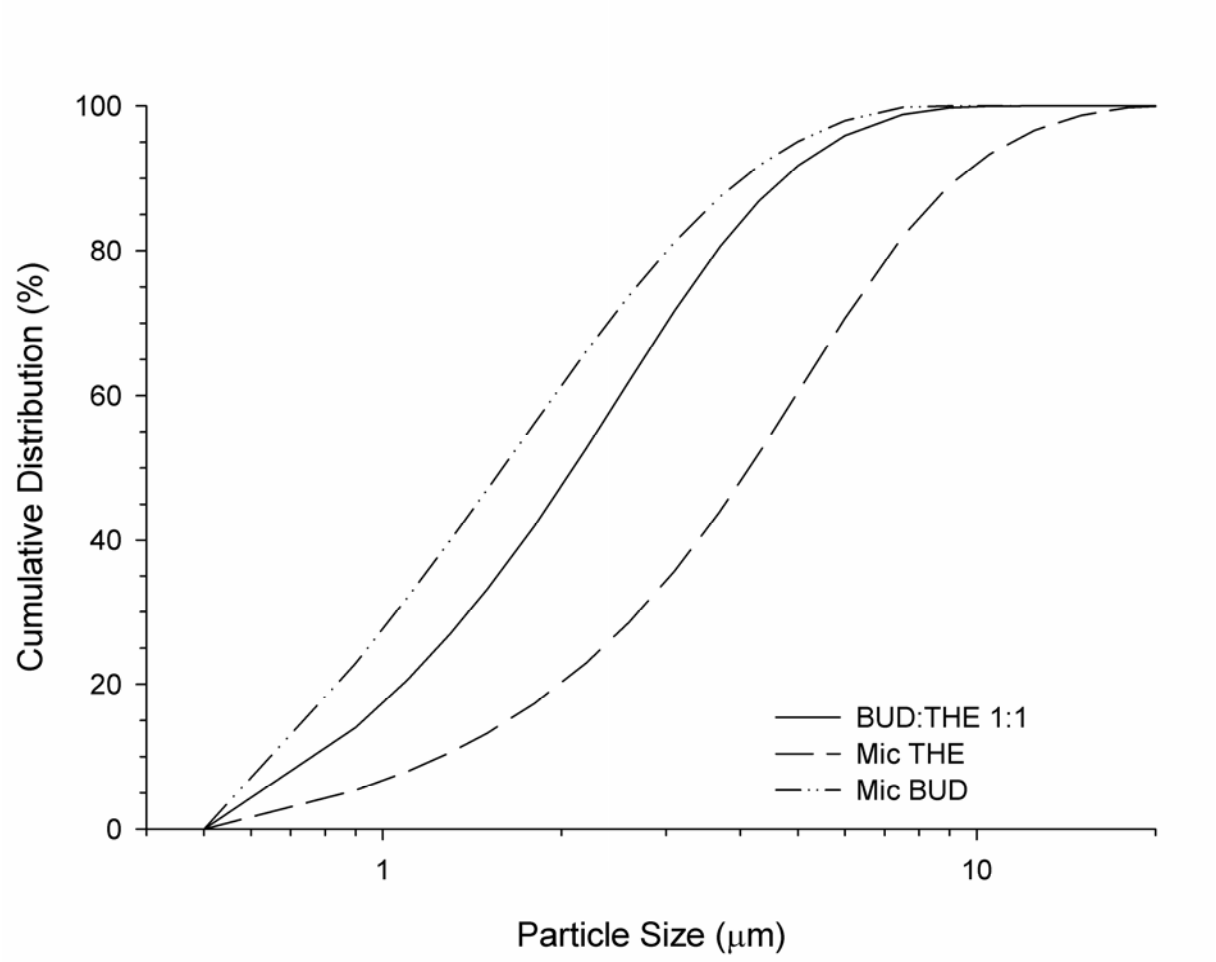

Figure 4.5: Particle size distribution of SAX produced BUD:THE 1:1 particles compared to micronised BUD and micronised THE.

Table 4.2: Particle size distribution of micronised THE, micronised BUD and SAX engineered BUD:THE 1:1 particles.

	Particle Size (µm) ±SD		
	d_{10}	d_{50}	d_{90}
THE	1.26 ± 0.02	4.15 ± 0.03	9.33 ±0.12
BUD	0.63 ± 0.01	1.60 ± 0.01	4.05 ± 0.04
BUD-THE	0.79 ± 0.01	2.10 ± 0.06	4.74 ± 0.16

The particle size will help control the deposition of the particles, however, any amorphous content within the system may cause the particles to be physically unstable

and therefore may agglomerate into larger particles (Elamin, Sebhatu et al. 1995; Hancock and Zografi 1997). Figure 4.6 shows the X-ray diffractograms for the SAX engineered FP:THE and BUD:THE particles compared to the raw materials. As shown, both compounds produced demonstrate a large number of peaks suggesting highly crystalline behaviour. The XRPD for the SAX material exhibits peaks that are also present in each of the raw materials and, therefore, confirms the presence of both raw materials in the SAX produced particles.

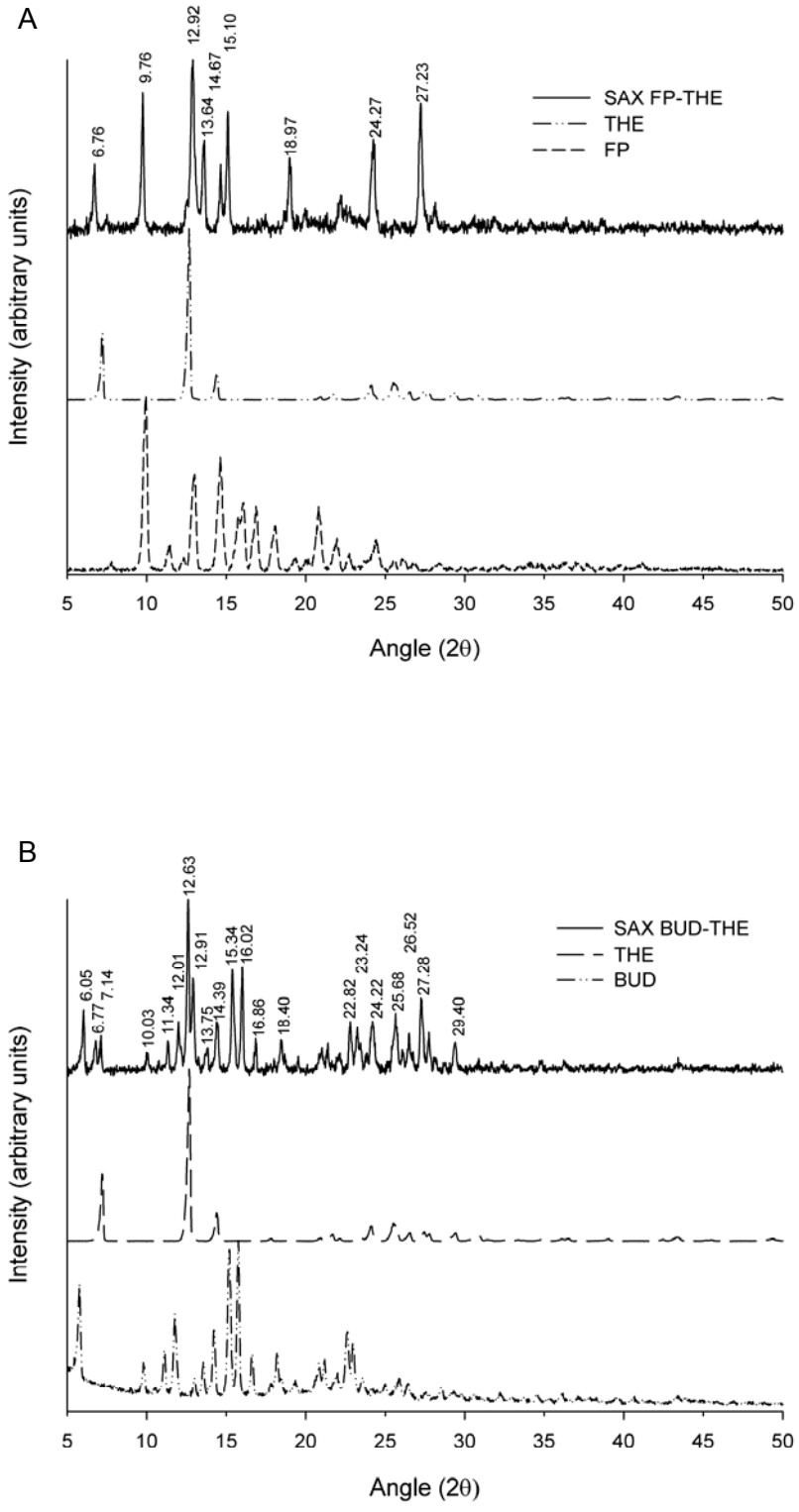

Figure 4.6: X-ray powder diffractogram of SAX engineered FP:THE 1:1 particles (a) and BUD:THE 1:1 particles (b) compared to their raw materials.

However, XRPD can only detect amorphous content that makes up ≥10% of the sample as this technique assesses the bulk sample (Salekigerhardt, Ahlneck et al. 1994; Buckton and Darcey 1999). Water sorption techniques have the ability to detect

amorphous content at a much lower level (Salekigerhardt, Ahlneck et al. 1994; Buckton and Darcy 1995; Buckton 1997; Buckton and Darcey 1999). DVS data for the SAX engineered FP:THE 1:1 particles shows that the particles are predominantly crystalline in nature with a small inflection during the first sorption cycle at 70 and 80% RH as shown in figure 4.7A. The same event can be seen in the SAX engineered BUD:THE 1:1 particles, but is more pronounced in the latter, as shown in figure 4.7B.

The FP:THE particles show a small weight increase at the end of the first of ~0.02% w/w while this is not seen in the BUD:THE particles. This suggests that the recrystallisation event occurring in the FP:THE particles could be the formation of an irreversible hydrate, possibly by the conversion of THE to theophylline monohydrate, as seen in figure 2.11A. This is supported by the fact that raw THE demonstrated a recrystallisation event at 70% RH. In addition, micronised THE shows a rapid mass increase after 70% RH to form a hydrate.

The desorption of the SAX engineered FP:THE 1:1 particles could be described in three distinct stages; 90 to 40% RH showing a linear decrease in mass with the reduction in RH; 40 to 20% RH demonstrating an accelerated mass loss with respect to the first part of the desorption cycle, and; 20 to 0% RH demonstrating a slower mass loss rate then between 40 and 20% RH. The second sorption and desorption cycles then follow this trend.

As for the SAX engineered BUD:THE 1:1 particles, the desorption cycle demonstrates two distinct section either side of 50% RH with 90 to 50% RH appearing to be more gradual than the 50 to 0% RH. The second sorption cycle then shows a gradual increase in mass up to 80% RH which is lower than the mass during the desorption cycle. The mass then increases to match that during the first cycle at 90% RH with the second desorption cycle matching the first.

Interestingly, both raw BUD and raw THE show a mass increase after the first sorption-desorption cycle suggesting that a hydrate may have been formed. However, this is not the case for the SAX engineered BUD:THE 1:1 particles. This suggested that the two drugs may have formed a crystal lattice thus resulting in a reduced reactivity to water. This is echoed by the fact that there are some new peaks in the XRPD as well as some missing compared to the raw materials for both FP:THE and BUD:THE particles.

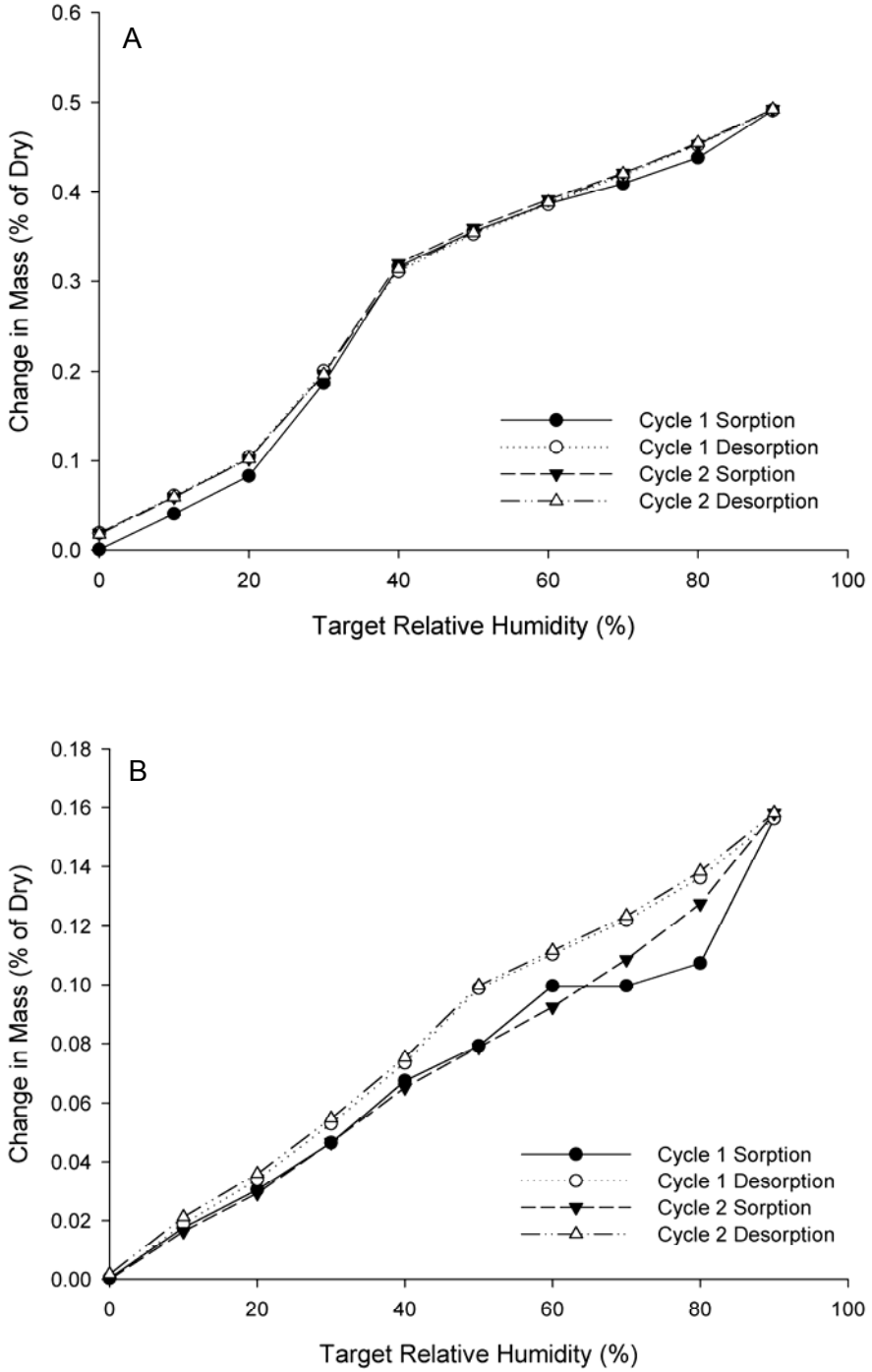

Figure 4.7: DVS isotherm at 25°C for SAX engineered FP:THE 1:1 (a) and BUD:THE 1:1 (b) particles

Table 4.3 details the peaks that appear in the raw material but not in the SAX engineered FP:THE particles as well as the new peaks in the SAX engineered particles while table 4.4 details the same for BUD:THE particles.

As shown, there are a large number of differences between the raw products and the SAX engineered particles. This suggests that a new crystalline lattice may have been formed which combines either FP or BUD with THE.

Table 4.3: Table detailing missing and new peaks from XRPD trace for SAX engineered FP:THE 1:1 particles compared to raw material.

Raw material	FP	THE
Angle (2θ) of missing peak	9.94, 11.56, 12.42, 15.75, 16.13, 16.90, 18.04, 20.80, 21.94, 22.90, 24.42.	7.28, 14.42, 24.13, 25.57
Angle (2θ) of additional peaks	6.76, 9.76, 13.64, 15.10, 18.97, 24.27, 27.23	

Table 4.4: Table detailing missing and new peaks from XRPD trace for SAX engineered BUD:THE 1:1 particles compared to raw material.

Raw material	BUD	THE
Angle (2θ) of missing peak	5.75, 9.85, 11.09, 11.76, 13.66, 15.66, 18.14, 19.28, 20.80, 22.52	None
Angle (2θ) of additional peaks	6.05, 6.77, 10.03, 11.34, 12.01, 12.91, 16.02, 18.40, 23.24,24.22, 26.52, 27.28, 29.40	

DSC analysis shows that the SAX engineered particles demonstrate an individual onset of melt separate from that of either pure material, as shown in figure 4.8. The onset and peak melting temperatures of the SAX engineered particles as well as the raw materials are presented in table 4.5. This suggested that a new crystalline lattice has been produced, as above.

Table 4.5: Onset and peak melting points for the SAX engineered particles compared to the raw materials.

Drug/Mixture	Onset of melt (°C)	Peak melting point (°C)
FP	284.50	292.92
BUD	258.13	261.86
THE	271.75	273.21
SAX FP:THE 1:1	252.54	255.50
SAX BUD:THE 1:1	223.26	228.28

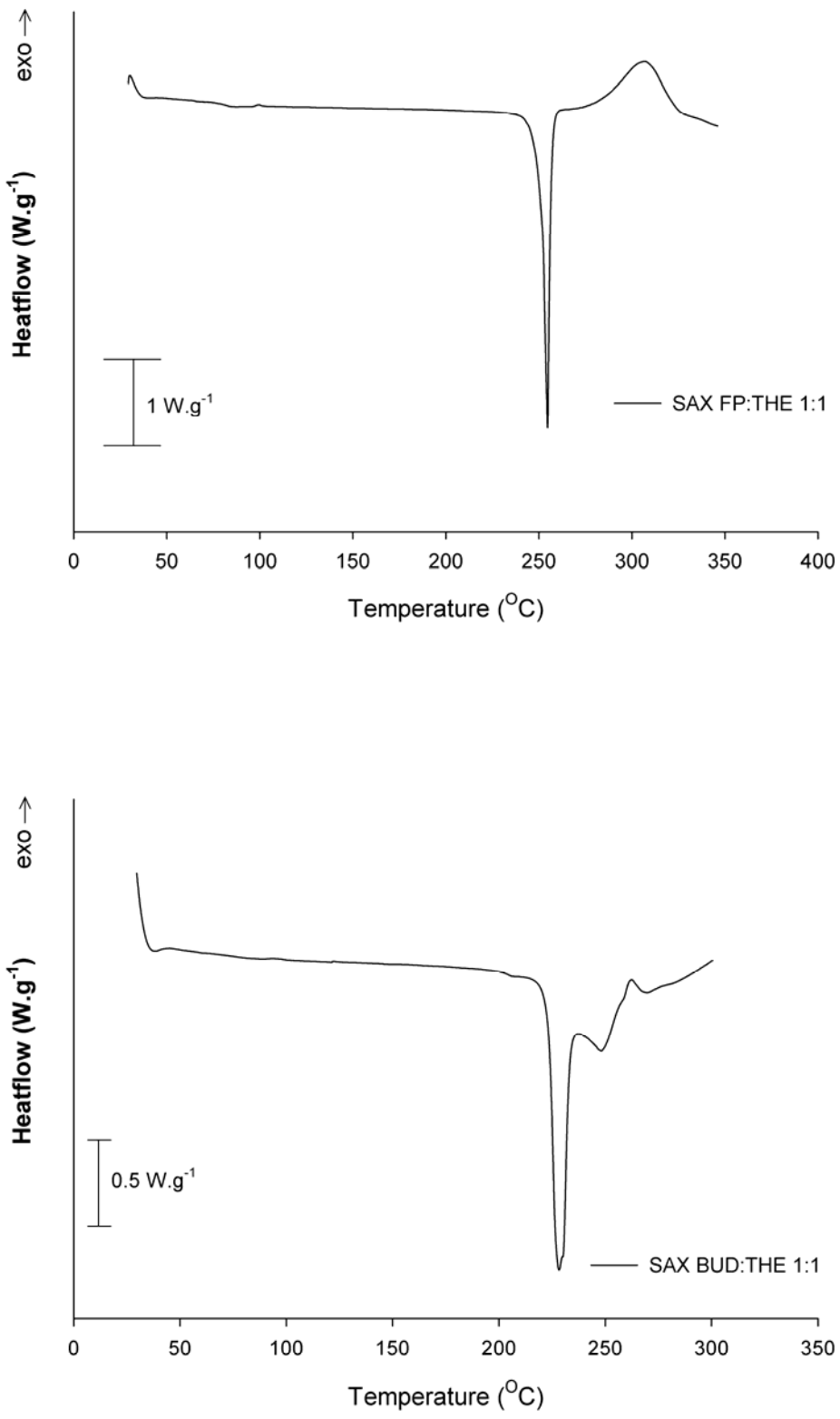

Figure 4.8: DSC thermograms of SAX engineered FP:THE and BUD:THE particles.

4.4.2 Pressurised metered dose inhaler (pMDI)

4.4.2.1 Drug impactor deposition measurements

The emitted dose (ED) and the fine particle dose (FPD) for FP and THE in both the micronised and the SAX engineered particles formulation are shown in Figure 4.9 with the data being summarised in Table 4.6. The micronised formulation resulted in a greater variability in the dose emitted for both FP and THE compared to the SAX equivalent formulation. There was no significant difference between either micronised FP or SAX FP. However, there was significantly ($P<0.05$) more THE emitted from the micronised formulation compared to the SAX.

Micronised FP demonstrated a significantly ($P<0.05$) greater FPD compared to either micronised THE or SAX FP but there was no significant difference between the fine particle dose for SAX FP or SAX THE. This difference could be due to the particle size distributions for each compound with FP having the smallest particle size distribution and therefore being able to deposit on the lower stages of the impactor while micronised THE demonstrated the largest mean particle size resulting in its collection earlier in the ACI. The SAX particles contain both FP and THE, with the same particle size distribution, in the correct ratio of 1:1, which would, therefore, result in similarity between the emitted dose and fine particle dose for FP and THE in the formulation and therefore co-deposition of both FP and THE resulting in the potential reversal of steroid resistance at these sites and allow for the FP to reduce any inflammation within the lungs. In contrast, due to the large difference between the FPD of micronised FP and micronised THE, only some of the THE would make it to the same site of action as the FP and, therefore, may not be able to reverse the steroid resistance throughout the lung of a COPD patient.

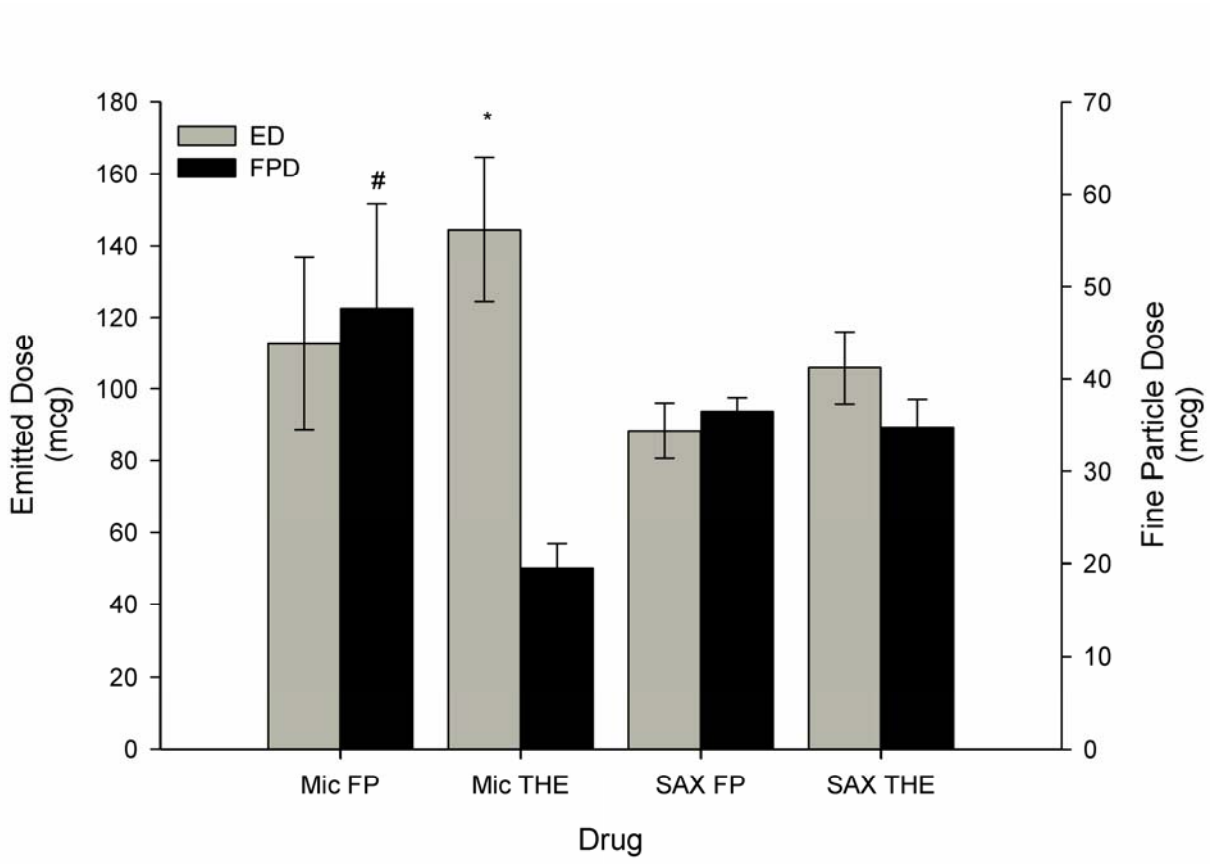

*Figure 4.9: Graphical representation of emitted dose (ED) and fine particle dose (FPD) for micronised FP:THE 1:1 and the SAX equivalent formulation. #= significant difference (P<0.05) between compounds in the same formulation; *=significant difference (P<0.05) between compounds across formulations*

The mean mass per shoot deposited on each stage of the ACI for micronised FP:THE 1:1 and the SAX engineered FP:THE 1:1 particles pMDI formulations is shown in table 4.6 and figure 4.10. Table 4.6 also details the emitted dose (ED), fine particle dose (FPD), fine particle fraction of emitted dose (FPF_{ED}), the mass median aerodynamic diameter (MMAD) and the geometric standard deviation of the MMAD (GSD). Figure 4.10 shows the stages of the ACI that had a significant difference (P<0.05) between the amount of FP and THE deposited for the micronised (*) and the SAX (#) formulations.

Figure 4.11 shows the mass of drug deposited between stages 0 to filter of the ACI for the micronised and SAX formulations. As shown, there was a significant difference (P<0.05) between the amount of micronised FP deposited compared to the amount of micronised THE deposited on stages 0, 1, 3, 4 and 5 while the SAX formulation showed a difference on stages 3, 4 and 5. This suggested that the particles may not contain FP and THE each particle. However, the SAX engineered particles have enabled better control of the dose ratio compared to having two individual micronised

components, as suggested in figure 4.12, which may be due to the fact that the SAX process allows for the particle size to be controlled in one easy step (Kaerger and Price 2004; Pitchayajittipong, Shur et al. 2009). The combination of FP and THE in one solution allows for the co-processing of both drugs in a single step operation and thus drugs could be expected to have the same particle size distribution and hence similar deposition profiles *In-vitro*. This may provide adequate co-deposition to reverse steroid resistance within COPD lungs. However, these data do not explain the appearance of new peaks in the XRPD which suggest a new crystalline lattice.

Stages 5 and 6 deposition had significantly ($P<0.05$) more FP deposited then THE for the SAX formulation. This, therefore, aids the argument that both compounds were co-processed and could suggest that both FP and THE crystallised out such a way that they may have lost co-association with one another, possibly upon actuation via a pMDI device.

The co-processing may have occurred as a result of using two solvents in equal measures for the initial drug solution resulting in a possible density gradient throughout the solution with the two compounds being inter-dispersed throughout. As a result, the solid material obtained may have been a eutectic mixture of the compounds and not the combination particles as produced by others (Pitchayajittipong, Shur et al. 2009).

Table 4.6: ACI deposition per shoot of drug delivered from micronised FP:THE 1:1 and SAX engineered FP:THE 1:1 particles pMDI formulations; FP=fluticasone propionate; THE=theophylline; MP&T= mouthpiece and throat; S=stage; F=filter.

Formulation	Drug	Mean Drug Deposition on Impactor Stages											Mean ED (µg±SD)	Mean FPD (µg±SD)	Mean FPF_{ED} (%±SD)	MMAD µm (GSD)
		Device	MP &T	S0	S1	S2	S3	S4	S5	S6	S7	F				
Micronised	FP	22.02 ± 2.91	51.90 ± 9.09	3.67 ± 1.24	3.99 ± 1.20	5.56 ± 1.80	14.81 ± 3.28	18.21 ± 4.02	11.48 ± 2.73	1.44 ± 0.29	0.47 ± 0.43	1.28 ± 2.03	112.82 ± 24.09	47.69 ± 11.28	42.13 ± 1.47	2.84 (2.18)
	THE	34.28 ± 4.71	94.29 ±13.41	13.99 ± 1.65	9.24 ± 2.18	7.41 ± 2.02	8.64 ± 1.63	4.55 ± 0.33	1.94 ± 0.31	0.95 ± 0.69	1.36 ± 1.35	2.08 ± 0.42	144.46 ± 20.16	19.53 ± 2.61	13.57 ± 1.11	6.34 (4.02)
SAX	FP	17.69 ± 2.18	41.40 ± 4.56	2.53 ± 1.12	2.89 ± 0.59	5.07 ± 0.57	10.75 ± 1.05	12.51 ± 0.71	10.53 ± 0.54	1.64 ± 0.24	1.07 ± 0.94	0.00 ± 0.00	88.38 ± 7.74	36.50 ± 1.50	41.44 ± 2.54	3.09 (1.73)
	THE	23.01 ± 0.95	60.53 ± 5.22	2.58 ± 0.55	2.92 ± 0.74	5.10 ± 0.70	14.38 ± 1.53	15.21 ± 0.86	5.00 ± 0.50	0.14 ± 0.24	0.06 ± 0.10	0.00 ± 0.00	105.90 ± 10.01	34.78 ± 3.04	32.86 ± 0.31	3.60 (1.64)

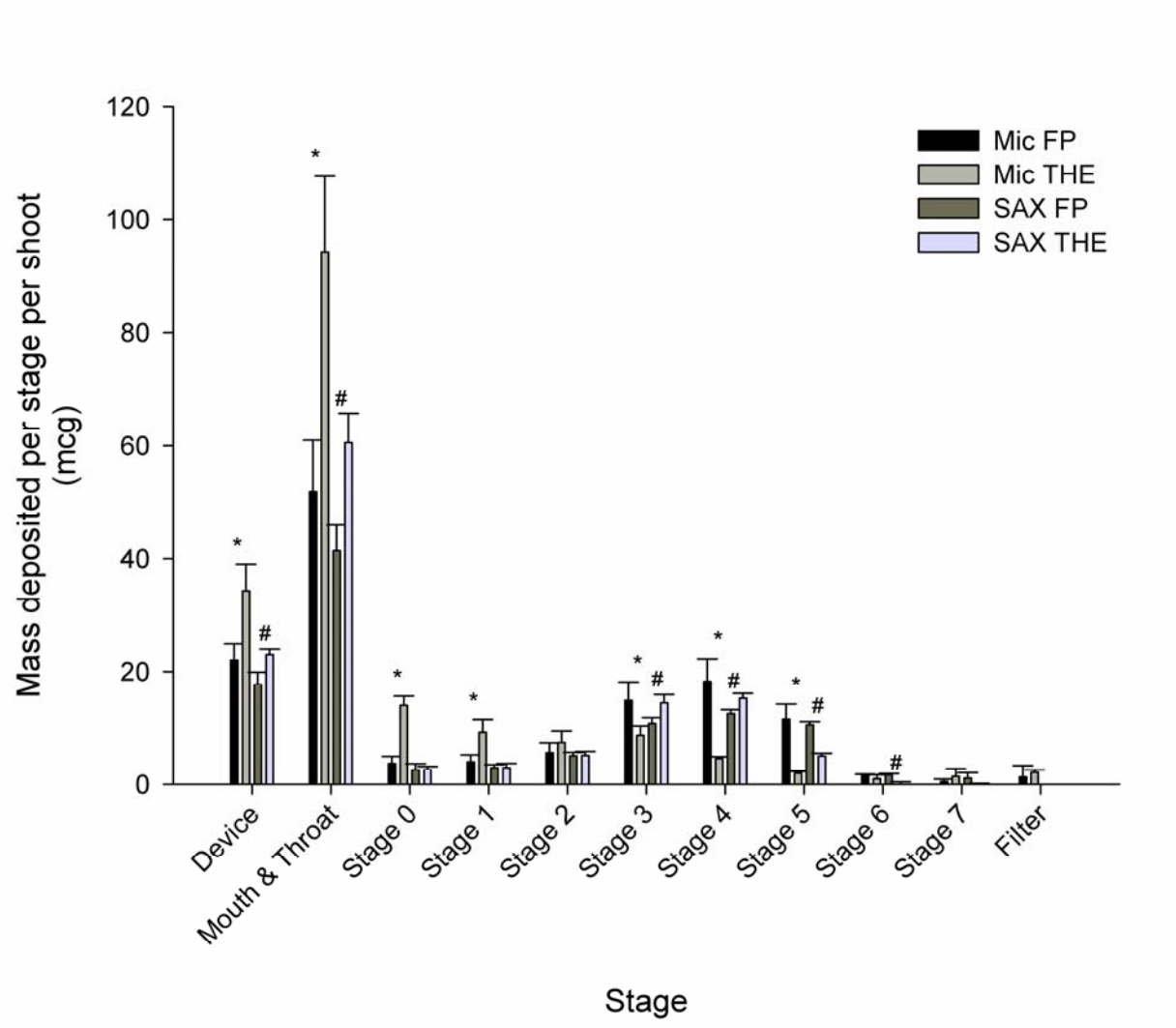

*Figure 4.10: ACI deposition per shoot of micronised FP:THE 1:1 and SAX engineered FP:THE 1:1 particles in a pMDI formulation. *=significant difference (P<0.05) between micronised FP and micronised THE. #=significant difference (P<0.05) between FP and THE in SAX formulation.*

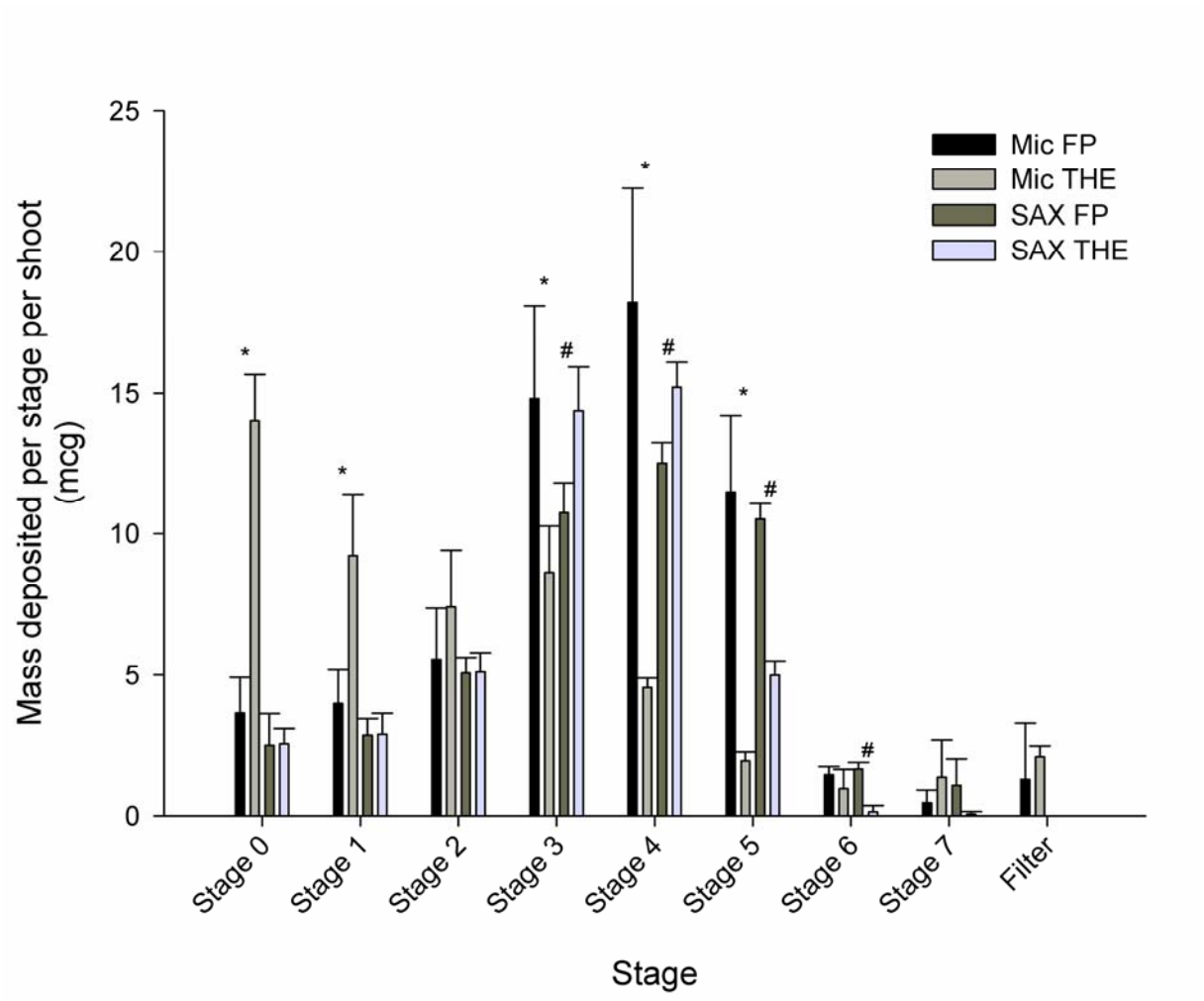

*Figure 4.11: ACI deposition per shoot on stages 0 to filter for micronised FP:THE 1:1 and SAX engineered FP:THE 1:1 particles in a pMDI formulation. *=significant difference (P<0.05) between micronised FP and micronised THE. #=significant difference (P<0.05) between FP and THE in SAX formulation.*

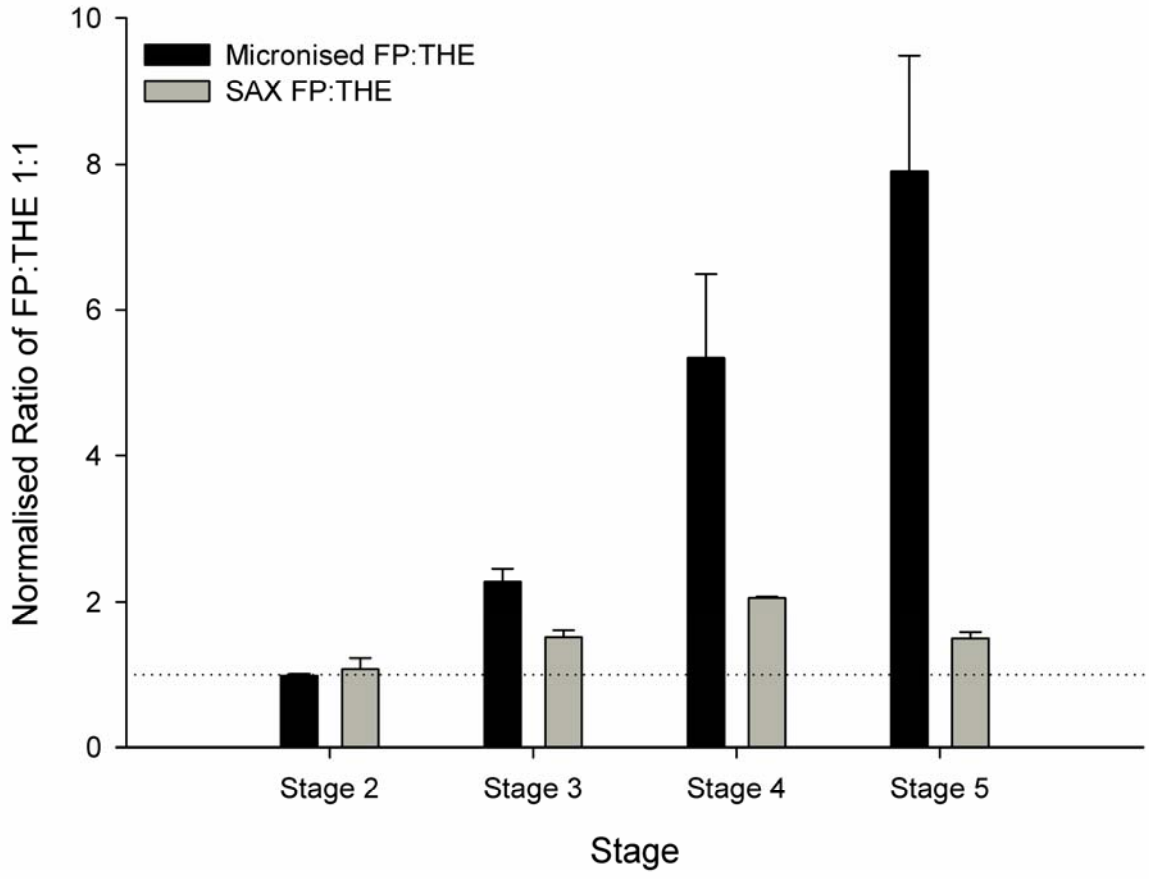

Figure 4.12: Graphical representation of the ratio between FP and THE for micronised and SAX formulations.

The emitted dose (ED) and the fine particle dose (FPD) for BUD and THE in both the micronised and the SAX engineered particles formulation are shown in Figure 4.13 with these data being summarised in table 4.7. The SAX formulation delivered a wider variability in the emitted dose; however, there was no significant difference between the emitted dose of any of the compounds.

As with the FP:THE micronised formulation, there was a significant difference ($P<0.05$) between the amount of micronised BUD delivered compared to micronised THE. This maybe due to the smaller particle size of BUD than THE. No significant difference was observed in the FPD between BUD and THE in the SAX formulation, as shown in figure 4.13. These data suggested that both BUD and THE may have been combined into one particle during the SAX process.

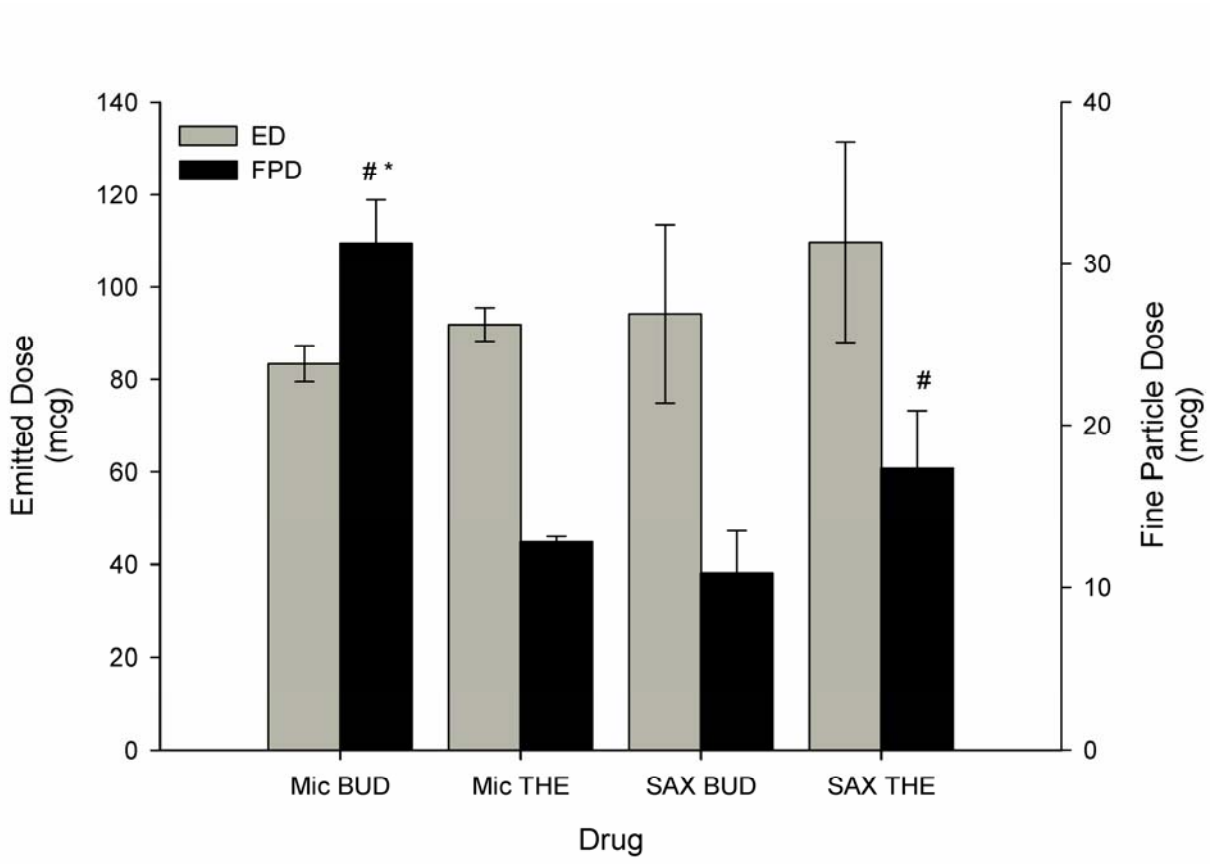

*Figure 4.13: Graphical representation of emitted dose (ED) and fine particle dose (FPD) for micronised BUD:THE 1:1 and the SAX equivalent formulation. #= significant difference (P<0.05) between compounds in the same formulation; *=significant difference (P<0.05) between compounds across formulations*

The mean mass per shot deposited on each stage of the ACI for micronised BUD:THE 1:1 and the SAX engineered BUD:THE 1:1 particles pMDI formulations are shown in table 4.7 and figure 4.14. Table 4.7 also details the emitted dose (ED), fine particle dose (FPD), fine particle fraction of emitted dose (FPF_{ED}), the mass median aerodynamic diameter (MMAD) and the geometric standard deviation of the MMAD (GSD). Figure 4.14 shows the stages of the ACI that had a significant difference (P<0.05) between the amount of BUD and THE deposited for the micronised (*) and the SAX (#) formulations while figure 4.15 shows only stages 0 to filter.

The MMAD for the SAX particles is greater than either BUD or THE in the micronised formulation. This does not follow the particle size distribution and could suggest that there was some agglomeration occurring in the SAX formulation which could be due to the suspected amorphous content (Aguilera, del Valle et al. 1995; Ticehurst, Basford et al. 2000). As a result, there was no BUD or THE deposited on stages 6, 7 or filter in the ACI for the SAX formulation.

The mass deposited on each stage of the ACI for both BUD and THE in both the micronised and SAX pMDI formulations with figure 4.15 showing only stages 0 to filter. The micronised formulation demonstrated a significant difference ($P<0.05$) between the amount of BUD and THE deposited in the mouth & throat as well as stages 1, 3, 4, 5, 6 and filter. In contrast to this, the SAX formulation only showed a significant difference ($P<0.05$) on stages 4 and 5.

The relative ratio between BUD and THE for the micronised formulation demonstrated a wide variability between all stages, as depicted in figure 4.16, while the ratio was more stable in the SAX formulation in comparison. This suggested that the SAX formulation is more likely to provide the co-deposition of BUD and THE to the same site of action within the lungs and, and therefore, allow for THE to be present at the same site of action as BUD to aid in the prevention of the inflammatory process. However, the slight variability in the relative ratio of BUD to THE suggested that the compounds may not be combined into one particle, as was the case for the FP:THE particles above.

Table 4.7: ACI deposition per shoot of drug delivered from micronised BUD:THE 1:1 and SAX engineered BUD:THE 1:1 particles pMDI formulations; BUD=budesonide; THE=theophylline; MP&T= mouthpiece and throat; S=stage; F=filter.

Formulation	Drug	Mean Drug Deposition on Impactor Stages											Mean ED (µg±SD)	Mean FPD (µg±SD)	Mean FPF_{ED} (%±SD)	MMAD µm (GSD)
		Device	MP &T	S0	S1	S2	S3	S4	S5	S6	S7	F				
Micronised	BUD	22.25 ± 2.84	42.37 ±2.65	3.40 ± 2.84	2.23 ± 0.10	4.14 ± 0.56	10.87 ± 0.79	14.27 ± 3.41	5.22 ± 0.73	0.61 ± 0.08	0.14 ± 0.05	0.17 ± 0.03	83.42 ± 3.87	31.28 ± 2.67	37.56 ± 3.93	3.33 (1.98)
	THE	24.18 ± 2.53	60.24 ± 4.16	7.74 ± 0.82	6.08 ± 0.88	5.08 ± 0.52	6.19 ± 0.37	3.10 ± 0.18	1.52 ± 0.16	0.84 ± 0.02	0.71 ± 0.36	0.43 ± 0.10	91.95 ± 3.65	12.79 ± 0.34	13.92 ± 0.46	5.76 (3.04)
SAX	BUD	17.80 ± 2.94	48.48 ±11.47	8.00 ± 1.27	5.15 ± 1.14	3.94 ± 1.42	6.42 ± 1.69	3.26 ± 0.68	1.19 ± 0.22	0.00 ± 0.00	0.00 ± 0.00	0.00 ± 0.00	76.45 ± 17.76	10.88 ± 2.59	14.21 ± 0.50	6.10 (1.68)
	THE	20.99 ± 3.70	54.79 ±12.86	7.62 ± 1.01	4.89 ± 0.96	4.17 ± 1.43	8.21 ± 2.12	6.28 ± 1.01	2.84 ± 0.48	0.00 ± 0.00	0.00 ± 0.00	0.00 ± 0.00	88.79 ± 19.71	17.33 ± 3.58	19.56 ± 0.33	6.80 (1.64)

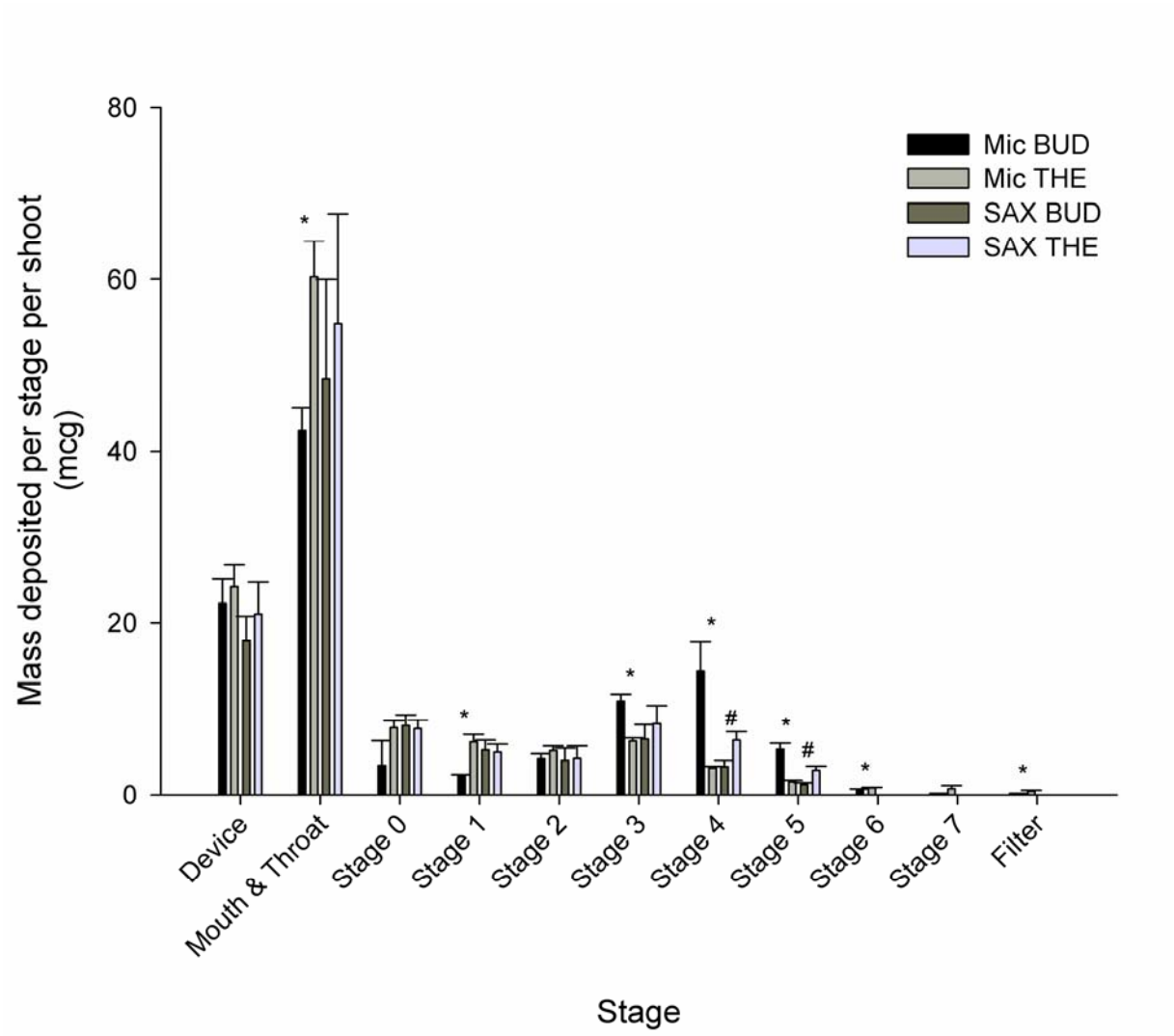

*Figure 4.14: ACI deposition per shoot of micronised BUD:THE 1:1 and SAX engineered BUD:THE 1:1 particles in a pMDI formulation. *=significant difference (P<0.05) between micronised BUD and micronised THE. #=significant difference (P<0.05) between BUD and THE in SAX formulation.*

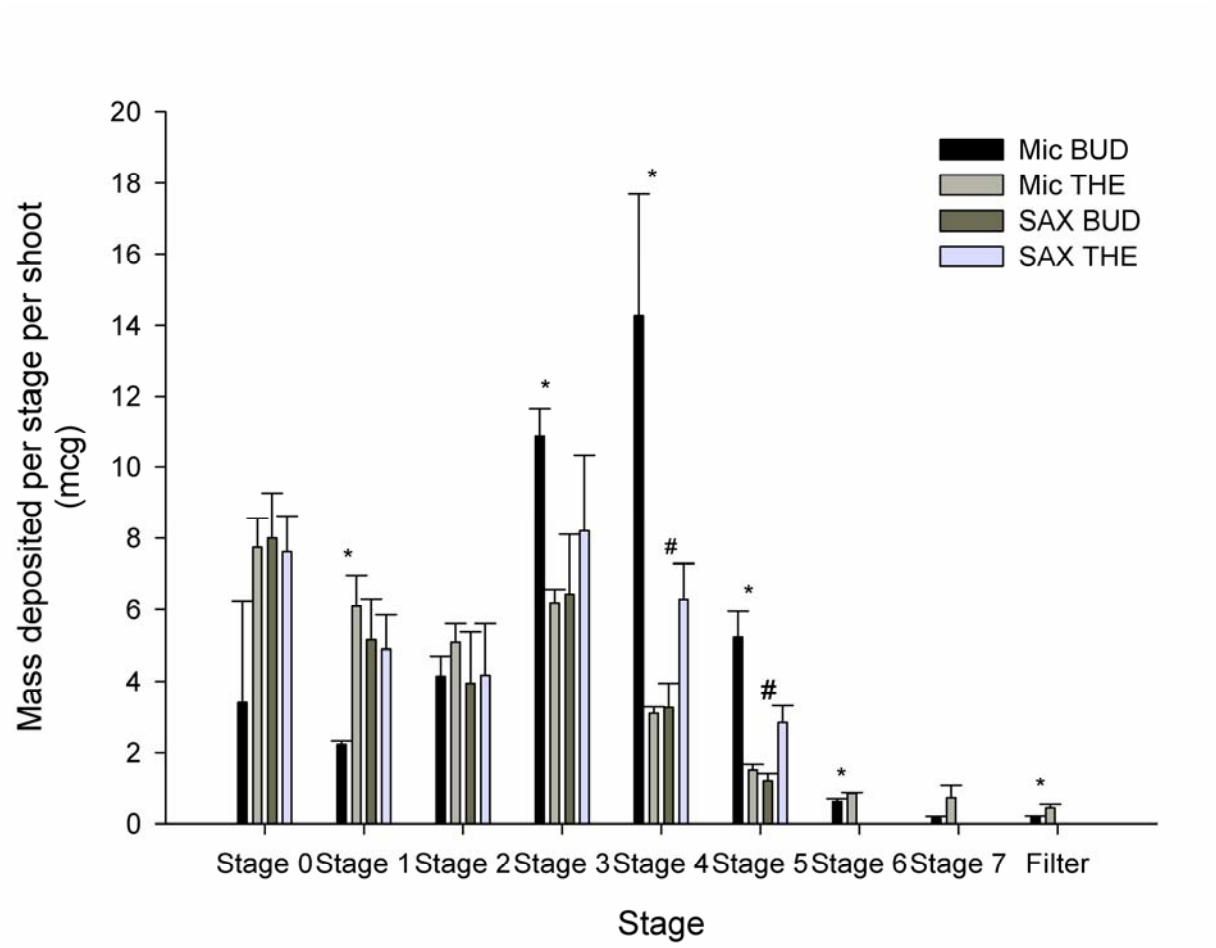

*Figure 4.15: ACI deposition per shoot on stages 0 to filter for micronised BUD:THE 1:1 and SAX engineered BUD:THE 1:1 particles in a pMDI formulation. *=significant difference (P<0.05) between micronised BUD and micronised THE. #=significant difference (P<0.05) between BUD and THE in SAX formulation.*

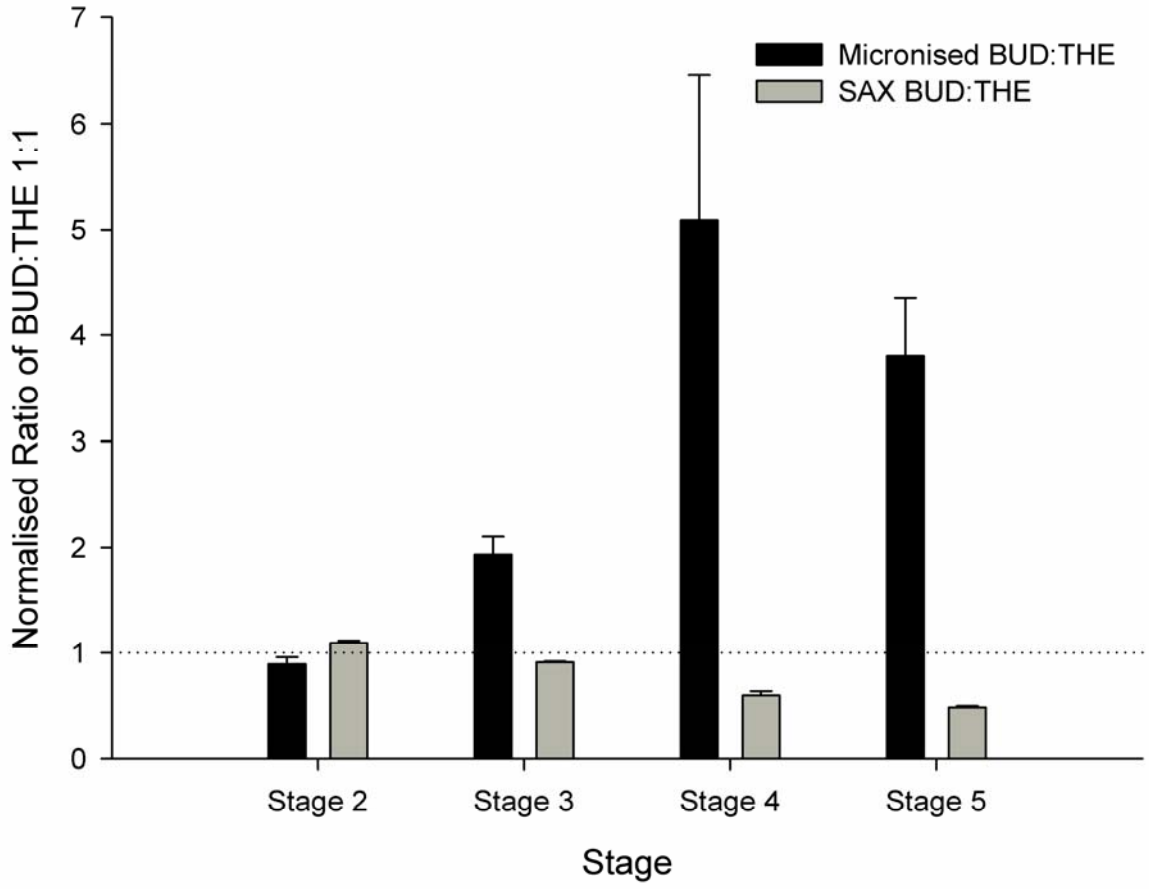

Figure 4.16: Graphical representation of the ratio between BUD and THE for micronised and SAX formulations.

4.4.3 Dry Powder Inhalers (DPI's)

4.4.3.1 Content uniformity.

The accepted coefficient of variation (CV) of a drug content within a dry powder inhaler formulation is <6%. The CV for FP and BUD, regardless of the formulation, were <6% (5.47, 4.07, 3.08 and 1.56% for micronised FP, SAX FP, micronised BUD and SAX BUD, respectively). However, the CV of THE for both micronised and SAX formulations as detailed in table 4.8 was greater than 6 %.

The SAX formulations demonstrated satisfactory results for the steroid used whilst THE was not well dispersed in the blend. These data suggest that the particles may not contain the steroid and THE, but may have produced a mixture that allowed for the two compounds to be loosely associated with each other. Another alternative is that the SAX process, having allowed for the two compounds to be co-processed, produced a dispersion of steroid with THE. However, when the mixture was processed with lactose, each compound separated from this mixture and acted as an individual component with regard to its own adhesive-cohesive nature with regard to the lactose carrier. This may explain how CV_{THE} was similar for similar formulations but greater than 6%.

Table 4.8: Coefficient of variation (CV) of THE in each of the DPI formulations.

Formulation	Micronised FP:THE 1:1	SAX FP:THE 1:1	Micronised BUD:THE 1:1	SAX BUD:THE 1:1
CV_{THE} (%)	6.55	7.16	11.36	11.53

The emitted dose (ED) and the fine particle dose (FPD) for FP and THE in both the micronised and the SAX engineered particles formulation are shown in Figure 4.17 with the data being summarised in table 4.9. Despite the CV_{THE} being greater than 6 %, the ED for THE was similar to that of FP.

The SAX formulation demonstrated a significantly ($P<0.05$) increased FPD for both FP and THE compared to the micronised formulation, however, there was a significant difference ($P<0.05$) between the two with a greater amount of THE being delivered to the lower stages of the NGI. This aids the argument that SAX can be used to process compounds that are difficult to mill using an air jet mill.

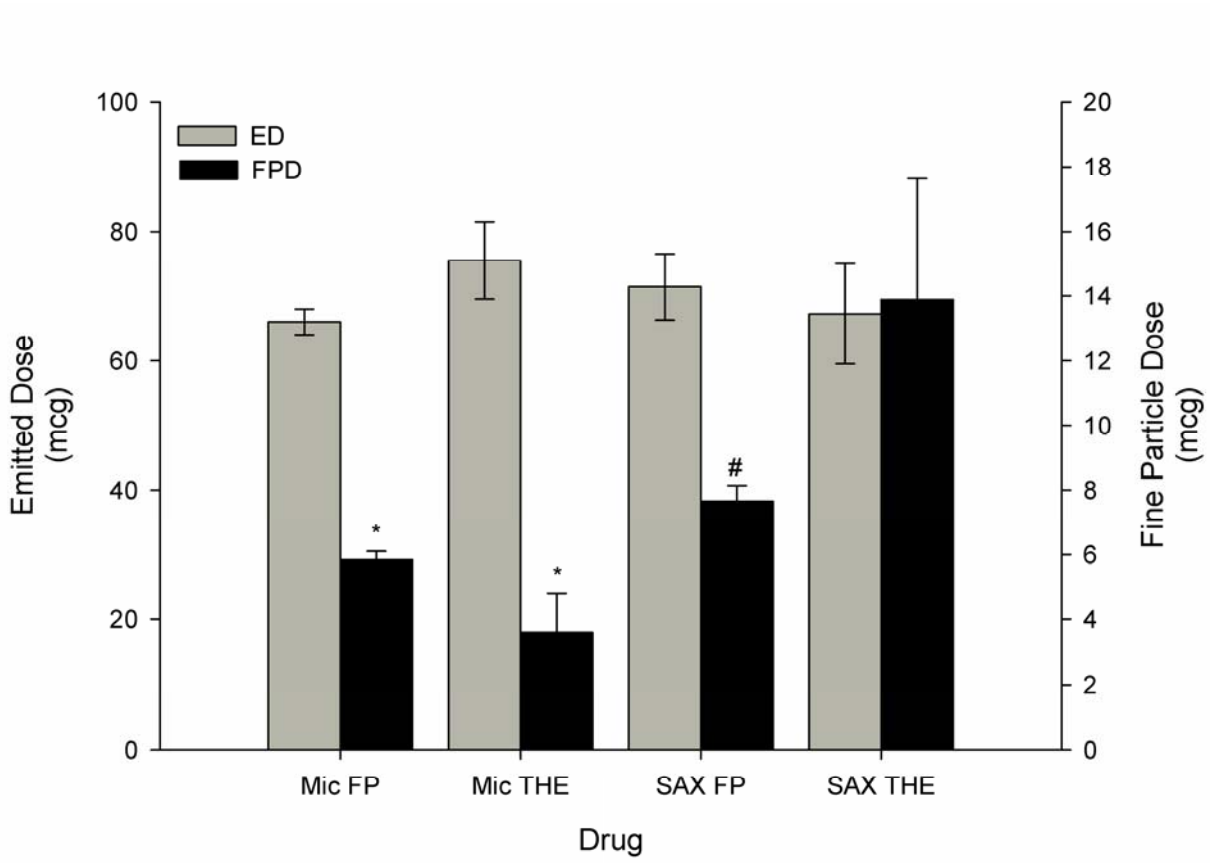

*Figure 4.17: Graphical representation of emitted dose (ED) and fine particle dose (FPD) for micronised FP:THE 1:1 and the SAX equivalent DPI formulations. #= significant difference (P<0.05) between compounds in the same formulation; *=significant difference (P<0.05) between compounds across formulations*

The mean mass per shoot deposited on each stage of the NGI for micronised FP:THE 1:1 and the SAX engineered FP:THE 1:1 particles DPI formulations is shown in table 4.9 and figure 4.18. Table 4.9 also details the emitted dose (ED), fine particle dose (FPD), fine particle fraction of emitted dose (FPF_{ED}), the mass median aerodynamic diameter (MMAD) and the geometric standard deviation of the MMAD (GSD). Figure 4.18 shows the stage deposition of the NGI that had a significant difference (P<0.05) between the amount of FP and THE deposited for the micronised (*) and the SAX (#) formulations while figure 4.19 shows only stages 1 to MOC.

The SAX formulation allowed for a better dose ratio between FP and THE to be delivered, compared to the micronised formulation. The micronised formulation demonstrated a significant difference (P<0.05) in the mass of FP to THE delivered to every stage up to and including stage 4, while the SAX formulation only showed a significant difference (P<0.05) in the pre-separator and stages 5 and 6. In the remaining stages, there was no significant difference between the mass deposited. This suggests that, even thought the FP and THE may not be combined in one particle, the co-processing via SAX allows for a consistent dose ratio to be delivered regardless

of the aerosolisation method used compared to a micronised formulation and is, therefore, more likely to help deal with steroid resistance in patients with COPD.

Table 4.9: NGI deposition per shoot of drug delivered from micronised FP:THE 1:1 and SAX engineered FP:THE 1:1 particles DPI formulations; FP = fluticasone propionate; THE=theophylline; C&D= capsules and device; PS = pre-separator; MP&T= mouthpiece and throat; S=stage; MOC = micro orifice collector.

Formulation	Drug	Mean Drug Deposition on Impactor Stages											Mean ED (µg±SD)	Mean FPD (µg±SD)	Mean FPF_{ED} (%±SD)	MMAD µm (GSD)
		C&D	MP &T	PS	S1	S2	S3	S4	S5	S6	S7	MOC				
Micronised	FP	29.81 ± 3.85	13.41 ± 0.93	71.23 ± 1.61	1.82 ± 0.11	4.11 ± 0.22	4.81 ± 0.28	5.22 ± 0.94	1.41 ± 0.12	0.24 ± 0.04	0.00 ± 0.00	0.00 ± 0.00	102.26 ± 0.85	11.68 ± 0.51	11.42 ± 0.49	2.74 (2.58)
	THE	64.54 ±13.65	33.74 ±7.12	35.51 ± 5.67	4.53 ±1.16	5.50 ± 0.35	3.72 ± 0.38	1.91 ± 1.66	1.24 ± 0.16	0.23 ± 0.20	0.08 ± 0.14	0.00 ± 0.00	86.45 ± 1.62	7.18 ± 2.45	8.28 ± 2.74	4.65 (3.12)
SAX	FP	43.44 ± 3.72	28.89 ±12.57	57.81 ± 0.17	2.19 ± 0.07	5.16 ± 0.24	5.59 ± 0.44	5.47 ± 0.63	3.06 ± 0.30	1.00 ± 0.28	0.20 ± 0.06	0.00 ± 0.00	99.38 ± 13.61	15.32 ± 0.96	15.51 ± 1.08	2.39 (2.60)
	THE	50.47 ± 3.99	12.02 ± 5.40	36.81 ±10.78	2.75 ± 1.30	4.71 ± 1.88	8.18 ± 3.27	11.75 ± 4.55	5.11 ± 1.14	1.53 ± 0.07	0.91 ± 0.71	0.27 ± 0.47	84.04 ± 19.49	27.76 ± 7.51	33.39 ± 7.67	2.16 (2.26)

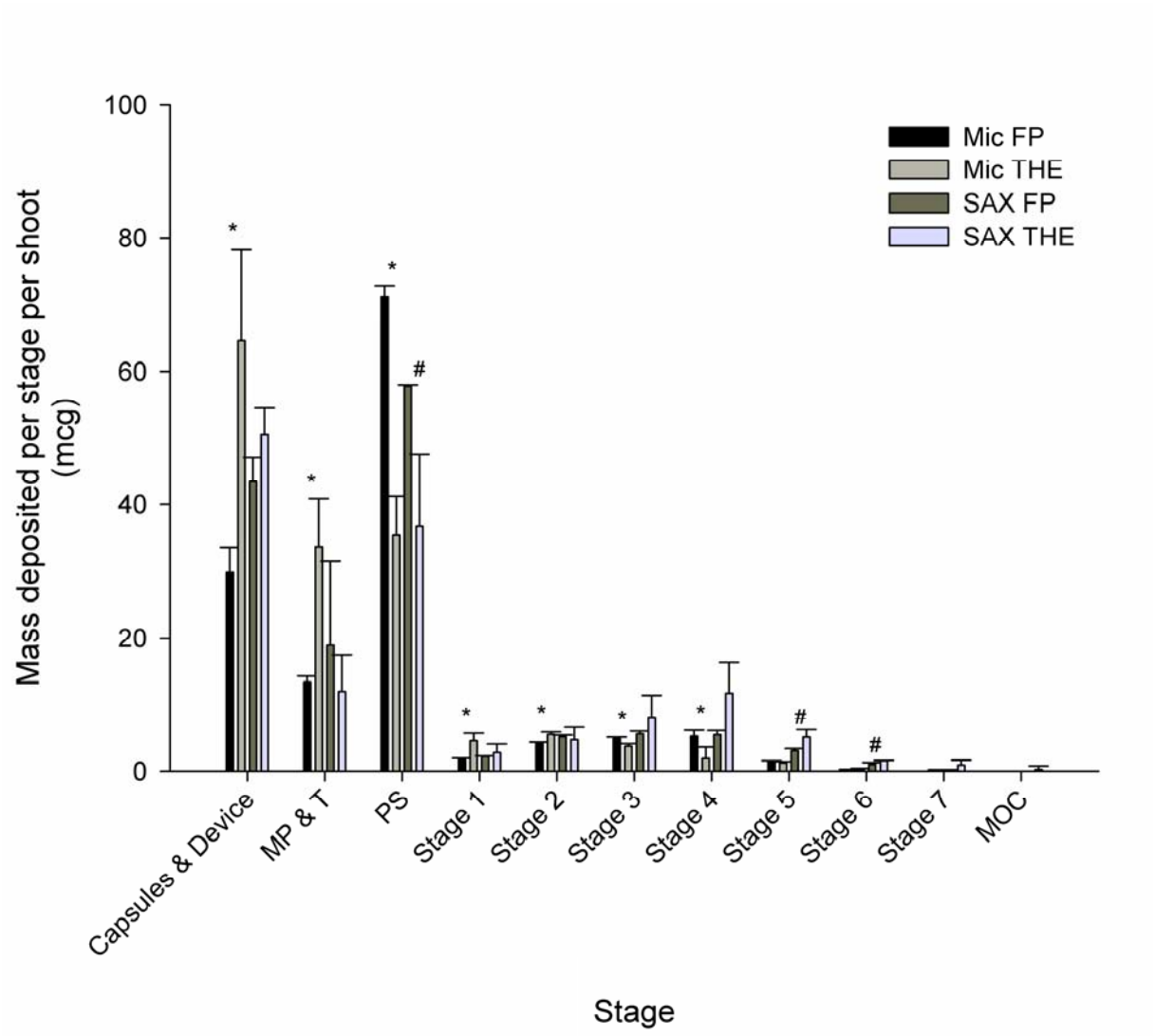

*Figure 4.18: NGI deposition per shoot of micronised FP:THE 1:1 and SAX engineered FP:THE 1:1 particles in a DPI formulation. *=significant difference (P<0.05) between micronised FP and micronised THE. #=significant difference (P<0.05) between FP and THE in SAX formulation.*

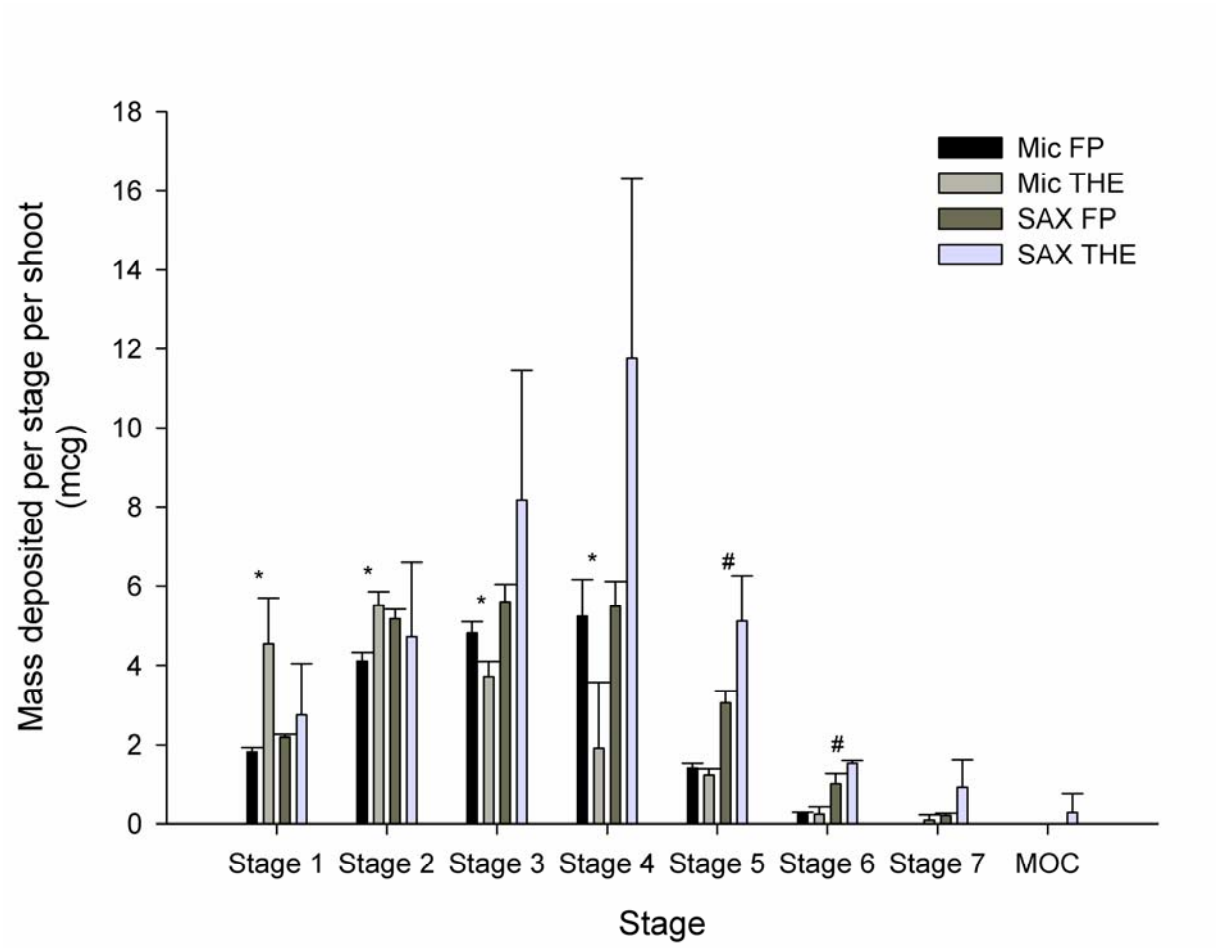

*Figure 4.19: NGI deposition per shoot on stages 1 to MOC for micronised FP:THE 1:1 and SAX engineered FP:THE 1:1 particles in a DPI formulation. *=significant difference (P<0.05) between micronised FP and micronised THE. #=significant difference (P<0.05) between FP and THE in SAX formulation.*

The ratio between the percentage of recovered dose (%RD) for FP and THE for both the SAX and micronised formulation in the NGI is represented in figure 4.20. As shown, neither the micronised or the SAX formulations maintained the ratio between FP and THE, suggesting therefore that the two compounds were not joined in one particle when the formulation was aerosolised.

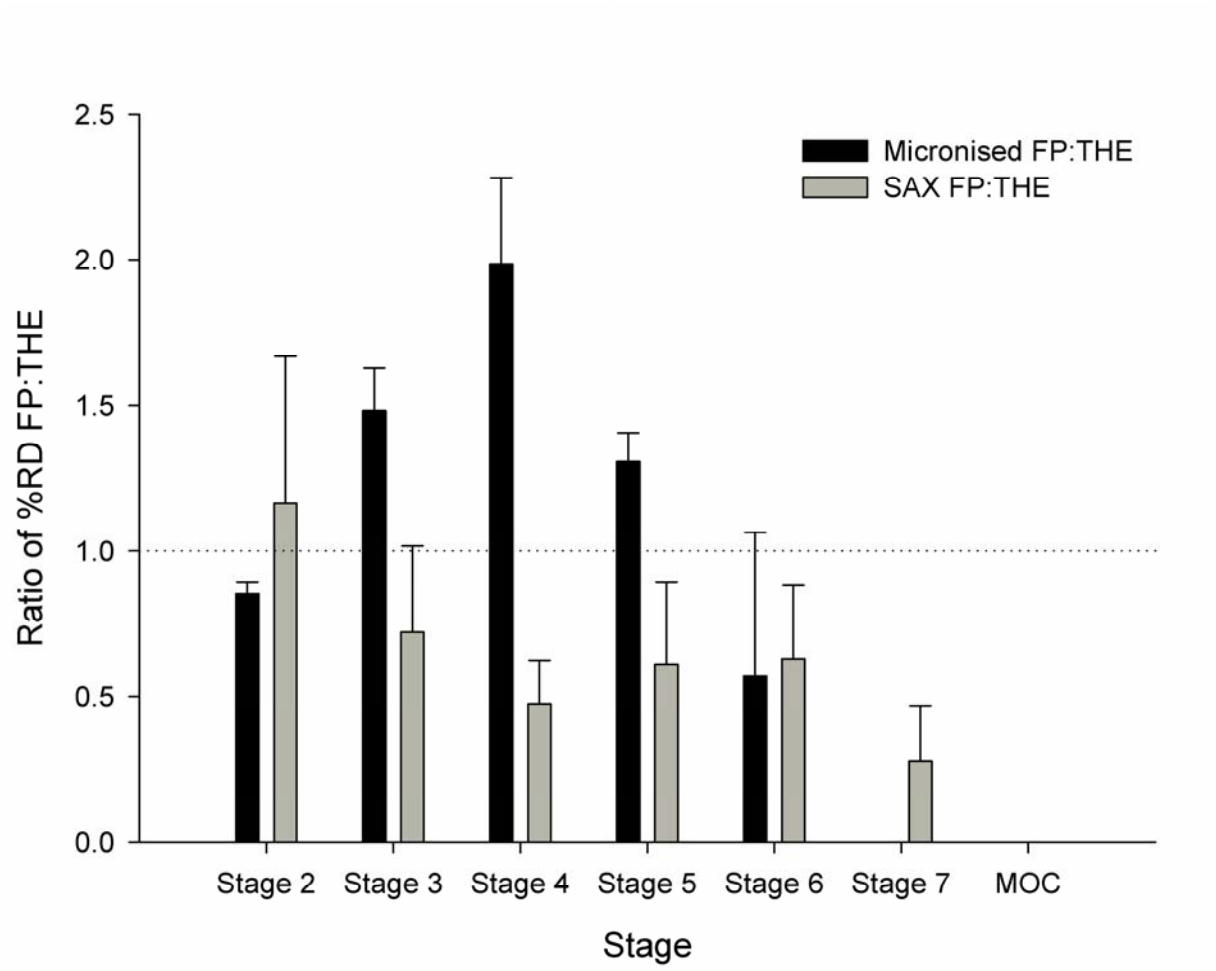

Figure 4.20: Graphical representation of the ratio between FP and THE for micronised and SAX formulations.

Figure 4.21 shows the ED and FPD for BUD and THE in both the micronised and the SAX engineered particles formulation with the data being summarised in table 4.10. As shown, the SAX formulation delivered a significantly ($P<0.05$) greater amount of BUD compared to the micronised formulation with a corresponding increase in FPD. There was no difference between the amount of BUD emitted compared to THE in either formulation, or no statistical difference between the amount of THE delivered in the micronised or SAX formulation. However, there was a difference in the FPD of the SAX BUD and SAX THE. This suggested that the BUD and THE easily separated during the formulation and aerosolisation process in a DPI formulation.

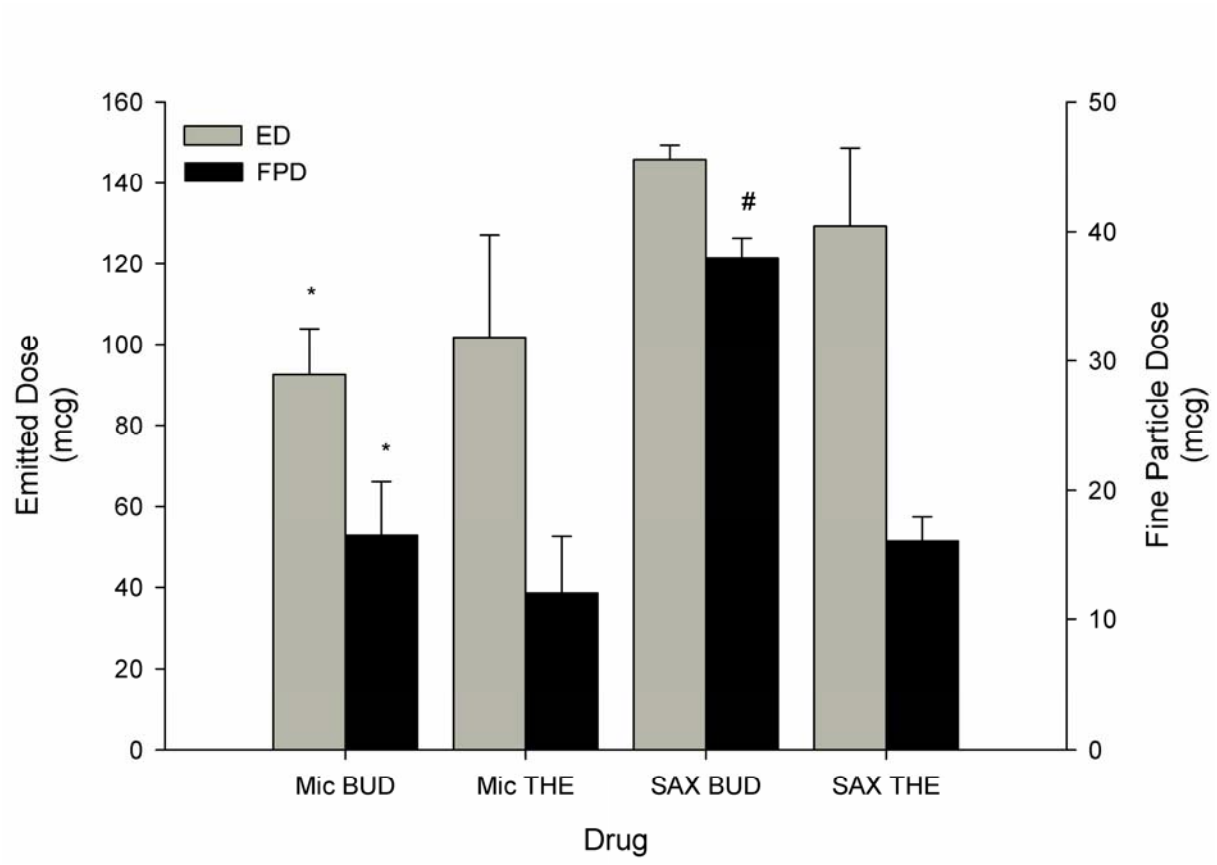

*Figure 4.21: Graphical representation of emitted dose (ED) and fine particle dose (FPD) for micronised BUD:THE 1:1 and the SAX equivalent DPI formulations. #= significant difference (P<0.05) between compounds in the same formulation; *=significant difference (P<0.05) between compounds across formulations*

The mean mass per shot deposited on each stage of the NGI for micronised BUD:THE 1:1 and the SAX engineered BUD:THE 1:1 particles DPI formulations is shown in table 4.10 and figure 4.22. Table 4.10 also details the emitted dose (ED), fine particle dose (FPD), fine particle fraction of emitted dose (FPF_{ED}), the mass median aerodynamic diameter (MMAD) and the geometric standard deviation of the MMAD (GSD). Figure 4.22 shows the stages of the NGI that had a significant difference (P<0.05) between the amount of BUD and THE deposited for the micronised (*) and the SAX (#) formulations while figure 4.23 shows only stages 1 to MOC.

As shown, the SAX formulation demonstrated significant differences (P<0.05) between the mass of BUD delivered compared to THE on the majority of stages while the micronised formulation only showed a difference in the pre-separator and stage 1. Therefore, it appears that a formulation containing micronised BUD and micronised THE provides better dose consistency than the SAX equivalent formulation. This contradicts these data seen in the pMDI formulation but indicates that the particles

containing BUD and THE are in a lose agglomeration which is easily broken up during processing and aerosolisation.

Table 4.10: NGI deposition per shoot of drug delivered from micronised BUD:THE 1:1 and SAX engineered BUD:THE 1:1 particles DPI formulations; BUD= budesonide; THE= theophylline; C&D= capsules and device; PS = pre-separator; MP&T= mouthpiece and throat; S=stage; MOC = micro orifice collector.

Formulation	**Drug**	**Mean Drug Deposition on Impactor Stages**											**Mean ED (µg±SD)**	**Mean FPD (µg±SD)**	**Mean FPF_{ED} (%±SD)**	**MMAD µm (GSD)**
		C&D	**MP &T**	**PS**	**S1**	**S2**	**S3**	**S4**	**S5**	**S6**	**S7**	**MOC**				
Micronised	**BUD**	43.21 ± 7.81	15.41 ± 5.59	53.33 ± 1.88	2.24 ± 0.28	5.06 ± 0.90	5.97 ± 1.33	6.68 ± 1.68	2.94 ± 0.78	0.81 ± 0.32	0.07 ± 0.12	0.00 ± 0.00	92.51 ± 11.44	16.47 ± 4.21	17.62 ± 2.23	2.70 (1.73)
	THE	75.99 ±21.36	38.79 ±14.85	40.62 ± 3.63	4.16 ± 0.81	6.20 ± 2.54	5.20 ± 2.22	4.15 ± 1.21	2.12 ± 0.45	0.39 ± 0.07	0.09 ± 0.15	0.14 ± 0.24	101.86 ± 25.33	12.09 ± 4.31	11.68 ± 1.20	3.53 (2.49)
SAX	**BUD**	54.71 ± 3.28	30.17 ± 1.86	59.84 ± 2.03	5.91 ± 0.40	11.97 ± 0.58	13.89 ± 0.56	14.55 ± 0.44	7.08 ± 0.27	2.00 v 0.14	0.40 ± 0.12	0.04 ± 0.06	145.85 ± 3.61	37.96 ± 1.53	26.02 ± 0.83	2.70 (2.06)
	THE	59.69 ± 5.02	28.07 ± 5.76	76.32 ± 9.84	3.20 ±0.74	5.79 ± 1.43	7.30 ± 1.65	7.52 ± 1.02	0.89 ± 0.41	0.20 ± 0.05	0.13 ± 0.03	0.00 ± 0.00	129.41 ± 19.34	16.03 ± 1.92	12.43 ± 0.49	3.16 (1.82)

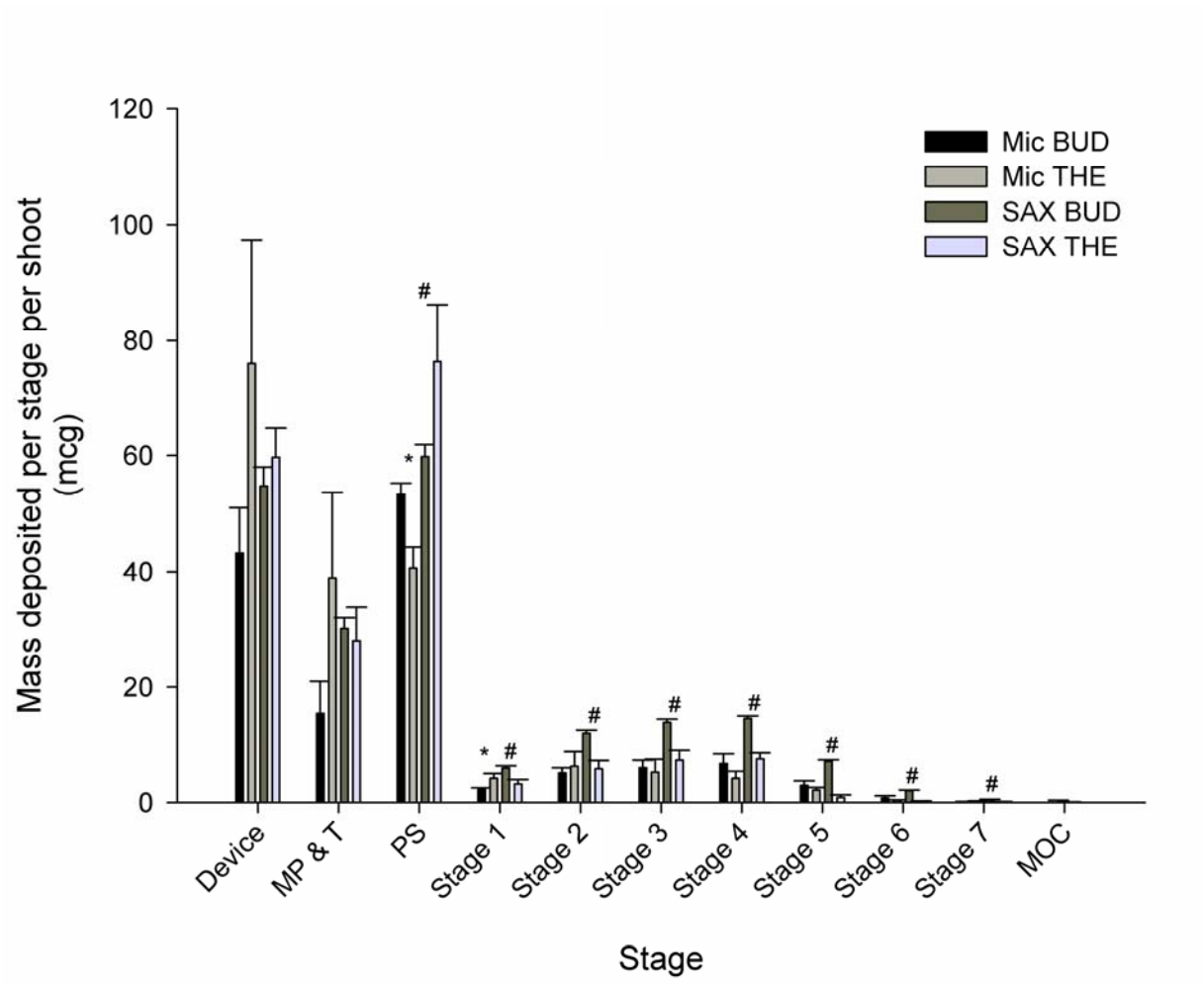

*Figure 4.22: NGI deposition per shoot of micronised BUD:THE 1:1 and SAX engineered BUD:THE 1:1 particles in a DPI formulation. *=significant difference (P<0.05) between micronised BUD and micronised THE. #=significant difference (P<0.05) between BUD and THE in SAX formulation.*

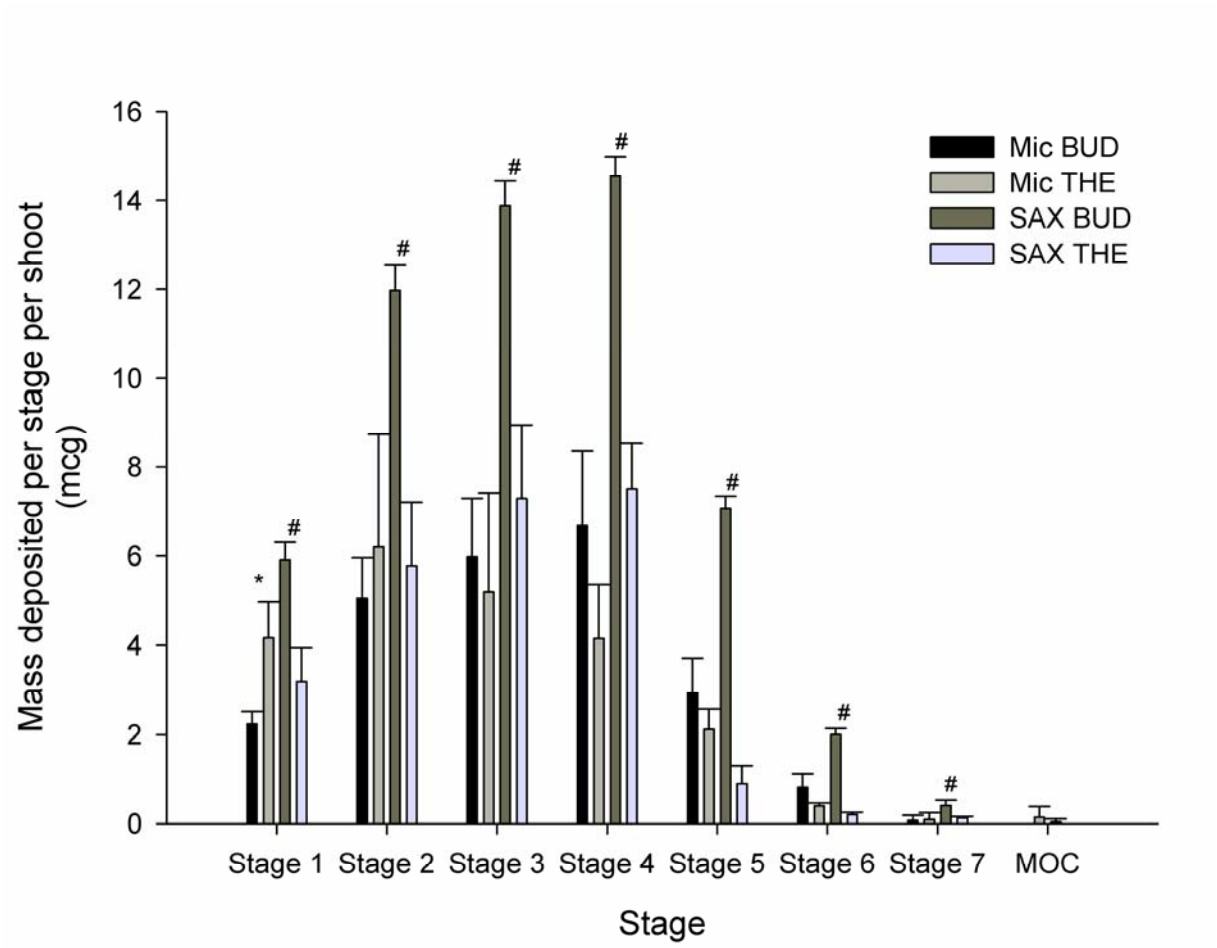

*Figure 4.23: NGI deposition per shoot on stages 1 to MOC for micronised BUD:THE 1:1 and SAX engineered BUD:THE 1:1 particles in a DPI formulation. *=significant difference (P<0.05) between micronised BUD and micronised THE. #=significant difference (P<0.05) between BUD and THE in SAX formulation.*

Figure 4.24 is a graphical representation of the ratio between the $\%RD_{BUD}$ and $\%RD_{THE}$ for both the SAX and micronised formulation. As shown, neither formulation provided a consistent dose ratio throughout the NGI with the SAX formulation demonstrating larger fluctuations in the ratio between BUD and THE than the micronised formulation.

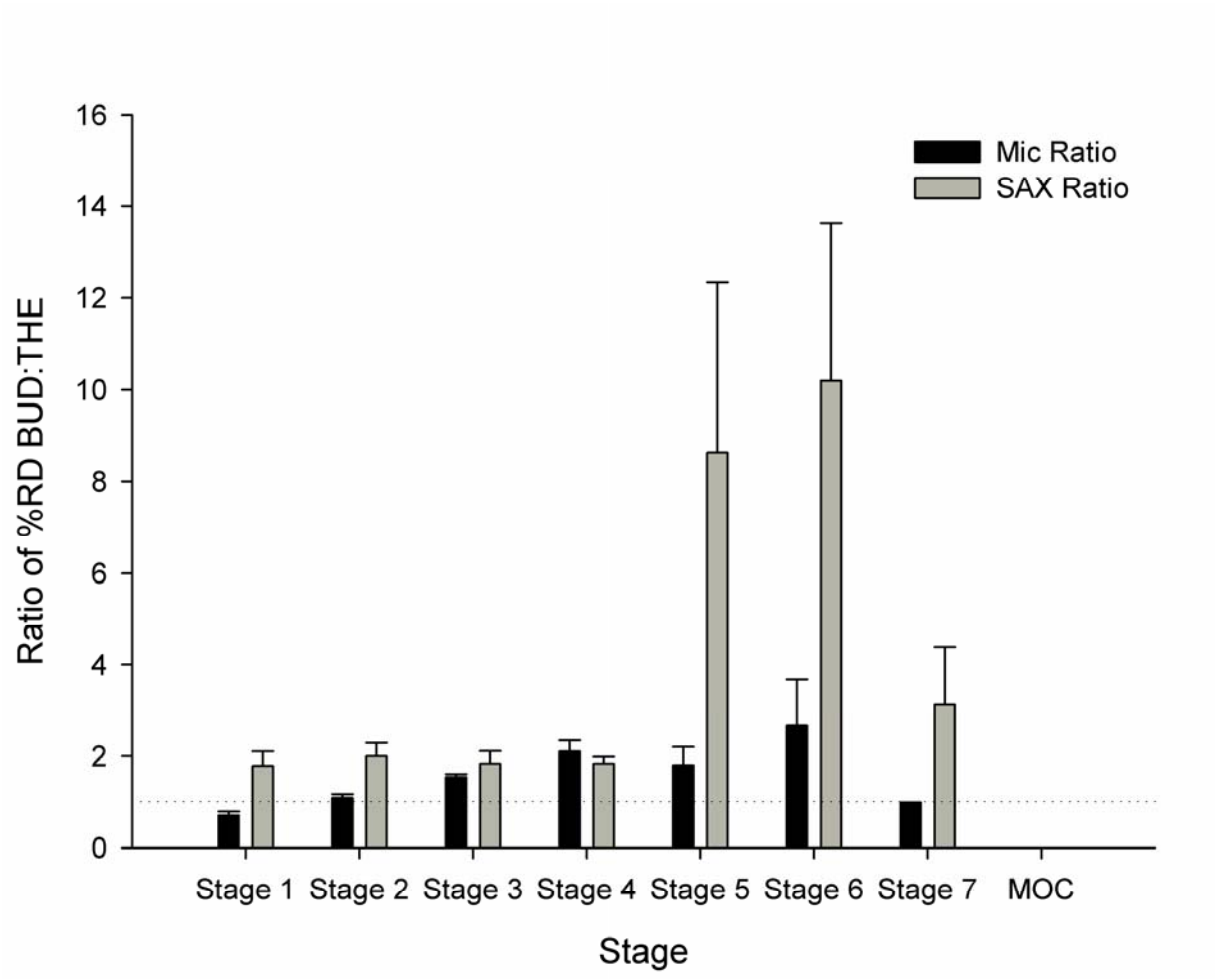

Figure 4.24: Graphical representation of the ratio between FP and THE for micronised and SAX formulations.

All of the DPI results suggested that the SAX process was unable to produce particles containing a steroid (either FP or BUD) with THE. However, the pMDI results show a positive correlation between the amount of steroid and THE delivered when fired into the ACI and suggests that a pMDI formulation containing an ICS with THE can be used to co-deposit the two compounds into a COPD patient lung with the possibility of reversing steroid resistance.

This may imply that the SAX process may have produced particles that contain a steroid and particles that contain THE with similar particle size distributions which may have separated during aerosolisation in the pMDI and would have different affinities to the lactose in a DPI formulation therefore resulting in a variability in the amount delivered (Begat, Morton et al. 2004; Jones, Harris et al. 2008) as well as the uniformity of the mixtures.

The difference between this work and that conducted by others could be due to the dose ratios; Pitchayajittipong used a dose ratio of 1:10 while this work was conducted using a dose ratio of 1:1 by mass. Alternatively, the solvent used may have made a

difference. For example, the SX:FP 1:10 particles were produced from an acetone solution while the FP:THE and BUD:THE particles were produced from a solution where the solvent consisted of 50% dichloromethane and 50% methanol by volume. The relative vapour pressure of the pure solvents for these studies are represented in Table 4.11. As shown, acetone has the greatest vapour pressure and, therefore, will evaporate more readily giving rise to greater viscosity within the collected droplets. Dichloromethane has the next highest vapour pressure with methanol having the lowest out of the three. The addition of methanol to dichloromethane will result in a vapour pressure between the two values for the pure solvents. As a result, the vapour pressure may not be sufficient to form a super-saturated droplet before being submerged into the anti-solvent.

Table 4.11: Vapour pressure of pure solvents at 25°C (CHERIC).

Solvent	Vapour pressure at 25°C (kPa)
Acetone	6.633
Dichloromethane	4.055
Methanol	2.826

The presence of excess solvent could result in a reduction of the crystallisation kinetics as the drug would be able to dissolve back into the solvent. This in turn would allow for slow crystal growth and the possibility of the particles growing as per their crystal habit allows and not forming a spherical particle. This could allow for the two compounds to precipitate out separately in the anti-solvent or produce some twinning between the compounds which can be subsequently fractured during the DPI formulation process but be maintained in the pMDI drug only formulation.

4.5 Conclusion

These data suggest that combination particles containing a lose association between an ICS and theophylline can be produced by the SAX process. The resultant particles were predominantly crystalline in nature. The *In-vitro* performance of a pMDI, drug only formulation showed that the two compounds can be delivered in combination via a pMDI formulation resulting in the co-deposition at the same site of action of the ICS and THE. However, a DPI formulation of the same particles appears to break up the combination so that the *In-vitro* NGI results do not show a consistent dose ratio throughout.

This may be due to the vapour pressure of the solvent used being too low to produce a highly viscous droplet by the time the particle has reached the anti-solvent and

therefore allowing for the drugs to have the opportunity to separate during crystallisation. Alternatively, the combination of solvents used to produce the initial solution may have allowed for different regions of the solution to have different amounts of each compound. Therefore resulting in the co-processing of the drugs rather than the combination of the two in one particle.

Chapter 5 - Novel Triple Formulations for the Treatment of COPD Containing a LABA, ICS and Theophylline.

5.1 Introduction

Chronic obstructive pulmonary disease (COPD) is a growing health concern within the global community (Mannino and Buist 2007; Pearce, It-Khaled et al. 2007). It is characterised by progressive, irreversible bronchoconstriction and airway inflammation (Barnes, Chung et al. 1998; Barnes, Shapiro et al. 2003).

Administration of LABA's appears to have reduced efficacy in COPD patients compared to asthmatics (Barnes 2003; Caramori and Adcock 2003). In addition, COPD patients are reported to be resistant to the effects of ICS's (Barnes 2000; Caramori and Adcock 2003; Barnes 2008) due to the oxidative and nitrative stress that inhibit the activity of histone deacetylase 2 (HDAC2) (Barnes 1998; Adcock, Maneechotesuwan et al. 2002; Barnes 2003; Barnes 2005; Ito, Ito et al. 2005; Ito, Yamamura et al. 2006). However, combination based therapy using both LABA and ICS together shows greater efficacy compared with monotherapy treatments with the individual components (Barnes 2001; Adcock, Maneechotesuwan et al. 2002; Calverley, Boonsawat et al. 2003; Sin and Man 2006), with suggestions of reduced mortality rates in COPD achieved by individual therapies (Soriano, Vestbo et al. 2002; Sin and Man 2007; Hanania 2008). This apparent synergistic effect is related to the up-regulation of key receptors by the LABA and ICS on which each class molecule will exert its effect (Mak, Nishikawa et al. 1995; Barnes 2001; Adcock, Maneechotesuwan et al. 2002; Barnes 2002). In addition to this, however, recent work has shown that the combination of fluticasone propionate (FP) and salmeterol xinafoate (SX), and ICS and LABA respectively, can reduce the amount of IL-8 released from stimulated neutorphils and macrophages (Edwards, Johnson et al. 2006; Mortaz, Rad et al. 2008; Marshall 2009). As a result, there will be a reduced influx of inflammatory cells to the lungs.

New insights into the molecular basis of chronic inflammation in COPD suggest that HDAC2 activity is reduced in the peripheral lung and in alveolar macrophages (Ito, Ito et al. 2005). As HDAC2 suppresses inflammatory gene expression and is required by corticosteroids for their anti-inflammatory activity; reduced levels of HDAC amplify the inflammatory response and account for corticosteroid resistance in COPD (Barnes, Ito et al. 2004). It has been reported that low doses of theophylline can activate HDAC suggesting that inhaled theophylline (THE) and ICS may act synergistically to suppress inflammation. The addition of a xanthine, such as theophylline (THE), to an ICS, may reverse the steroid resistance (Barnes and Pauwels 1994; Ito, Lim et al. 2002; Cosio,

Tsaprouni et al. 2004; Barnes 2006). The addition of THE to SX and FP may, therefore, provide additional benefit to COPD by increasing the efficacy of FP (Barnes and Pauwels 1994; Ukena, Harnest et al. 1997; Barnes and Woolcock 1998; Markham and Faulds 1998; Lim, Jatakanon et al. 2000; Lim, Tomita et al. 2001).

As previously discussed, current combination formulations consist of the active component being processed individually and then combined during the formulation stage. As a result, the prospect of co-depositing of both actives to the same site of action in the correct dose ratio is rather limited and cannot be controlled (Taki and Marriott; Taki, Zeng et al. 2006). Hence, these dosage forms are subject to greater variability in fine particle delivery of each active.

Previously, we have shown that the SAX process maybe employed to engineer single particles that contain two active ingredients (fluticasone propionate (FP) and salmeterol xinafoate (SX)) in the correct weight ratio. This approach was shown to reduce variability in fine drug particle delivery of both molecules *In-vitro*, and provided significant advantages to conventional methods of preparing combined inhalation dosage forms (Pitchayajittipong, Shur et al. 2009). The aim of this study was to engineer particles containing salmeterol xinafoate (SX), theophylline (THE) and fluticasone propionate (FP) so that the three drugs can be co-deposited in a fixed ratio, using the SAX process (Pitchayajittipong, Shur et al. 2009).

5.2 Materials

Micronised FP and SX were obtained from sources stated in Chapter 2, as was theophylline and lactose monohydrate. All organic solvents were of at least analytical grade and were supplied by Fisher Chemicals (Loughborough, UK). Water was prepared by MilliQ from reverse osmosis (Milipore, Molsheim, France).

5.3 Methods

5.3.1 Production of SAX-produced SX:FP:THE Particles

Combined SAX SX:FP:THE particles were prepared by atomisation of a 2% w/v solution containing SX:FP:THE in the ratio 1:10:10 in a co-solvent of dichloromethane:methanol (50:50). Atomisation was conducted using a SU11 co-axial two-fluid atomiser with an internal mix (Spraying Systems Co., Illinois, USA). The atomiser was used at a sprayed rate of 4 $ml.min^{-1}$ with air pressure at 2.5 bar in a lab scale SAX process. Atomisation was conducted over a 60 cm separation distance and positive pressure of 30 $L.min^{-1}$. The resultant droplets were collected in a non-solvent of hexane at 5˚C, and exposed to sonic energy using a sonic horn (P100, Sonic

Systems, Somerset, UK) operating at a fixed wavelength of 20 kHz and capable of inducing a maximum power output of 750 W. The ultrasonic horn (horn diameter ~13 mm) was immersed 5 mm in the processing liquid to aid nucleation and crystal growth. The resulting particles were isolated using supercritical CO_2 extraction of hexane, as described in Chapter 2.

5.3.2. Formulation Production

5.3.2.1: Pressurised metered dose inhalers (pMDI's)

Drug-only pressurised metered dose inhaler (pMDI) formulations containing 0.30 % w/w of combination SAX particles of SX, FP and THE was produced by weighing the appropriate amount of powder into an aluminium canister (Bespak, King's Lynn, UK) before being sealed with a 50 µl metering valve (Bespak, King's Lynn, UK) and the appropriate amount of HFA-134a (Ineos Fluor, Runcorn, UK) propellant being added. The canisters were then sonicated for 20 minutes and allowed to stand for 24 hours before testing. An equivalent formulation containing micronised SX, micronised FP and micronised THE was also prepared.

5.3.2.2: Dry powder inhaler (DPI) formulation

A formulation, containing 1.6% w/w combined SAX SX:FP:THE, was prepared by geometric blending with a sieved grade of inhalation lactose monohydrate (Respitose, SV003). The combined SAX particles and SV003 were mixed in a 15 ml glass tube for 60 seconds in a Whirlimixer (Fisons Scientific Equipment, Loughborough, UK). The resultant blend was further processed using a Turbula mixer (Willy A Bachofen AG, Basel, Switzerland) at 46 rpm for 45 minutes.

In order to compare the *in-vitro* inhalation performance of SAX particles, a micronised combination formulation containing 0.08% w/w of micronised SX, 0.76% w/w of micronised FP and 0.76% w/w micronised THE, was prepared by geometric blending SV003 lactose. The drug and SV003 were mixed in a 15 ml glass tube for 60 seconds in a Whirlimixer (Fisons Scientific Equipment, Loughborough, UK). The resultant blend was then mixed using a Turbula mixer (Willy A Bachofen AG, Basel, Switzerland) at 46 rpm for 45 minutes. Both the formulations containing either combined SAX particles or micronised equivalent blends were stored at 44 % RH and 25 °C for 24 h before formulation testing.

5.3.3 Content Uniformity Determination

Upon blending of the DPI formulation, the content uniformity of formulations was assessed. Each blend was spread over a clean surface and ten samples of 25 $\pm$ 1 mg

taken from random positions. Each sample was dissolved with 15 minutes sonication in 100 ml final volume of 50% methanol 50% water and drug concentration assessed by high performance liquid chromatography (HPLC). The proportion of drug in each sample was calculated and the content uniformity expressed as the coefficient of variation (Equation 3.1).

5.3.4 Capsule Filling

The DPI formulations were manually loaded into size 3 hydroxypropyl methylcellulose (HPMC) capsules (Qualicaps, Madrid, Spain). Fill weight was 25 ± 1 mg, giving a nominal dose of 400 ± 16 µg total drug per capsule for each formulations used. Following filling, capsules were stored in a sealed container containing a saturated solution of potassium carbonate (RH = 44%, (Rockland 1960)) for at least 24 hours prior to analysis.

5.3.5 *In-Vitro* Performance Analaysis

5.3.5.1 Andersen Cascade Impactor (ACI)

In-vitro pMDI performance may be assessed using an Andersen Cascade Impactor (ACI, Copley Scientific, Nottingham, UK). Prior to assembly, each impaction plate was immersed in a 1% v/v solution of silicon oil (Acros Organics, Geel, Belgium) in hexane and allowed to air dry. The ACI was then assembled and connected to a vacuum pump (Gaast, Benton Harbour, MI, USA). The flow rate at the inlet to the throat was set to 28.3 $L.min^{-1}$ using a digital flow meter with model DFM 2000 (Copley Scientific Ltd., Nottingham, UK).

For each analysis, the first five shots of each pMDI were fired to waste following shaking the can for 10s between each actuation. The manufactured pMDIs were inserted into a specially constructed mouthpiece and actuated in a fixed position. With the pump on, the solenoid valve was opened for 12s. A 3s delay was employed, after the pump was engaged, to allow equilibrium of the pump before the actuator was pressed for 4s to allow sufficient time for firing. After this, the pump was allowed to continue for a further 5s before the solenoid valve was closed, as in chapter 3. Three consecutive doses, with vigorous shaking of the canister between each dose, for each formulation were released into the impactor.

The pMDI actuator, mouthpiece adaptor, throat assembly, collection plates from stage zero to seven and filter stage were thoroughly rinsed into suitable volumetric flasks with dilution solvent (50:50 (V/V) methanol:water) and made up to the mark. The actuator, mouthpiece adaptor, throat assembly and ACI collection plates were then washed in

water and rinsed with distilled water followed by methanol, and dried at 40°C in an oven for 30 min. The ACI components were left to cool for 30 min, reassembled and re-used. For each formulation, ACI investigations were carried out in triplicate. All samples were analysed by HPLC from which the mass of drug deposited on each stage could be determined.

The emitted dose (ED) was defined as the mass of drug recovered from all parts of the ACI and mouthpiece adaptor. The fine particle dose (FPD) was the mass of drug recovered from stage 3 and below of the ACI and the fine particle fraction (FPF_{ED}) was the FPD expressed as a percentage of the ED.

5.3.5.2 Next Generation Impactor (NGI)

In-vitro DPI performance was assessed using a Next Generation Impactor (NGI, Copley Scientific Ltd, Nottingham, UK). The NGI collection cups were immersed in a 1% v/v solution of silicone oil (Acros Organics, Geel, Belgium) in hexane and allowed to air dry. The NGI was then assembled with pre-separator (containing 15 ml of wash solvent) and connected to a vacuum pump (Gaast, Benton Harbour, MI, USA) *via* a solenoid valve. The flow rate at the inlet to the throat was set to 85 $L.min^{-1}$ using a digital flow meter with model DFM 2000 (Copley Scientific Ltd., Nottingham, UK). An Aerolizer DPI device was attached to the throat of the NGI using a specially created mouthpiece. A capsule was inserted in the Aerolizer and pierced by eight sharp pins to generate four small holes at each end of the capsule. The contents of the capsule were then aerosolised into the NGI by drawing air through the apparatus at 85 $L.min^{-1}$ for 2.8 seconds (controlled by the solenoid valve). Once the contents of three capsules were aerosolised in this way, the device was disconnected, and capsules and each stage were thoroughly rinsed into suitable volumetric flasks with dilution solvent (50:50 (V/V) methanol:water) and made up to the mark. The concentration of drug in each solution was investigated by HPLC, from which the mass of drug deposited on each stage of the NGI could be determined at stages 1 to 7 and the MOC. Between experiments, the NGI was washed in water and methanol, dried in an oven, and allowed to cool to room temperature before re-use.

Each formulation was tested in triplicate. The emitted dose (ED) was defined as the mass of drug recovered from all parts of the NGI and the mouthpiece. The fine particle dose (FPD) was the mass of drug recovered from stage 3 and below of the NGI and the fine particle fraction (FPF_{ED}) was the FPD expressed as a percentage of the ED.

5.3.6 High Performance Liquid Chromatography

Drug concentrations were determined by HPLC. The HPLC system consisted of a PU-980 intelligent HPLC pump, an AS950 intelligent autosampler and a UV-975 inteligent UV/VIS detector (all from Jasco, Japan). Data were collected and analysed using Azur v4.0 software (Datalys, Saint Martin D'Heres, France). Unknown sample concentration was determined from duplicate injections by comparison of peak area with reference peaks from external standard solutions of known concentration.

All compounds were analysed using the same HPLC apparatus and wash solution. This employed a 4.6 mm x 150 mm C18, 5 µm Hypersil column (Phenominex, Macclesfield, Cheshire, UK). The flow rate was 1.5 $ml.min^{-1}$; with the injection volume of 100 µl. FP and SX drug concentrations were assessed using 75:25 (v/v) 0.6% w/v aqueous ammonium acetate:methanol with a detection wavelength of 228nm while THE drug concentrations were assessed using 10mM Aqueous Ammonium acetate:MeOH:ACN 86:7:7 (v/v) with a detection wavelength of 271nm

Drug retention times were 2.38, 3.75 and 4.20 minutes for SX, FP and THE respectively, so a run time of 5 minutes was employed.

The relationship between drug concentration (0.1, 1, 5, 10 and 50 $\mu g.ml^{-1}$) and peak area for each drug was found to be linear, with linear regression analysis yielding a coefficient of determination (R^2) of 1.0 for FP and THE and 0.997 for SX (Figure 5.1). Calibration curves were produced prior to each experimental assay.

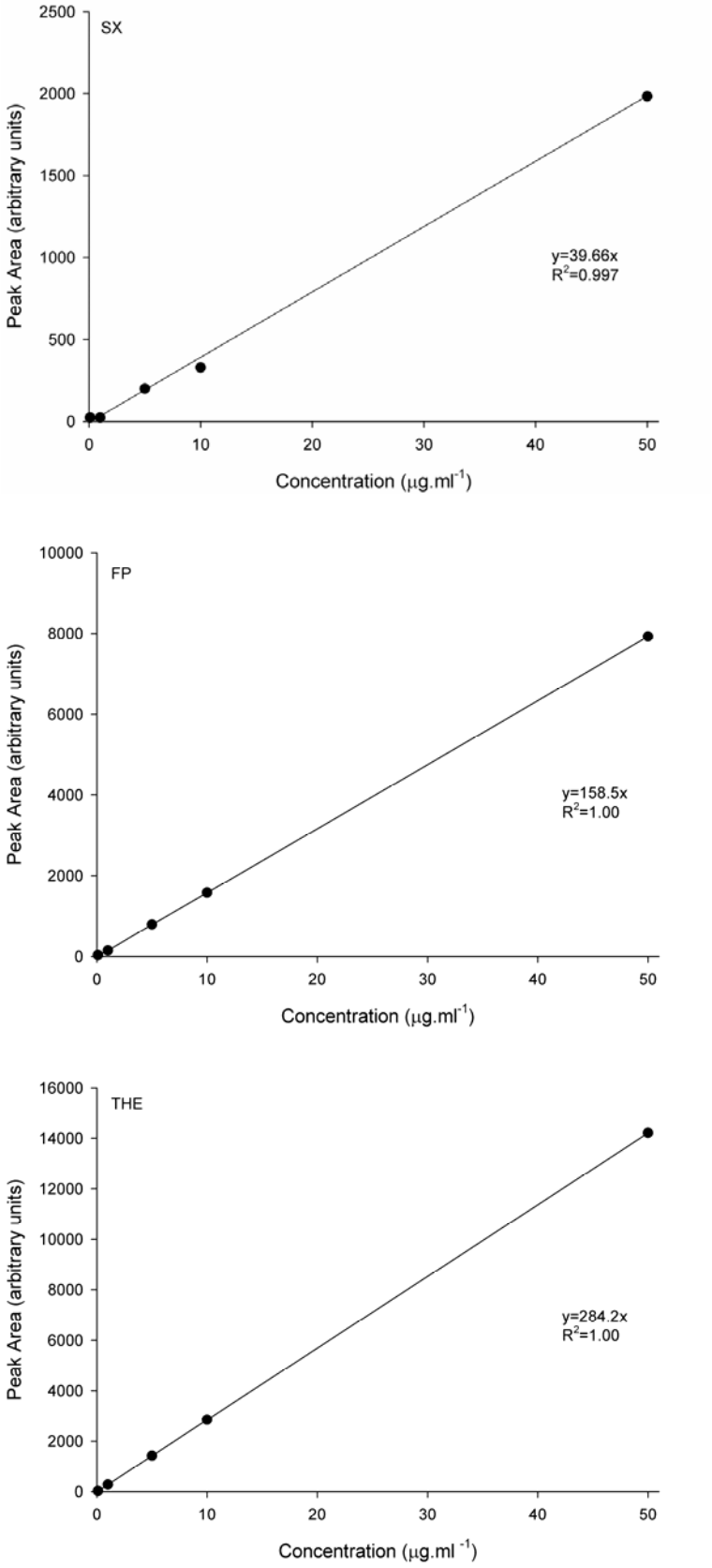

Figure 5.1: HPLC calibration curves for SX, FP, and THE.

5.4 Results and Discussion.

5.4.1 Physical characterisation

As in chapter 3, the physical morphology of SX can be modified depending on the operating conditions of the SAX process. Figure 5.2 shows the SEM micrograph images of micronised SX (5.2A) compared to SAX SX produced from an acetone solution (5.2B).

As shown, the micronised SX appear to be flat plate like particles of approximately 10µm in width whilst the SAX SX appears as spherical particles.

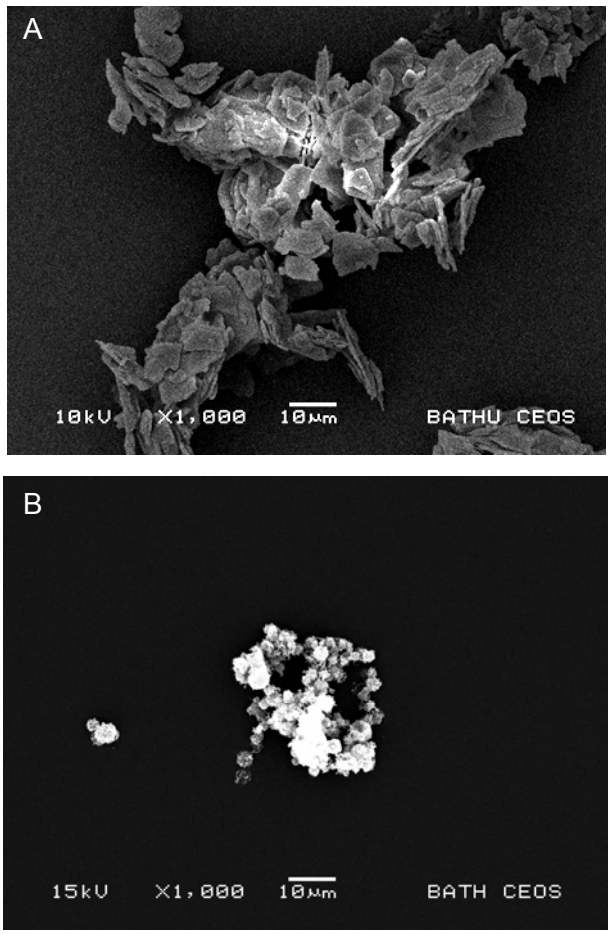

Figure 5.2: SEM micrograph images of micronised SX (a) and SAX SX (b).

Figure 5.3 shows the SEM micrograph images of SX, FP and THE (1:10:10 ratio by mass) particles when produced in combination via SAX. Three distinct crystal habits are evident: long needle like particles, flatter plate like particles and small fibres.

As discussed, Pitchayajittipong *et.al.* have shown that FP and SX can be combined in one particle using SAX resulting in the production of spherical particles (as shown in figure 5.4) that can be delivered via a DPI formulation. These particles allowed for the

ratio between FP and SX to be maintained at a ratio of 10:1, respectively, throughout the in vitro NGI apparatus (Pitchayajittipong, Shur et al. 2009). It appears that the addition of THE resulted in the breakdown of the combination between FP and SX. This could be due to the presence of the methanol in the solvent causing a reduction in the vapour pressure of the dichloromethane, as seen in chapter 3, resulting in a solution reaching the anti-solvent instead of a highly viscous droplet, containing all three compounds. This subsequently could result in the individual materials precipitating out of solution as the solvent dissipates into the anti-solvent. The high magnification SEM image in Figure 5.3b, suggests that this process may have occurred. The differences in the particle shapes and sizes indicates that they may not have a similar aerodynamic diameter and, therefore, will not be able to maintain a consistent dose ratio in either a pMDI or a DPI formulation.

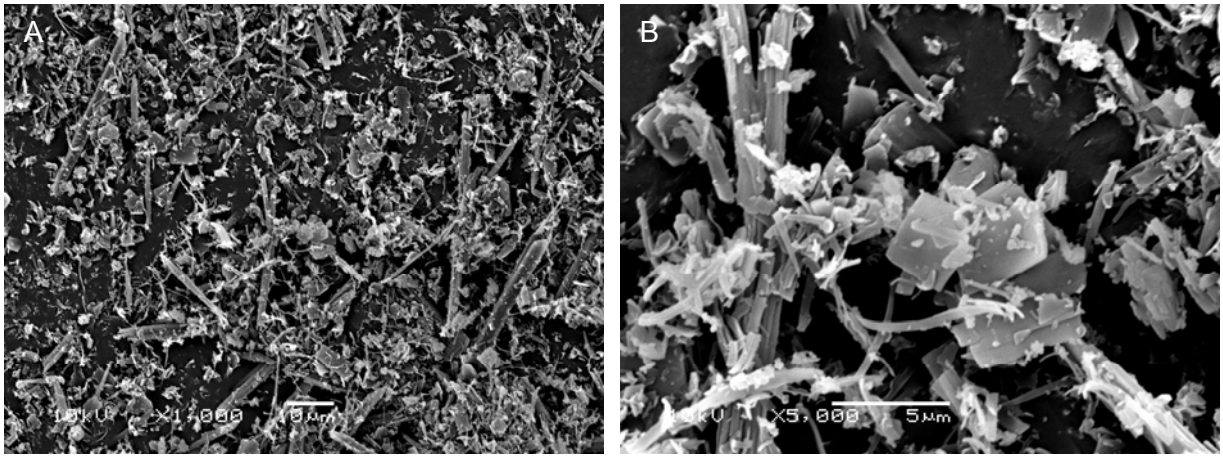

Figure 5.3: SEM micrograph images of SX:FP:THE 1:10:10 particles produced by SAX at 100x (a) and 5000x (b) magnification.

Figure 5.4: SEM micrograph images of SAX SX:FP 1:10 particle (Pitchayajittipong, Shur et al. 2009)

Figure 5.5 shows a graphical representation of the particle size distribution of the SAX produced SX:FP:THE 1:10:10 particles compared to the micronised equivalent particles with the data also being represented in table 5.1. The particle size distribution of the SAX material is larger then that of the micronised SX and micronised FP but smaller then the micronised THE. This suggested that the SAX particles may deposit on the lower stages of the impactor compared to the micronised THE but not as far as the micronised FP or SX.

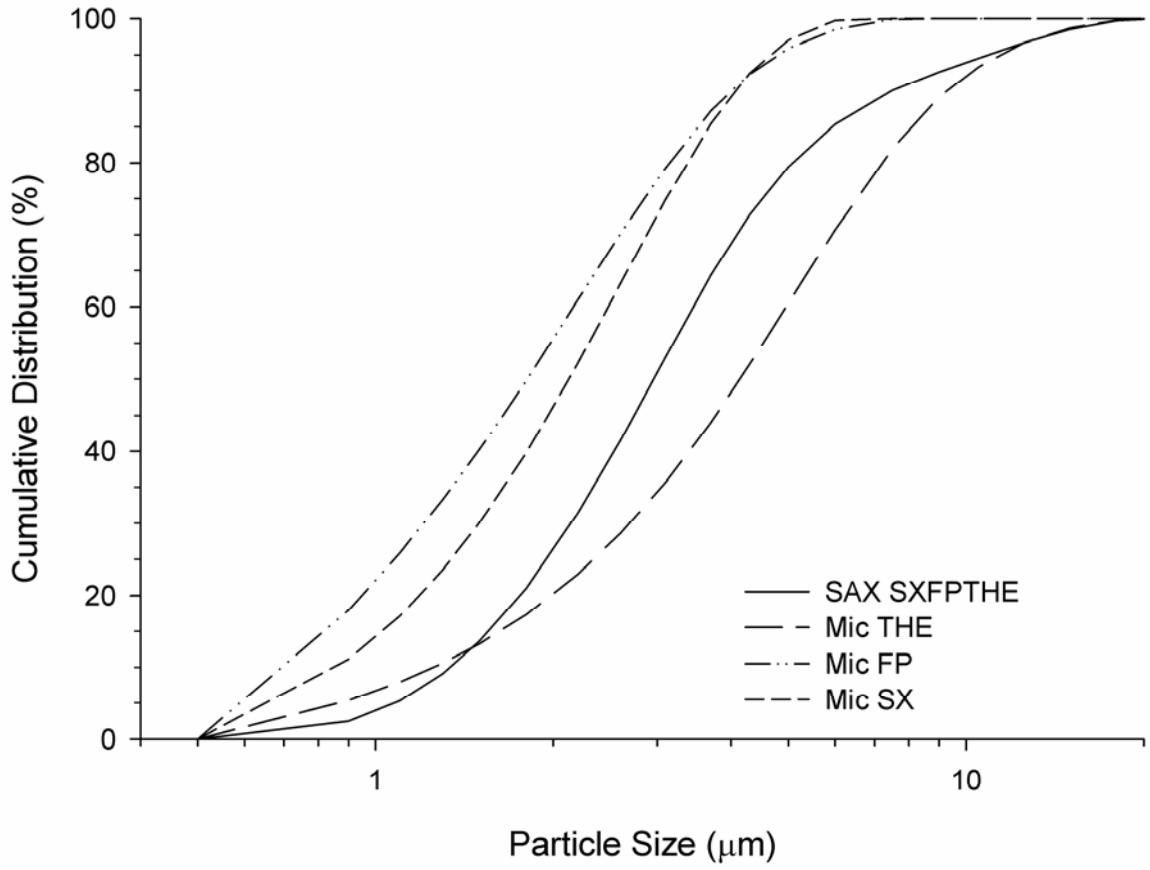

Figure 5.5: Particle size distribution of SAX produced SX:FP:THE 1:10:10 particles compared to micronised SX, micronised FP and micronised THE.

Table 5.1: Particle size distribution of micronised SX, micronised FP, micronised THE and SAX engineered SX:FP:THE 1:10:10 particles.

	Particle Size (μm ± SD)		
	d_{10}	d_{50}	d_{90}
SX	0.86 ± 0.01	2.13 ± 0.01	4.10 ± 0.01
FP	0.72 ± 0.01	1.81 ± 0.01	4.03 ± 0.05
THE	1.26 ± 0.02	4.15 ± 0.03	9.33 ± 0.12
SX:FP:THE	1.34 ± 0.01	2.97 ± 0.01	7.52 ±0.07

Figure 5.6 shows the XRPD diffractogram of the SAX engineered SX:FP:THE 1:10:10 material compared to the diffractograms of the micronised materials. The SAX diffractogram demonstrated several peaks suggesting that the material produced was crystalline. However, the peaks shown can all be related to either FP or THE with no peaks being presented that can be used for the confirmation of the presence of SX within the sample. This may be related to the small amount of SX within the sample,

which may have resulted insufficient peak intensity to register any difference to the baseline in comparison to FP and THE within the sample. In addition to this, there does not seem to be any new peaks in the XRPD to suggest the formation of a new crystalline lattice, as shown in chapter 4.

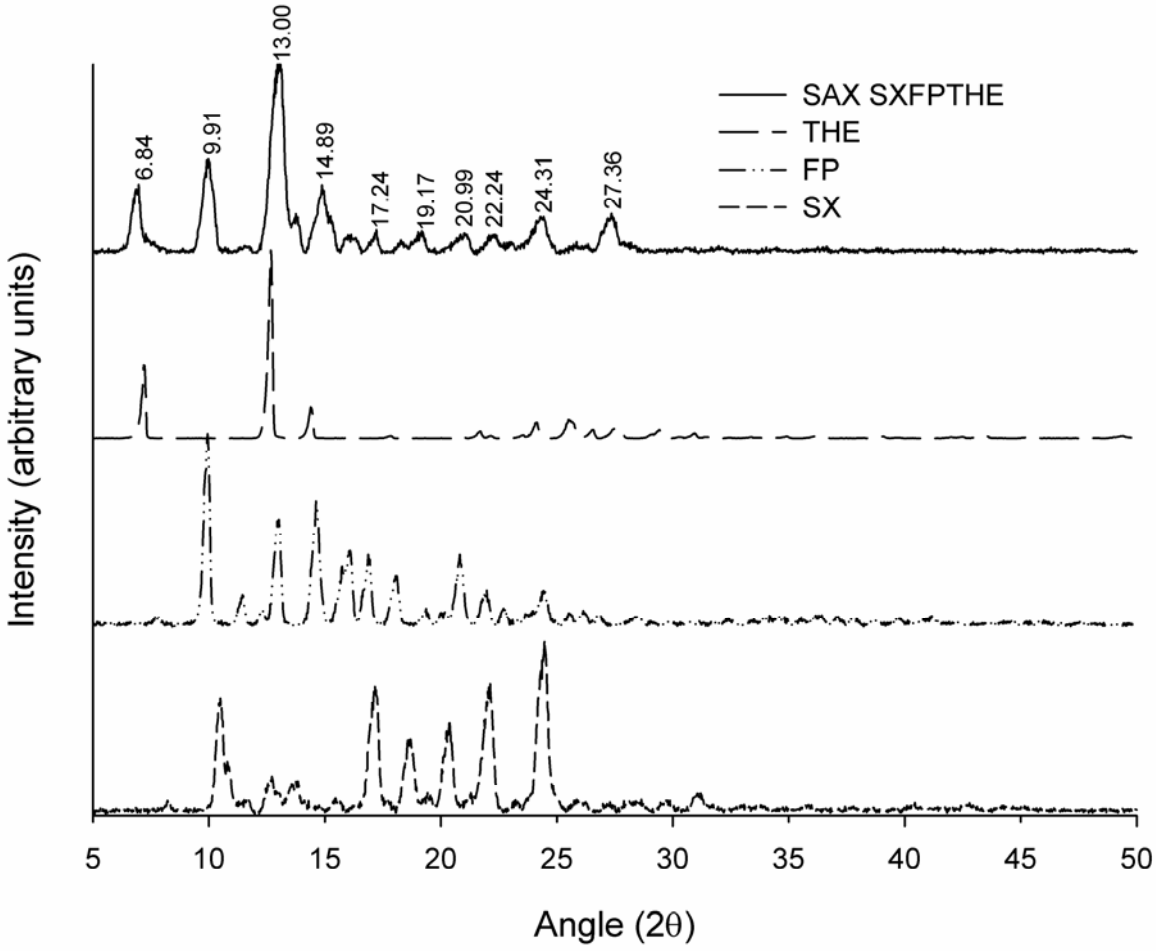

Figure 5.6: XRPD diffractogram of SAX engineered SX:FP:THE (1:10:10) particles compared to the raw materials

Figure 5.7 shows the DSC thermogram of the SAX produced SX:FP:THE particles compared to their respective raw materials. The SAX material demonstrates two distinct endothermic responses: the first demonstrating a peak melting temperature at 117.24°C and the second at 252.52°C with onsets of melt at 111.72°C and 250.53°C respectively. These temperatures are slightly lower than the peak melting temperatures for SX form I and the FP:THE particles in chapter 3. The shift in peak melting point could be due to the other compounds within the formulation acting as impurities and therefore shifting the melting point down. This also supports the argument that the material produced in chapter 4 was not a new crystalline lattice but a combination of FP

and THE and therefore could explain why the DPI formulation did not allow for the co-deposition of FP and THE with the same ratio throughout the NGI. However, these data confirm the presence of SX within the mixture produced by SAX.

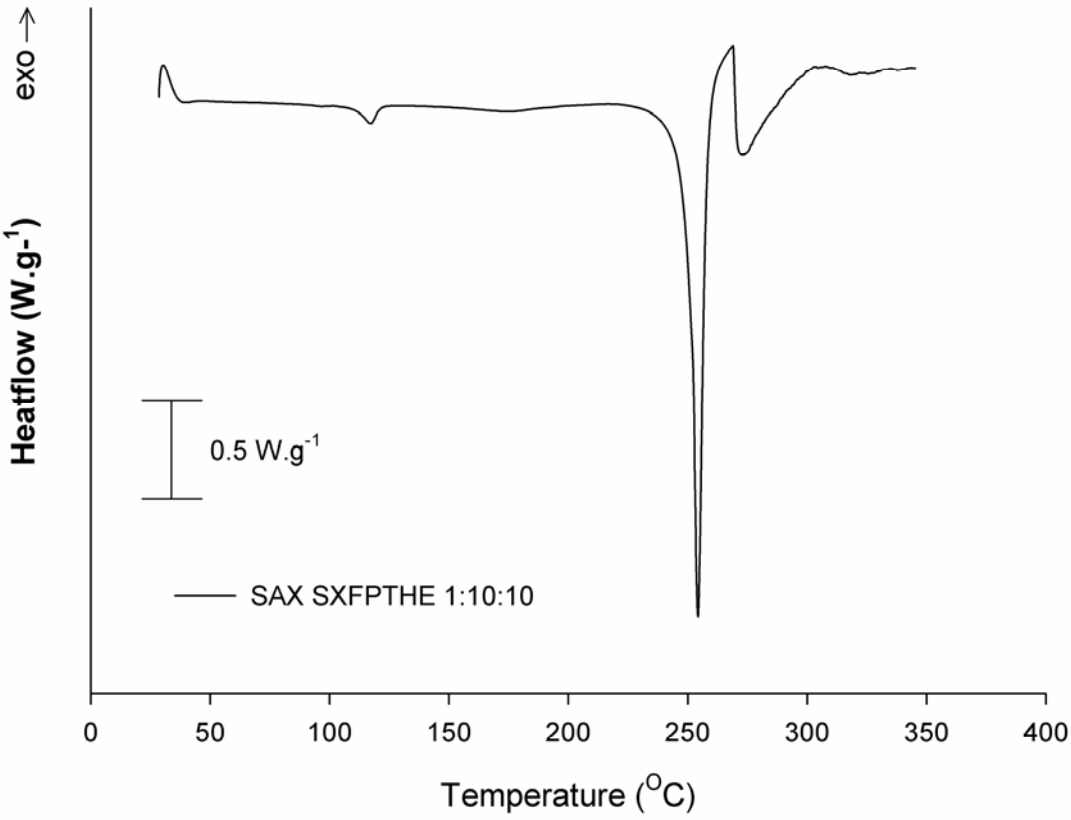

Figure 5.7: DSC thermogram of SAX engineered SX:FP:THE 1:10:10 particles.

Figure 5.8 shows the DVS isotherm plot for the SX:FP:THE 1:10:10 particles produced by SAX at 25°C. The first sorption cycle shows a gradual increase in weight with a slight deviation between 40 and 70% RH. The desorption cycle demonstrated a slightly higher weight of sample between 80 and 40% RH compared to the sorption cycle.

After the first sorption/de-sorption cycle, there was no change in mass. These data suggest that there was no incorporation or loss of water from the crystal lattice during the run and, therefore, the particles were predominantly crystalline.

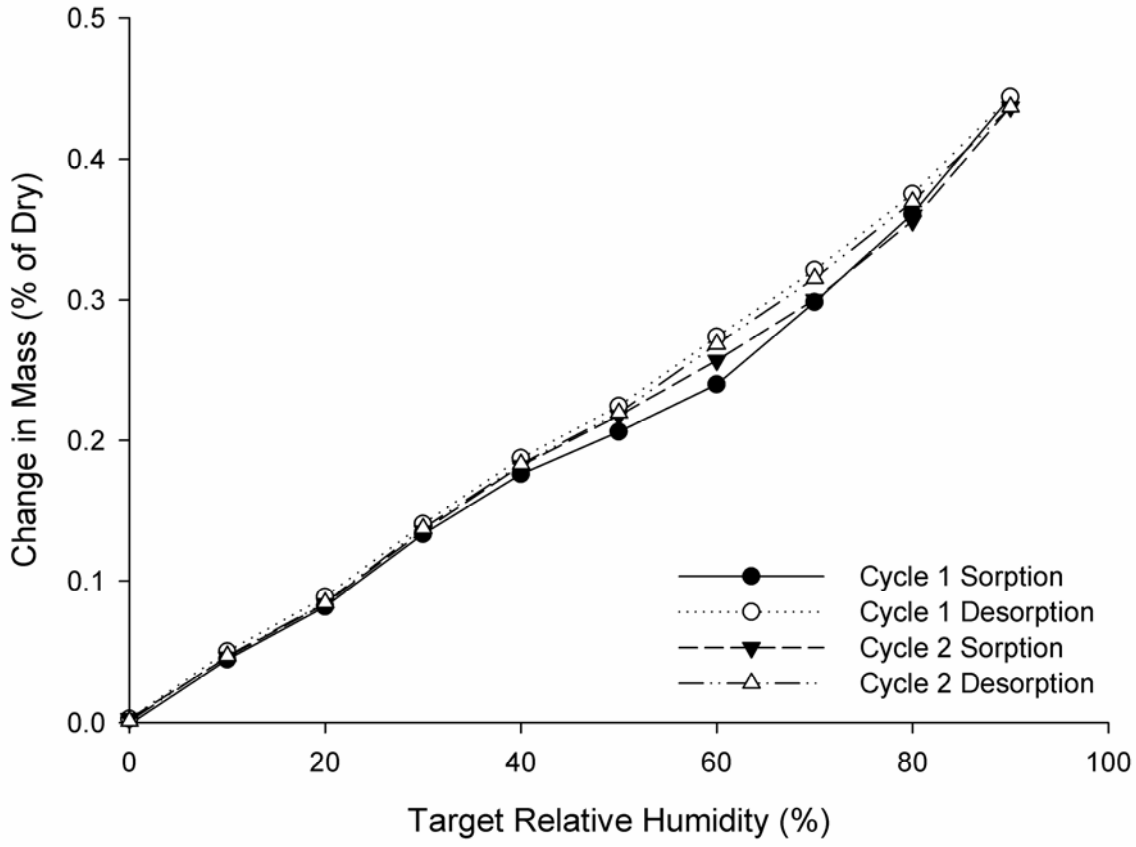

Figure 5.8: DVS isotherm at 25°C for SAX engineered SX:FP:THE 1:10:10 particles

5.4.2 In-vitro performance of pMDI formulations

Figure 5.9 shows the fine particle fraction of the emitted dose (FPF_{ED}) for the SAX pMDI formulation compared to the micronised equivalent. The FPF data, along with the mass deposited on each stage, emitted dose (ED), fine particle dose (FPD), the mass median aerodynamic diameter (MMAD) and the geometric standard deviation of the MMAD (GSD), are also tabulated in table 5.2.

As shown, the FPF_{ED} for SX, FP and THE varied in the micronised formulation with all three compounds demonstrating significantly different values ($P<0.05$). The FPF_{ED} values follow the particle size data with FP having the smallest geometric particle size and the highest FPF_{ED}, followed by SX and THE being the largest particles and therefore, the smallest fine particle fraction. The SAX formulation shows that SX and FP had similar FPF_{ED} values while THE was significantly lower ($P<0.05$). These data suggest that the dual processing of SX and FP allows for the similar deposition *in-vitro* and may, therefore, aid in the reduction of IL-8 production (Barnes 2002; Mortaz, Rad et al. 2008). The significant lower FPF_{ED} for THE means that a sub-optimal dose of

THE may reach the deep lung and therefore the steroid resistance may not be reversed.

In addition to this, the SAX formulation delivered more SX and FP to the lower stages of the ACI compared to the micronised formulation. Conversely, micronised THE had a greater FPF_{ED} than the SAX equivalent.

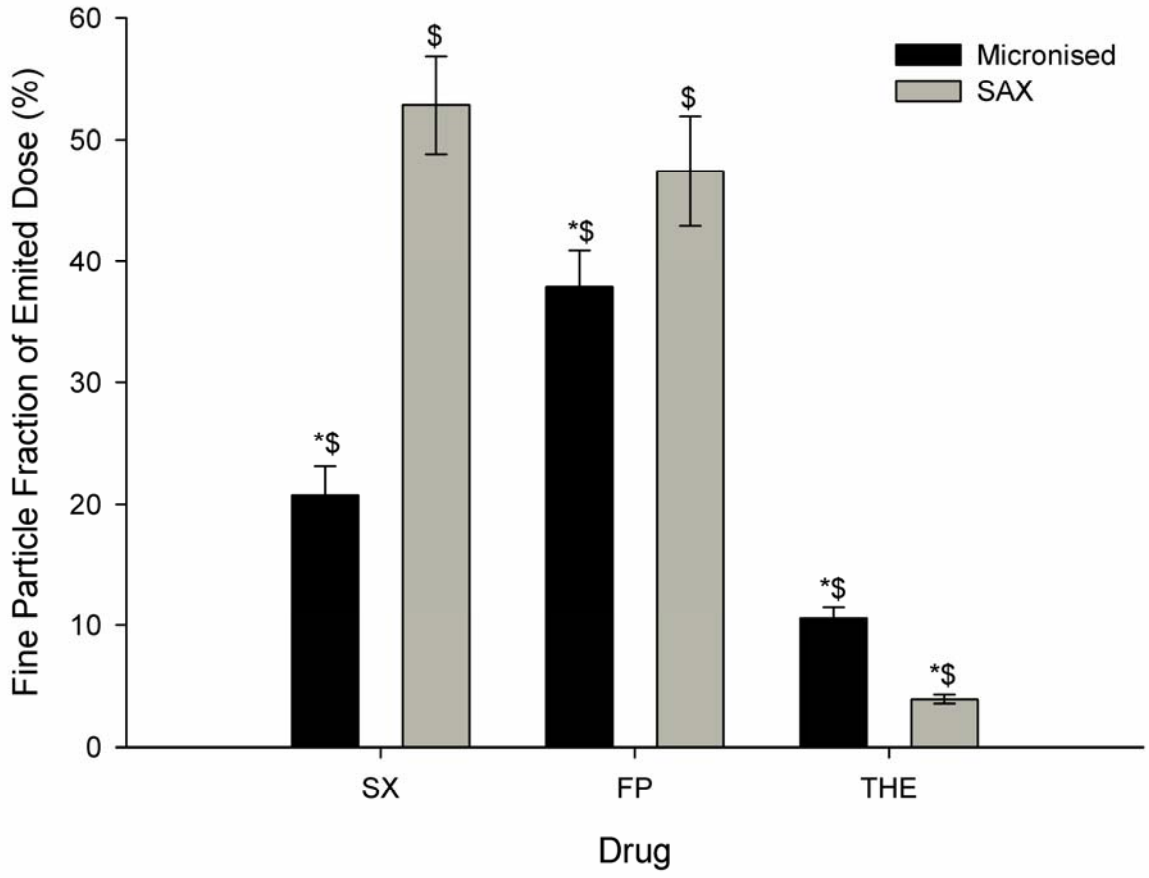

*Figure 5.9: Graphical representation of FPF_{ED} for all the compounds in both the SAX and micronised formulations. *=significant difference compared to compounds in same formulation $=significant difference across formulations (P<0.05)*

Table 5.2: ACI deposition per shoot of drug delivered from micronised SX:FP:THE 1:10:10 and SAX engineered SX:FP:THE 1:10:10 particles pMDI formulations;

SX=salmeterol xinafoate, FP=fluticasone propionate; THE=theophylline; MP&T= mouthpiece and throat; S=stage; F=filter.

Formulation	Drug	Mean Drug Deposition on Impactor Stages											Mean ED (µg±SD)	Mean FPD (µg±SD)	Mean FPF_{ED} (%±SD)	MMAD µm (GSD)
		Device	MP &T	S0	S1	S2	S3	S4	S5	S6	S7	F				
Micronised	SX	4.80 ± 4.07	8.22 ± 2.10	0.65 ± 0.36	0.57 ± 0.18	1.00 ± 0.10	1.08 ± 0.56	0.90 ± 0.21	0.43 ± 0.05	0.25 ± 0.01	0.11 ± 0.12	0.00 ± 0.00	13.21 ± 2.72	2.77 ± 0.79	20.77 ± 2.33	3.94 (1.95)
	FP	24.32 ± 8.96	71.86 ±18.95	2.33 ± 1.53	3.83 ± 0.93	6.48 ± 1.09	15.75 ± 2.65	20.72 ± 1.60	11.93 ± 1.67	1.59 ± 0.56	0.24 ± 0.24	0.52 ± 0.45	135.26 ± 25.02	50.75 ± 5.82	37.86 ± 3.05	2.85 (1.96)
	THE	21.43 ±18.56	77.30 ±33.83	8.83 ± 1.22	6.33 ± 0.58	6.68 ± 0.76	7.49 ± 2.59	2.81 ± 0.81	0.89 ± 0.28	0.19 ± 0.09	0.08 ± 0.13	0.00 ± 0.00	110.58 ± 36.64	11.45 ± 2.89	10.56 ± 0.93	6.01 (1.91)
SAX	SX	4.71 ± 2.12	4.62 ± 0.32	1.65 ± 0.58	1.58 ± 0.68	1.53 ± 0.58	1.55 ± 0.69	2.31 ± 0.44	2.77 ± 0.59	2.04 ± 0.78	1.57 ± 0.27	0.30 ± 0.26	19.9 ± 3.3	10.5 ± 2.0	52.8 ± 4.0	2.57 (2.74)
	FP	17.99 ± 4.15	44.38 ± 2.14	3.22 ± 0.47	2.41 ± 0.17	2.86 ± 1.18	9.18 ± 2.26	18.36 ± 3.18	16.60 ± 3.29	2.71 ± 0.36	0.91 ± 0.76	0.37 ± 0.32	101.0 ± 10.8	48.1 ± 8.8	47.4 ± 4.5	2.59 (2.0)
	THE	22.00 ± 4.31	71.88 ± 1.65	12.77 ± 2.74	5.23 ± 0.28	1.82 ± 0.54	1.35 ± 0.35	0.92 ± 0.15	0.64 ± 0.12	0.35 ± 0.11	0.24 ± 0.06	0.28 ± 0.03	95.5 ± 5.6	3.8 ± 0.6	3.9 ± 0.4	17.88 (4.83)

Figure 5.10 shows the amount of each drug deposited on each stage as a percentage of the total recovered dose (%RD) for each drug in both formulations. The device showed no significant difference in the %RD for any drug in both formulations. The micronised formulation also maintained the ratio between the compounds at the mouth and throat stage. The ratio between SX and FP is maintained down to stage 3 for the micronised formulation. On stages 3, 4 and 5, the ratio varied. From stage 6 onwards, the micronised formulation shows very little or no drug deposition.

In the SAX formulation, the ratio between the drugs is constantly changing throughout the ACI. The ratio of the %RD for each drug in both formulations on each stage of the ACI is also represented in figure 5.12.

These data confirmed that the SAX process has produced a eutectic mixture of all of the compounds, which upon aerosolisation from a pMDI formulation does not maintain a consistent dose ratio of all drugs throughout the ACI. These data also suggest that the drugs are less likely to act at the same site of action. However, an advantage of such an eutectic mixture produced by SAX maybe to enable accurate metering of all the drugs in the required dose.

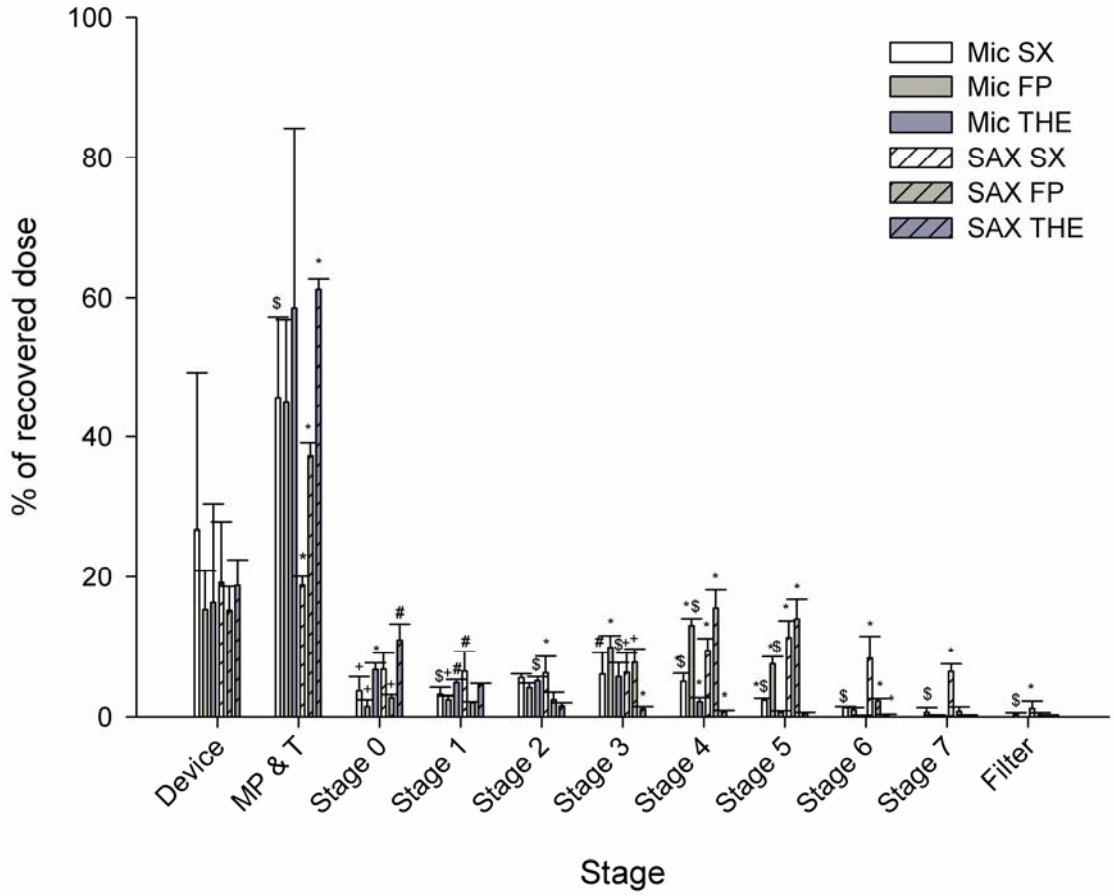

Figure 5.10: Graphical representation of the percentage of recovered dose (RD) collected on each stage of the ACI.=significant difference from other compounds in the same formulation, $=significant difference between same drug in different formulations, £=significant difference from $\%RD_{SX}$ in the same formulation, #=significant difference from $\%RD_{FP}$ in the same formulation and +=significant difference in $\%RD_{THE}$ in the same formulation (all P<0.05)*

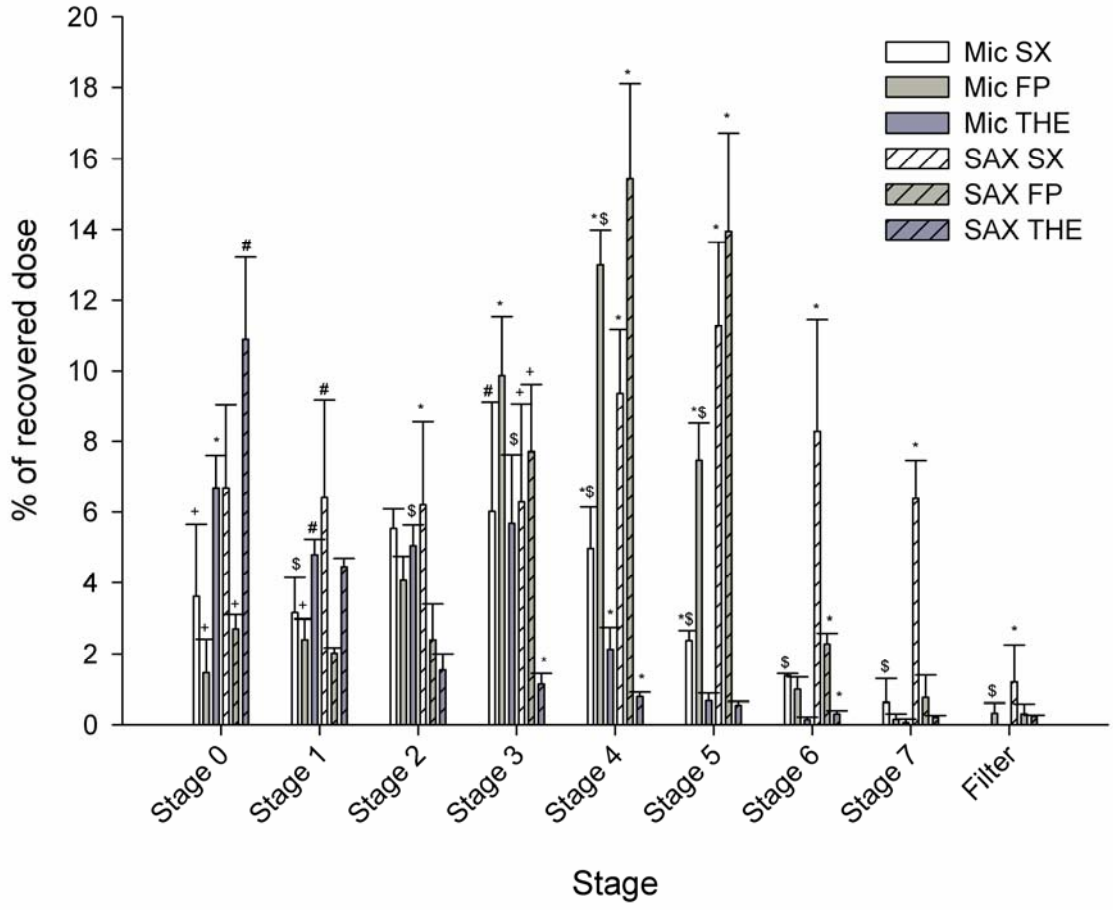

Figure 5.11: Graphical representation of the percentage of recovered dose (RD) collected on stages 0 to filter of the ACI.=significant difference from other compounds in the same formulation, $=significant difference between same drug in different formulations, £=significant difference from $\%RD_{SX}$ in the same formulation, #=significant difference from $\%RD_{FP}$ in the same formulation and +=significant difference in $\%RD_{THE}$ in the same formulation (all $P<0.05$)*

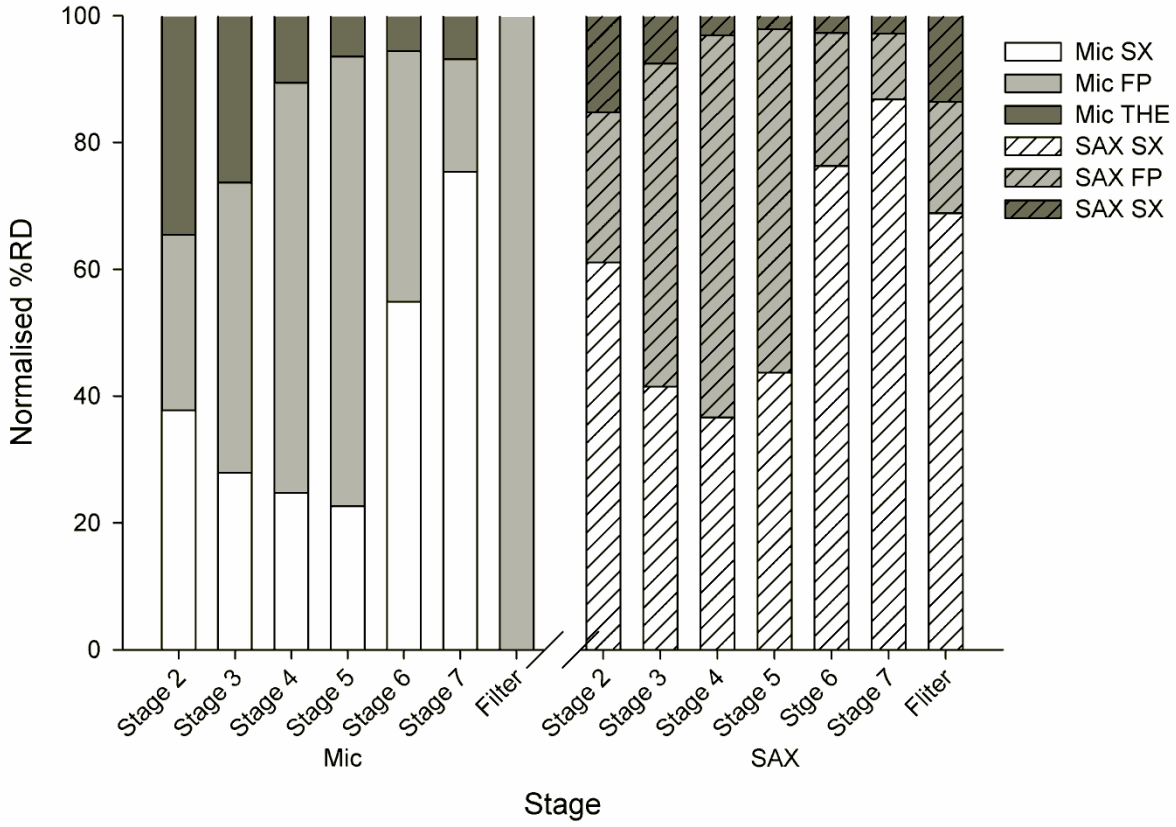

Figure 5.12:Graphical representation of the ratio between the %RD for each drug between stage 2 and filter of the ACI for both formulations.

5.4.3 *In-vitro* performance of DPI formulations

Figure 5.13 shows the FPF_{ED} of SX, FP and THE from the SAX formulation. No fine particle fraction of SX following aerosolisation of the micronised formulation was detected. This maybe related to the content uniformity demonstrating a CV of 24.30%. In comparison, both SX and FP had CV's less than 6% for the SAX formulation with THE being just over at 8.18%. These data demonstrated the difficulty of producing triple carrier-based DPI formulations using micronised material. The formation of a eutectic mixture of all three APIs using SAX provides a route whereby all three drugs maybe formulated as a DPI formulation.

The FPF_{ED} for SX and FP are similar while that for THE was significantly lower ($P<0.05$). These data suggested that the FP and SX may be delivered in the correct ratio even where the two are not combined into one particle. Similar results were also observed for the pMDI formulation containing all three APIs.

The FPF_{ED} data, along with the mass deposited on each stage, emitted dose (ED), fine particle dose (FPD), the mass median aerodynamic diameter (MMAD) and the geometric standard deviation of the MMAD (GSD) for the SAX formulation, are also represented in table 5.3.

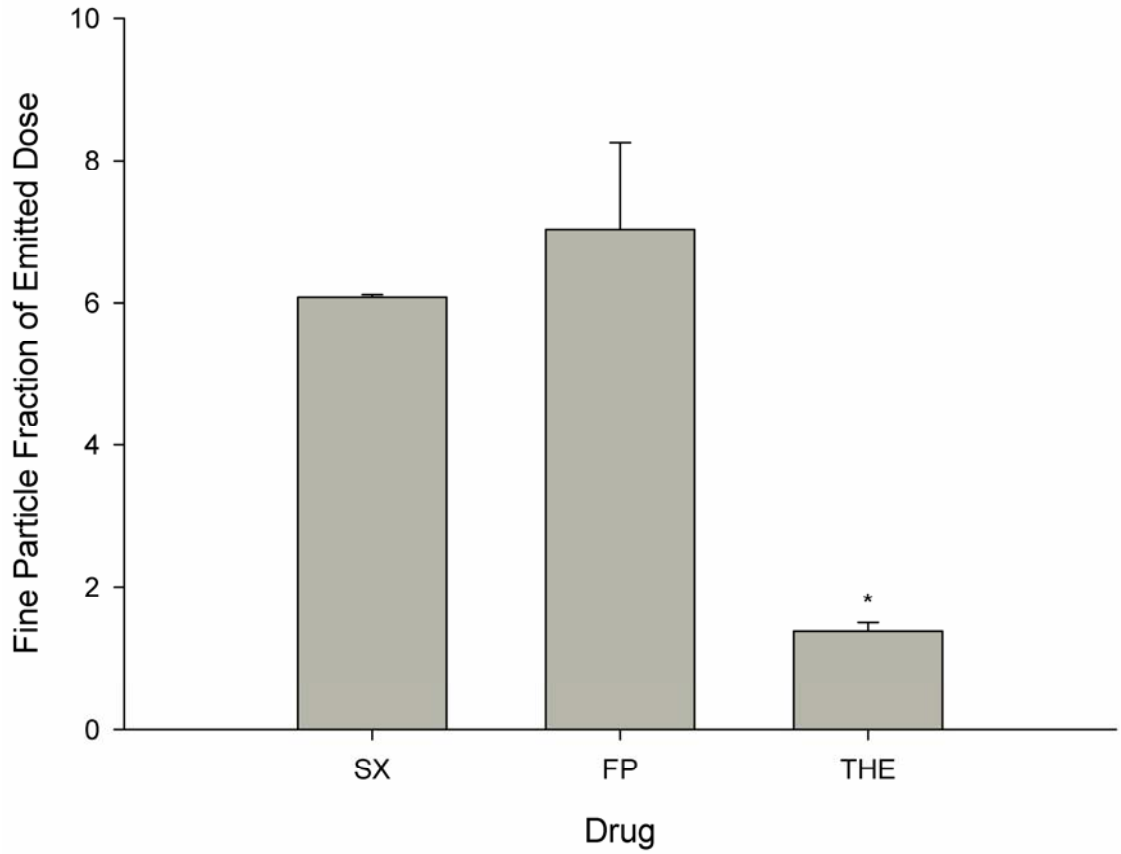

*Figure 5.13: Fine particle fraction of the emiited dose from the SAX formulation. *=significantly different (P<0.05) from others in formulation.*

Table 5.3: NGI deposition per shoot of drug delivered from micronised SX:FP:THE 1:10:10 and SAX engineered SX:FP:THE 1:10:10 particles pMDI formulations;

SX=salmeterol xinafoate, FP=fluticasone propionate; THE=theophylline; C&D= Capsules and Device; MP&T= mouthpiece and throat; PS=Pre-separator; S=stage; MOC= micro orifice collector.

Formulation	Drug	Mean Drug Deposition on Impactor Stages												Mean ED (µg±SD)	Mean FPD (µg±SD)	Mean FPF_{ED} (%±SD)	MMAD µm (GSD)
		CV (%)	C&D	MP &T	PS	S1	S2	S3	S4	S5	S6	S7	MOC				
Micronised	SX	24.30															
	FP	4.04															
	THE	6.53															
SAX	SX	3.82	9.42 ± 4.02	3.48 ± 1.79	13.58 ±2.26	0.63 ±0.12	0.53 ±0.06	0.47 ±0.07	0.38 ±0.13	0.23 ±0.05	0.08 ±0.02	0.00 ±0.00	0.02 ±0.04	29.09 ± 5.77	1.77 ± 0.34	6.08 ± 0.03	3.90 (2.73)
	FP	3.16	44.61 ±32.72	16.92 ±3.16	123.43 ±24.38	4.47 ±0.82	4.45 ±0.68	3.74 ±0.66	4.10 ±0.89	2.32 ±0.67	0.91 ±0.26	0.06 ±0.06	0.06 ±0.10	240.68 ± 44.15	16.78 ± 3.63	7.03 ± 1.22	3.32 (2.39)
	THE	8.18	89.46 ±28.59	54.14 ±12.88	24.57 ±6.54	5.77 ±1.80	2.17 ±0.64	0.73 ±0.24	0.44 ±0.14	0.05 ±0.01	0.02 ±0.02	0.00 ±0.00	0.00 ±0.00	131.82 ± 32.31	1.84 ± 0.60	1.38 ± 0.12	8.49 (2.13)

Figure 5.14 shows the percentage of total recovered dose collected on each stage throughout the NGI for the SAX engineered particles, with stages 1 to MOC having been expanded in Figure 5.15. The ratio between SX and FP was maintained throughout the NGI. This suggested, as for the pMDI formulation, it appears to be possible to deliver these two compounds in a fixed ratio providing that they were processed together.

However, the amount of THE reaching each stage of the NGI compared to SX and FP was variable. The capsule and device recovery showed that the correct amount of THE compared to both SX and FP was present. However, there was significantly greater ($p<0.05$) amount of THE present in the mouth and throat. As a result, the lower stages received significantly less ($P<0.05$) THE compared to SX and FP. These data suggested that during the formulation process, THE may agglomerate together resulting in larger particles which would be deposited further up the NGI.

These data are also depicted in figure 5.16 by the normalised %RD, which suggested that the SAX particles do not contain SX, FP and THE in a single aersosol particle. However, the co-processing of SX and FP allows for the two to be delivered in a fixed ratio in both pMDI and DPI formulations. As a result, these particles may be of benefit in COPD patients in order to reduce IL-8 production by lung macrophages, and, therefore, reduce inflammatory cell migration towards the lungs (Barnes 2001; Barnes 2002; Barnes, Qiu et al. 2006).

Recent studies have shown that relatively low doses of theophylline are needed to reduce HDAC inactivity (To, Ito et al.; Cosio, Iglesias et al. 2009). This may suggest that, even though the three drugs were not combined into a single particle, the formulations produced may be beneficial in reversing HDAC inactivity in COPD patients.

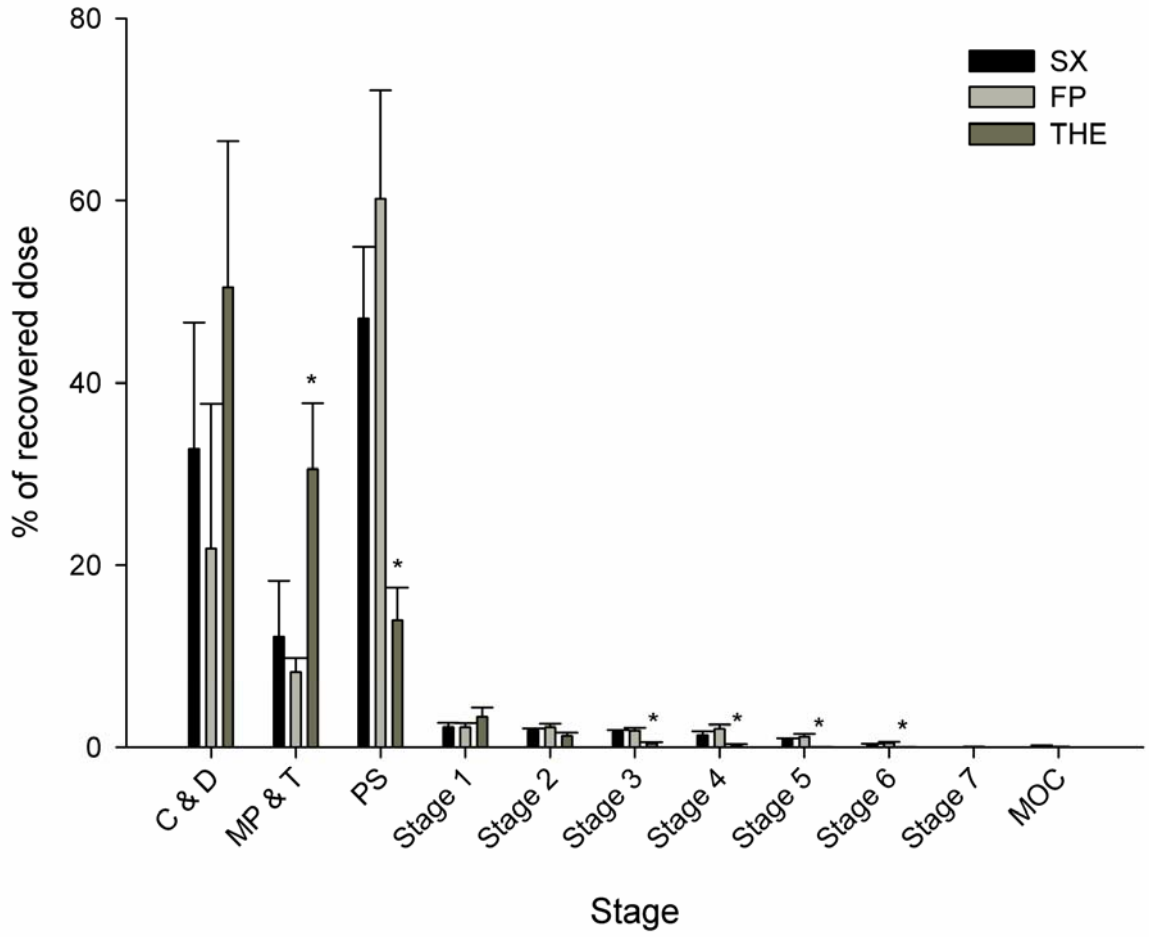

Figure 5.14: Graphical representation of the percentage of recovered dose (RD) collected on each stage of the NGI for the SAX formulation.=significant difference from other compounds in the same formulation (P<0.05).*

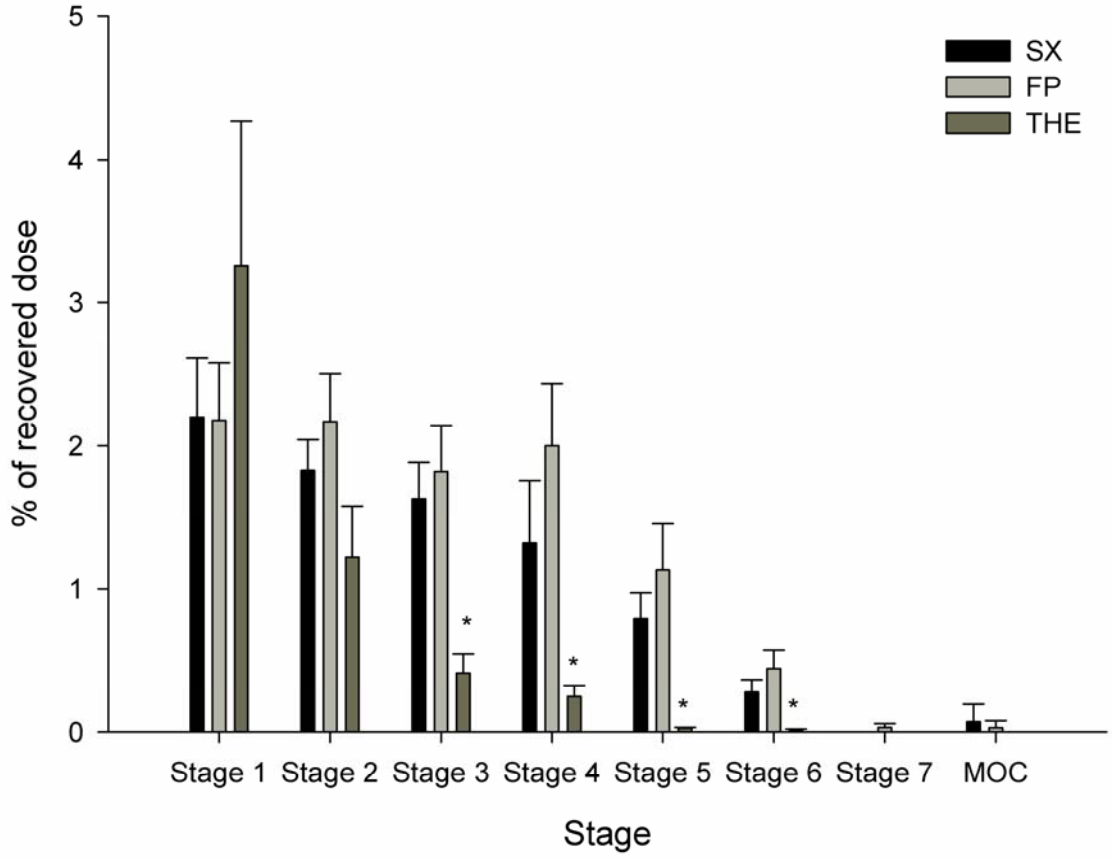

Figure 5.15: Graphical representation of the percentage of recovered dose (RD) collected on each stage of the NGI.=significant difference from other compounds in the same formulation (P<0.05).*

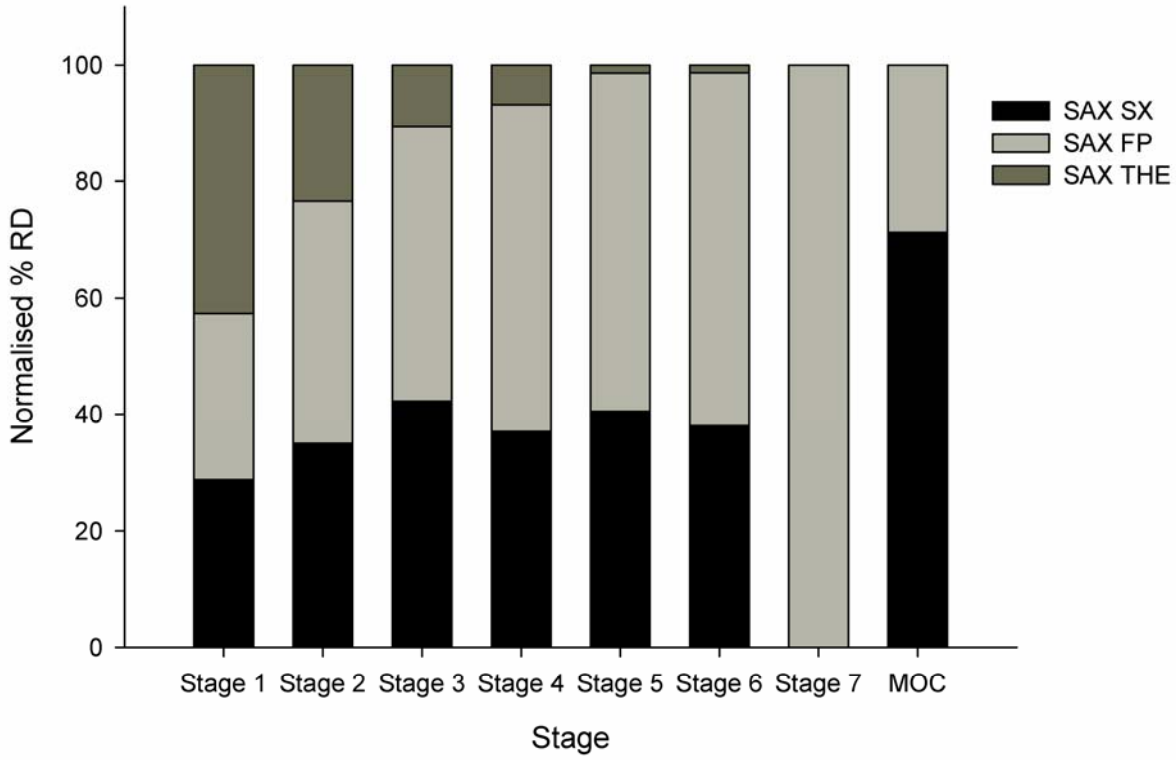

Figure 5.16:Graphical representation of the ratio between the %RD for each drug between stage 1 and MOC of the NGI.

There could be many reasons for the particles to deaggregate during processing. In the pMDI formulation, the pressure and shear forces generated at the actuator orifice could cause the drugs to separate. Alternatively, the vapour pressure for HFA-134_a is high enough for it to evaporate as soon as it is released from the pMDI. This vapourisation of the liquid propellant could be sufficient to break any lose association between the compounds. This could explain the lack of dose consistency in the pMDI yet allowing for the DPI formulation to maintain the dose relationship between SX and FP.

As for the DPI formulation, the shear forces generated during formulation preparation could be responsible for the separation of THE from the rest of the components.

The fact that the particles do not appear to contain all three compounds in a single respirable particles, maybe also be related to the low vapour pressure of dichloromethane as result of the presence of methanol. As a result, as the solution is sprayed through SAX, the droplets may have a low viscosity on reaching the anti-solvent. This may allow for the particles to crystallise out individually. Methanol must be present in the solution to allow for THE to be dissolved along with SX and FP. In

addition to this, the energy provided by the ultrasonic probe may have been sufficient to break up particles that may have contained more than one compound.

5.5 Conclusion

The SAX process allows for the production of crystalline SX, FP and THE, but not in one particle. The *in-vitro* performance of these particles from a pMDI formulation shows that the particles all break up during atomisation resulting in the loss of the dose ratio consistency. In contrast, a DPI formulation allows for the ratio between SX and FP to be maintained. This shows that a dose ratio relationship between SX and FP can be maintained as long as the two compounds have been co-processed prior to formulation in a DPI blend.

The particles may not have contained all three compounds due to the vapour pressure being reduced by the presence of methanol in the solvent. This could result in a low viscous droplet reaching the anti-solvent, in SAX, and, therefore, resulting in the compounds crystallising out separately.

Chapter 6 - Cocrystal Engineering of Indomethacin and Carbmazepine

6.1 Introduction

6.1.1 Pharmaceutical cocrystals

In recent years, drug molecules with limited aqueous solubility are becoming increasingly prevalent due to pharmaceutical companies searching extensively for new therapeutic molecules during high throughput drug discovery screening (Bastin, Bowker et al. 2000). Currently, over 40 % of new chemical entities (NCEs) present intrinsic solubilities (solubility of neutral or unionized form) of less than 1 $\mu g.ml^{-1}$ (Hu, Johnston et al. 2004; 2008). As a result, the pharmaceutical industries have a large number of compounds that have not been developed due to the fact that they are poorly water soluble and difficult to formulate (Wu and Benet 2005).

Recently, Almarrson *et al*. patented the production of pharmaceutical cocrystals containing a drug (Carbamazepine) and a crystal former (e.g. saccharin or nicotinamide) joined together by hydrogen bonds of complimentary groups forming a new crystalline lattice. Cocrystals can be defined as entities where both components i.e. the API and cocrystal former are solid entities at room temperature (Almarsson and Zaworotko 2004; Almarsson, Hickey et al. 2007).

Hickey et al compared the solubility of the 1:1 molar ratio Carbamazepine:Saccharin cocrystal (200mg formulation with respect to anhydrous Carbamazepine) with Tegretol®, a 200mg immediate release carmazepine tablet, in fasted beagle dogs (Hickey, Peterson et al. 2007). They found that the elimination of the Carbamazepine was unaffected by producing the cocrystal ,however, the time to reach peak plasma concentration was reduced from approximately 1.75 hours to about 1.0 hour on average. The area under the curve (AUC), and therefore the total amount of Carbamazepine absorbed by the dogs, increased for the cocrystal suggesting that the cocrystallisation of Saccharin into the crystalline lattice of the API improved the absorption of the Carbamazepine (Hickey, Peterson et al. 2007).

Remenar et al have also shown using an anti-fungal agent, Itraconazole, that a cocrystal of the API can be used to improve solubility. They showed that crystalline Itraconazole has a much lower solubility then the amorphous form that is on the market (Sopranox) as shown in Figure 6.1. The study, however, showed the dramatic effect

that different cocrystal formers had on the rate of dissolution of the API (Remenar, Morissette et al. 2003)

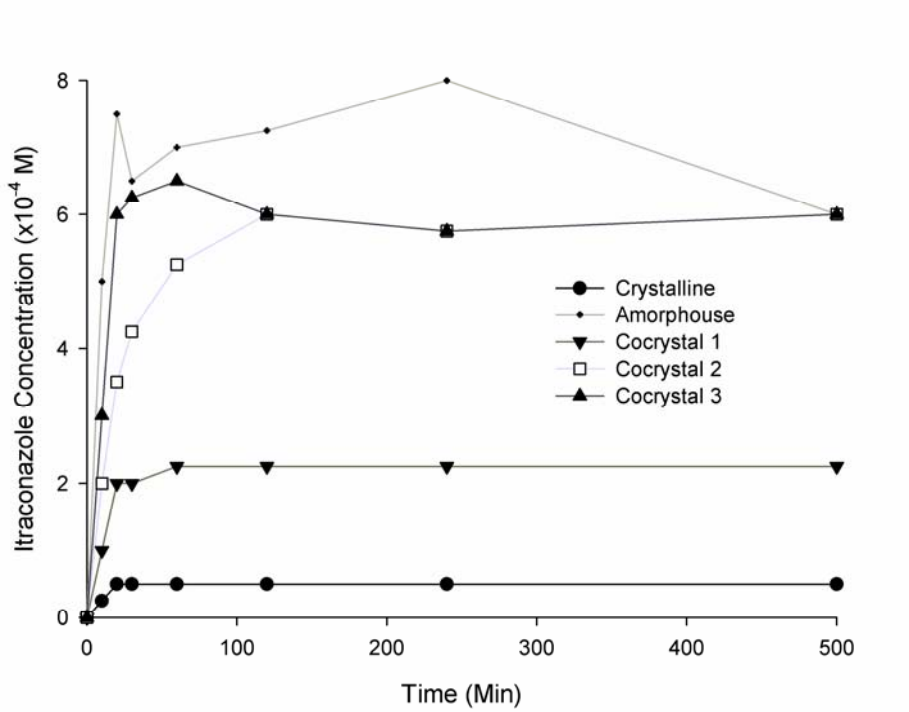

Figure 6.1: *Graph adapted from Remenar et al showing the effect of different cocrystals on the solubility of crystalline itracoanzole compared to the amorphous marketed product (Remenar, Morissette et al. 2003).*

6.1.2. Current methods for producing cocrystals

Conventionally cocrystals have been produced via an evaporation based crystallisation process. The active pharmaceutical ingredient (API) and the crystal former are dissolved in a volatile solvent in a defined stoichometric ratio. The volatile solvent is allowed to evaporate forming a supersaturated solution for nucleation and crystal growth (Pedireddi, Jones et al. 1996; Fleischman, Kuduva et al. 2003; Almarsson and Zaworotko 2004; Vishweshwar, McMahon et al. 2006).

Cocrystals have also been isolated upon milling an API and cocrystal former in a ball mill. In this process, a drop of a suitable solvent can be used to increase the inter-conversion rate of cocrystal formation. This adapted process is called solvent drop grinding. Both of these methods work by inducing amorphous regions on the API and the crystal former. These amorphous regions then interact to form the cocrystal (Jayasankar 2006; Vishweshwar, McMahon et al. 2006).

These various methods for producing cocrystals do not produce ideal particles for pharmaceutical use. For example, the solvent evaporation method does not produce cocrystals with a narrow particle size distribution without the need of secondary processing of the cocrystals. Furthermore, due to the slow nature of evaporation, either the API and/or the cocrystal former may reach saturation before the other resulting in nucleation and growth of the pure API or cocrystal former as well as the cocrystal. Thus, requiring the laborious use of reactive crystallisation where the addition of fresh solute is required to maintain the stoichiometry in solution for cocrystal formation (Nehm, Rodriguez-Spong et al. 2005). In addition, some of the solvent may bond with the API forming a solvate (Almarsson and Zaworotko 2004; Vishweshwar, McMahon et al. 2006).

The use of a ball milling process or solvent drop grinding process can only be used to make a small quantity of material and is generally applicable to cocrystal screening. These processes may result in amorphous regions on the surface of the cocrystals (Gaffet and Harmelin 1990; Begat, Young et al. 2003), which will interact with other materials or even increase the rate of degradation of the material (Buckton 1997) . Furthermore, the industrial scale-up of such a process is limited.

Previous work within this thesis has suggested that theophylline and an ICS may form a novel crystalline lattice, as suggested by XRPD diffractograms in chapter 4, section 4.4.1. In this study, the potential use of the SAX process in the production of cocrystals was explored. Two model compounds: carbamazepine (CBZ) and indomethacin (IND) with either nicotinamide (NIC) or saccharin (SAC) as the cocrystal former were investigated.

6.1.3 Cocrystal Engineering using SAX

The SAX process has previously been used to produce crystalline particles containing two compounds in a well-defined ratio (Pitchayajittipong, Shur et al. 2009). Due to the very nature of the SAX process, each droplet produced is crystallised into an individual particle containing the two compounds in the initial ratio (Pitchayajittipong, Shur et al. 2009).

The solvent used to completely solubilise both the API and cocrystal former provides the means for the individual molecules of drug and former to form a homegenous solution, which subsequently leads, upon aerosolisation, to the formation of highly supersaturated droplets containing both API and cocrystal former in the correct stoichmetric ratio. The solvent of choice needs to be sufficiently volatile to vaporise before the highly viscous droplets reach the crystallisation vessel (Kaerger and Price

2004; Pitchayajittipong, Shur et al. 2009). The atomiser, along with the vapour pressure of the solvent, allow for fine particle size control to be achieved. Changes in the atomiser used, solvent flow rate to the atomiser or atomising gas flow/pressure may result in a different particle size distribution (Kaerger and Price 2004; Pitchayajittipong, Shur et al. 2009). The separation distance between the atomiser nozzle and anti-solvent can also be controlled to allow sufficient time for vaporisation of the solvent. If the distance is too short, excess solvent within the droplets would reach the anti-solvent and the individual components may disperse in the non-solvent in the crystallisation vessel. However, if the distance is too large, the viscosity of the supersaturated solution of API and cocrystal former droplets may be too high, thus, forming an amorphous solid which cannot be crystallised into a cocrystal due to insufficient molecular mobility to induce the nucleation and crystal growth (Kaerger and Price 2004; Pitchayajittipong, Shur et al. 2009).

The formation of supersaturated droplets with sufficient viscosity is necessary for the formation of cocrystals using the SAX process as the solvent concentration is at its lowest level, whilst maintaining sufficient mobility of molecules. At this stage, the crystallisation is not limited by thermodynamics but the kinetics of nucleation and growth (Hancock and Zografi 1997). Crystallising within the supersaturated droplets during the aerolisation process would be very difficult to control and as a result the SAX process was purposefully designed to re-capture the viscous droplets in an non-solvent for controlled crystallisation (Mullin 1992). In addition, the non-solvent, which is typically miscible with the solvent used for solubilising the API and cocrystal former, allows for any remaining solvent within the droplets to be removed, thus preventing the formation of a solvate between the API and the solvent. To ensure that the cocrystals are not soluble in the non-solvent, the temperature can be reduced (Mullin 1992).

To induce the nucleation and crystal growth in the highly viscous droplets, ultrasonic energy and/or a sharp temperature drop upon entering the non-solvent can be used (Chow, Blindt et al. 2003; Kaerger and Price 2004; Ruecroft, Hipkiss et al. 2005; Abbas, Srour et al. 2007; Bucar and MacGillivray 2007; Dhumal, Biradar et al. 2009) (Kaerger 2003; Kaerger and Price 2004; Pitchayajittipong, Shur et al. 2009).

6.1.4 Aim

Carbamazepine (CBZ), a major anti-epileptic drug, has been reported to have a wide distribution in the time taken to reach a peak plasma concentration (Bertilsson 1978; El-Zein, Riad et al. 1998; Lake, Olling et al. 1999). The major reason for this is due to its low water solubility (Bertilsson 1978; El-Zein, Riad et al. 1998).

Indomethacin (IND) is an anti-inflammatory compound that reaches a peak plasma concentration in about 1.3 hours and has an oral bioavailability of around 98% (Oberbauer, Krivanek et al. 1993; Thummel and Shen 2001). However, despite this fact, like CBZ, IND demonstrates low aqueous solubility and thus falls under group II of the biopharmaceutical classification system (BCS, low solubility high permeability compounds), as discussed in chapter 1, section 1.5.1 (Wu and Benet 2005).

As previously mentioned, cocrystals containing CBZ and saccharin can increase the dissolution rate of CBZ (Hickey, Peterson et al. 2007) with a correlating increase in drug bioavailability (Hickey, Peterson et al. 2007). For this reason, along with the wealth of knowledge available on the different cocrystal for CBZ, it would be an ideal candidate compound for assessing the use of SAX in producing cocrystals.

More recently, cocrystals of IND and saccharin have also been developed (Basavoju, Boström et al. 2008; Padrela, Rodrigues et al. 2009). As a result, this was also chosen as a suitable candidate for assessing the applicability of SAX for the production of cocrystals with a defined particle size distribution.

6.2 Materials

Carbamazepine, indomethacin, nicotinamide and saccharin were obtained from sources stated in Chapter 2. All organic solvents were of at least analytical grade and were supplied by Fisher Chemicals (Loughborough, UK).

6.3 Methods

6.3.1 Production of reference cocrystals by conventional evaporation based crystallisation

Cocrystals of carbamazepine and either nicotinamide or saccharin were prepared by accurately measuring 1g of carbamazepine and dissolving in excess methanol with either 0.489g of nicotinamide or 0.733g of saccharin to form a 1:1 molar ratio of carbamazepine to either nicotinamide or saccharin (Fleischman, Kuduva et al. 2003). The methanol was then allowed to evaporate to produce cocrystals.

Indomethacin-saccharin cocrystals were prepared by accurately measuring 1g of indomethacin and 0.512g of saccharin to produce a 1:1 molar ratio. The compounds were then placed in a crystallisation dish and dissolved in excess methanol. The methanol was then allowed to evaporate.

6.3.2. Production of carbamazepint cocrystals via SAX

Cocrystal particles of CBZ:NIC (1:1 molar ratio) or CBZ:SAC (1:1 molar ratio) were prepared by atomising a 3% w/v solution containing carbamazepine with either nicotinamide (1.978g CBZ and 1.022g NIC) or saccharin (1.690g CBZ and 1.310g SAC) in methanol solvent.

6.3.2.1: SAX processing of cocrystals – Set-up A

Atomisation was conducted using a pneumatic atomiser (Büchi Mini Spray Dryer B-191, Flawil, Switzerland), operated with compressed air consumption at 600 $L.h^{-1}$ with the solution being provided at a rate of 2 $ml.min^{-1}$. The separation distance between the atomiser nozzle and the collection vessel was set to 60 cm. The volumetric air flow rate through the system was set to 30 $L.min^{-1}$. The particles were collected in a crystallisation vessel which contained an ultrasonic probe (Sonic processor P100, Sonic system, Somerset, UK) which was immersed in a solution of hexane maintained at 5˚C via a jacketed vessel. The resulting SAX particles were isolated from solution using supercritical CO_2 extraction of the hexane, as described in Chapter 2.

6.3.2.2: SAX processing of cocrystals – Set-up B

To achieve finer sized particles, the atomisation nozzle was replaced with a SU11 co-axial two-fluid atomiser with an internal mix (Spraying Systems Co., Illinois, USA). The flow rate through the atomiser was offset to 4 $ml.min^{-1}$ and an air pressure of 2.5 bar was used to induce the atomisation. The separation distance between the atomiser nozzle and the collection vessel was, as in set-up A, set to 60 cm. The volumetric air flow rate through the system was set to 30 $L.min^{-1}$. The particles were collected in a crystallisation vessel which contained an ultrasonic probe (Sonic processor P100, Sonic system, Somerset, UK) which was immersed in a solution of hexane maintained at 5˚C via a jacketed vessel. The resulting SAX particles were isolated from solution using supercritical CO_2 extraction of the hexane, as described in Chapter 2.

6.3.3 Indomethacin-saccharin cocrystals

Cocrystal particles of IND:SAC (1:1 molar ratio) were prepared by atomisation of a 3% w/v solution containing indomethacin with saccharin in methanol.

Atomisation was conducted using a SU11 co-axial two-fluid atomiser with an internal mixing chamber of the solution and the pressured air (Spraying Systems Co., Illinois, USA). The atomiser flow rate was set to 4 $ml.min^{-1}$ with a supporting air pressure of 2.5 bar. The separation distance between the atomiser nozzle and the collection vessel was set to 60 cm. The volumetric air flow rate through the system was set to 30 $L.min^{-}$

[1]. The particles were collected in a crystallisation vessel which contained an ultrasonic probe (Sonic processor P100, Sonic system, Somerset, UK) which was immersed in a solution of hexane maintained at 5˚C via a jacketed vessel. The resulting SAX particles were isolated from solution using supercritical CO_2 extraction of the hexane, as described in Chapter 2.

6.3.4 Crystal and particle characterisation

The crystals formed by evaporation and via the SAX process were characterised using SEM, DSC, PSD and XRPD, as described in chapter 2. Predicted XRPD diffractogram traces were produced using the published crystallographic data and PowderCell for Windows (Federal Institute for Material Research and Testing, Berlin, Germany)(Kraus and Nolze 1996).

6.4 Results and discussion.

6.4.1 Carbamazepine-nicotinamide (CBZ-NIC) cocrystals

Previous reports describe the crystal structure of twelve carbamazepine cocrystals including those containing nicotinamide and saccharin (Fleischman, Kuduva et al. 2003; Spong 2005). The structure and assembly of the carbamazepine:nicotinamide cocrystal is shown in Figure 6.2. As shown, the carbamazepine drug molecules form hydrogen bonds between the carboxamide groups. The same can be seen for nicotinamide along with a hydrogen bond between the nitrogen of pyridine ring of one molecule and the carboxamide of the next (Almarsson and Zaworotko 2004). In the CBZ-NIC cocrystal, hydrogen bonds are formed between the carboxamide groups of both compounds with two CBZ and two NIC molecules in the unit cell (Fleischman, Kuduva et al. 2003; Spong 2005; Almarsson, Hickey et al. 2007). The cocrystal is further stabilised by the presence of $\pi\ldots\pi$ interactions between the CBZ and NIC aromatic ring (Fleischman, Kuduva et al. 2003; Spong 2005).

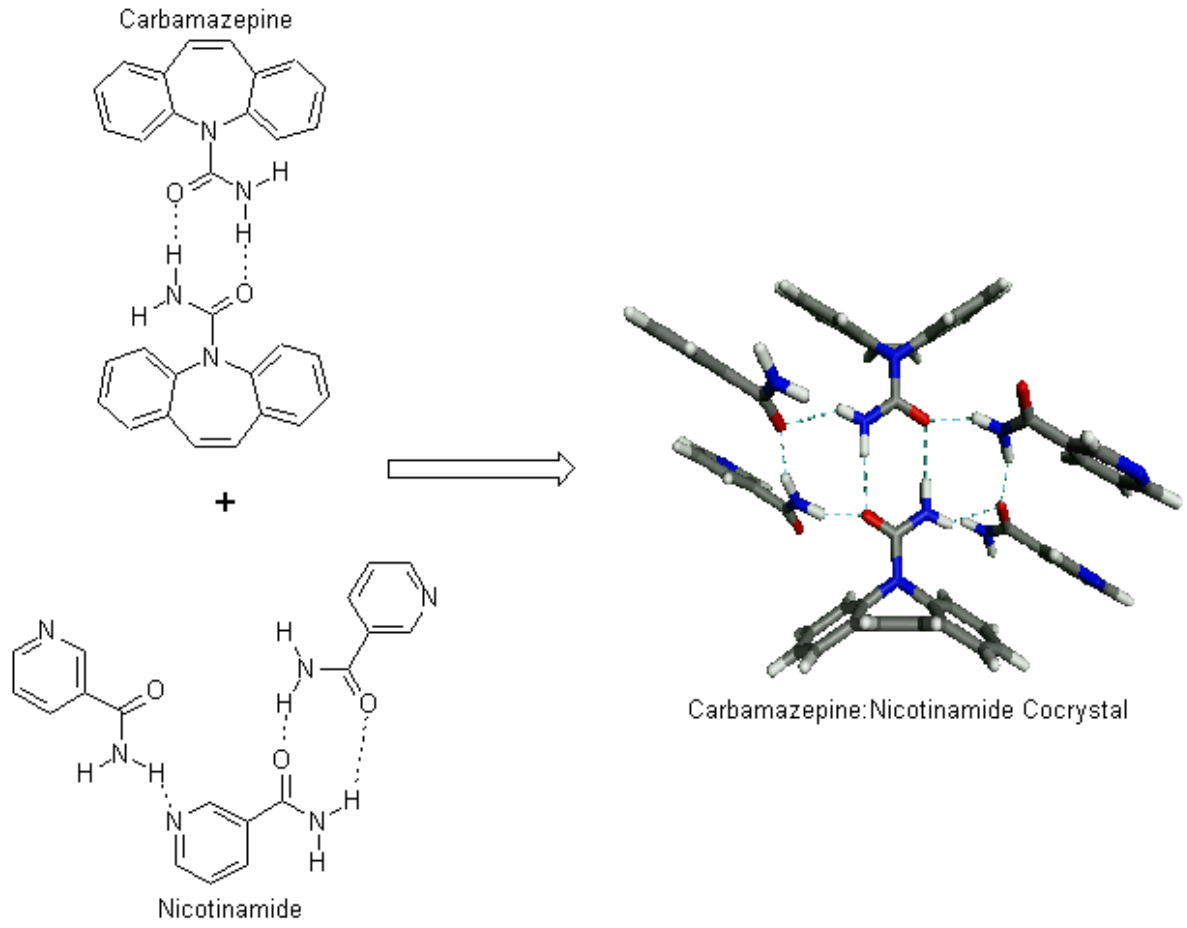

Figure 6.2: *Graphical representation of carbamazepine and nicotinamide unit cells and resultant CBZ:NIC cocrystal (edited from Fleischman, Kuduva et al. 2003; Spong 2005)*

The particle morphology of the CBZ:NIC cocrystals produced by evaporation induced crystallisation can be seen in Figure 6.3A along with a photographic image of a much larger crystal, shown in figure 6.3B. As shown, the crystals appear to form elongated plates or needles with no two crystals appearing to be the same size. The larger crystal, in figure 6.3B was too large for the SEM and is a representative image of one of the larger crystals formed during the evaporation of methanol from solution. The particle size distribution of the evaporated material ranged between 100µm to approximately 10mm, which is indicative of the evaporation of the solvent leading to extensive agglomeration of the particles. This variation in particle size suggests that further processing of the evaporation produced cocrystals will be required to produce particles of the same particle size distribution to ensure good flowability during tablet manufacture to ensure consistent drug content uniformity (Brittain 1995; 2002; GAD 2008). In addition, the larger particles will result in smaller total surface area for the same mass of drug (Bisrat and Nyström 1988) resulting in a slower dissolution rate (Lauwo 1985; Narurkar, Sheen et al. 1987; Bisrat and Nyström 1988; Brittain 1995), therefore potentially reversing any benefit obtained from producing a cocrystal.

In contrast, the particles produced from the SAX-A process all appear to be uniformly needle shaped particles of approximately 5μm in length (figure 6.3C). The uniform particle size distribution suggests the material requires no additional processing and can be directly included in a dosage form. Similar results were observed for SAX-B (figure 6.3D), however, the particles appear to be slightly smaller than SAX-A.

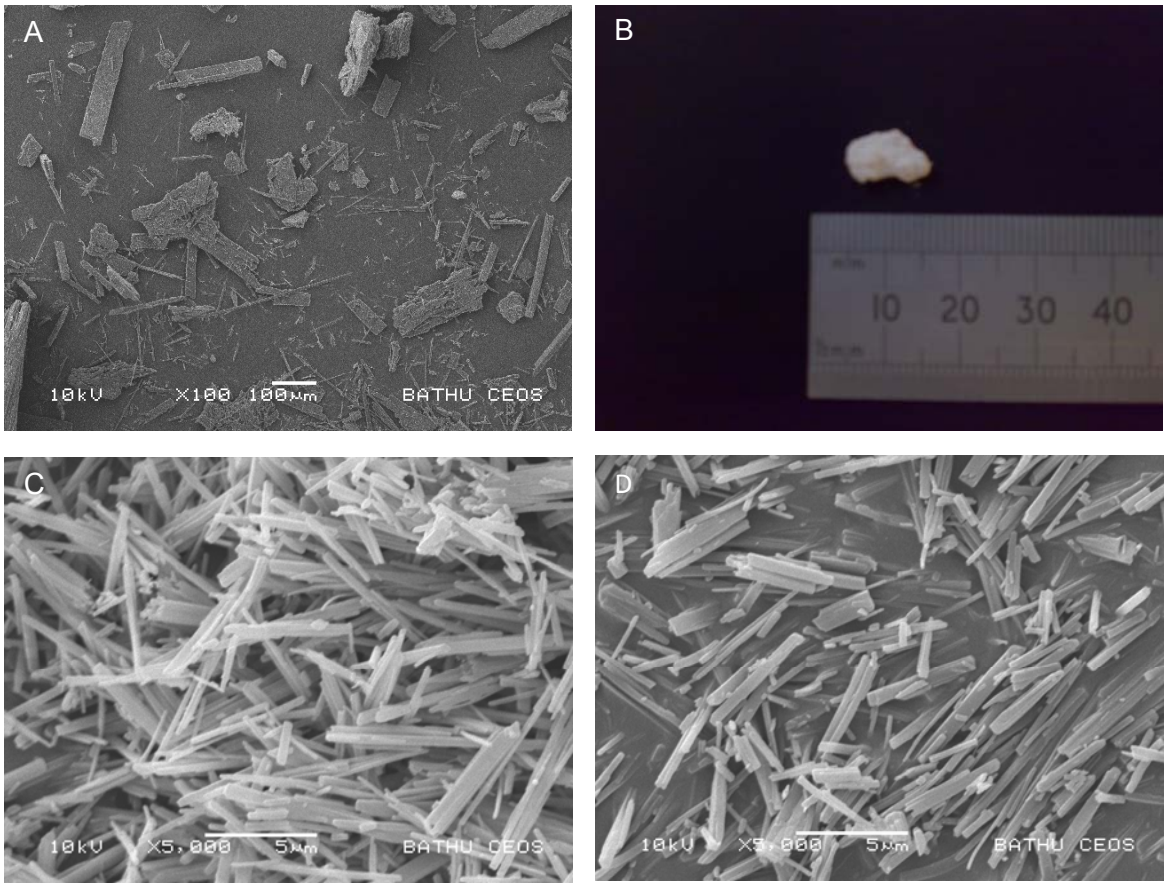

Figure 6.3. *Scanning electron micrograph images for carbamazepine-nicotinamide cocrystals made by evaporation (a) at 100x magnification with photographic image of crystal (b, scale in mm) compared to those made using SAX with settings A (c) and B (d) at 5000x magnification.*

The particle size distribution analysis of the three batches of cocrystals are shown in Figure 6.4. These data are also summarised in Table 6.1. The SAX produced cocrystals demonstrate a significantly smaller particle size compared to the evaporated material, and were characteristic of the size distribution of a micronized material with a median diameter (d_{50}) of 5.69μm and 2.13μm for SAX-A and SAX-B, respectively).

For the SAX processed cocrystals, the atomisation step produces micrometre sized droplets of the solute in a solution of a high vapour pressure liquid. Together with the high surface area, and the non-saturated environment of the supporting air flow, allows rapid evaporation of the solvent resulting in supersaturated droplets of the API and the

cocrystal former (Kaerger and Price 2004; Pitchayajittipong, Shur et al. 2009) in the correct stoichiometric ratio within each of the droplet. As a result, the influence of the solvent is negligible and the particle size distribution of the cocrystals can be controlled and modified by the atomisation process.

The span of the particle size distribution can be calculated using equation 6.1. This gives an indication as to the particle size control with a wider distribution having a larger span. These data are summarised in table 6.1.

$$Span = \frac{d_{90} - d_{50}}{d_{50}}$$ Equation 6.1

The span of the evaporated cocrystal was not measured due to the upper limit of the lens in the particle size was 100μm. The SAX produced particles produced very similar span values, indication that the different atomisers used produced similar distributions in aerosol droplets.

The particles produced by SAX-A were larger then SAX-B, which is most likely due to the different mechanisms used by the atomisers in producing the spray. The Büchi atomiser is an external mix atomiser where the atomizing air and solvent do not meet until the solvent leaves the atomiser while the SU11 is an internal mix atomiser. Here the high pressure liquid is mixed with the liquid before being forced through the atomizing orifice (Dietrich 1990). Internal mix atomisers produce finer droplets which would result in a smaller particle size of the cocrystal (Dietrich 1990). The particle size distribution can be adjusted by altering the liquid supply rate, atomization pressure and type of atomiser used (Pitchayajittipong, Shur et al. 2009). This, therefore, shows that SAX can be used to control particle size distribution of cocrystals which may aid dissolution without further processing resulting in an increased dissolution rate.

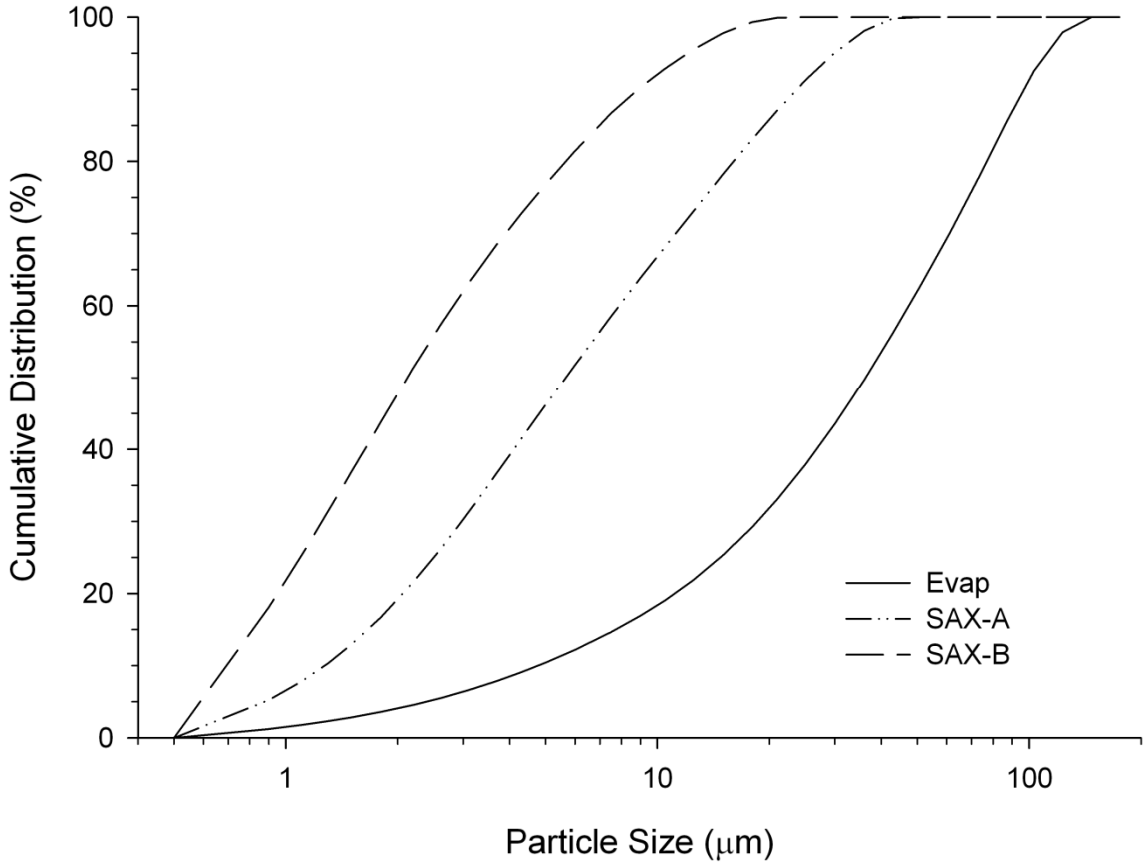

Figure 6.4: *particle size distribution of carbamazepine-nicotinamide cocrystals produced by evaporation, SAX-A and SAX-B.*

Table 6.1: Particle size distribution of carbamazepine-nicotinamide cocrystals produced by evaporation, SAX-A and SAX-B.

CBZNIC	d_{10}(μm) ±SD	d_{50}(μm) ±SD	d_{90}(μm) ±SD	Span
EVAP	4.77 ± 0.13	36.30 ± 0.38	97.27 ± 1.04	-
SAX-A	1.27±0.01	5.69±0.081	23.81±0.33	3.18
SAX-B	0.72±0.01	2.13±0.07	8.93±0.83	3.19

The DSC thermograms of the raw materials used to produce cocrystals are shown in Figure 6.5. The as received CBZ showed two endothermic melts with peak temperatures at 175.95 and 193.54°C while NIC only shows one melt at 132.21°C. The DSC thermograms of the resulting cocrystals are shown in Figure 6.6. The thermogram of the evaporated material demonstrated three distinct endothermic peaks at 80.61, 126.88 and 161.23°C. In comparison, the SAX produced particles only demonstrated a

single endothermic peak at 161.23°C. The appearance of a new melting endotherm at 161.23°C suggests that a new crystalline lattice has been produced in all experiments. Previous studies have reported the melting endotherm for the CBZ:NIC cocrystal to between 151-161°C (Fleischman, Kuduva et al. 2003; Spong 2005; Almarsson, Hickey et al. 2007; Seefeldt, Miller et al. 2007), suggesting that the CBZ:NIC cocrystal has been formed for the evaporation induced crystallisation and the SAX process.

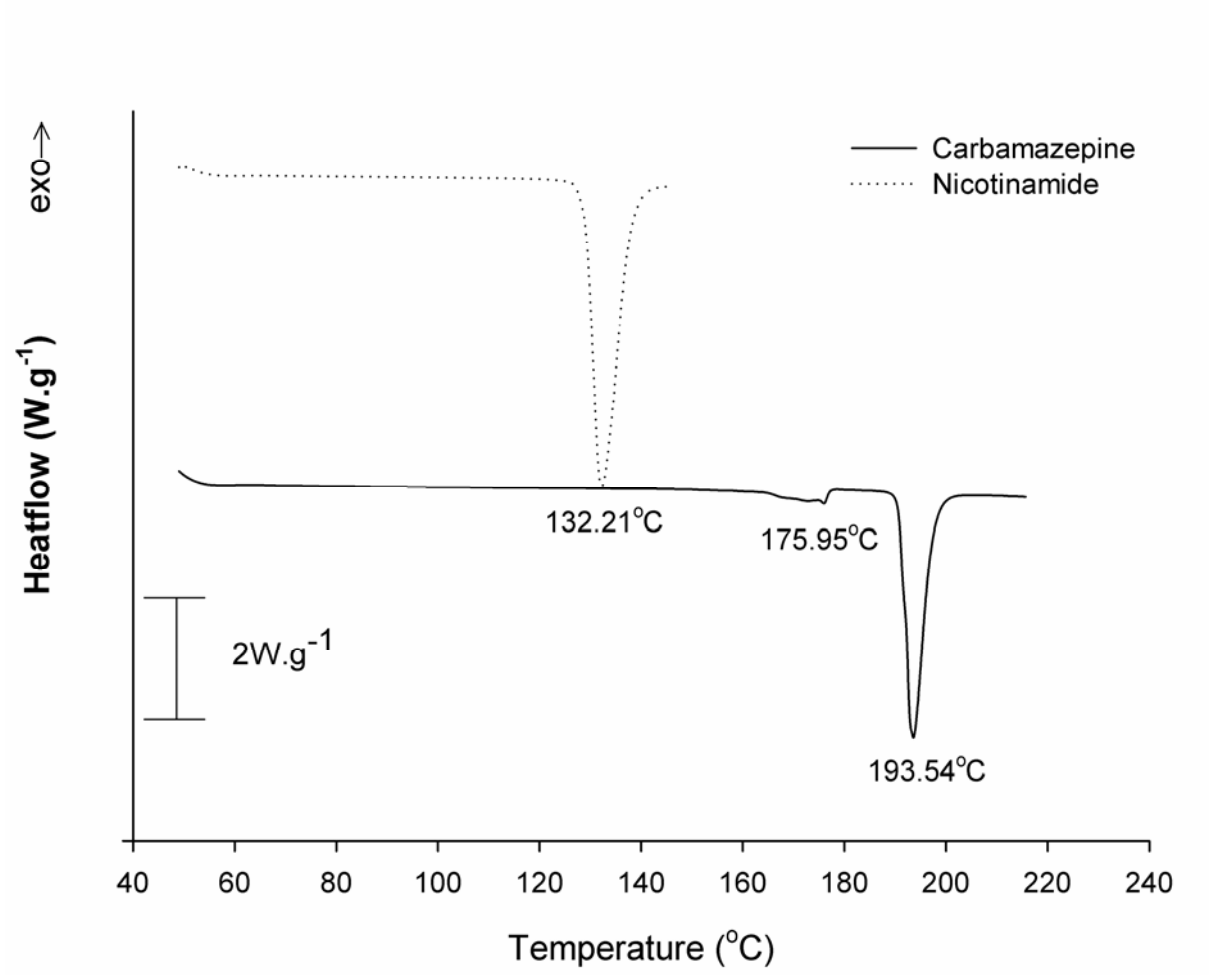

Figure 6.5: *DSC thermograms of raw carbamazepine and nicotinamide.*

However, it appears from the DSC therogram of the evaporated cocrystals that the endotherm at 126.88°C may be a traceable amount of the cocrystal former (Nictoniamide) being crystallised out during the evaporation induced crystallisation. The peaks below 100°C for the evaporated cocrystals suggest the possible presence of solvent in the solid material.

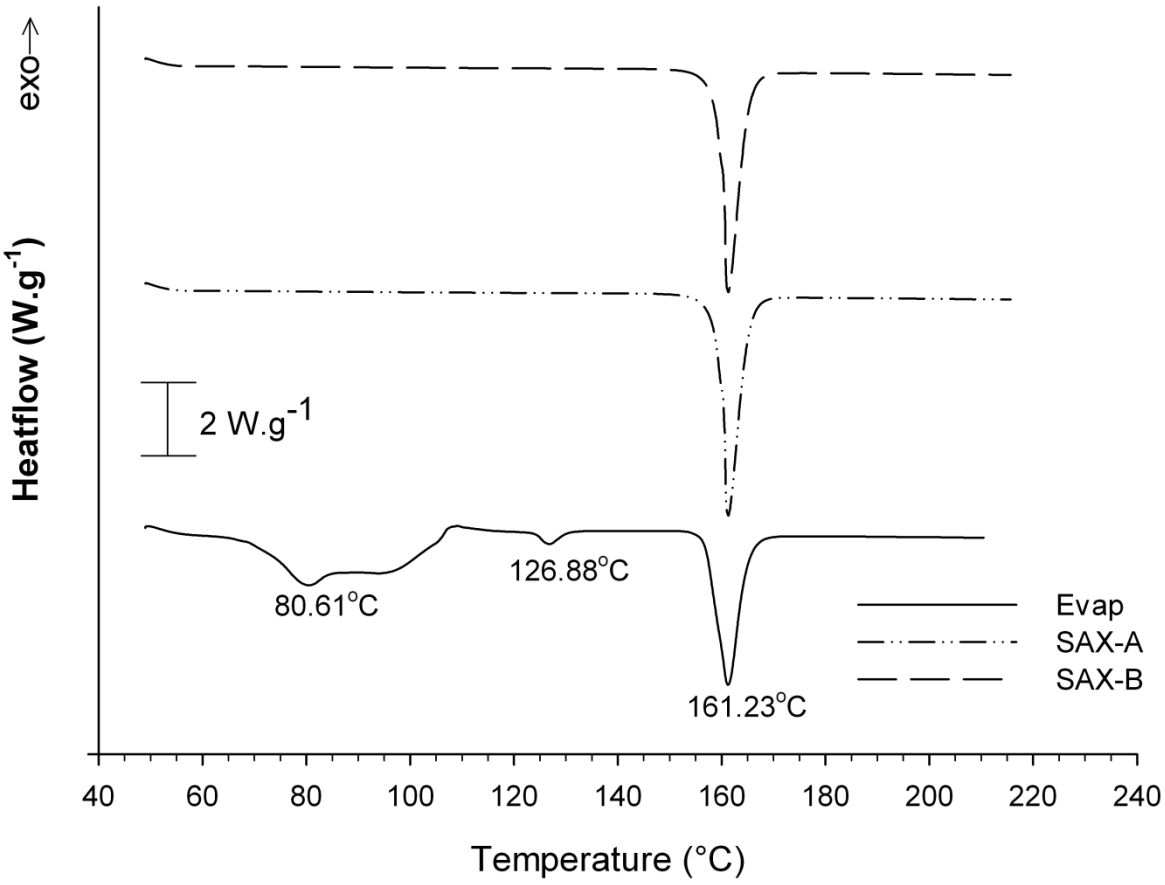

Figure 6.6:*DSC thermograms of carbamazepine-nicotinamide cocrystals produced by evaporation, SAX-A and SAX-B.*

The inclusion of solvent in the evaporated cocrystals appears to be confirmed by thermogravimetry (TGA) analysis of the sample shown in figure 6.7. The evaporated material appears to have lost approximately 1.5% of its initial weight before reaching 100°C. The low temperature involved suggests that some solvent may have still been incorporated in or bound to the surface of the crystalline material. In comparison, the SAX produced cocrystals did not demonstrate any step changes in their TGA thermogram. These data suggest that only one entity was present in the SAX cocrystals.

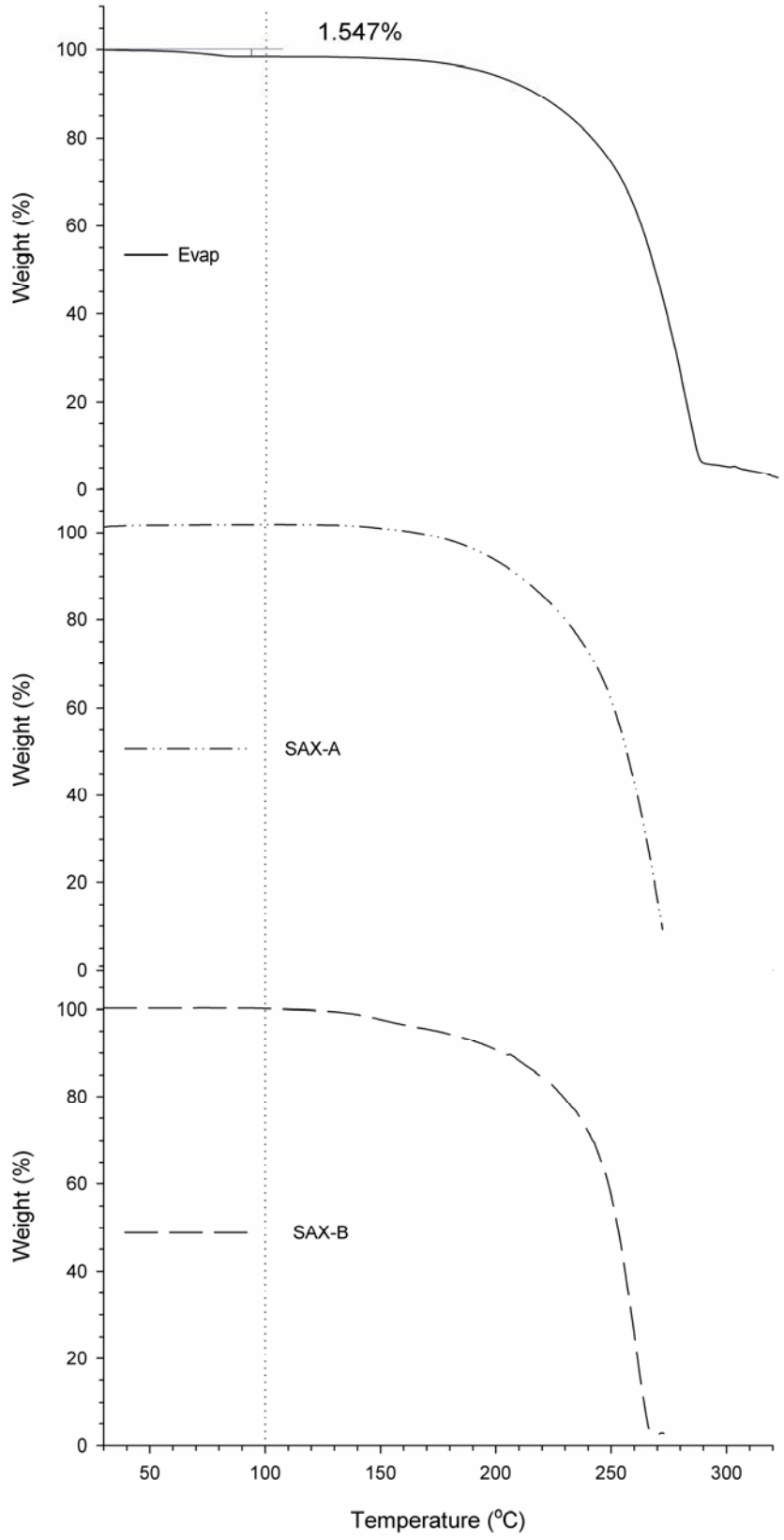

Figure 6.7: *TGA analysis of the cocrystals produced by evaporation, SAX-A and SAX-B.*

XRPD diffractograms of the cocrystals formed and their corresponding raw material are shown in Figure 6.8. The raw materials do not show any peaks below 10° 2θ while the processed materials exhibit two peaks (one at 6.69° and the other at 8.89° 2θ). These data suggest that the raw materials have crystallised in a manner that has produced a new lattice structure that was not present in the raw materials. In addition to the two peaks at <10° 2θ, the cocrystals produced by evaporation appear to have peaks that do not appear in either of the SAX produced materials. These peaks are at 12.37°, 14.70°, 24.81° and 43.14° 2θ. The peak at 14.70° 2θ may relate to the corresponding peak in nicotinamide, therefore suggesting that there was an excess of nicotinamide in the solution that was not incorporated into the new crystalline lattice. However, the peak at 24.81° 2θ also appears in the carbamazepine trace. These data suggest that during evaporation, some of the raw materials were not fully transformed into cocrystals.

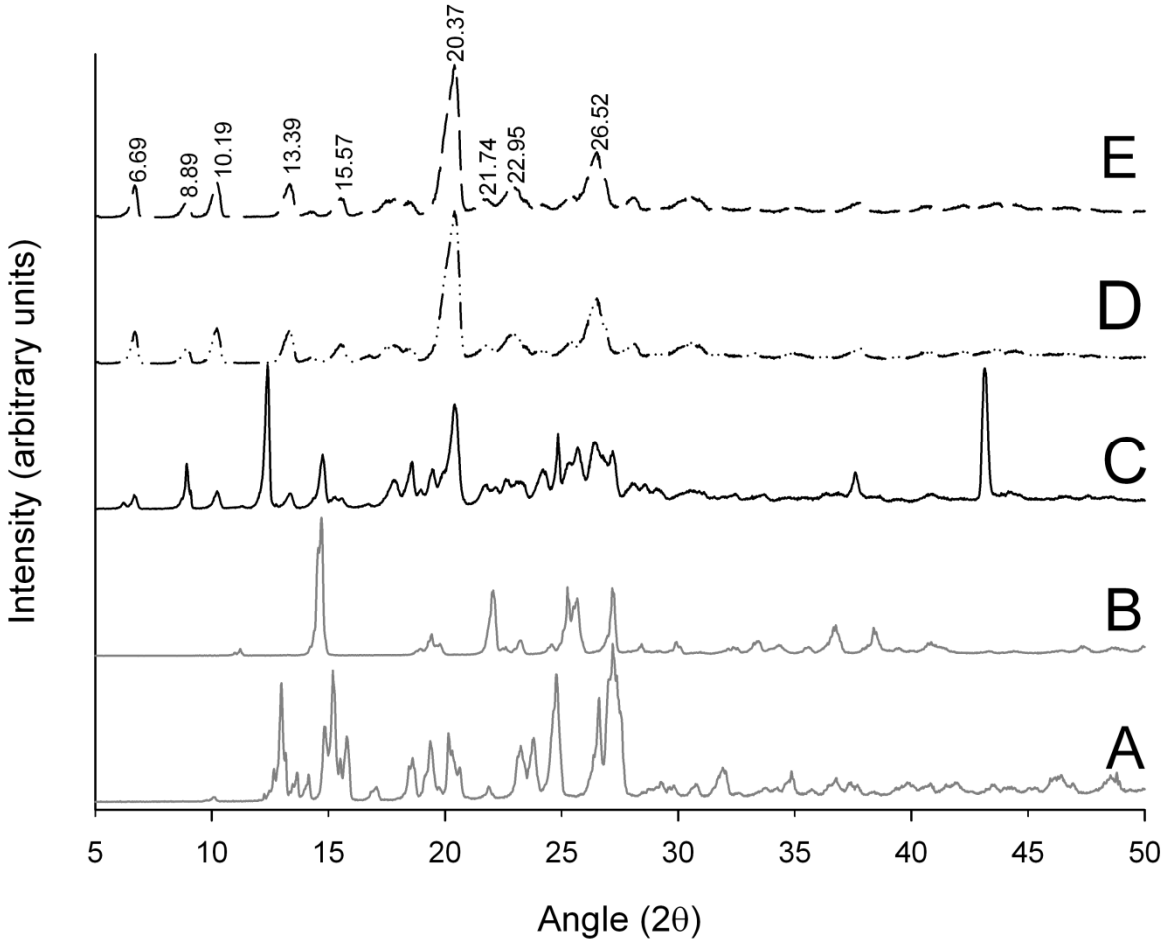

Figure 6.8: *X-ray powder diffractogram of (A) carbamazepine, (B) nicotinamide and carbamazepine-nicotinamide cocrystals produced by (C) evaporation, (D) SAX-A and (E) SAX-B.*

Figure 6.9 shows the XRPD diffractogram of the cocrystals compared to an XRPD diffractogram produced form published crystallographic data (Fleischman, Kuduva et al. 2003). The peak at 24.81° 2θ is not in the predicted trace confirming that it is not part of the cocrystal, neither is the peak at 43.14° 2θ. These additional peaks may be from some form of contamination remaining from the evaporation process as suggested earlier.

Fleischman *et.al* grew their cocrystals slowly from a solution while the evaporated crystals were allowed to grow naturally suggests that differences between the respective diffractograms may due to the rate of crystal growth. The faster rate of crystal growth of the cocrystals produced from evaporation may have resulted in some crystals incorporating the solvent. The predicted trace appears to have a couple of extra peaks compared to the other diffractograms. The first of which is at 10.99° 2θ

which could relate to the small peak in the NIC trace above. The second is at 16.90° 2θ which could be due to CBZ.

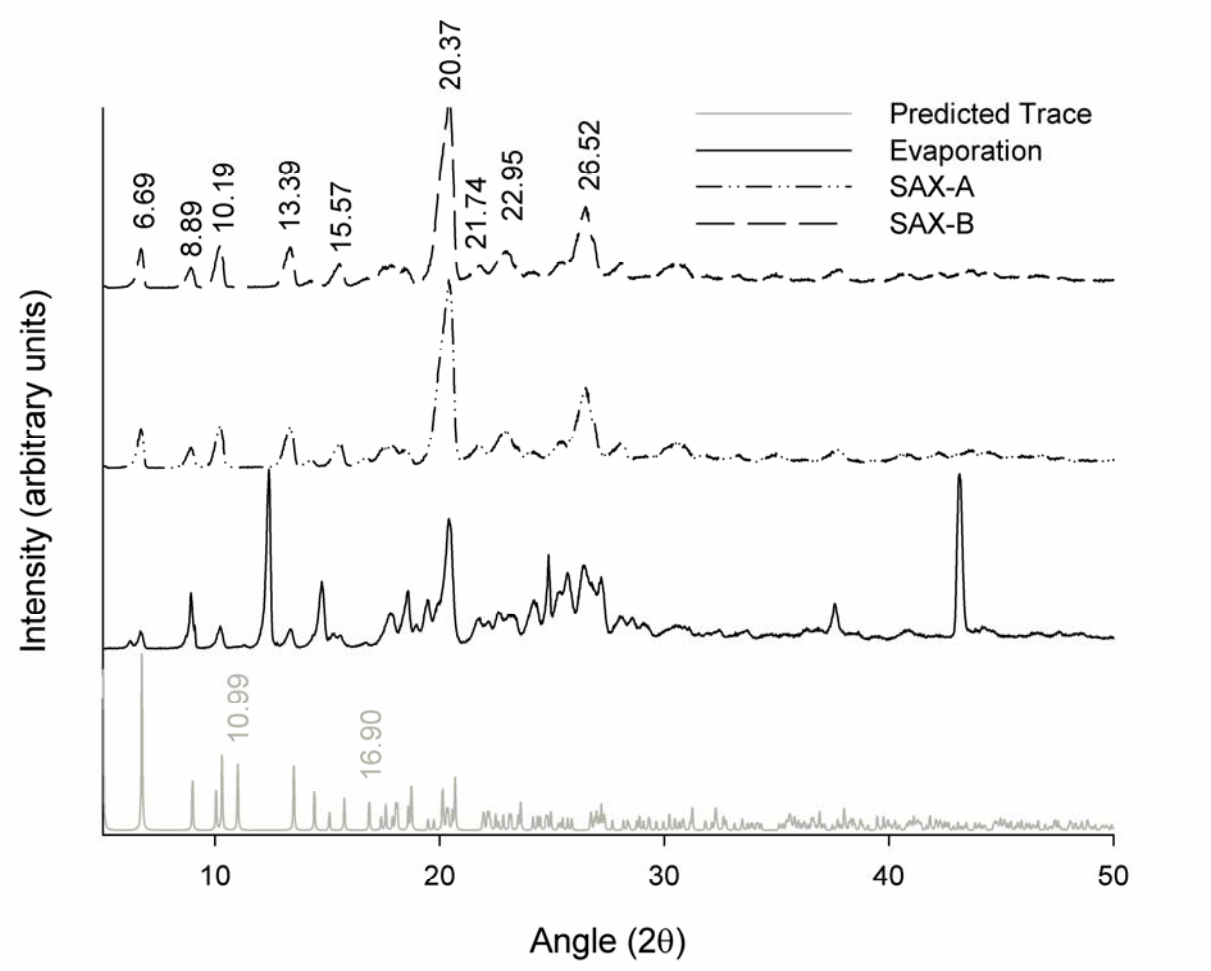

Figure 6.9: *X-ray powder diffractogram of carbamazepine-nicotinamide cocrystals produced by evaporation, SAX-A and SAX-B compared to the predicted trace.*

The presence of the raw material in the XRPD diffractogram shows that it can be difficult to balance ensure that both drug and cocrystal former remain in solution in equi-molar concentrations prior to solution based crystallisation. However, in the SAX system, the solvent evaporates from the droplets resulting in a supersaturated droplets containing the correct ratio of both the drug and cocrystal former (Kaerger 2003; Kaerger and Price 2004; Pitchayajittipong, Shur et al. 2009). In this state, neither drug nor cocrystal former have crystallised out. The non-solvent, which is miscible with the solvent used to solubilise the API and cocrystal former, may facilitate the removal of any remaining solvent within the droplets. The sonication energy provides the molecular mobility to overcome the kinetic barrier for the drug and cocrystal former molecules to nucleate and crystal growth to occur within the highly viscous droplets. (Lorimer and Mason 1987; Kaerger and Price 2004; Abbas, Srour et al. 2007; Bucar

and MacGillivray 2007; Ruecroft 2007; Dhumal, Biradar et al. 2009; Pitchayajittipong, Shur et al. 2009).

6.4.2 Carbamazepine-saccharin (CBZ-SAC) cocrystals

The structure of the raw materials and cocrystal unit cell for the carbamazepine saccharin cocrystal are shown in Figure 6.10. As shown, saccharin forms hydrogen bonds between the amide on one ring and carboxide group on the next ring. In the cocrystal, the saccharin forms hydrogen bonds using the sulphonamide as well as hydrogen groups of the benzene ring (Fleischman, Kuduva et al. 2003).

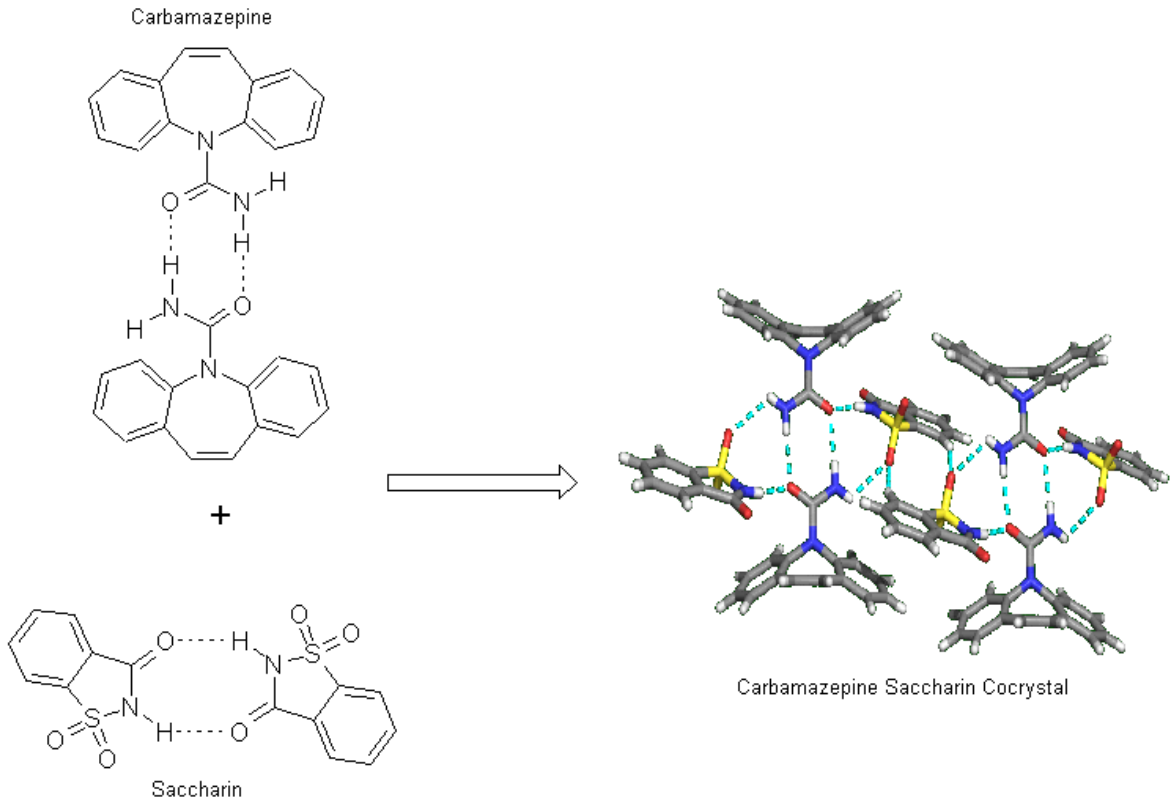

Figure 6.10: *Graphical representation of raw carbamazepine and nicotinamide unit cells and resultant CBZ:NIC cocrystal (edited from Fleischman, Kuduva et al. 2003; Spong 2005)*

SEM images of the cocrystals produced by evaporation (Figure 6.11A) and by SAX (Figure 6.11B) suggest that the CBZ:SAC cocrystals appears to be morphologically different from the CBZ:NIC cocrystals. The evaporation method produced material that appeared in a variety of shapes; some appearing as needles, some as plates and others as large non-descript blocks. These larger blocks may have formed by the twinning of smaller crystals during the evoparation process (Mullin 1992). In comparison, the SAX produced crystals appear to form plates or needles. Previous

reports have confirmed that cocrystals of CBZ:SAC to form rhombic plates (Spong 2005).

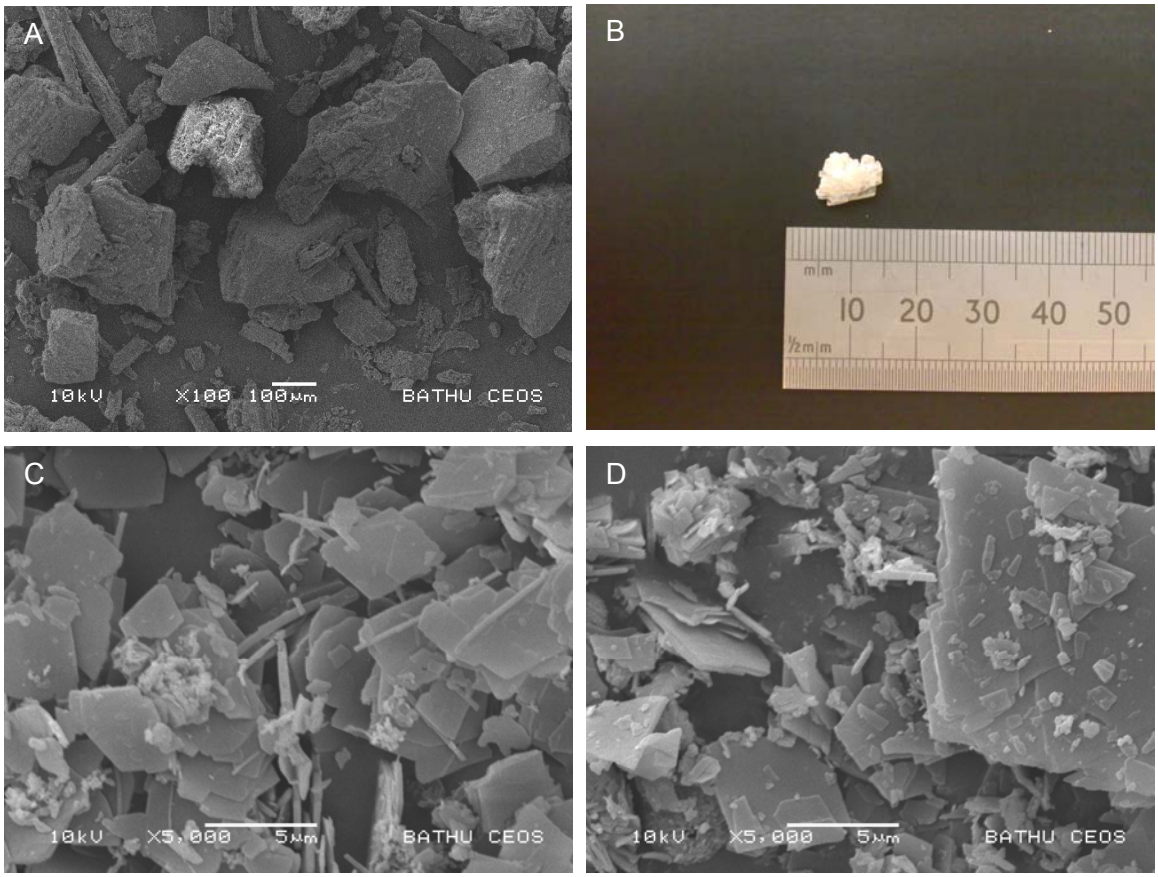

Figure 6.11: *Scanning electron micrograph images for carbamazepine-saccharin cocrystals made by evaporation (a) at 100x magnification with photographic image of crystal (b, scale in mm) compared to those made using SAX with settings A (c) and B (d) at 5000x magnification.*

The particle size distributions (Figure 6.12 and Table 6.2) show that the crystals produced by evaporation were the largest crystals (d_{50} of 20.34µm), as had been shown for the carbamazepine-nictoinamide cocrystals. Similarly, SAX-A and SAX-B particles (d_{50} of 15.12 and 7.69µm respectively) produced significantly smaller particles, with the internal mixing atomiser producing smaller particles than the external mixer.

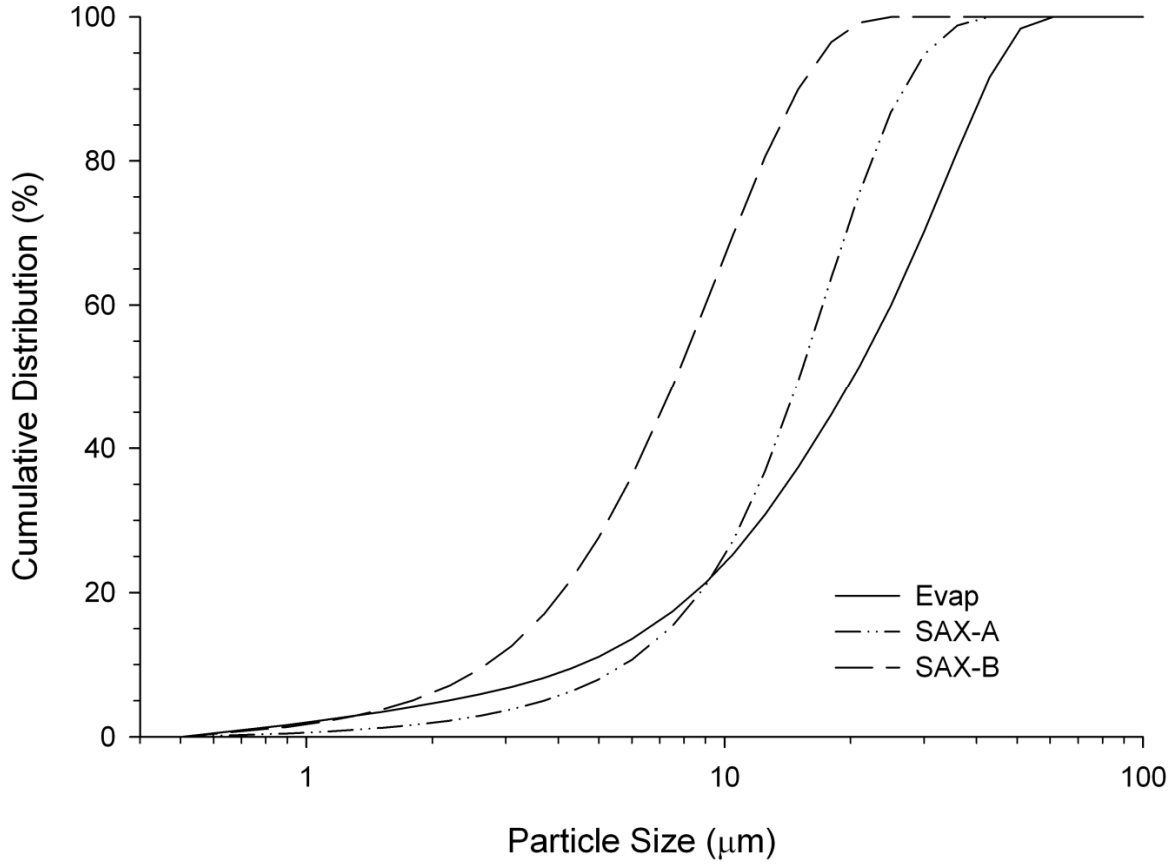

Figure 6.12: *Particle size distribution of carbamazepine-saccharin cocrystals produced by evaporation, SAX-A and SAX-B.*

Table 6.2. *Particle size distribution of carbamazepine-saccharin cocrystals produced by evaporation, SAX-A and SAX-B.*

CBZSAC	d_{10}(μm) ±SD	d_{50}(μm) ±SD	d_{90}(μm) ±SD	Span
EVAP	4.62 ± 0.75	20.34 ± 2.28	41.81 ± 1.21	-
SAX-A	5.75±0.01	15.12±0.01	27.01±0.04	0.79
SAX-B	2.69±0.02	7.69±0.04	15.02±0.06	0.95

The DSC thermograms of CBZ:SAC cocrystals produced by evaporation and SAX are shown in Figure 6.13. The endothermic response below 100°C for the cocrystals produced by evaporation may be related to solvent associated with the crystals. In

addition, the cocrystal produced by evaporation appears to demonstrate two conjoined melting endotherms. The first demonstrtaing a peak melting temperature of 164.75°C. This melt appears to co-inside with the melt of CBZ form III (Rustichelli, Gamberini et al. 2000; McGregor, Saunders et al. 2004) suggesting that there was an excess CBZ in the solution with no melt for excess SAC. The second endotherm appears to relate to the single endotherm for the SAX produced cocrystals of approximately 174°C. This relates to the melting point of the CBZ:SAC cocrystal, which is supported by previous studies (Fleischman, Kuduva et al. 2003; Spong 2005).

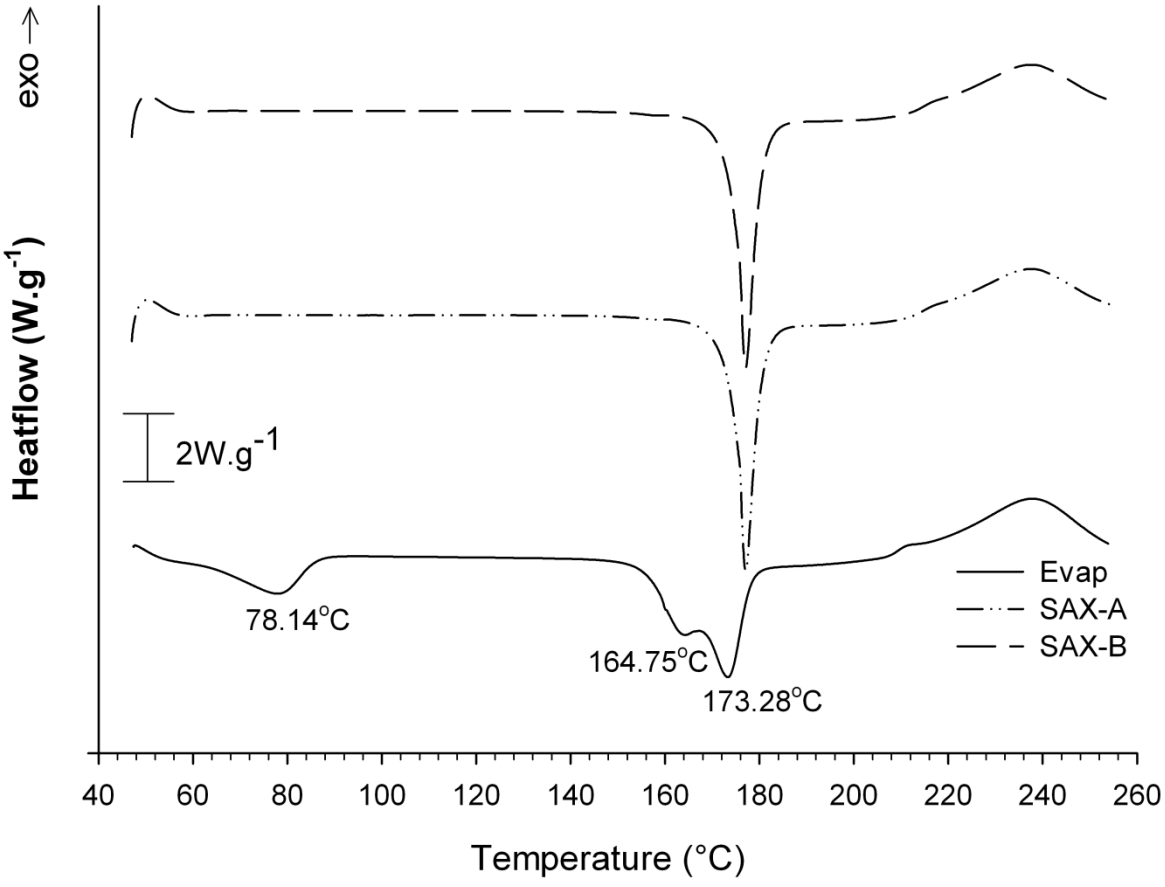

Figure 6.13: *DSC analysis of CBZ:SAC cocrystals made by evaporation, SAX-A and SAX-B.*

Surprisingly, the TGA analysis does not show any residual solvent in the CBZ:SAC crystals produced by evaporation (figure 6.14). The TGA also confirmed that no solvent was associated with the SAX cocrystals as indicated by a single degradation step when heated in Figure 6.14.

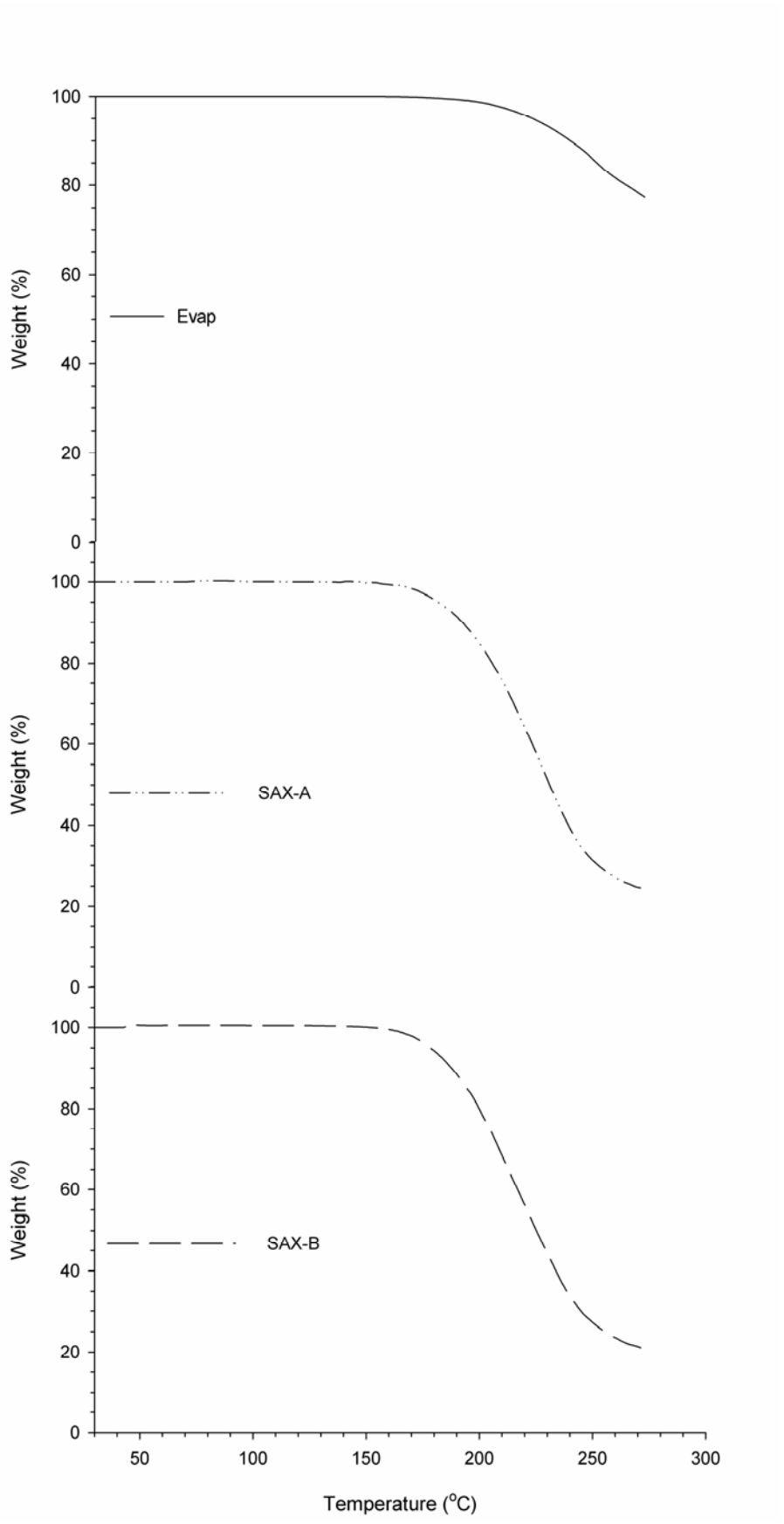

Figure 6.14: *TGA analysis of cocrystals made by evaporation, SAX-A and SAX-B.*

The XRPD analysis shows the presence of a single CBZ peak in the cocrystals produced by evaporation at about 10° 2θ. There are only a few peaks in the XRPD trace for the crystals produced by evaporation, as the crystals were too large for powder diffraction so single crystal diffraction was conducted. There appears to be only one extra peak <10° 2θ in the cocrystals XRPD trace, at 6.99° 2θ, compared to the raw materials with another strong new peak appearing at 14.03° 2θ. The remainder of the peaks can be found in the cocrystals produced by SAX and in one of the traces produced by either CBZ or SAC raw materials, thus confirming their presence.

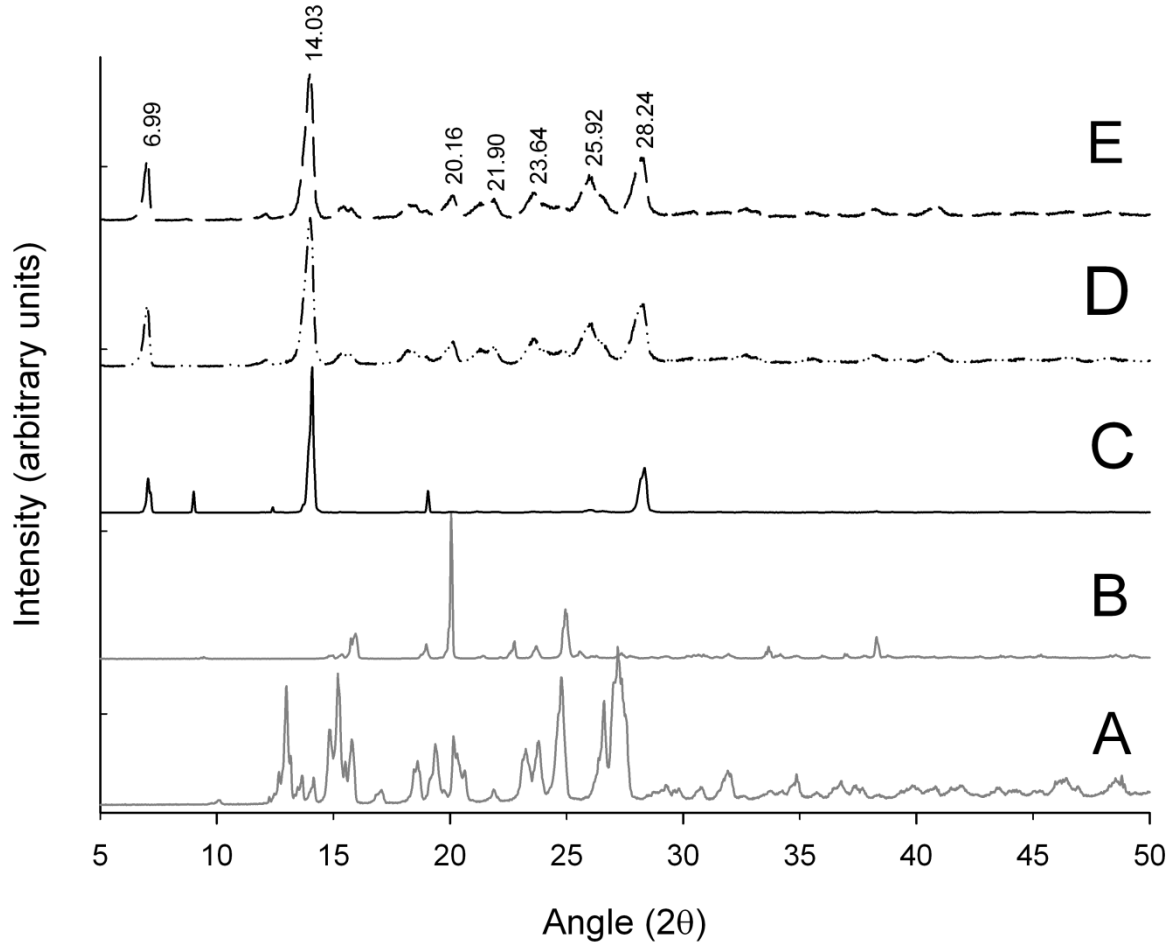

Figure 6.15: *X-ray powder diffractogram of carbamazepine (a), saccharin (b) and carbamazepine-saccharin cocrystals produced by evaporation (c), SAX-A (d) and SAX-B (e).*

Figure 6.16 shows the XRPD trace for the cocrystals produced by evaporation and SAX compared to the XRPD trace produced from the crystallographic data used to generate the unit cell shown in figure 6.10 (Fleischman, Kuduva et al. 2003). The predicted trace appears to have many more peaks compared to the cocrystals produced by SAX or evaporation. Many of these peaks relate to raw materials used, as for those between 8.79 and 13.79° 2θ. However, the peaks that appear in the XRPD

trace for the cocrystals produced by evaporation and SAX also appear in the predicted trace produced from crystallographic data. This confirms that the materials produced were cocrsytals of CBZ and SAC.

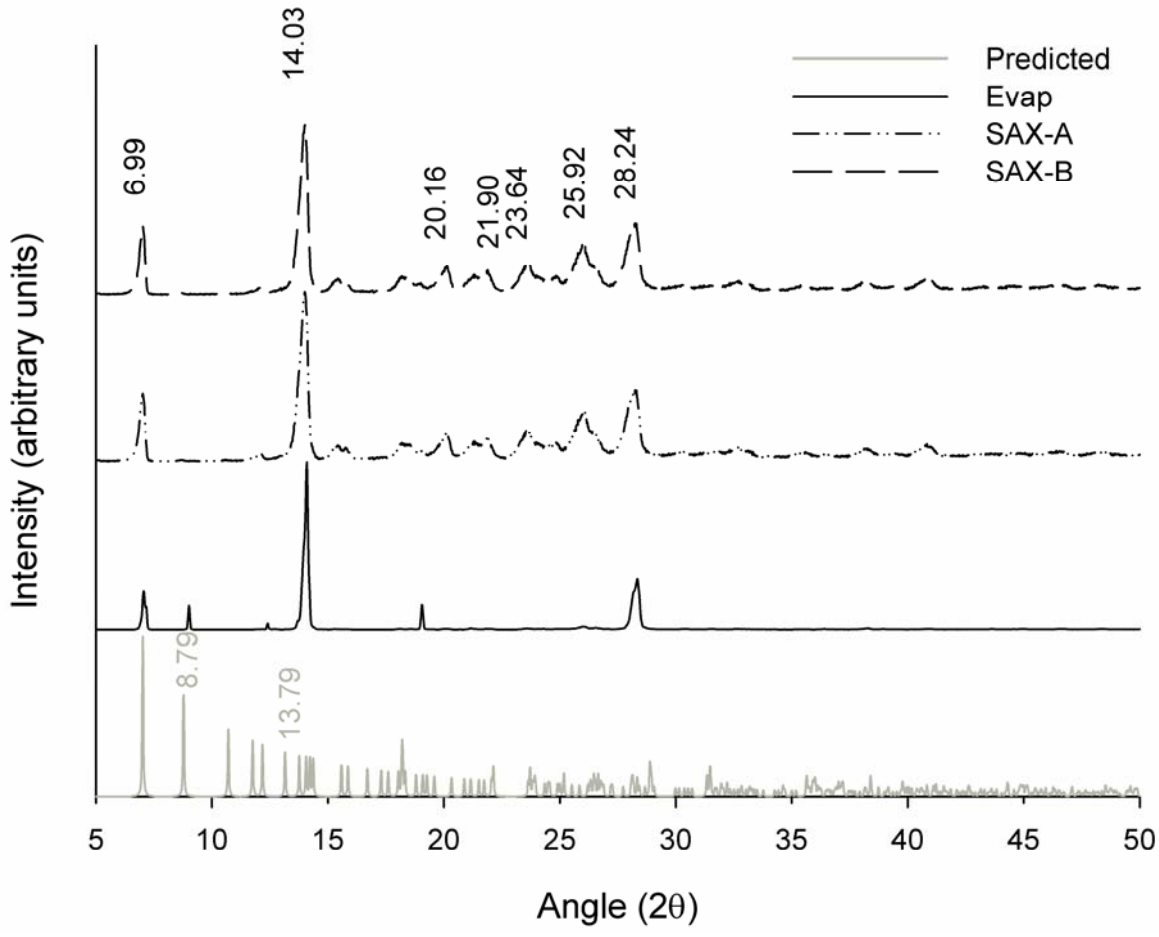

Figure 6.16: *XRPD diffractogram of carbamazepine-saccharin cocrystals made by evaporation, SAX-A and SAX-B compared to the predicted trace.*

6.4.3 Indomethacin-saccharin (IND-SAC) cocrystals

Recently, Alles et al. have demonstrated that indomethacin can form cocrystals with saccharin (Alles, xf et al. 2008; Basavoju, Boström et al. 2008). They found that indomethacin formed a single hydrogen bond with the saccharin between carboxamine group of indomethacin and the pyridine ring of saccharin as shown in Figure 6.17.

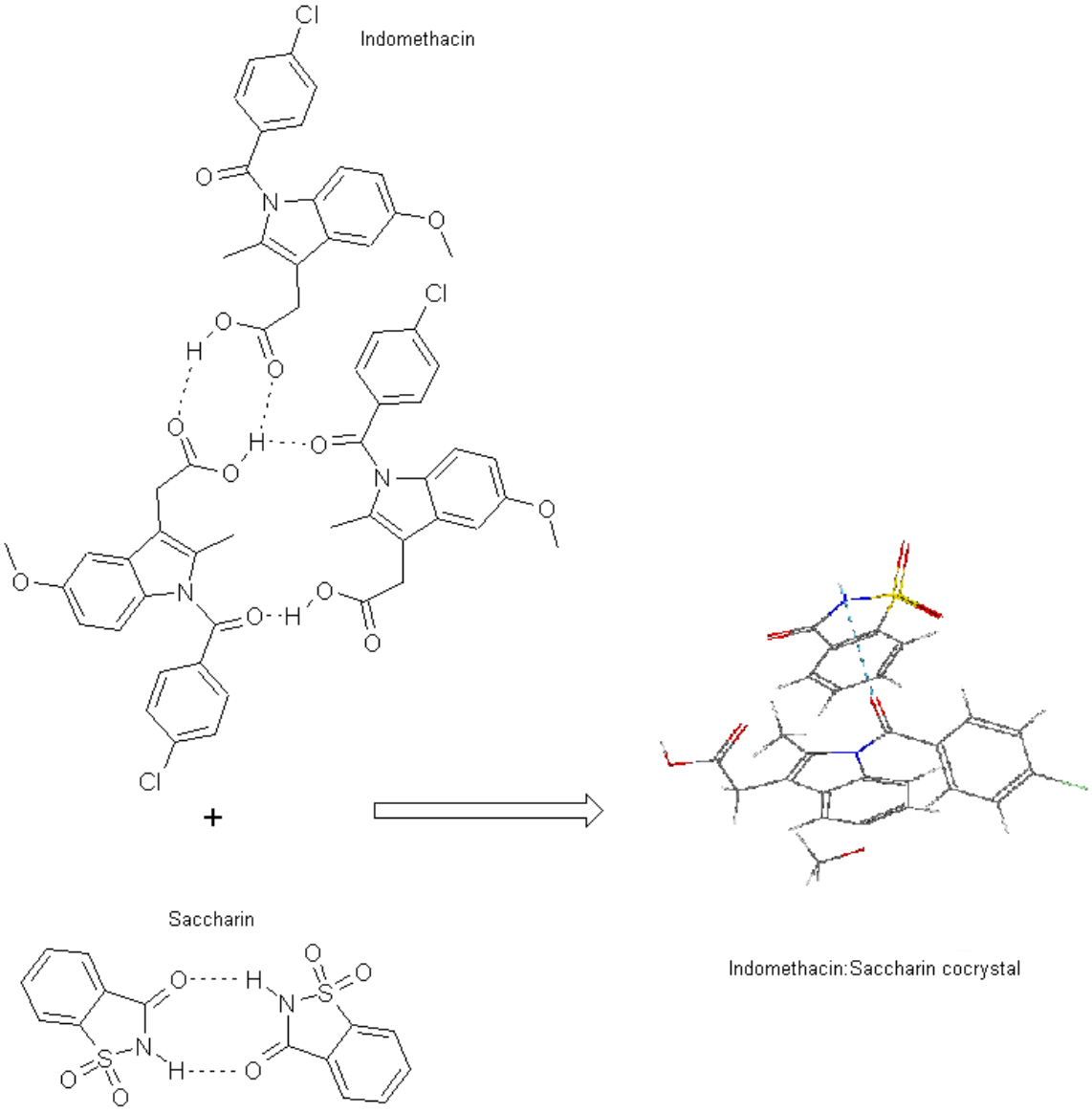

Figure 6.17: *Graphical representation of indomethacin and saccharin cells and resultant IND:SAC cocrystal (edited from Basavoju, Boström et al. 2008).*

SEM micrograph images of SAX produced cocrystals of IND:SAC and those made by evaporation are shown in Figure 6.18. Both sets of crystals appear to form needle shaped particles with the solvent evaporation crystallisation process production forming larger particles than the SAX process. Despite using a different solvent, Basavoju *et al.* also produced needle shaped particles of indomethacin saccharin in a 1:1 molar ratio by evaporation.

In correlation to the CBZ cocrystals, the particles produced by evaporation appear to have a broad particle size distribution ranging from a couple of micrometers to about 60µm in length. This is also confirmed by the particle size distribution (figure 6.19 and table 6.3). However, yet again, this is not completely representative of the entire

sample as some particles produced by evaporation were too large for the detector ring and so could not be measured by the lens.

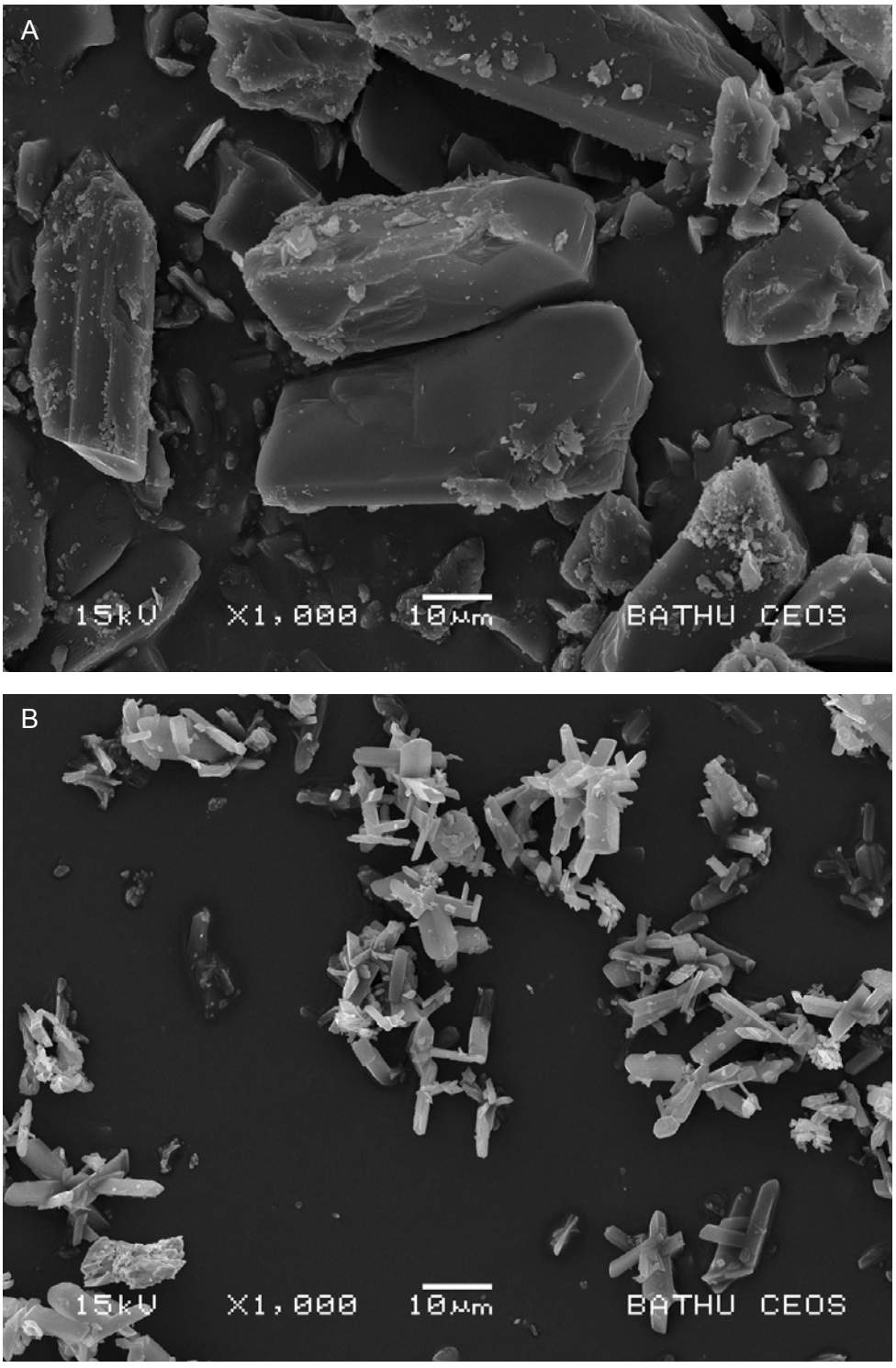

Figure 6.18: *SEM micrograph images of indomehtacin-saccharin cocrystals produced by evaporation (a) and SAX (b).*

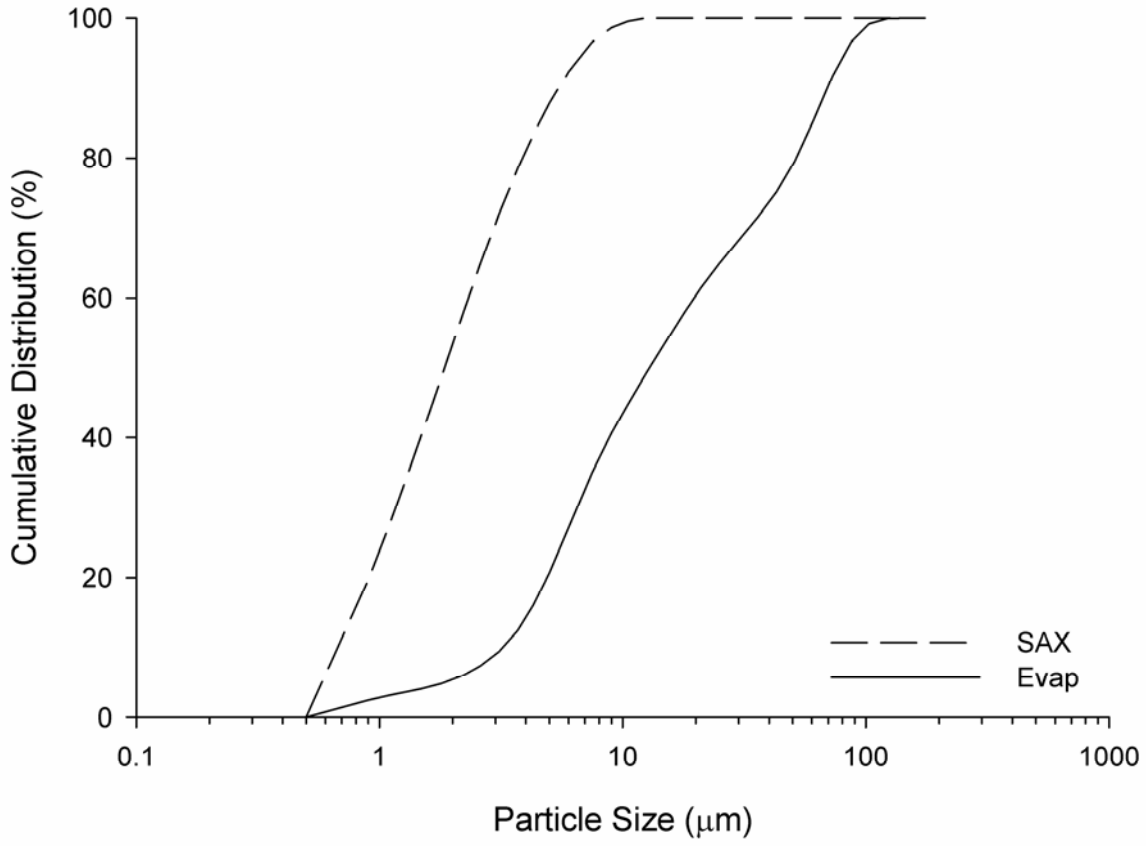

Figure 6.19: *Particle size distribution of IND:SAC cocrystals produced by evaporation and SAX.*

Table 6.3: Particle *size distribution of IND:SAC cocrystals produced by evaporation and SAX.*

IND:SAC	d_{10}(μm) ±SD	d_{50}(μm) ±SD	d_{90}(μm) ±SD	Span
EVAP	2.94 ± 0.131	9.88 ± 0.153	75.19 ± 1.71	-
SAX	0.725 ± 0.035	1.99 ± 0.184	5.61 ± 0.184	1.82

DSC analysis shows that the melting endotherm of the co-crystal produced by evaporation is different to either raw IND or raw SAC, as shown in figure 6.20. The raw materials have a peak melting points of 160.60 and 228.76°C, respectively, while the cocrystals produced by evaporation demonstrated a melt at 185.38°C as well as a second melt further on at a peak temperature of 252.98°C. This temperature does not correlate with either of the raw materials, however, the melt has an onset temperature of 249.83°C which is very close to the melt of SAC. In addition to this, there appears to

be a step in the baseline at about 107°C shifting the baseline. These data suggest that associated solvent may have been lost resulting in less energy being needed to maintain a ramp rate of 10°C.min^{-1} and therefore a small shift in the baseline. In contrast, the SAX produced cocrystals demonstrate only one melt at a peak melting point of 181.96°C. This melting point correlates with information found in the literature (Basavoju, Boström et al. 2008; Padrela, Rodrigues et al. 2009).

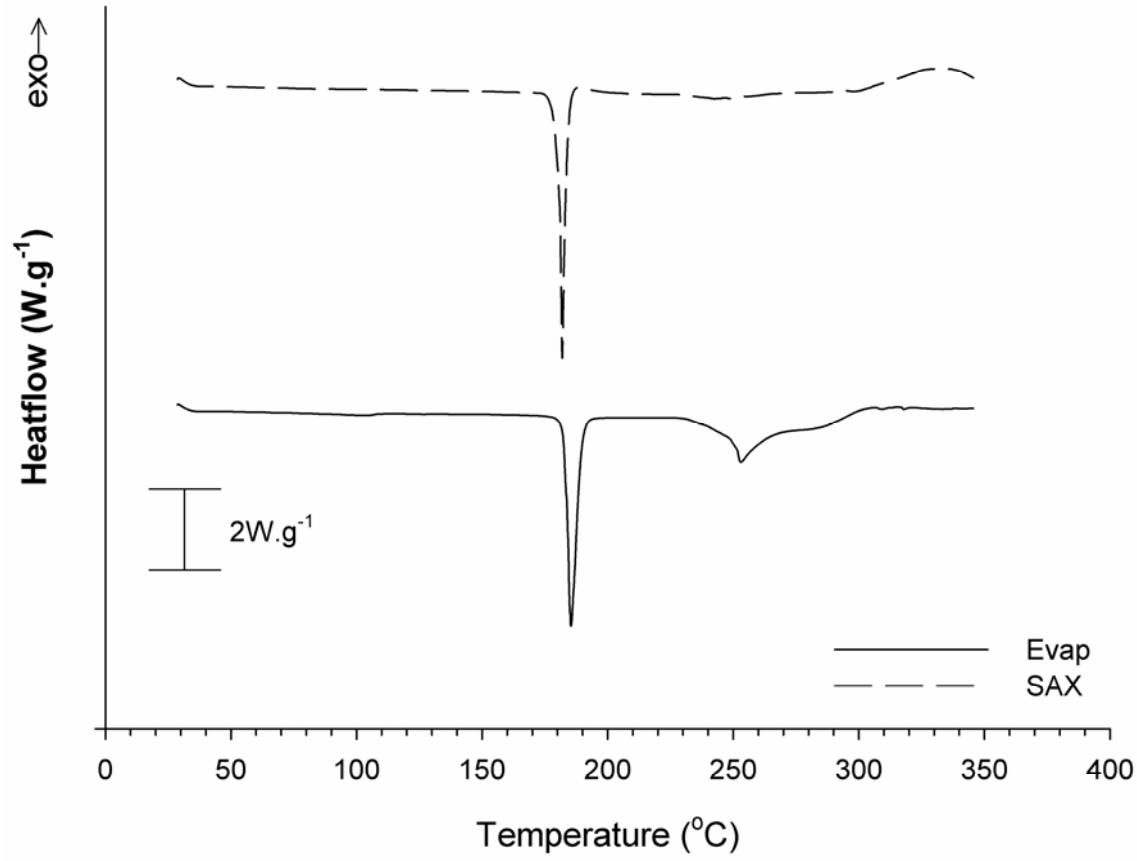

Figure 6.20: *DSC analysis of IND:SAC cocrystals produced by evaporation and SAX.*

XRPD diffractogram for the IND:SAC cocrystals produced by evaporation and SAX compared to the raw materials are shown in Figure 6.21. The XRPD diffractogram for the cocrystals produced by evaporation and SAX appear to be identical. Both traces show three new peaks compared to the raw materials (5.27 14.22 and 21.09° 2θ respectively), which suggest the formation of a cocrystal. The remaining peaks can be found in the raw materials and therefore, confirms the presence of both materials.

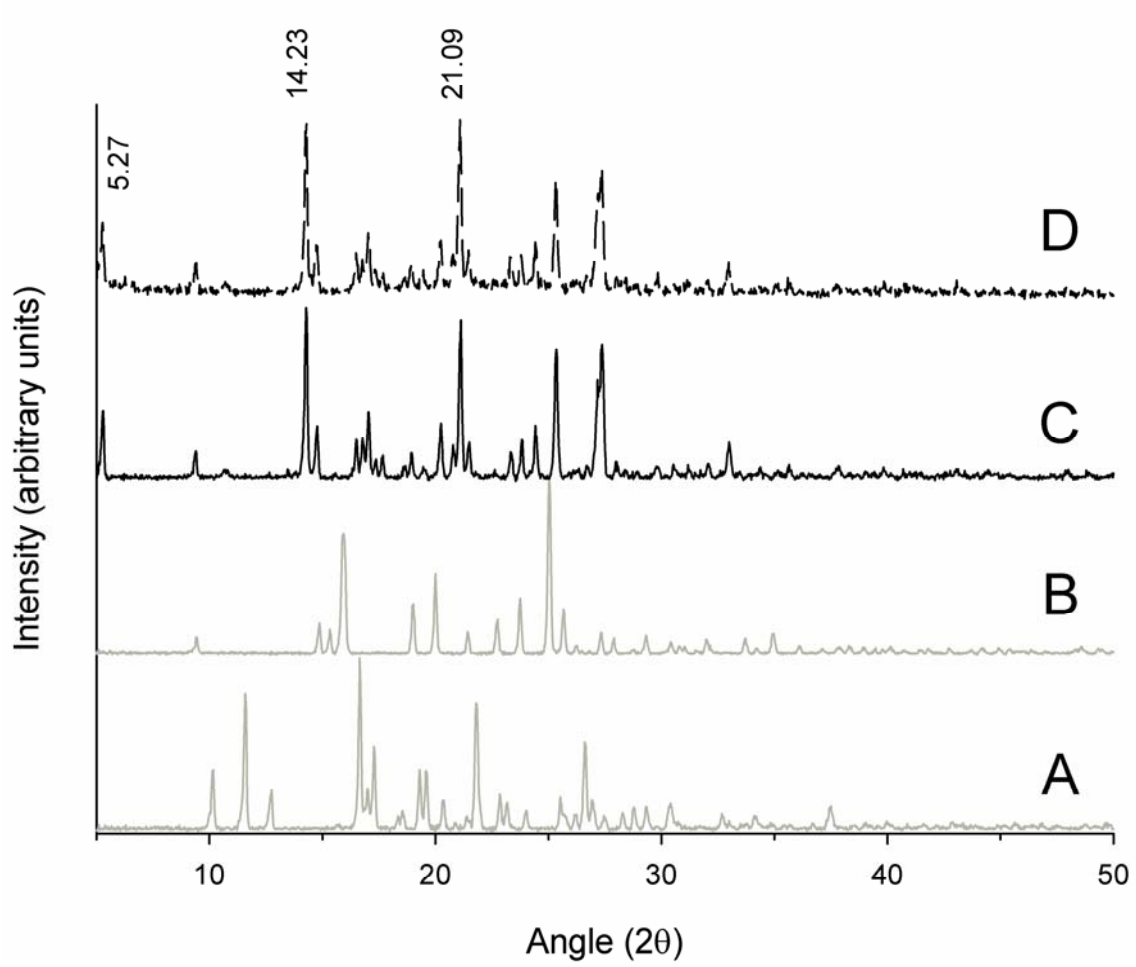

Figure 6.21: *XRPD diffractogram of (A) IND, (B) SAC and IND:SAC cocrystals produced by (C) evaporation and (D) SAX.*

Figure 6.22 shows the XRPD diffractograms of the cocrystals produced by evaporation and SAX compared to the diffractogram produced from crystallographic data used to produce the unit cell shown in figure 6.17 (Basavoju, Boström et al. 2008). The new peaks seen in the XRPD diffractogram for both the evaporation and SAX produced cocrystals appear in the predicted XRPD. However, the predicted tract also shows several other peaks between 10 and 14° 2θ. These peaks appear to co-inside with peaks from raw IND and SAC above.

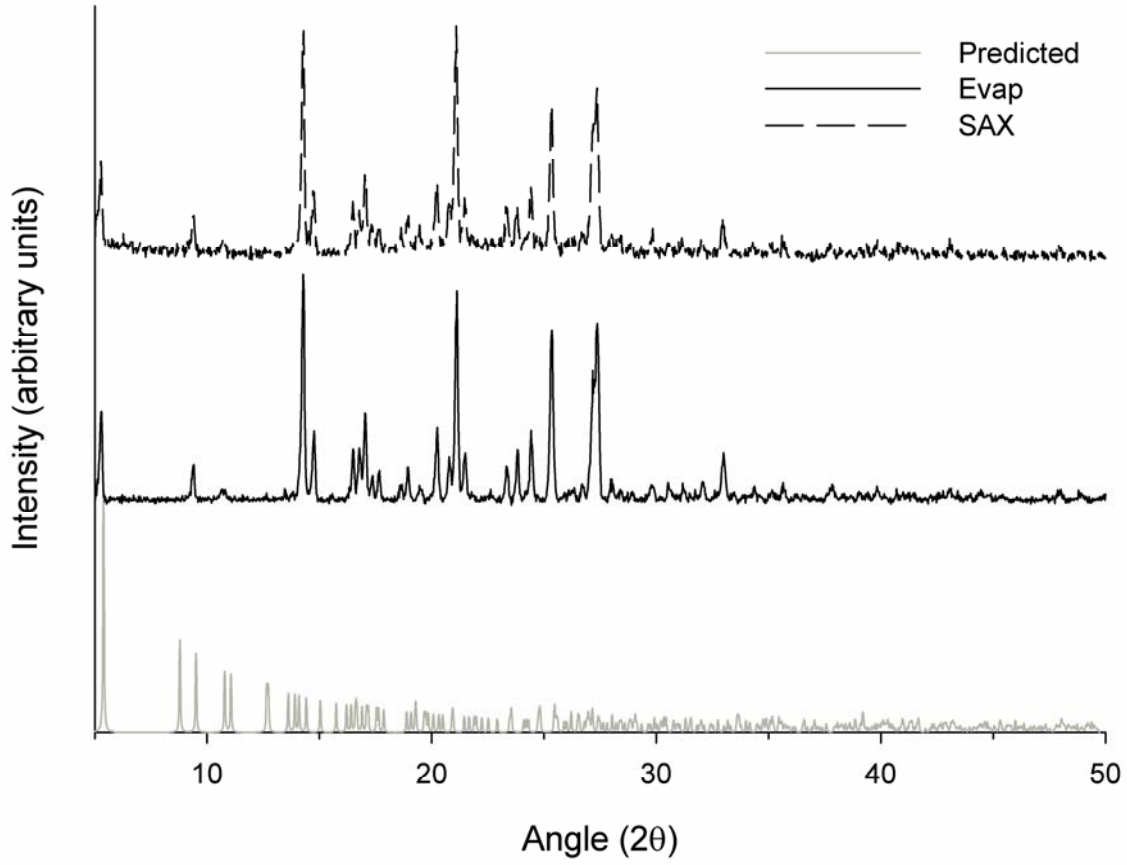

Figure 6.22: *XRPD diffractogram of IND:SAC cocrystals produced by evaproration and SAX compared to the predicted trace generated from crystallographic data (Basavoju, Boström et al. 2008).*

These data suggest that the SAX process may be used to produce a variety of cocrystals of several compounds within a defined particle size distribution. Each of the resultant cocrystals produced were crystalline in nature, with the cocrystals produced via SAX appearing to have fewer impurities (e.g. residual solvent) incorporated into the crystalline lattice.

6.5 Conclusion

This work shows that SAX can be used to produce cocrystals containing a variety of API's and cocrystal formers. In addition, the cocrystals produced appear to be of a higher purity with less excess solvent present for some cocrystals and a defined particle size distribution.

Chapter 7 - General Conclusions and Further Work

7.1 Inhalation

7.1.1 Introduction

The treatment for chronic obstructive pulmonary disease (COPD) has traditionally relied on symptomatic treatment based on asthma therapy. This has resulted in no single combination formulation being produced for the treatment of COPD patients.

7.1.2 Summary of results

The SAX process was applied as a single step droplet-to-particle operation to process drug particles for delivery to the respiratory tract. In chapter 4, novel particles containing theophylline (THE) and a steroid, either fluticasone propionate (FP) or budesonide (BUD) were prepared.

The FP:THE particles appeared to be slightly large for inhaled drug delivery with a d_{90} of 7.82μm, while the BUD:THE particles were of the correct size for respiratory delivery. The FP:THE particles produced needle shaped particles, while the BUD:THE particles appeared to be plate like.

Both sets of particles appeared to be crystalline in nature each demonstrating only one melting endotherm during DSC analysis. This, as well as the addition of new peaks in the XRPD diffractogram, may suggest the presence of a new crystalline structure, but may also be due to the presence of one compound effecting the melting of the other and the orientation of the compounds in the XRPD.

In-vitro analysis shows that the two compounds may not have been combined into one particle but rather a eutectic mixture. Despite this, the SAX formulations did provide a better dose ratio throughout the Andersen Cascade Impactor (ACI) and the Next Generation Impactor (NGI) compared to the micronised equivalent formulations. This may be due to the fact that THE was not as efficiently micronised compared to the industrially micronised FP and BUD.

Novel particles containing ipratropium bromide (IB) along with salmeterol xinafoate (SX) and FP, were prepared to produce a short acting muscarinic agonist (SAMA), long acting β_2 agonist, inhaled corticosteroid (ICS) combination.

These particles appeared to be spherical in nature within the inhalable range, but did not appear to be fully crystalline in nature. The presence of all three compounds could only be confirmed by XRPD as DSC analysis did not produce any melting endotherms.

In a pressurised metered dose inhaler (pMDI) system the fine particle fraction as a function of emitted dose (FPF_{ED}) appeared to be similar for SX and FP in the SAX formulations, while the IB and SX were similar in the micronised formulation.

This differed for the dry powder inhaler (DPI) formulation which showed the FPF_{ED} for the SAX prepared particles being similar for all three drugs while the micronized formulation demonstrated significant differences for each drug. In addition, the coefficient of variation (CV) for the micronised formulation demonstrated vast differences between the compounds. The SAX formulation showed less of a variation, but both formulations demonstrated a CV greater than 6%.

The ratios for the emitted dose varied between the two formulations. This suggests that the particles may not have contained the compounds in the correct dose ratio and may account for the difference seen in the CV.

Despite this fact, both the pMDI and DPI SAX formulations appeared to deliver a consistent dose ratio the compounds across the lower stages of the ACI and the NGI compared to the micronised equivalent formulation.

The final triple formulation produced consisted of a combination of SX, FP and THE. This resulted in the formation of crystalline particles. However, it is obvious from the SEM images that the compounds were not combined into one particle.

The resultant *in-vitro* analysis proved that the compounds were not combined, but did provide a DPI formulation where all of the compounds had similar CV values while the micronised equivalent did not.

7.1.3 Discussion

None of the inhalation formulations were ideal. One of the reasons for this may be due to the physic-chemical properties of the compounds used in the formulations. For example, in the steroid, THE combinations, the steroids are more hydrophobic in nature compared to the THE (as shown in table 2.2).

This may be part of the reason why a combination of solvents had to be used (dichloromethane and methanol in a 50:50 ratio). The steroid, being more hydrophobic in nature, would preferentially dissolve in the dichloromethane, while the THE would prefer the methanol as it is more hydrophilic in nature.

Both of the triple formulation contained SX and FP, which have similar log P values, as seen in table 2.2. As a result, they can be combined by using a single solvent, as demonstrated by Pitchayajittipong et.al (Pitchayajittipong, Shur et al. 2009). For the IB:SX:FP triple formulation, the amount of IB introduced into the mixture is small, hence

a small amount of secondary solvent is needed, while the amount of THE in the SX:FP:THE particles is quite large, resulting in a larger amount of methanol being needed.

The addition of a secondary solvent can have a variety of consequences. The first may be due to a phase separation of the solvents due to their differing densities resulting in one solvent being passed through SAX before the other, hence one set of compounds being processed before the other.

In addition, the use of combination solvents may result in one solvent evaporating preferentially compared to the other resulting in one (or a set) of compounds reaching saturation before the other, and therefore crystallising out before the other.

7.2 Production of cocrystals.

7.2.1 Introduction

Drug solubility can be an issue when delivering medication via the oral route. This stage could be the rate limiting step for compounds that are well absorbed by the body but appear to exhibit a slow dissolution rate.

Several methods exist in improving the drug dissolution rate. However, these all appear to demonstrate one drawback or another. A novel method that may provide the solution is by the formation of cocrystals.

The simplest method for the production of cocrystals is via solvent evaporation from a solution containing the drug and cocrystal former. However, this can result in crystals with a large particle size and further processing may result in the loss of cocrystals.

7.2.2 Summary of results and discussion

The SAX process was applied to produce cocrystals with a small particle size distribution. This could improve the dissolution rate by two methods: (a) the cocrystal will provide an increased dissolution rate, and (b) a smaller particle size distribution also aids in the increase in dissolution rate.

Two drugs that demonstrate a high bioavailability but low dissolution rate are carbamazepine (CBZ) and indomethacin (IND). Both of these compounds have been show to produce cocrystals with saccharin (SAC).

Both CBZ:SAC and IND:SAC cocrystals were successfully produced via the SAX method. The particles were all crystalline and demonstrated a particle size distribution less than 30μm.

In addition, the SAX system has the ability to change the particle size distribution by changing a single setting (such as the atomiser used). This was shown during the production of CBZ:SAC and CBZ:nicotinamide (NIC) cocrystals.

Finally, the cocrystals produced via SAX appear to have fewer impurities compared to the conventional method.

7.3 Limitations

As discussed, solvent evaporation was not taken into consideration. It was assumed that a combination of solvents would evaporate at the same rate, when one may evaporate more readily then the other in a combination situation. This difference in evaporation profiles may result in solubility differences between the compounds in the mixture resulting in one (or more) compounds reaching saturation before the others.

In addition, using combinations of solvents may result in a phase separation due to the solvent densities. This impact of this was reduced by using miscible solvents and using the mixture soon after it was prepared.

The particles produced were not assessed for their content, due to the fact that a low yield was produced. If a sufficient yield could be obtained, the drug content ratio could be assessed to ensure the particles contain the correct ratio of compounds prior to formulation. This could be used in combination with techniques such as Raman spectroscopy and environmental SEM to ensure all of the drugs are in each particle. However, these techniques may not be sensitive enough to provide the answer. For cocrystals, the actual ratio of the active pharmaceutical ingredient (API) to cocrystal former was not assessed.

Dissolution work was not conducted. As a result, the actual benefit for the patient cannot be assessed. Previous work has shown that producing cocrystals can improve the bioavailability of BSC class II compounds. In addition, reducing particle size is known to have an impact on improving dissolution rate. For both of these reasons, it was felt that dissolution testing was not needed.

Finally, supercritical carbon dioxide was not assessed as a variable in this work. This may have an effect on the ratio of API to former in the final product.

7.4 General Conclusion

The SAX process can be used to produce novel combination formulations and novel triple formulations for the treatment of respiratory diseases such as asthma and COPD. In addition, it can also be used as a one step process method in the production of cocrystals with a defined particle size.

However, the solvent/anti-solvent combination need to be carefully considered prior to processing as an incorrect combination could result in loss of required characteristics. Despite some issues, the inhalation combinations produced from particles developed via SAX appear to deliver better dose ratios then conventional methods.

In addition to this, the SAX process can produce a novel crystalline lattice containing a drug and a pharmacologically acceptable cocrystal former, providing the cocrystal is thermodynamically favourable.

7.5 Further Work

According to data presented in the thesis, the SAX approach may have the ability to produce novel combination/triple formulations for the treatment of respiratory diseases. However, the actual dose ratio between some of the compounds has not been investigated and therefore arbitrary values were used. This leads on to asking what ratio of ICS and theophylline would produce a beneficial response in COPD patients before developing better particles.

In addition, IB is a short acting anti-muscarinic compound while SX and FP are considered to be long acting compounds. Tiotropium is a long acting anti-muscarinic compound (British Medical Association and Royal Pharmaceutical Society of Great Britain 2009). However, this may have compatibility issues with SX and/or FP in solution (tiotropium predicted log P of -1.35,Tetko, Gasteiger et al. 2005; VCCLAB 2005). In order to improve on the mixing of different types of particles, surfactants may be used to reduce the interfacial tension and promote mixing.

Also, it has been shown that the SAX process can produce a batch of cocrystals in a single run. This could be up to 8 hours in duration for the lab scale SAX system. Compared to conventional solvent evaporation, the SAX process may provide a rapid screening process for future development of cocrystals. However, the ratio of API to cocrystal former may have an effect on the cocrystal formed. Differing ratios may still be able to produce cocrystals. The SAX process allows for the rapid screening of different ratios within a short amount of time.

References:

(2002). Modern Pharmaceutics. Basel, Marcel Dekker.
(2004). "Managing stable COPD." Thorax **59**(90001): i39-130.
(2006). Saccharin. Handbook of Pharmaceutical Excipients. Raymond C Rowe, P. J. Sheskey and S. C. Owen. London, Pharmaceutical Press**:** 638-640.
(2008). Water-Insoluble Drug Formulation. New York, CRC Press.
Aaron, S. D., K. L. Vandemheen, et al. (2007). "Tiotropium in Combination with Placebo, Salmeterol, or Fluticasone Salmeterol for Treatment of Chronic Obstructive Pulmonary Disease: A Randomized Trial." Ann Intern Med **146**(8): 545-555.
Abbas, A., M. Srour, et al. (2007). "Sonocrystallisation of sodium chloride particles for inhalation." Chem Eng Sci **62**(9): 2445-2453.
Abdine, H., F. Belal Heba, et al. (2003). Ipratropium Bromide: Physical Properties. Profiles of Drug Substances, Excipients and Related Methodology, Academic Press. **Volume 30:** 59-83.
Adcock, I. M. and K. F. Chung (2008). Overcoming Steroid Insensitivity in Respiratory Disease. Chichester, Willey.
Adcock, I. M., K. Maneechotesuwan, et al. (2002). "Molecular interactions between glucocorticoids and long-acting β2-agonists." J.Allergy Clin.Immunol. **110**(6, Part 2).
Aguilera, J., J. del Valle, et al. (1995). "Caking phenomena in amorphous food powders." Trends Food Sci Technol **6**(5): 149-155.
Akbarieh, M. and R. Tawashi (1987). "Morphic features of solid particles after micronization in the fluid energy mill." Int. J. Pharm. **35**(1-2): 81-89.
Allen, T. (1990). Particle size measurement. London, Chapman and Hall.
Alles, xf, et al. (2008). "Near-Infrared Spectroscopy for Cocrystal Screening. A Comparative Study with Raman Spectroscopy." Anal. Chem. **80**(20): 7755-7764.
Almarsson, O., M. B. Hickey, et al. (2007). Pharmaceutical Co-crystal Compositions. United States Patent Application Publication. United States, TransForm Pharmaceuticals, Inc, University of South Florida, The Regents of The University of Michigan.
Almarsson, O. and M. Zaworotko (2004). "Crystal engineering of the composition of pharmaceutical phases. Do pharmaceutical co-crystals represent a new path to improved medicines?" Chem. Commun.(17): 1889-1896.
Ando, H., M. Ishii, et al. (1995). "Effect of Crystallization of Theophylline on Physical Properties of Tablets." Drug Dev. Ind. Pharm. **21**(19): 2227.
Asgharian, B. and S. Anjilvel (1994). "Inertial and Gravitational Deposition of Particles in A Square Cross-Section Bifurcating Airway." Aerosol Sci. Tech. **20**(2): 177-193.
Aulton, M. E. (2002). Pharmaceutics: The Science of Dosage Form Design. London, Churchill Livingstone.
Austin, L. G. and O. Trass (1997). Size Reduction of Solids Crushing and Grinding Equipment. Handbook of Powder Science and Technology. M. E. Fayed and L. Otten. London, Chapman & Hall.
Balashazy, I. and W. Hofmann (1993). "Particle deposition in airway bifurcations. 1. inspiratory flow." J.Aerosol Sci. **24**(6).
Barnes, N. C., Y. S. Qiu, et al. (2006). "Antiinflammatory Effects of Salmeterol/Fluticasone Propionate in Chronic Obstructive Lung Disease." Am. J. Respir. Crit. Care Med. **173**(7): 736-743.
Barnes, P., J. (2008). "Immunology of asthma and chronic obstructive pulmonary disease." Nat. Rev. Immunol. **8**(3): 183-192.
Barnes, P. J. (1998). "New therapies for chronic obstructive pulmonary disease." Thorax **53**(2): 137-147.

Barnes, P. J. (1999). "Novel Approaches and Targets for Treatment of Chronic Obstructive Pulmonary Disease." Am. J. Respir. Crit. Care Med. **160**(5): S72-79.

Barnes, P. J. (2000). "Chronic Obstructive Pulmonary Disease." N Engl J Med **343**(4): 269-280.

Barnes, P. J. (2000). "Inhaled Corticosteroids Are Not Beneficial in Chronic Obstructive Pulmonary Disease." Am. J. Respir. Crit. Care Med. **161**(2): 342-344.

Barnes, P. J. (2001). "Clinical outcome of adding long-acting β-agonists to inhaled corticosteroids." Resp.Med. **95**(Supplement 2).

Barnes, P. J. (2002). "Scientific rationale for inhaled combination therapy with long-acting β_2-agonists and corticosteroids." Eur Respir J **19**(1): 182-191.

Barnes, P. J. (2003). "Therapy of chronic obstructive pulmonary disease." Pharmacol. Therapeut. **97**(1): 87-94.

Barnes, P. J. (2004). "Mediators of chronic obstructive pulmonary disease." Pharmacol. Rev. **56**: 515-548.

Barnes, P. J. (2005). "Theophylline in Chronic Obstructive Pulmonary Disease: New Horizons." Proc Am Thorac Soc **2**(4): 334-339.

Barnes, P. J. (2006). "Reduced Histone Deacetylase in COPD: Clinical Implications." Chest **129**(1): 151-155.

Barnes, P. J. (2006). "Theophylline for COPD." Thorax **61**(9): 742-743.

Barnes, P. J. (2008). "Frontrunners in novel pharmacotherapy of COPD." Curr. Opin. Pharmacol. **8**(3): 300-307.

Barnes, P. J. (2008). "Immunology of asthma and chronic obstructive pulmonary disease." Nature Reviews Immunology **8**(3): 183-192.

Barnes, P. J., K. F. Chung, et al. (1998). "Inflammatory mediators of asthma: an update." Pharmacol. Rev. **50**: 515-596.

Barnes, P. J., K. Ito, et al. (2004). "Corticosteroid resistance in chronic obstructive pulmonary disease: inactivation of histone deacetylase." Lancet (British edition) **363**(9410): 731-733.

Barnes, P. J. and R. A. Pauwels (1994). "Theophylline in the management of asthma: time for reappraisal?" Eur Respir J **7**(3): 579-591.

Barnes, P. J., S. D. Shapiro, et al. (2003). "Chronic obstructive pulmonary disease: molecular and cellular mechanisms." Eur Respir J **22**(4): 672-688.

Barnes, P. J. and R. A. Stockley (2005). "COPD: current therapeutic interventions and future approaches." Eur Respir J **25**(6): 1084-1106.

Barnes, P. J. and A. J. Woolcock (1998). "Difficult asthma." Eur Respir J **12**(5): 1209-1218.

Basavoju, S., D. Boström, et al. (2008). "Indomethacin–Saccharin Cocrystal: Design, Synthesis and Preliminary Pharmaceutical Characterization." Pharm Res **25**(3): 530-541.

Bastin, R. J., M. J. Bowker, et al. (2000). "Salt Selection and Optimisation Procedures for Pharmaceutical New Chemical Entities." Org. Process Res. Dev. **4**(5): 427-435.

Beach, S., D. Latham, et al. (1999). "Control of the physical form of salmeterol xinofoate." Org.Process Res.Dev. **3**(5).

Beavo, J. A. and D. H. Reifsnyder (1990). "Primary sequence of cyclic nucleotide phosphodiesterase isozymes and the design of selective inhibitors." Trends Pharmacol. Sci. **11**(4): 150-155.

Begat, P., D. A. V. Morton, et al. (2004). "The cohesive-adhesive balances in dry powder inhaler formulations II: Influence on fine particle delivery characteristics." Pharm. Res. **21**(10): 1826-1833.

Begat, P., P. M. Young, et al. (2003). "The effect of mechanical processing on surface stability of pharmaceutical powders: Visualization by atomic force microscopy." J. Pharm. Sci. **92**(3): 611-620.

Behme, R. J. and D. Brooke (1991). "Heat of fusion measurement of a low melting polymorph of carbamazepine that undergoes multiple-phase changes during differential scanning calorimetry analysis." J. Pharm. Sci. **80**(10): 986-990.

Bertilsson (1978). "Clinical Pharmacokinetics of Carbamazepine." Clin. Pharmacokinet. **3**(2): 128-143.

Bisrat, M. and C. Nyström (1988). "Physicochemical aspects of drug release. VIII. The relation between particle size and surface specific dissolution rate in agitated suspensions." Int. J. Pharm. **47**(1-3): 223-231.

Biwer, A., G. Antranikian, et al. (2002). "Enzymatic production of cyclodextrins." Applied Microbiology and Biotechnology **59**(6): 609-617.

Bosquillon, C., C. Lombry, et al. (2001). "Comparison of particle sizing techniques in the case of inhalation dry powders." J. Pharm. Sci. **90**(12): 2032-2041.

Botsaris, G. D. and J. W. Mullins (1976). Secondary nucleation: A review. Industrial crystallization. New York, USA, Plenum Press. **2nd**.

Boucher, R. C. (1994). "State of Art: Human airway ion transport." Am. J. Respir. Crit. Care Med. **150** 271-593.

Bousquet, J., R. Dahk, et al. (2007). "Global alliance against chronic respiratory diseases." Allergy **62**: 216-223.

British Medical Association and Royal Pharmaceutical Society of Great Britain (2009). British National Formulary. London, Pharmaceutical Press.

Brittain, H. G. (1995). Physical characterisation of Pharmaceutical Solids. New York, Marcel Dekkar.

Brittain, H. G., S. J. Bogdanowich, et al. (1991). "Physical characterisation of pharmaceutical solids." Pharm. Res. **8**: 963-973.

Bucar, D. K. and L. R. MacGillivray (2007). "Preparation and Reactivity of Nanocrystalline Cocrystals Formed via Sonocrystallization." J.Am.Chem.Soc. **129**(1).

Buckton, G. (1997). "Characterisation of small changes in the physical properties of powders of significance for dry powder inhaler formulations." Adv. Drug Delivery Rev. **26**: 17-27.

Buckton, G. and P. Darcey (1999). "Assessment of disorder in crystalline powders - a review of analytical techniques and their application." Int. J. Pharm. **179** 141-158.

Buckton, G. and P. Darcy (1995). "The use of gravimetric studies to assess the degree of crystallinity of predominantly crystalline powders." Int.J.Pharm. **123**(2).

Calverley, P., R. Pauwels, et al. (2003). "Combined salmeterol and fluticasone in the treatment of chronic obstructive pulmonary disease: a randomised controlled trial." Lancet **361**(9356): 449-456.

Calverley, P. M., W. Boonsawat, et al. (2003). "Maintenance therapy with budesonide and formoterol in chronicobstructive pulmonary disease." Eur.Respir.J. **22**(6).

Caramori, G. and I. Adcock (2003). "Pharmacology of airway inflammation in asthma and COPD." Pulm. Pharmacol. Ther. **16**(5): 247-277.

Cazzola, M., N. A. Hanania, et al. (2008). "It's about time - directing our attention toward modifying the course of COPD." Resp.Med. **102**(Supplement 1).

Cazzola, M. and M. G. Matera (2008). "To Add, or Not To Add an Inhaled Corticosteroid in Moderate COPD: That Is the Question." Chest **134**(2): 223-225.

CHERIC. Retrieved 29th June, 2009, from http://www.cheric.org/research/kdb/hcprop/cmpsrch.php.

Chow, R., R. Blindt, et al. (2003). "The sonocrystallisation of ice in sucrose solutions: primary and secondary nucleation." Ultrasonics **41**(8): 595-604.

Clark, A. R. and M. Egan (1994). "Modeling the Deposition of Inhaled Powdered Drug Aerosols." J Aerosol Sci **25**(1): 175-186.

Commission, B. P. (2003). Appendix XII F. Aerodynamic assessment of fine particles - fine particle sode and particle size disrtibution. British Pharmacopoeia. London, Stationaery Office.

Corrigan, D. O., O. I. Corrigan, et al. (2006). "Physicochemical and in vitro deposition properties of salbutamol sulphate/ipratropium bromide and salbutamol sulphate/excipient spray dried mixtures for use in dry powder inhalers." Int. J. Pharm. **322**(1-2): 22-30.

Cosio, B. G., A. Iglesias, et al. (2009). "Low-dose theophylline enhances the anti-inflammatory effects of steroids during exacerbations of COPD." Thorax **64**(5): 424-429.

Cosio, B. G., L. Tsaprouni, et al. (2004). "Theophylline Restores Histone Deacetylase Activity and Steroid Responses in COPD Macrophages." J. Exp. Med. **200**(5): 689-695.

Crowder, T. M., J. A. Rosati, et al. (2002). "Fundamental effects of particle morphology on lung delivery: Predictions of Stokes' law and the particular relevance to dry powder inhaler formulation and development." Pharm.Res. **19**(3).

Crower, T. M., A. Hickey, et al. (2003). A guide to pharmaceutical particulate science. London, Interpharm/CRC.

Culpitt, S. V., C. de Matos, et al. (2002). "Effect of Theophylline on Induced Sputum Inflammatory Indices and Neutrophil Chemotaxis in Chronic Obstructive Pulmonary Disease." Am. J. Respir. Crit. Care Med. **165**(10): 1371-1376.

Cushley, M. J. and S. T. Holgate (1985). "Bronchodilator actions of xanthine derivatives administered by inhalation in asthma." Thorax **40**(3): 176-179.

Cushley, M. J., A. E. Tattersfield, et al. (1984). "Adenosine-induced bronchoconstriction in asthma. Antagonism by inhaled theophylline." Am Rev Respir Dis. **129**: 380-4.

D'Alonzo, G. E., R. A. Nathan, et al. (1994). "Salmeterol Xinafoate as Maintenance Therapy Compared With Albuterol in Patients With Asthma." JAMA **271**(18): 1412-1416.

Dalby, R., M. Spallek, et al. (2004). "A review of the development of Respimat(R) Soft Mist(TM) Inhaler." Int. J. Pharm. **283**(1-2): 1-9.

Dalby, R. and J. Suman (2003). "Inhalation therapy: technological milestones in asthma treatment." Adv. Drug Deliver. Rev. **55**(7): 779-791.

Davis, B. (2008). "The winner's cirlce." Pharm. Tech. Eur. **20**(9): 86-92.

de Boer, A. H., D. Gjaltema, et al. (2002). "Characterization of inhalation aerosols: a critical evaluation of cascade impactor analysis and laser diffraction technique." Int.J.Pharm. **249**(1-2).

Dean, T. P., Y. Dai, et al. (1993). "Interleukin-8 Concentrations Are Elevated in Bronchoalveolar Lavage, Sputum, and Sera of Children with Cystic-Fibrosis." Pediatr Res **34**(2): 159-161.

Dhumal, R. S., S. V. Biradar, et al. (2009). "Particle engineering using sonocrystallization: Salbutamol sulphate for pulmonary delivery." Int. J. Pharm. **368**(1-2): 129-137.

Dietrich, D. E. (1990). "A Partial Theory of Atomization in Internal Mix Swirl Nozzles." Aerosol Sci. Tech. **12**(3): 654-664.

Duncanhewitt, W. C. and D. J. W. Grant (1986). "True density and thermal expansivity of pharmaceutical Solids - Comparison of methods and assessment of crystallinity." Int. J. Pharm. **28**(1): 75-84.

Ebisuzaki, Y., P. Boyle, D., et al. (1997). "Methylxanthines. I. Anhydrous Theophylline." Acta Crystallographica Section C **53**(6): 777-779.

Edwards, M. R., M. W. Johnson, et al. (2006). "Combination Therapy: Synergistic Suppression of Virus-Induced Chemokines in Airway Epithelial Cells." Am. J. Respir. Cell Mol. Biol. **34**(5): 616-624.

El-Zein, H., L. Riad, et al. (1998). "Enhancement of carbamazepine dissolution: in vitro and in vivo evaluation." Int. J. Pharm. **168**(2): 209-220.

Elajnaf, A., P. Carter, et al. (2007). "The Effect of Relative Humidity on Electrostatic Charge Decay of Drugs and Excipient Used in Dry Powder Inhaler Formulation." Drug Dev. Ind. Pharm. **33**(9): 967-974.

Elamin, A. A., T. Sebhatu, et al. (1995). "The use of amorphous model substances to study mechanically activated materials in the solid state." Int.J.Pharm. **119**(1).

Evans, D. J., D. A. Taylor, et al. (1997). "A Comparison of Low-Dose Inhaled Budesonide plus Theophylline and High-Dose Inhaled Budesonide for Moderate Asthma." N Engl J Med **337**(20): 1412-1419.

Feoktistov, I., I. Biaggioni, et al. (1998). "Adenosine A2B receptors: a novel therapeutic target in asthma?" Trends Pharmacol Sci **19**(4): 148-153.

Fleischman, S. G., S. S. Kuduva, et al. (2003). "Crystal Engineering of the Composition of Pharmaceutical Phases: Multiple-Component Crystalline Solids Involving Carbamazepine." Crystal Growth & Design **3**(6): 909-919.

Fleischman, S. G., S. S. Kuduva, et al. (2003). "Crystal Engineering of the Composition of Pharmaceutical Phases: Multiple-Component Crystalline Solids Involving Carbamazepine." Cryst. Growth Des. **3**(6): 909-919.

Florence, A. T. and D. Attwood (2006). Physicochemical Principles of Pharmacy. London, Pharmaceutical Press.

Fredholm, B. B. and C. Persson (1982). "Xanthine derivatives as adenosine receptor antagonists." Eur. J. Pharmacol. **81**: 673-76.

GAD, S. C. (2008). Pharmaceutical Manufacturing Handbook: Production and Processes. New Jersy, Wiley-Interscience.

Gaffet, E. and M. Harmelin (1990). "Crystal-amorphous phase transition induced by ball-milling in silicon." J. Less-Common Met. **157**(2): 201-222.

Gross, N. J. (1988). "Ipratropium bromide." N Engl J Med **319**(8): 486-494.

Guchardi, R., M. Frei, et al. (2008). "Influence of fine lactose and magnesium stearate on low dose dry powder inhaler formulations." Int. J. Pharm. **348**(1-2): 10-17.

Gurney, J. W. (1991). "Cross-Sectional Physiology of the Lung." Radiology **178**(1): 1-10.

H. Abdine, F. B. Heba, et al. (2003). Ipratropium Bromide: Physical Properties. Profiles of Drug Substances, Excipients and Related Methodology, Academic Press. **Volume 30:** 59-83.

Halbert, R., J. L. Natoli, et al. (2006). "Global burden of COPD: systematic review and meta-analysis." Eur Respir J **28**(3): 523-532.

Hanania, N. A. (2008). "The impact of inhaled corticosteroid and long-acting β-agonist combination therapy on outcomes in COPD." Pulm. Pharmacol. Ther. **21**: 540-550.

Hancock, B. C. and G. Zografi (1997). "Characteristics and significance of the amorphous state in pharmaceutical systems." J.Pharm.Sci. **86**(1).

Harris, D. (2007). "Testing Inhalers." Pharmaceutical Technology Europe **11**(11): 11-11.

Henningson, E. W. and M. S. Ahlberg (1994). "Evaluation of microbiological aerosol samplers: A review." J Aerosol Sci **25**(8): 1459-1492.

Heyder, J., J. Gebhart, et al. (1986). "Depoistion of particles in the human respiratory tract in the size range 0.005-15mM." J Aerosol Sci **17** (5): 811-825.

Hickey, M. B., M. L. Peterson, et al. (2007). "Performance comparison of a co-crystal of carbamazepine with marketed product." Eur. J. Pharm. Biopharm. **67**(1): 112-119.

Hillery, A. M., A. W. Lloyd, et al. (2001). Drug Delivery and Targeting for Pharmacists and Pharmaceutical Scientists. New Fetter Lane, London, UK, Taylor & Francis.

Hoffman, B. B. and P. Taylor (2001). Neurotransmission: The Autonomic and Somatic Motor Nervous System. Goodman & Gilman's The Pharmacological Basis of Therapeutics. J. G. Hardman, L. E. Limbird and A. G. Gilman. London, McGraw-Hill.

Hu, J. H., K. P. Johnston, et al. (2004). "Nanoparticle engineering processes for enhancing the dissolution rates of poorly water soluble drugs." Drug Dev.Ind.Pharm. **30**(3).

Ito, K., M. Ito, et al. (2005). "Decreased Histone Deacetylase Activity in Chronic Obstructive Pulmonary Disease." N Engl J Med **352**(19): 1967-1976.

Ito, K., S. Lim, et al. (2002). "A molecular mechanism of action of theophylline: Induction of histone deacetylase activity to decrease inflammatory gene expression." P. Natl. Acad. Sci. USA **99**(13): 8921-8926.

Ito, K., S. Yamamura, et al. (2006). "Histone deacetylase 2-mediated deacetylation of the glucocorticoid receptor enables NF-κB suppression." J. Exp. Med. **203**(1): 7-13.

Jacoby, D. B. and A. D. Fryer (2001). "Anticholinergic therapy for airway diseases " Life Sciences **68**(22-23): 2565-2572.

Jayasankar, A. (2006). "Cocrystal formation during cogrinding and storage is mediated by amorphous phase." Pharmaceutical research **23**(10): 2381-2392.

Jayasankar, A., D. J. Good, et al. (2007). "Mechanisms by Which Moisture Generates Cocrystals." Mol. Pharmaceutics **4**(3): 360-372.

Johnson, M. and R. A. Coleman (1995). Mechanism of action of β_2-adrenoceptor agonists. Aasthma and Rhinitis. W. W. Busse and S. T. Holgate. Cambridge, Blackwell Scientific Publications**:** 1278-1295.

Jones, M. D., H. Harris, et al. (2008). "An investigation into the relationship between carrier-based dry powder inhalation performance and formulation cohesive-adhesive force balances." Eur. J. Pharm. Biopharm. **69**(2): 496-507.

Kaerger, J. S. (2003). Controlled Crystallisation of Mesoscopic Partices. Pharmacy & Pharmacology. Bath, University of Bath. **Doctor of Philosophy**.

Kaerger, J. S. and R. Price (2004). "Processing of spherical crystalline particles via a novel solution atomization and crystallization by sonication (SAXS) technique." Pharm Res **21**(2): 372-81.

Kamada, A. K., J. D. Spahn, et al. (1994). "Salmeterol: its place in asthma management." Ann Pharmacother **28**(9): 1100-1102.

Keating, G. M. and P. L. McCormack (2007). "Salmeterol/fluticasone propionate: A review of its use in the treatment of chronic obstructive pulmonary disease." Drugs **67**(16): 2383-2406.

Keatings, V. M., A. Jatakanon, et al. (1997). "Effects of inhaled and oral glucocorticoids on inflammatory indices in asthma and COPD." Am. J. Respir. Crit. Care Med. **155**(2): 542-548.

Kent, L., L. Smyth, et al. (2008). "Cigarette smoke extract induced cytokine and chemokine gene expression changes in COPD macrophages." Cytokine **42**(2): 205-216.

Kirsten, D. K., R. E. Wegner, et al. (1993). "Effects of theophylline withdrawal in severe chronic obstructive pulmonary disease [published erratum appears in Chest 1994 Jul;106(1):328]." Chest **104**(4): 1101-1107.

Kraus, W. and G. Nolze (1996). "POWDER CELL - a program for the representation and manipulation of crystal structures and calculation of the resulting X-ray powder patterns." J. Appl. Crystallogr. **29**(3): 301-303.

Lake, O. A., M. Olling, et al. (1999). "In vitro/in vivo correlations of dissolution data of carbamazepine immediate release tablets with pharmacokinetic data obtained in healthy volunteers." Eur. J. Pharm. Biopharm. **48**(1): 13-19.

Lauwo, J. A. K. (1985). "Effect of Particle Size and Excipients on the Dissolution Rate of Metronidazole from Solid Dosage Forms: I." Drug Dev. Ind. Pharm. **11**(8): 1565 - 1576.

Lewis, D. A., B. J. Meakin, et al. (2006). Pharmaceutical solution formulation for pressurized metered dose inhaler. United States Patent Office. USA, Chiesi Farmaceutici S.p.A.

Li, S. F. (2005). "Investigation of solubility and dissolution of a free base and two different salt forms as a function of pH." Pharmaceutical Research **22**(4): 628-635.

Lichtenstein, L. M. and S. Margolis (1968). "Histamine release in vitro:inhibition by chatecholamines and methylxanthines." Science **161**: 902-3.

Lim, S., A. Jatakanon, et al. (2000). "Comparison of high dose inhaled steroids, low dose inhaled steroids plus low dose theophylline, and low dose inhaled steroids alone in chronic asthma in general practice." Thorax **55**(10): 837-841.

Lim, S. A. M., K. Tomita, et al. (2001). "Low-dose Theophylline Reduces Eosinophilic Inflammation but Not Exhaled Nitric Oxide in Mild Asthma." Am. J. Respir. Crit. Care Med. **164**(2): 273-276.

Lindenberg, M., S. Kopp, et al. (2004). "Classification of orally administered drugs on the World Health Organization Model list of Essential Medicines according to

the biopharmaceutics classification system." Eur. J. Pharm. Biopharm. **58**(2): 265-278.
Lippmann, M., D. B. Yeates, et al. (1980). "Deposition, Retention, and Clearance of Inhaled Particles." Brit. J. Ind. Med. **37**(4): 337-362.
Liversidge, G. G. and K. C. Cundy (1995). "Particle-Size Reduction for Improvement of Oral Bioavailability of Hydrophobic Drugs .1. Absolute Oral Bioavailability of Nanocrystalline Danazol in Beagle Dogs." Int. J. Pharm. **125**(1): 91-97.
Lodewyckx, P. and E. F. Vansant (1997). "The dynamic adsorption of water vapour on activated carbon." Carbon **35**(2): 310-311.
Lopez, A. D. and C. Mathers (2006). "Measuring the global burden of disease and epidemiological transitions: 2002-2030." Ann. Trop. Med. Parasit. **100**(5-6): 481-499.
Lorimer, J. P. and T. J. Mason (1987). "Sonochemistry Part 1-The Physical Aspects." Chemical Society Reviews **16**: 239-274.
Lorimer, J. P. and T. J. Mason (1987). "Sonochemistry. Part 1—The physical aspects." Chem. Soc. Rev.(16): 239-274.
Louey, M. D., M. Van Oort, et al. (2004). "Aerosol dispersion of respirable particles in narrow size distributions produced by jet-milling and spray-drying techniques." Pharm Res **21**(7): 1200-1206.
Mak, J. C. W., M. Nishikawa, et al. (1995). "Glucocorticosteroids Increase β_2-Adrenergic Receptor Transcription in Human Lung." Am. J. Physiol-Lung C. **12**(1): L41-L46.
Mannhold, R., H. Kubinyi, et al. (2003). Drug Bioavailability: Estimation of Solubility Permeability, Absorption and Bioavailability. Germany, Wiley-VCH.
Mannino, D. M. and A. S. Buist (2007). "Global burden of COPD: risk factors, prevalence, and future trends." Lancet **370**(9589): 765-773.
Markham, A. and D. Faulds (1998). "Theophylline: A Review of its Potential Steroid Sparing Effects in Asthma." Drugs **56**(6): 1081-91.
Marple, V. A., B. A. Olson, et al. (2003). "Next generation pharmaceutical impactor (a new impactor for pharmaceutical inhaler testing). Part II: Archival calibration." J. Aerosol Sci. **16**(3): 301-24.
Marple, V. A., D. L. Roberts, et al. (2003). "Next generation pharmaceutical impactor (a new impactor for pharmaceutical inhaler testing). Part I: Design." J. Aerosol Med. **16**(3): 283-99.
Marshall, L. (2009). IL-8 suppression of micronised salmeterol xinafoate and fluticasone propionate either alone, in combination or co-processed via SAX.
Martonen, T. B. and I. Katz (1993). "Deposition Patterns of Polydisperse Aerosols Within Human Lungs." J. Aerosol Med. **6**(4): 251-274.
Martonen, T. B., I. Katz, et al. (1992). "Use of Analytically Defined Estimates of Aerosol Respirable Fraction to Predict Lung Deposition Patterns." Pharm Res **9**(12): 1634-1639.
McGregor, C., M. H. Saunders, et al. (2004). "The use of high-speed differential scanning calorimetry (Hyper-DSC(TM)) to study the thermal properties of carbamazepine polymorphs." Thermochimica Acta **417**(2): 231-237.
Mie, G. (1908). "Contributions to the optics of diffuse media." Ann.Phys. **25**.
Minoru, Y., C. H. Bruno, et al. (1994). "Crystallization of indomethacin from the amorphous state below and above its glass transition temperature." J. Pharm. Sci. **83**(12): 1700-1705.
Morrison, F. A. (1974). "Inertial impaction in stagnation flow." J.Aerosol Sci. **5**(3).
Mortaz, E., M. V. Rad, et al. (2008). "Salmeterol with fluticasone enhances the suppression of IL-8 release and increases the translocation of glucocorticoid receptor by human neutrophils stimulated with cigarette smoke." J. Mol. Med.-Jmm **86**(9): 1045-1056.
Mullin, J. W. (1992). Crystallization. Oxford, UK, Butterworth-Heinemann.
Narurkar, A., P.-C. Sheen, et al. (1987). "Effect of Particle Size on the Dissolution Characteristics of Chlorthalidone." Drug Dev. Ind. Pharm. **13**(2): 319 - 328.

Nehm, S. J., B. Rodriguez-Spong, et al. (2005). "Phase Solubility Diagrams of Cocrystals Are Explained by Solubility Product and Solution Complexation." cryst. Growth Des. **6**(2): 592-600.

Nelson, H. S., K. R. Chapman, et al. (2003). "Enhanced synergy between fluticasone propionate and salmeterol inhaled from a single inhaler versus separate inhalers." J.Allergy Clin.Immun. **112**(1).

Oberbauer, R., P. Krivanek, et al. (1993). "Pharmacokinetics of Indomethacin in the Elderly." Clin. Pharmacokinet. **24**(5): 428-434.

Padrela, L., M. A. Rodrigues, et al. (2009). "Formation of indomethacin-saccharin cocrystals using supercritical fluid technology." Eur. J. Pharm. Sci. **38**(1): 9-17.

Park, S. H. and K. W. Lee (2000). "Lognormal size distribution theory for deposition of polydisperse aerosol particles." Nucl Sci Eng **135**(3): 288-295.

Pauwels, R. A., A. S. Buist, et al. (2001). "Global Strategy for the Diagnosis, Management, and Prevention of Chronic Obstructive Pulmonary Disease . NHLBI/WHO Global Initiative for Chronic Obstructive Lung Disease (GOLD) Workshop Summary." Am.J.Respir.Crit.Care Med. **163**(5): 1256-1276.

Pauwels, R. A. and K. F. Rabe (2004). "Burden and clinical features of chronic obstructive pulmonary disease (COPD)." Lancet **364**(9434): 613-620.

Peachell, P. T., M. Columbo, et al. (1988). "Adenosine potentiates mediator release from human lung mast cells." Am Rev Respir Dis. **138**: 1143-51.

Pearce, N., N. It-Khaled, et al. (2007). "Worldwide trends in the prevalence of asthma symptoms: phase III of the International Study of Asthma and Allergies in Childhood (ISAAC)." Thorax **62**(9): 757-765.

Pedireddi, V. R., W. Jones, et al. (1996). "Creation of crystalline supramolecular arrays: A comparison of co-crystal formation from solution and by solid state grinding." Chemical Communications(8): 987-988.

Pfeiffer-Brodka, K., P. Langguth, et al. (2003). "Influence of mechanical activation on the physical stability of salbutamol sulphate." Eur. J. Pharm. Biopharm. **56**: 393-400.

Pinkerton, K. E., A. R. Brody, et al. (1983). "Characterization of three types of chrysotile asbestos after aerosolization." Environ Res. **31**(1): 32-53.

Pitchayajittipong, C., J. Shur, et al. (2009). "Engineering of Crystalline Combination Inhalation Particles of a Long-Acting β2-agonist and a Corticosteroid." Pharm Res **26**(12): 2657-2666.

Price, R. (2005). Investigation into the cohesive adhesive properties in dry powder inhalation systems (influence of surface roughness and MgST processed lactose particles, Nanopharm Ltd**:** 1-45.

Rasenack, N. and B. W. Muller (2004). "Micron-Size Drug Particles: Common and Novel Micronization Techniques." Pharm. Dev. Technol. **9**(1): 1-13.

Remenar, J. F., S. L. Morissette, et al. (2003). "Crystal Engineering of Novel Cocrystals of a Triazole Drug with 1,4-Dicarboxylic Acids." J. Am. Chem. Soc. **125**(28): 8456-8457.

Rockland, L. B. (1960). "Saturated Salt Solutions for Static Control of Relative Humidity between 5o and 40o C." Anal. Chem. **32**(10): 1375-1376.

Rodrigo, G. J. and C. Rodrigo (2003). "Triple Inhaled Drug Protocol for the Treatment of Acute Severe Asthma." Chest **123**(6): 1908-1915.

Ruecroft, G. (2007). "Power ultrasound and particle engineering - Crystals for drug delivery and formulation." Chimica Oggi-Chemistry Today **25**(3): 12-14.

Ruecroft, G., D. Hipkiss, et al. (2005). "Sonocrystallization: The Use of Ultrasound for Improved Industrial Crystallization." Org.Process Res.Dev. **9**(6).

Rustichelli, C., G. Gamberini, et al. (2000). "Solid-state study of polymorphic drugs: carbamazepine." J Pharm Biomed Anal **23**(1): 41-54.

Salekigerhardt, A., C. Ahlneck, et al. (1994). "Assessment of disorder in crystalline solids." Int. J. Pharm. **101**(3): 237-247.

Seefeldt, K., J. Miller, et al. (2007). "Crystallization pathways and kinetics of carbamazepine-nicotinamide cocrystals from the amorphous state by *in situ*

thermomicroscopy, spectroscopy, and calorimetry studies." J. Pharm. Sci. **96**(5): 1147-1158.

Shekunov, B. Y., P. Chattopadhyay, et al. (2007). "Particle size analysis in pharmaceutics: Principles, methods and applications." Pharm Res **24**(2): 203-227.

Shekunov, B. Y. and P. York (2000). "Crystallization processes in pharmaceutical technology and drug delivery design." J Cryst Growth **211**(1-4): 122-136.

Sin, D. D. and S. F. P. Man (2006). "Corticosteroids and adrenoceptor agonists: The compliments for combination therapy in chronic airways diseases." Eur J Pharmacol **533**(1-3): 28-35.

Sin, D. D. and S. F. P. Man (2007). "Do chronic inhaled steroids alone or in combination with a bronchodilator prolong life in chronic obstructive pulmonary disease patients?" Curr Opin Pulm Med **13**(2): 90-97.

Singh, D., J. Brooks, et al. (2008). "Superiority of "triple" therapy with salmeterol/fluticasone propionate and tiotropium bromide versus individual components in moderate to severe COPD." Thorax **63**(7): 592-598.

Smith, E. D. L., R. B. Hammond, et al. (2001). "The Determination of the Crystal Structure of Anhydrous Theophylline by X-ray Powder Diffraction with a Systematic Search Algorithm, Lattice Energy Calculations, and 13C and 15N Solid-State NMR: A Question of Polymorphism in a Given Unit Cell." J. Phys. Chem. B **105**(24): 5818-5826.

Soriano, J. B., J. Vestbo, et al. (2002). "Survival in COPD patients after regular use of fluticasone propionate and salmeterol in general practice." Eur Respir J **20**(4): 819-825.

Spong, B. R. (2005). Enhancing the pharmaceutical behavior of poorly soluble drugs through the formation of cocrystals and mesophases. Michigan, University of Michigan. **Doctor of Philosophy (Pharmaceutics)**.

Steckel, H., L. Pichert, et al. (2004). "Influence of process parameters in the ASES process on particle properties of budesonide for pulmonary delivery." Eur.J.Pharm.Biopharm. **57**(3).

Stempel, D. A., S. W. Stoloff, et al. (2005). "Adherence to asthma controller medication regimens." Resp. Med. **99**(10): 1263-1267.

Stokes, G. G. (1908). "Mathematical and physical papers." Astrophys. J. **23**: 173.

Suihko, E., J. Ketolainen, et al. (1997). "Dehydration of theophylline monohydrate - a two step process." Int. J. Pharm. **158**(1): 47-55.

Suryabarayanan, R. and H. G. Brittain (1995). X-ray powder diffractometry. Physical Charcaterization of Pharmaceutical Solids. New York, Marcel Dekker**:** 187-221.

Taki, M. and C. Marriott Combination formulations for inhalation: Benefits and challenges. Proceedings of Drug Delivery to the Lungs 18, The Aerosol Society, Bristol, UK.

Taki, M., X. M. Zeng, et al. (2006). "A comparison of the in-vitro deposition profiles of drugs from a combination dry powder inhaler (DIPI) using the Next Generation Impactor (NGI)." J Pharm Pharmacol **58**: A65-A65.

Taulbee, D. B. and C. P. Yu (1975). "Theory of Aerosol Deposition in Human Respiratory-Tract." J Appl Physiol **38**(1): 77-85.

Taylor, M. K., A. J. Hickey, et al. (2006). "Manufacture, Characterization, and Pharmacodynamic Evaluation of Engineered Ipratropium Bromide Particles." Pharm. Dev. Technol. **11**(3): 321-336.

Telko, M. and A. J. Hickey (2005). "Dry powder inhaler formulations." Respir. Care **50**(9): 1209-1227.

Tetko, I. V., J. Gasteiger, et al. (2005). "Virtual computational chemistry laboratory - design and description." J. Comput. Aid. Mol. Des. **19**: 453-63.

Tetsumi, I. and U. Kaneto (1997). "Pharmaceutical applications of cyclodextrins. III. Toxicological issues and safety evaluation." J. Pharm. Sci. **86**(2): 147-162.

The British Thoracic Society (2008). British Guidelines on the Managment of Asthma, The British Thoracic Society.

Theophilus, A., A. Moore, et al. (2006). "Co-deposition of salmeterol and fluticasone propionate by a combination inhaler." Int. J. Pharm. **313**(1-2): 14-22.

Threlfall, T. (2000). "Crystallisation of Polymorphs: Thermodynamic Insight into the Role of Solvent." Org. Process Res. Dev. **4**(5): 384-390.

Thummel, K. E. and D. D. Shen (2001). Design and Optimization of Dosage Regimens: Pharmacokinetic Data. Goodman & Gilman's The Pharmacological Basis of Therapeurics. J. G. Hardman and L. E. Limbird. London, McGraw-Hill.

Ticehurst, M. D., P. A. Basford, et al. (2000). "Characterisation of the influence of micronisation on the crystallinity and physical stability of revatropate hydrobromide." Int. J. Pharm. **193**(2): 247-259.

Timsina, M. P., G. P. Martin, et al. (1994). "Drug delivery to the respiratory tract using dry powder inhalers." International Journal of Pharmaceutics **101**(1-2): 1-13.

To, Y., K. Ito, et al. "Targeting Phosphoinositide-3-kinase-{delta} with Theophylline Reverses Corticosteroid Insensitivity COPD." Am. J. Respir. Crit. Care Med.: 200906-0937OC.

Tong, H. H. Y., B. Y. Shekunov, et al. (2003). "Thermal analysis of trace levels of polymorphic impurity in salmeterol xinafoate samples." Pharm. Res. **20**(9): 1423-1429.

Torphy, T. J., B. J. Undem, et al. (1993). "Identification, characterization and functional role of phosphodiesterase isozymes in human airway smooth muscle." J Pharmacol Exp Ther **265**(3): 1213-1223.

Traini, D. (2005). Physical Properties and Interactions in Pressurised Metered Dose Inhalers. Pharmacy & Pharmacology. Bath, University of Bath. **Doctor of Philosophy**.

Tsuda, A., J. P. Butler, et al. (1994). "Effects of alveolated duct structure on aerosol kinetics. 2. Gravitational sedimentation and inertial impaction." J.Appl.Physiol. **76**(6): 2510 - 2516.

Ukena, D., U. Harnest, et al. (1997). "Comparison of addition of theophylline to inhaled steroid with doubling of the dose of inhaled steroid in asthma." Eur Respir J **10**(12): 2754-2760.

VCCLAB. (2005). "Virtual Computational Chemistry Laboratory,." Retrieved 29th August 2010, 2010, from http://www.vcclab.org.

Vishweshwar, P., J. A. McMahon, et al. (2006). "Pharmaceutical co-crystals." Journal of Pharmaceutical Sciences **95**(3): 499-516.

Vishweshwar, P., J. A. McMahon, et al. (2006). "Pharmaceutical co-crystals." J. Pharm. Sci. **95**(3): 499-516.

Vora, K. L., G. Buckton, et al. (2004). "The use of dynamic vapour sorption and near infra-red spectroscopy (DVS-NIR) to study the crystal transitions of theophylline and the report of a new solid-state transition." Eur. J. Pharm. Sci. **22**(2-3): 97-105.

Washington, C. (1992). Particle Size Analysis in Pharmaceutics and Other Industries: Theory and Practice. London, Ellis Horwood.

Wendlandt, W. W. (1986). Thermal Analysis. New York, John Wiley & Sons.

Williams, R. O., J. Brown, et al. (1999). "Influence of micronization method on the performance of a suspension triamcinolone acetonide pressurized metered-dose inhaler formulation." Pharm.Dev.Technol. **4**(2).

Wu, C.-Y. and L. Z. Benet (2005). "Predicting Drug Disposition via Application of BCS: Transport/Absorption/ Elimination Interplay and Development of a Biopharmaceutics Drug Disposition Classification System." Pharm Res **22**(1): 11-23.

Yeomans, A. H., E. E. Rogers, et al. (1949). "Deposition of Aerosol Particles." J Econ Entomol **42**(4): 591-596.

Young, P. M., S. Edge, et al. (2005). "Dynamic vapor sorption properties of sodium starch glycolate disintegrants." Pharm. Dev. Technol. **10**(2): 249-259.